

A STUDY OF ORE GENESIS AND GEOCHRONOLOGY  
IN THE SUB-VOLCANIC TIN BELT OF THE  
EASTERN ANDES, BOLIVIA

by

John Nigel Murray Grant

A thesis submitted for the degree of  
Doctor of Philosophy in the University  
of London.

Department of Mining  
Geology, Imperial  
College of Science  
and Technology,  
London, England

December 1978.

A study of Ore Genesis and Geochronology in the  
Sub-Volcanic Tin Belt of the Eastern Andes, Bolivia  
by J.N.M. Grant

ABSTRACT

Most of the important mineral deposits in the southern part of the Bolivian tin belt are vein and disseminated ore systems associated with acid igneous eruptive complexes of Tertiary age. Evidence from geological, fluid inclusion and stable isotope studies suggest a genetic model involving an initially shallow magmatic supply of heat, fluid and ore components in the porphyry- and breccia-filled volcanic vents. Patterns of early pervasive rock alteration and dispersed ore mineral deposition were controlled by mixing of the high-temperature fluid with cool dilute water of probable meteoric origin. Later, as hydrothermal activity declined at the high level, the major vein structures were formed and tapped the deeper magmatic source. Hydrothermal circulation and ore deposition were then confined to the veins, which cross-cut the earlier patterns of pervasive alteration and mineralization.

K-Ar dating of the complexes shows that their ages fall into two groups. The northern group (north of Potosi) give ages of approximately 19 Ma to 23 Ma, while the southern group give 12 Ma to 17 Ma. The ages of the northern group overlap with previously published ages for the southernmost batholiths of the northern tin belt showing that there is not, as previously believed, a major time break between them. The data show that the various metal associations of the eruptive complexes are not consistently related to their age, but appear to depend on the level in the crust at which the deposits were formed. This suggests that the metal zonation displayed by the tin belt as a whole, from tin-tungsten in the north to tin-silver-lead-zinc in the south, reflects the depth of formation of the deposits and hence the variation in the level of erosion, rather than changes in magma composition.

## CONTENTS

	Page
Abstract	(I)
List of Figures	(VII)
List of Tables	(X)
List of Plates	(XI)
Acknowledgements	(XIII)
Abbreviations and Symbols	(XV)
CHAPTER 1. REGIONAL GEOLOGY AND MINERALIZATION OF THE CENTRAL ANDES	
1.1. The Morpho-Tectonic Units	1
1.2. Tectonics and Magmatism	6
1.2.1. Pre-Andean tectonics and magmatism	8
1.2.2. Andean tectonics and magmatism	10
1.3. Mineralization	23
1.3.1. Pre-Andean mineral deposits	24
1.3.2. Andean mineralization	25
CHAPTER 2. GEOLOGY OF THE BOLIVIAN TIN BELT AND SUB-VOLCANIC TIN DEPOSITS	
2.1. General Geology and Mineralization	28
2.1.1. Geology	28
A. The northern section	30
B. The southern section	33
2.1.2. The mineral deposits	40
A. The metallogenic province	40
B. The mineral deposits of the northern section	42
C. The mineral deposits of the southern section	45
2.2. Detailed Studies of the Geology and Mineralization of Selected Deposits	48
2.2.1. Introduction	48
2.2.2. Chorolque	
A. Regional setting	50
B. Rock types	51
C. Alteration types	56
D. Alteration zoning	61

CHAPTER 2 (continued).	Page
E. Mineralization and metal zoning	63
2.2.3. Llallagua	
A. Regional setting	71
B. Rock types	72
C. Alteration	78
D. Mineralization	79
E. Alteration and mineral zoning	83
2.2.4. Potosí	83
A. Rock types	84
B. Alteration and mineralization	86
2.2.5. Colquechaca	
A. Introduction, geological setting	87
B. Alteration and mineralization	90
2.2.6. Other deposits	91
A. The San Pablo-Morococala area	91
B. Chocaya	96
C. Tatasi	98
D. Isca-Isca	100
E. Tasna	100
2.3. Discussion	101
2.3.1. Hydrothermal brecciation	101
2.3.2. Hydrothermal alteration	108
A. Pervasive alteration, types and zoning	108
B. Vein wall-rock alteration	113
2.3.3. The chemistry of some altered and unaltered rocks	
A. Introduction	115
B. The whole-rock analyses	115
C. Results	117
D. Semi-quantitative analyses	130
 CHAPTER 3. FLUID INCLUSION STUDIES	
3.1. Introduction	135
3.2. Principles of Fluid Inclusion Study	136
3.2.1. Mechanisms of trapping of primary inclusions	137

CHAPTER 3 (continued).	Page
3.2.2. The distinction between primary, secondary and pseudo-secondary inclusions	138
3.2.3. Leakage, and other changes since trapping	141
3.2.4. Temperature-pressure relationships and the homogenization method of microthermometry	144
3.2.5. Fluid salinity, depression of freezing point and daughter minerals	151
3.2.6. The composition of fluid inclusions	153
3.3. Experimental Methods	154
3.3.1. Sample preparation	155
3.3.2. Homogenization temperature determination	156
3.3.3. Freezing temperature determination	159
3.3.4. Analytical procedures	160
A. Non-destructive tests of daughter minerals	161
B. On-stage optical and chemical tests on extracted daughter minerals	161
C. Electron-probe microanalysis	162
D. The scanning electron microscope	163
E. Crushing and leaching	167
F. Laser microprobe analysis	169
3.4. Results	175
3.4.1. Chorolque	175
A. Material studied	175
B. Classification of inclusion types	176
C. Distribution of inclusion types	179
D. Temperature and salinity data	181
E. Chemical data	190
1. Daughter mineral identification	190
2. General chemical data	193
a) The scanning electron microscope data	194
b) Data from crushing and leaching	196
c) Laser microprobe data	197
3.4.2. Llallagua	
A. Previous investigations	199

CHAPTER 3 (continued).	Page
B. Material studied	201
C. Classification and distribution of inclusion types	201
D. Temperature data	205
3.4.3. Potosí	209
A. Material studied and inclusion types	209
B. Results	211
3.4.4. Other deposits	215
3.5. Discussion	218
CHAPTER 4. OXYGEN AND HYDROGEN ISOTOPE STUDY	
4.1. Introduction	228
4.2. Principles	229
4.3. Analytical Methods	233
4.4. Samples Studied, and Results	235
4.5. Discussion	241
4.5.1. Surface water data	241
4.5.2. Clay data	244
4.5.3. Biotite data	245
4.5.4. Quartz-tourmaline alteration and vein data	246
4.5.5. Sericite data	248
4.6. Conclusions	251
CHAPTER 5. A GEOCHRONOLOGICAL STUDY OF THE SOUTHERN PART OF THE BOLIVIAN TIN BELT	
5.1. Introduction	256
5.2. Previous Geochronological Data	256
5.3. Location and Description of Samples	258
5.4. The Principles of the Potassium-Argon Method of Age Determination	259
5.4.1. The K-Ar age equation	260
5.4.2. Extraneous argon	263
5.4.3. Argon loss	265
A. Thermal disturbance	267
B. Hydrothermal alteration	269

CHAPTER5 (continued).	Page
5.5. Experimental Methods	272
5.5.1. Sample preparation	272
5.5.2. Analytical methods	273
A. Potassium analysis	273
B. Argon isotopic analysis	274
5.6. Precision and Resolution	275
5.7. Results	279
5.7.1. San Pablo-Morococala region	279
5.7.2. Llallagua, the Salvadora stock	285
5.7.3. Colquechaca	289
5.7.4. The Potosí region	292
5.7.5. The mineralized igneous centres of the Quechisla region	298
5.8. Discussion	302
5.8.1. General considerations	302
5.8.2. Geochronology of the southern tin belt	306
CHAPTER 6. SUMMARY AND CONCLUSIONS	
6.1. Origin of the Tin Belt	312
6.2. Geochronology of the Southern Part of the Tin Belt	318
6.3. A genetic Model for the Sub-Volcanic Tin Deposits	320
6.4. The Transport and Deposition of Tin in Hydrothermal Systems	328
APPENDICES	
I. Petrographic Descriptions of Analysed Rocks	332
II. Calculations in K-Ar Dating	340
REFERENCES	349

## LIST OF FIGURES

CHAPTER 1	Page
1.1. The central Andes, morpho-tectonic units	2
1.2. The central Andes, schematic cross-section	5
1.3. Plate configuration, South American region	7
1.4. Major igneous provinces of the Eastern Cordillera of the central Andes, with locations of relevant age data	11
1.5. Tectonic segmentation of the Andes	14
1.6. Age relationships of igneous rocks in the transect across the Andes between 26° and 29° south latitude	19
1.7. Metallogenic belts of the central Andes	26
CHAPTER 2	
2.1. The Bolivian tin belt, general location map	29
2.2. The northern tin belt, location map	31
2.3. The southern tin belt, location map	34
2.4. Schematic cross-sections. Mineralized eruptive complexes of the southern tin belt	36
2.5. Chorolque, general geology map	52
2.6. Chorolque, geological cross-section	53
2.7. Chorolque, plan of alteration zones	62
2.8. Chorolque, underground rock geochemistry traverse, results	
A. Tin	66
B. Silver	67
C. Bismuth	68
D. Copper	69
2.9. Llallagua, the Salvadora stock, geological plan and cross-section	73
2.10. Potosí, the Cerro Rico stock, geological cross-section	85
2.11. Colquechaca, surface geology	89
2.12. San Pablo stock, surface geology	93
2.13. San Pablo-Morococala region, surface geology	95



CHAPTER 2 (continued).	Page
2.14. Chocaya, surface geology	97
2.15. Tatasí, surface geology	99
2.16. Alkali-silica diagrams, unaltered rocks	120
2.17. Composition variations, altered and unaltered rocks	123
2.18. K/Ca variation, altered and unaltered rocks	124
2.19. ACF diagram, altered and unaltered rocks	126
2.20. AKF diagram, altered and unaltered rocks	127
2.21. Sn/Ag variation, altered and unaltered rocks	133
2.22. Sn/Zn variation, altered and unaltered rocks	134
 CHAPTER 3	
3.1. P-T diagram for H <sub>2</sub> O	147
3.2. Heating stage calibration curves	157
3.3. Laser microprobe, schematic diagram	170
3.4. Chorolque, fluid inclusion homogenization data	185
3.5. Chorolque, schematic diagram of fluid temperature/salinity evolution with time	187
3.6. Llallagua, fluid inclusion homogenization data	206
3.7. Llallagua, schematic diagram of fluid temperature/salinity evolution with time	207
3.8. Potosí, fluid inclusion homogenization data	213
3.9. Relationship between the critical curve for NaCl - H <sub>2</sub> O and the melting curve for granite	219
 CHAPTER 4.	
4.1. Oxygen and hydrogen isotopic composition ranges for some natural waters	232
4.2. Plot of measured isotopic data for minerals and surface waters	240
4.3. Plot of calculated isotopic compositions of alteration and vein fluids	243
4.4. Schematic diagram showing possible evolution of hydrogen isotopic composition of fluids with time	253
4.5. Schematic diagram showing possible evolution of hydrogen isotopic composition of fluids with time	254

CHAPTER 5	Page
5.1. Plotted K-Ar data, San Pablo-Morococala area	286
5.2. Plotted K-Ar data, Llallagua	288
5.3. Plotted K-Ar data, Colquechaca	291
5.4. Surface geology and sample locations, Potosí region	293
5.5. Plotted K-Ar data, Potosí region	295
5.6. $^{40}\text{Ar}/\text{K}$ diagram, Potosí data	296
5.7. Plotted K-Ar data, Quechisla region	299
5.8. Summary plot of age data for the southern tin belt	308
CHAPTER 6	
6.1. Schematic diagram, evolution of the sub-volcanic systems, volcanic stage	321
6.2. Schematic diagram, porphyry intrusion stage	323
6.3. Schematic diagrams, pervasive alteration stage	
A. Main hydrothermal stage	324
B. Resulting alteration and dispersed mineralization pattern	325
6.4. Schematic diagram, vein stage	328

## LIST OF TABLES

	Page
1. Whole-rock (XRF) analytical results, major and minor elements	118
2. Whole-rock (XRF) analytical results, trace elements	121
3. Semi-quantitative whole-rock analyses, mean values	131
4. Chorolque: Fluid inclusion homogenization temperature and salinity data	182
5. Fluid inclusion crushing experiment, analytical results	198
6. Laser microprobe results	200
7. Llallagua: Fluid inclusion homogenization temperature and salinity data	202
8. Potosí: Fluid inclusion homogenization temperature and salinity data	212
9. Miscellaneous fluid inclusion homogenization results	216
10. Oxygen and hydrogen isotopic analyses, mineral, surface water, and inclusion fluid results	239
11. Calculated oxygen and hydrogen isotopic compositions of fluids	242
12. Potassium-argon analytical and age data	280

## LIST OF PLATES

	Page
1. Views of Chorolque	380
2. Chorolque; petrography of volcanics, and breccia texture of vent rock	381
3. Chorolque, petrography of altered rocks	382
4. Llallagua, igneous breccia	383
5. Llallagua, hydrothermal breccia types	384
6. Llallagua, hydrothermal breccia types	385
7. Llallagua, hydrothermal breccia	386
8. Llallagua, petrography of hydrothermal breccia matrix and black dyke	387
9. Llallagua, disseminated mineralization types	388
10. Colquechaca, general view of Cerro Yanakaka; San Pablo stock, breccia and alteration types	389
11. Santa Fé, hydrothermal breccia	390
12. Fluid inclusion analysis by laser microprobe	391
13. Fluid inclusion analysis by laser microprobe, scanning electron microscope image of crater produced by laser	392
14. As above	393
15. Chorolque, fluid inclusion types	394
16. Chorolque, fluid inclusion types	395
17. Chorolque, fluid inclusion types	396
18. Chorolque, fluid inclusion types	397
19. Chorolque, fluid inclusion types	398
20. Chorolque, fluid inclusion types	399
21. Chorolque, fluid inclusion types	400
22. Chorolque, fluid inclusions in sericitized volcanics	401
23. Chorolque, daughter minerals in Type IV and VI inclusions	402
24. Scanning electron microscope (SEM) investigations of daughter minerals	403
25. SEM investigation of daughter minerals	405
26. SEM investigation of daughter minerals	408

## LIST OF PLATES (continued).

	Page
27. SEM investigation of daughter minerals	413
28. Llallagua, fluid inclusion types	416
29. Potosí, fluid inclusion types	417
30. Huanuni, fluid inclusion types	418

## ACKNOWLEDGEMENTS

The research was financed by the Natural Environment Research Council. Of the large number of people who assisted I wish to thank in particular the following: At the Royal School of Mines; Professor G.R. Davis, Dr. Christopher Halls who introduced me to the tin deposits of Bolivia and supervised the research, Dr. A. Rankin for assistance with the fluid inclusion work, Dr. R. Sillitoe for encouragement and helpful discussion; the technical staff of the Geology and Applied Geochemistry Departments, in particular Mr. B. Foster and Miss E. Morris (sample preparation), Mr. N. Wilkinson (SEM and microprobe), Mr. A. Thompson and Mr. G. Bullen (rock analyses), Mr. R. Curtis (XRD), and research assistants Ian Ferriday, S. le Chevalier, and A. Stevens (mineral separation). At the Geochemical Division, Institute of Geological Sciences, London, Dr. N. Snelling and Mr. C. Rundle for permission to use the K-Ar facilities, instruction, and much helpful discussion. At the Scottish Universities Research Center, Dr. S.M.F. Sheppard and Mr. J. Borthwick for isotopic analyses and helpful discussion. At St Andrews University, Dr. P. Bowden and Dr. A. Maitland for encouraging the use of the laser microprobe, and Mr. J. Bennett for assistance with the experiments.

In Bolivia the work was carried out with the cooperation and assistance of the Servicio Geologico de Bolivia (GEOBOL) who provided transport and much geological assistance. I thank in particular Ingenieros Jose Torrez, then Director of GEOBOL, Alvaro Fernandez, present Director, Fernando Urquidi, and in

particular Waldo Avila with whom I shared many adventures throughout two field seasons and who provided invaluable knowledge of Bolivian geology. I thank the Management of the Corporacion Minera de Bolivia (COMIBOL) for permission to visit the mines and for providing accomodation and fuel, and numerous COMIBOL staff for their hospitality and geological assistance underground. Among these I thank in particular Ingenieros Mendiola and Delgado (Santa Fé - Japo), Mercado and Rivas (Llallgua), Rivera (Colquechaca), Oño (Quechisla group), Cabrera and Gonzales (Chorolque) and Anaya and Cortez (Caracoles).

The manuscript was typed by Cisca van Dijk. Finally, I thank my wife Lucy for her constant encouragement and assistance.

## ABBREVIATIONS AND SYMBOLS

$\text{\AA}$	angstrom units
bars	pressure (1 bar = 750.08 mm Hg at 0°C)
°C	temperature in degrees Centigrade
cm	centimetre
DC	direct current electricity
EPMA	electron probe microanalyser
f	fugacity of gas
gm	gram
K-Ar	potassium-argon age determination
kg	kilogram
km	kilometre
km <sup>2</sup>	area in square kilometres
kv	kilovolt
ln	natural (base <sub>e</sub> ) logarithm
m	metre
Ma	million (10 <sup>6</sup> ) years
mg	milligram
ml	millilitre
mm	millimetre
mv	millivolt
nl	nanolitre
P	pressure, except where used to denote parent isotope in radioactive decay equations (Chapter 5)
pH	negative logarithm of the hydrogen ion activity
ppm	parts per million
permil (‰)	parts per thousand
Rb:Sr	rubidium-strontium age determination
SEM	scanning electron microscope
T	temperature
U:Pb	uranium-lead age determination
2V	optic axial angle
XRD	X-ray diffraction



## ABBREVIATIONS AND SYMBOLS (continued)

yr	year
Wt%	weight percent
°	angular measurement in degrees
>	greater than
<	less than
$\lambda$	radioactive decay constant, general
$\lambda_{\epsilon}$	decay constant for $^{40}\text{K} \rightarrow ^{40}\text{Ar}$
$\lambda_{\beta}$	decay constant for $^{40}\text{K} \rightarrow ^{40}\text{Ca}$

## C H A P T E R 1

REGIONAL GEOLOGY AND MINERALIZATION OF THE CENTRAL ANDES1.1. The Morpho-Tectonic Units

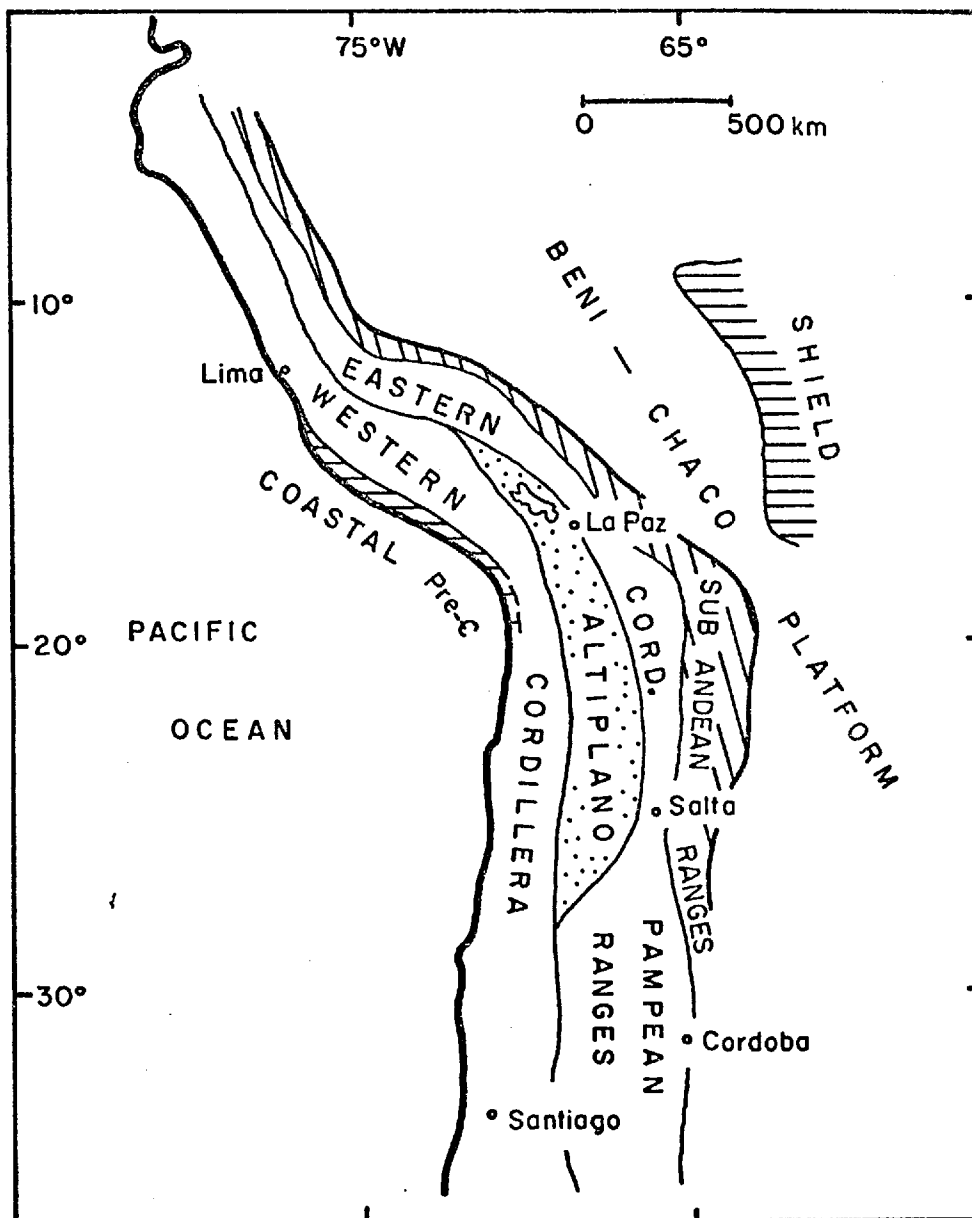
The Cordillera of the Andes runs the length of South America, bounded on the west by the Pacific ocean and on the east by the Precambrian shields of Guyana, Brazil and Argentina. The width across strike varies from about 100 to 500 km. The widest part is the central section described here, and here also there is a change in the direction of strike of the major structures from roughly northwest-southeast to north-south. I shall refer to the central Andes loosely as incorporating the Cordilleras in southern Peru, Bolivia, northern Chile and northwestern Argentina.

Within this zone rocks ranging in age from Precambrian to Recent are exposed. There is evidence that the entire width of the Andes is here underlain by a Precambrian crystalline basement. There are also very extensive terrains made up almost exclusively of Lower Palaeozoic sedimentary formations. However, the outstanding structural and morphological features, as well as many of the major rock units, are the result of orogenic activity which began in the Triassic and continued to the present. I shall follow most other workers in this region in using the term Andes when referring to the Cordillera in the geographic sense, and Andean when referring to the post-Palaeozoic orogeny.

Six morpho-tectonic units can be recognized throughout the length of the central Andes (Audebaud et al., 1976; Ahlfeld, 1972; Turner, 1970).

They are shown in Fig. 1.1.

FIG. I.I



THE CENTRAL ANDES, MORPHO-TECTONIC UNITS

a) The Coastal Zone. This is best displayed in southern Peru. It is a massif of Precambrian rocks which extends from the coast for about 80 km inland to the edge of the Coastal batholith. The extension of this zone southward into Chile is generally obscured by younger rocks; however, intermittent outcrops are present in northern Chile and it is well exposed farther south.

b) The Western Cordillera. This follows the main axis of sedimentation, volcanism and plutonism of the Andean orogen. It now forms the highest elevations of the Andes, reaching to over 6000 m altitude, and its crest is marked by a chain of young strato-volcanoes, some of which are still active.

c) The Altiplano. South of the region of Cuzco in central Peru, the single chain of the Andes is divided into two Cordilleras by the Altiplano intermontane basin. It is filled with continental clastic sediments eroded from the flanking ranges in the process of uplift during the Andean orogeny. It extends southward as far as northern Argentina, and the present day surface is a high-level plateau at an elevation of about 4000 m.

d) The Eastern Cordillera. This is composed predominantly of Palaeozoic sedimentary rocks though it owes its morpho-tectonic identity to the Andean orogeny. They form deeply incised plateau-like terrain, only moderately elevated above the Altiplano. Where the sedimentary rocks are intruded by Andean plutons, there are rugged mountain chains reaching altitudes of over 6000 m, as in the Cordillera Real in northern Bolivia and the Cordillera Vilcabamba in Peru.

e) The Sub-Andean Zone. This is a well-defined belt of marine and continental sedimentary rocks of the Andean orogeny,

lying between the Eastern Cordillera and the Brazilian shield. It was unaffected by the earlier phases of Andean movements, but was strongly deformed during the Pliocene, so that a tight en-echelon fold pattern and parallel high angle reverse faults were produced. These control the present-day topography, which comprises a series of parallel ranges of moderate elevation, deeply incised by the easterly-flowing drainage.

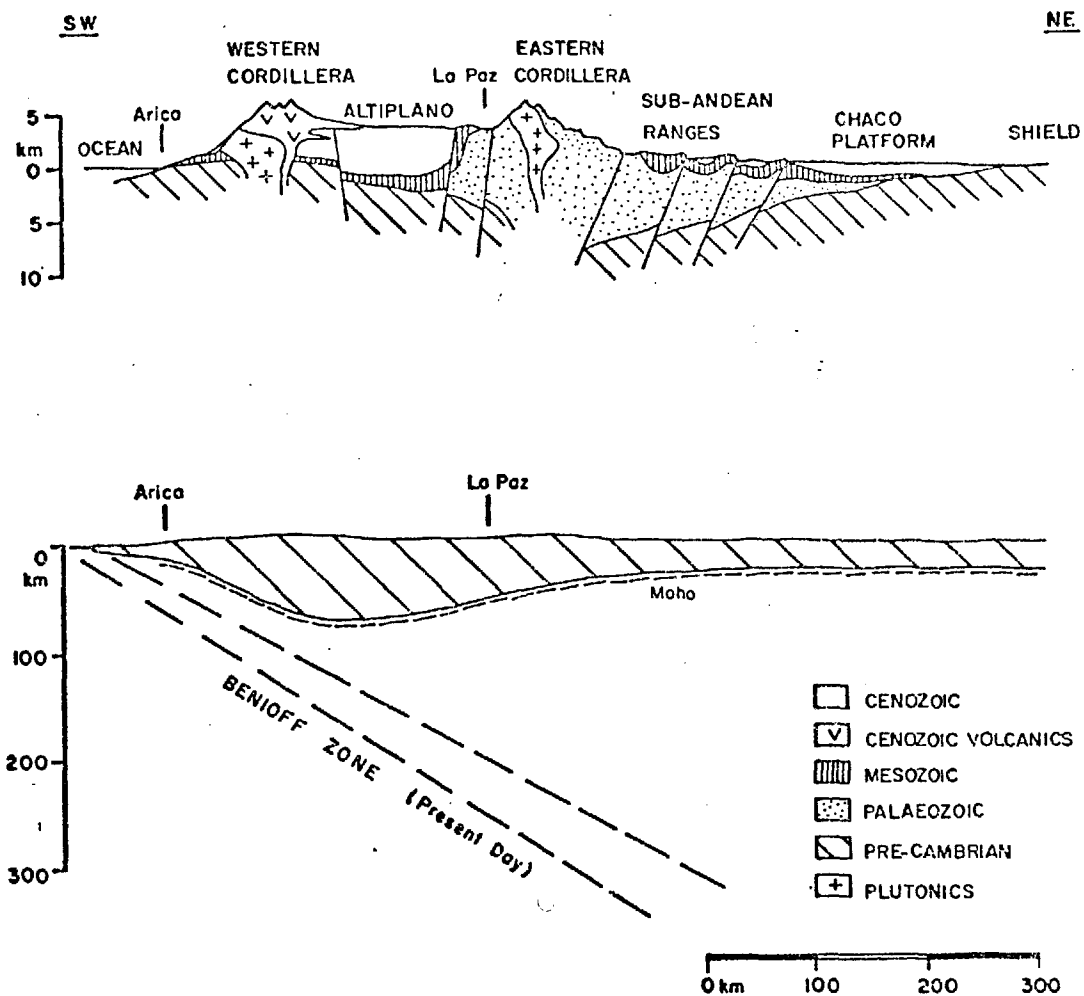
f) The Brazilian Shield. The Precambrian rocks are not exposed along the eastern border of the Andes. They underlie the lowlands east of the Sub-Andean zone (the Beni and Chaco platforms of Bolivia) but are covered with young clastic sedimentary rocks and alluvium.

The present-day structure of the crust beneath the central Andes has been partly investigated by seismic and gravity surveys (James, 1971a; Ocola et al., 1971). The continental crust thickens very rapidly eastward from the Chile-Peru trench, increasing from about 11 km in the ocean to 30 km along the coast and reaching a maximum of over 70 km beneath the crest of the Western Cordillera. The thickness decreases more gradually towards the craton, measuring 50-55 km under the Eastern Cordillera. The gravity data indicate a filling of over 10 km of sedimentary rocks in parts of the Altiplano basin. Fig 1.2 shows a schematic cross-section across the region. The central Andes are presently underlain by an active Benioff zone, the configuration of which is under investigation. Active underthrusting of oceanic lithosphere is apparently taking place down to depths of 300 km beneath the Eastern Cordillera (Swift and Carr, 1973; Stauder, 1973).

The morpho-tectonic units retained their separate identities throughout the Andean orogeny, and the stratigraphy of the Andean rocks can largely be interpreted in terms of vertical relative

FIG.1.2 CENTRAL ANDES — SCHEMATIC CROSS SECTION

(After JAMES, 1971b and COBBING and PITCHER, 1972a )



movement between them. However, the boundaries which delineate them almost certainly follow structural features of the basement which were reactivated in the Andean orogeny. The overall structural pattern is thus influenced by inherited basement structures, and superimposed purely Andean structures. Some of these involve the basement, while some were restricted to the Andean cover rocks.

The general geology of the central Andes has been described by numerous workers. Among the most useful papers are the following: for southern Peru, Audebaud et al., (1976); for Bolivia, Ahlfeld and Branisa (1960), Ahlfeld (1972), Schlatter and Nederlof (1966), Megard et al., (1971); for northern Argentina, Turner (1970), Mon (1976); for northern Chile, Segerstrom (1967), and Ruiz et al., (1965). Only a brief review of the tectonic and igneous evolution will be given here.

### 1.2. Tectonics and Magmatism

The tectonic evolution and the magmatism of the central Andes is related to the subduction of the Nazca plate, of Pacific oceanic crust, beneath the western edge of the South American continent (Fig. 1.3 ). The present rate of spreading of the Nazca plate eastward from the East Pacific Rise is about 6 cm/yr, and it has been estimated that some 5000 km of oceanic lithosphere have been consumed beneath the Andes since the Cretaceous alone ( Larson and Pitman, 1972). The rise into the crust of the enormous volumes of calc-alkaline magma so produced is regarded as one of the most important mechanisms of Andean tectonic evolution (James, 1971b). A detailed synthesis of the relationship between the tectonic evolution of the Andean orogen and the history of plate interaction is not possible; however, a considerable amount of information is now available on the time-space pattern of magmatism, as well as

FIG. 1.3

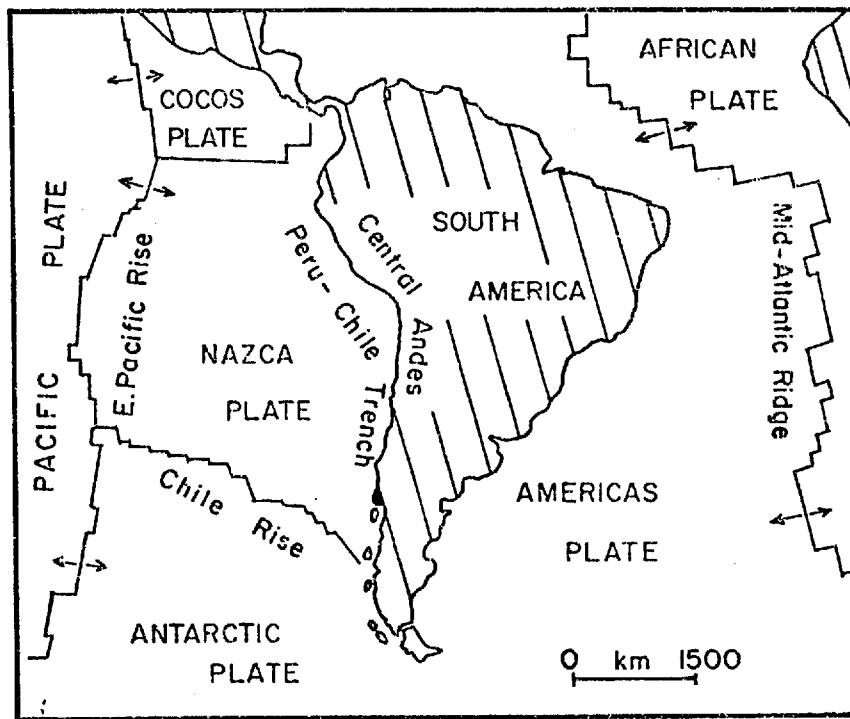


PLATE CONFIGURATION — SOUTH AMERICAN REGION



limited information on some important chemical and isotopic characteristics of the igneous rocks. Since most of the important mineralization in the central Andes is associated with igneous rocks, the metallogeny of the region must be considered in the light of this still very incomplete data, as well as in relation to the overall tectonic setting.

#### 1.2.1. Pre-Andean tectonics and magmatism

The tectonic evolution and magmatic history of the pre-Andean Palaeozoic and Precambrian basement is relatively poorly known. In his plate tectonic model for the evolution of the central Andes, James (1971b) described the Palaeozoic sedimentary rocks as continental-shelf deposits which had accumulated under essentially quiescent conditions on an 'Atlantic-type' (Dewey and Bird, 1970) continental margin. However, this appears to be something of an oversimplification, and it is now clear that there was a complex history of deformation and calc-alkaline magmatism during the Palaeozoic, especially in the southern part of the region in northern Argentina and Chile. In that region the stratigraphic record indicates a north-west trending continental margin which migrated to the west, away from the Brazilian shield, during the Palaeozoic. Parallel belts of granitic plutons and metamorphic rocks define successive orogenic zones. The main plutonic episodes have been dated as Cambrian, Upper Ordovician-Lower Devonian, and mid-Carboniferous in age, and correspond with regional unconformities in the sedimentary succession. There was a general westward migration of Palaeozoic plutonic activity with time, and the plutons in the basement on the Chilean side of the Cordillera are mid-Carboniferous to Upper Permian in age (Clark et al., 1976).

Farther to the north, in Bolivia, there are regional unconformities in the Palaeozoic sedimentary succession which correspond with those to the south, but deformation was less intense, metamorphism almost absent, and there are no igneous rocks older than Triassic. Some of the granitic plutons of the Cordillera Real in the northern Eastern Cordillera in Bolivia give Triassic apparent ages (Clark and Farrar, 1973). They can not readily be fitted into the sequence of westward-migrating belts of Palaeozoic plutonism outlined above for the region to the south. They are however, of critical importance in any interpretation of the metallogeny of the central Andes since they have important tin-tungsten deposits associated with them which constitute the earliest phase of mineralization in the well-defined north-south trending Bolivian tin belt. Tin deposits associated with acid magmatism were formed in this belt in a number of apparently discrete pulses from Triassic to Upper Miocene time. If, as discussed below, the Andean orogeny was initiated by the beginning of eastward subduction of the Nazca plate in the Upper Triassic, the problem then is to explain the generation and emplacement of these tin-bearing Upper Triassic batholiths, which took place over 300 km inland from the trench, before, or at the same time as the beginning of volcanism in the coastal region. Subsequent emplacement of tin-bearing igneous rocks in the tin belt during the Miocene can be more readily fitted into a coherent pattern of Andean magmatic evolution.

In southern Peru there were periods of tectonic activity in the Upper Ordovician and Devonian-Carboniferous time, but magmatic activity was minimal. There was however, important volcanic activity (the Mitu group) and emplacement of granitic plutons in the Eastern

Cordillera in the Permian (Lancelot et al., 1976). The geochronological data for the igneous rocks of the Eastern Cordillera in southern Peru, Bolivia, and northern Argentina are summarized in Fig. 1.4.

#### 1.2.2. Andean tectonics and magmatism

The beginning of the Andean orogeny is generally taken to be marked by the subsidence, marine transgression and volcanic activity which began in the coastal regions in the Upper Triassic (James, 1971b; Clark et al., 1976). However, the evidence of widespread calc-alkaline magmatic activity in the coastal region of Chile and in the Eastern Cordillera in Peru and Argentina during the Permian, and in the Western Cordillera of Bolivia in the Triassic, suggests a more complex picture. While it may be more realistic to consider that the Andean orogen first became active in the Permian (Sillitoe, 1976), the difficulty remains in relating the Permian and Triassic magmatic activity of the Eastern Cordillera to the initiation of eastward subduction of the Nazca plate beneath the Andes. This problem is discussed further, in the context of the metallogeny of the region, in Chapter 6. From the Upper Triassic onward, the tectonic and magmatic evolution of the central Andean orogen has been relatively simple. Outstanding characteristics include: the entirely intra-continental setting with the development of extreme crustal thickness; the dominance of vertical tectonic movement with relatively little crustal shortening; the predominance of continental sedimentation and sub-aerial volcanism, especially in the post-Cretaceous period; and the predominance of a tensional tectonic regime, with the formation of major longitudinal horst and graben structures, which existed during much of the development of

FIG.1.4

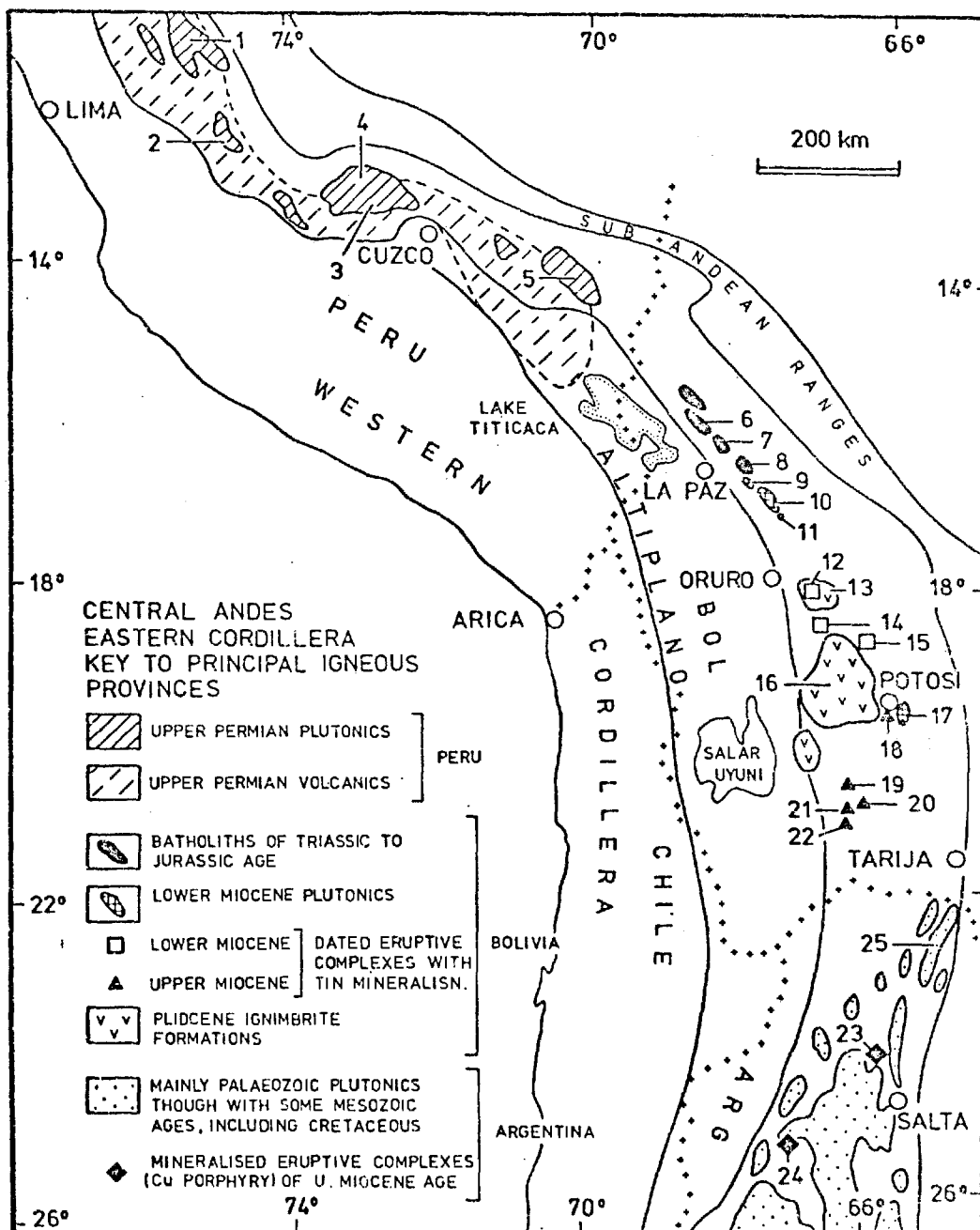


Fig. 1.4. Major igneous provinces of the Eastern Cordillera of the central Andes, with locations of relevant age data

Peru. Data reported in Lancelot et al. (1976)

1. San Ramon,  $252 \pm 18$  Ma (Rb: Sr)
2. Villa Azul, 251 Ma (K-Ar)
3. Machupicchu,  $246 \pm 10$  Ma (Rb: Sr)
4. Quillabamba,  $257 \pm 5$  Ma (U: Pb)
5. Coasa,  $238 \pm 11$  Ma (U: Pb)

Bolivia, the northern tin belt, K-Ar data reported in Clark and Farrar (1973) and Evernden et al. (1977)

6. Sorata, 180 Ma
7. Zongo, 150 to 211 Ma
8. Taquesi, 199 Ma
9. Illimani, 26 Ma
10. Quimsa Cruz, 26 Ma, and  $23.8 \pm 1.6$  Ma
11. Santa Vera Cruz,  $22.8 \pm 0.7$  Ma

Bolivia, the southern tin belt, K-Ar data reported in Chapter 5

12. San Pablo-Morococala,  $22.7 \pm 0.4$  Ma
13. Morococala ignimbrite,  $6.1 \pm 0.1$  Ma
14. Llallagua,  $20.5 \pm 0.4$  Ma
15. Colquechaca,  $22.1 \pm 0.4$  Ma
16. Los Frailes ignimbrite,  $7.3 \pm 0.2$  Ma
17. Kari-Kari batholith, 21 Ma
18. Cerro Rico stock, Potosi,  $13.5 \pm 0.3$  Ma
19. Tasna,  $16.0 \pm 0.3$  Ma
20. Chorolque,  $15.8 \pm 0.3$  Ma
21. Chocaya,  $13.4 \pm 0.2$  Ma
22. Tatasi,  $15.3 \pm 0.3$  Ma

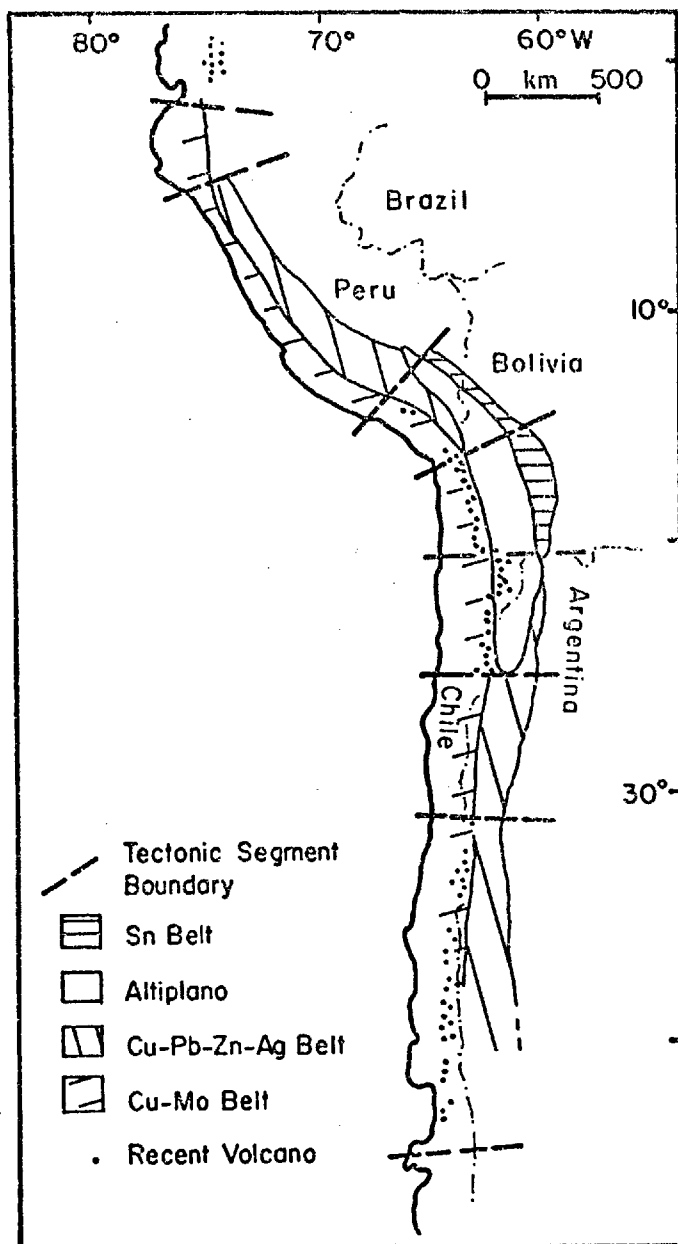
Argentina. Data reported in Sillitoe (1976 and 1977)

23. Pancho Arias,  $15.4 \pm 0.3$  Ma (K-Ar)
24. Inca Viejo,  $15.0 \pm 0.2$  Ma
25. Aguilar, 123-133 Ma (Rb: Sr).

the orogen, although back-arc spreading and the development of marginal ocean basins did not take place. Many of these characteristics, including the great vertical uplift which took place particularly in the late Tertiary, can perhaps be explained as the results of distension of the continental crust by the rise of enormous volumes of calc-alkaline magma (James, 1971b; Gough, 1973; Sillitoe, 1976).

The tectonics of the region have been dominated by the parallel development of a series of relatively well-defined linear zones. The zones run parallel to the overall trend of the orogen and have great linear extent. They can be distinguished from each other in particular by their history of relative vertical movement and differing igneous activity. Although this linear zonation is the most obvious feature, the orogen is also divided by rather poorly defined transverse boundaries into a series of tectonic segments which cross-cut the longitudinal continuity (Sillitoe, 1974). The boundaries between segments are generally marked by changes in geology and geomorphology but not by well-defined lineaments or fault zones (Fig. 1.5). Adjacent segments commonly show distinct differences in the time-space pattern of igneous activity, suggesting a sub-crustal control on the segmentation. In some cases however, distinct pulses of magmatism do not correspond with otherwise recognisable segment boundaries (see Chapter 5) suggesting that the distinction between segments did not exist throughout the entire period of Andean evolution. The breakdown of the major linear zones into short segments is particularly recognisable in the history of igneous activity in the Western Cordillera where, for

FIG. 1.5



TECTONIC SEGMENTATION OF THE ANDES  
After Sillitoe (1974).

example, present day volcanism is restricted to well-defined sections of limited length. Both the linear zonation and the cross-strike segmentation are reflected in the pattern of metallogeny of the Andes, as discussed below.

From the Upper Triassic onward, the magmatic activity has been particularly concentrated in what is now the Western Cordillera, although it has taken place to a lesser extent farther east, in the Altiplano and Eastern Cordillera. Almost all of the igneous rocks are calc-alkaline in character, although there are minor alkaline high-level intrusions in the eastern part of the Eastern Cordillera in Peru, Bolivia and Argentina (Stewart et al., 1974; Ahlfeld, 1972; Clark et al., 1976). Age dating of the igneous rocks is still fragmentary, although certain sections have been studied in some detail (Farrar et al., 1970; Clark et al., 1976).

Major igneous activity began in the coastal region in the Triassic to Lower Jurassic. Enormous volumes of andesite and keratophyre were erupted, and these were accompanied by intrusions of tonalite and granodiorite which marked the beginning of formation of the Coastal Batholith. The batholith extends for over a thousand kilometres through the western Andes from Ecuador to southern Chile (Gansser, 1973). In the central Andes it is made up of a series of disconnected composite plutons which intruded the pre-Andean rocks of the coastal zone, and the oldest Andean sediments and volcanics to the east, in what is now the western flank of the Western Cordillera. Many of the plutons of the batholith pass upward into centered sub-volcanic complexes, or are roofed by what are interpreted as the effusives of the same magma chamber. The composite plutons show a distinct basic to acid



compositional trend with time, from gabbro to adamellite, though granodiorite and tonalite are the dominant rock types (Cobbing and Pitcher, 1972b). In northern Chile the oldest plutonics of the batholith are Lower Jurassic in age, though the oldest ages so far measured in southern Peru are Middle Cretaceous. Farrar et al., (1970) showed that in northern Chile there is a distinct trend in the ages of the plutonic rocks, and that intrusion seems to have taken place in distinct pulses with little activity between them. The locus of intrusion appears to have migrated eastward with time, starting on the coast in Lower Jurassic and reaching 120 km inland in the Upper Eocene. Farther east the plutonic rocks are covered by younger volcanic formations of the high Western Cordillera. In Peru a similar trend is apparent. The bulk of the batholith seems to be made up of rocks of Cretaceous age, but there is a distinct belt of Tertiary plutons and small high-level stocks in the eastern flank of the Cordillera to the east of the main axis of the batholith (Stewart et al., 1974). Despite this general trend, it is clear that plutonic activity has taken place in the same relatively narrow zone of the Western Cordillera over a very long period of time, possibly from the Lower Jurassic to the Pliocene.

Noble et al., (1974) described the episodic nature of Cenozoic igneous activity and tectonics in the Peruvian Andes, and their findings probably apply throughout the region. Following a major period of igneous activity in the Cretaceous, there was a general decline in activity through the early Tertiary. A relatively weak pulse in the Upper Eocene was followed by a quiescent period. This ended in the Lower Miocene when there

was another major pulse. A relatively high level of activity was maintained from then on, through Pliocene and Recent time.

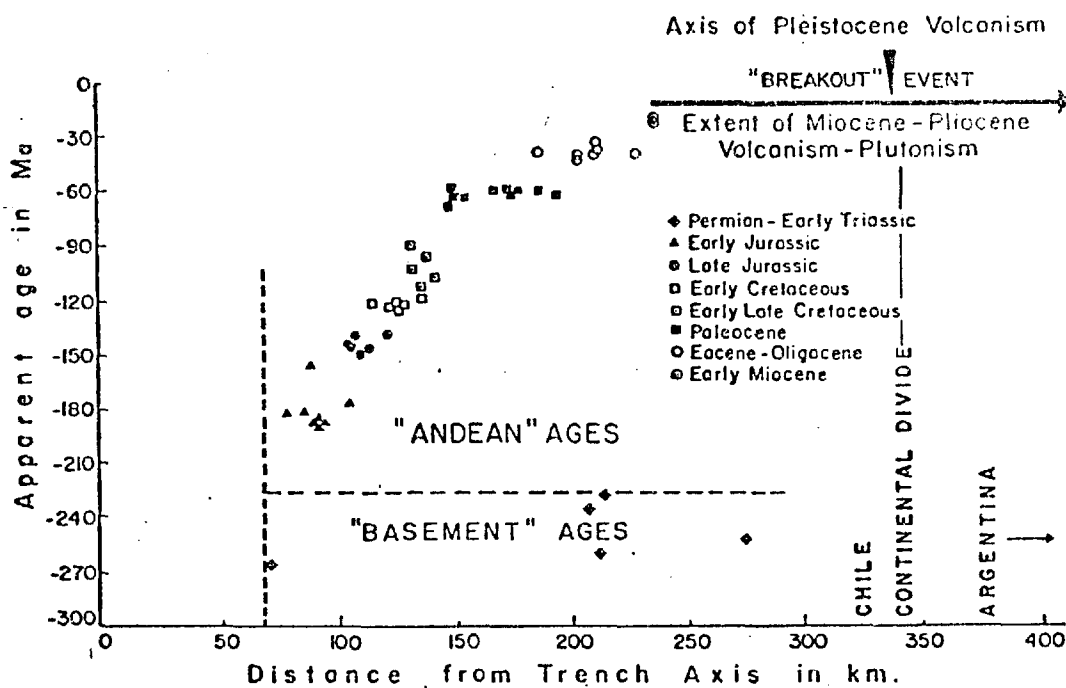
Considering the region as a whole, the Cretaceous activity was particularly concentrated in the Western Cordillera. There was little activity in the Cretaceous or Lower Tertiary in the Eastern Cordillera in Peru and Bolivia. However in the Lower Miocene there was a sudden "breakout" of magmatic activity toward the east, so that during the Miocene and Pliocene there was both plutonic and volcanic activity in the Western Cordillera, the Altiplano and in the Eastern Cordillera (Clark et al., 1976).

In Peru there is a belt of Lower Miocene or younger plutonic rocks running through the Western Cordillera to the east of the Coastal batholith. They include the Cordillera Blanca batholith to the north of Lima and numerous smaller high-level stocks farther south. Similar high-level plutons are found in Chile, and together they are of particular importance because of the numerous mineral deposits which are associated with them. There was also andesitic volcanism in the Western Cordillera during this period and it extended eastward onto the Altiplano. In Bolivia there are important andesitic volcanic centres of Lower Miocene age in the western and southern Altiplano (Ahlfeld, 1967), and some of the volcanics of the Cordillera de Lipez, which runs east-west across the Bolivian Altiplano near the Argentina frontier, are also of this age. In the Eastern Cordillera of central Bolivia there is a well-defined Lower Miocene igneous province which forms a southward continuation of the Triassic plutonic province. Its northern part is made up of high-level plutonics (the Illimani stock, Quimsa Cruz batholith, and Santa Vera Cruz stock) while

farther south there are volcanic and sub-volcanic centers and also the Kari-Kari batholith (Fig. 1.4). To the south of this there is an Upper Miocene province of volcanic and sub-volcanic centers. Some aspects of the geology, mineral deposits and geochronology of this region are the subject of this thesis and are discussed in detail below.

In Bolivia the Miocene igneous activity was followed by a period of erosion. There was a renewal of volcanism after this in the Eastern Cordillera, with the eruption of extensive ignimbrite sheets. Small alkalic plutons were emplaced in the Eastern Cordillera in Peru, Bolivia, and northern Argentina at this time also, while volcanic activity continued in the Altiplano and Western Cordillera. In northern Chile and Argentina the systematic eastward migration of magmatic activity, and the Miocene-Pliocene "breakout" have been particularly well documented by detailed geochronological work along a transect across the orogen between latitudes 26 degrees and 29 degrees south (Clark et al., 1976). Discrete episodes of magmatic activity have been dated, each pulse of activity was confined to a relatively narrow longitudinal belt lying to the east of the preceding one. During the Miocene there was an abrupt eastward spread so that igneous activity took place over a very wide zone during the Miocene-Lower Pliocene. The eastward migration of magmatic activity with time in this region is illustrated in Fig. 1.6. In the Upper Pliocene, following the "breakout" period, there was a contraction of igneous activity back towards the west. Volcanism continued in the western Altiplano and Western Cordillera, first with major rhyolitic ignimbrite eruptions, and then with the development of

FIG. 1.6



AGE RELATIONSHIPS OF IGNEOUS ROCKS IN THE TRANSECT ACROSS THE ANDES BETWEEN 26° AND 29° SOUTH LATITUDE. K/Ar MINERAL AGES PLOTTED AGAINST DISTANCE FROM PRESENT CHILE-PERU TRENCH.

(After CLARK et al., 1976)

andesitic strato-volcanoes along the crest of the Cordillera, but igneous activity virtually ceased in the eastern Altiplano and Eastern Cordillera.

Farther north, in the segments containing the tin belt, the timing of igneous activity is less well documented particularly in the Western Cordillera. Apart from the major problem posed by the Triassic batholiths of the Cordillera Real, a broadly similar pattern is evident. Plutonic and volcanic activity began on the coast in the Lower Jurassic and migrated gradually eastward in the Western Cordillera. The Lower Miocene "breakout" is well represented by the sudden beginning of igneous activity across the Altiplano and in the tin belt in the Eastern Cordillera, starting in the Lower Miocene and continuing until the Pliocene. After the Pliocene ignimbritic volcanic episode there was a retreat of volcanism back to the Western Cordillera.

The fluctuations in the general intensity of igneous and tectonic activity may be related to variations in the rate of subduction of the Nazca plate beneath the Andes. The general increase which took place at about the beginning of the Miocene can be recognised in a number of other circum-Pacific regions and may be the result of increased rotation of the Pacific plates in general. The "breakout" of igneous activity which was so well developed in parts of the central Andes apparently corresponded with the beginning of a period of very rapid spreading at the East Pacific Rise (Noble et al., 1974; Herron, 1972).

The plutonic rocks of the central Andes range in composition from gabbro to granite. In the Coastal batholith tonalite is probably the predominant rock type, with large volumes of granodiorite

and adamellite (Jenks and Harris, 1953; Cobbing and Pitcher, 1972b). Farther to the east, the batholiths and sub-volcanic plutons of the Eastern Cordillera are predominantly granodiorite and adamellite in composition (Turneure and Welker, 1947; Ahlfeld, 1967). The earlier volcanics of the Western Cordillera are mainly andesites, with a trend towards dacitic and rhyolitic composition with time; although, as noted above the most recent strato-volcanoes are again andesitic in composition. Basalts are present among the older volcanics but are rare in the younger volcanic terrain. Andesitic volcanics are found in the Altiplano, and the older volcanics in the Eastern Cordillera in Peru and Argentina are andesitic also. In the younger volcanoes and sub-volcanic eruptive complexes of the Eastern Cordillera, andesites are not common and the predominant rock-types are dacite and rhyodacite.

Important chemical and isotopic data have been obtained by Clark and his co-workers (Clark et al., 1976) for igneous rocks from the transect across the orogen between latitudes 26 degrees and 29 degrees south. Some important features of the chemistry of a wide range of plutonic and volcanic rocks of all ages are as follows:

a) The calc-alkaline volcanic and plutonic rocks of all ages show essentially similar chemical characteristics when compared with igneous rocks of the western Pacific island arcs. The only important differences are that the Andean rocks appear to be significantly enriched in Sn and Mo.

b) There is a well-defined eastward trend of increasing alkalinity.

c) There is a marked eastward increase in the potash index,

and application of the empirical potash index to depth relationship of Dickinson and Hatherton (1967) and Dickinson (1970) indicates that the inferred depth of magma generation corresponds closely with the known depth to the present-day Benioff zone.

d) There is no systematic spatial trend in the concentration of most of the minor elements, and the levels of Cu, Zn, Pb, Mo, Ti and Sn are the same for volcanic rocks of similar silica content right across the orogen. As discussed below there is no zonation of mineralization in this region, unlike the regions to the north. Copper deposits are found here right across the orogen from the coastal region to the Eastern Cordillera, and there are no Andean tin deposits.

e) Analysis of the chlorine and fluorine content of the rocks has not shown any systematic trends with time or space, nor has it shown a relationship between halogen concentration and the degree of mineralization in a given pluton. Analysis of the hydrothermal biotites from some of the porphyry copper deposits has shown a strong enrichment in F but not in Cl.

f) The initial strontium isotope ratios of igneous rocks of all ages give a restricted overall range from 0.7022 to 0.7077. The older plutons (Jurassic) give variable ratios from 0.7042 to 0.7059. However from the mid-Cretaceous onward the rocks show a systematic age-dependent increase in the ratio, from 0.7022 to 0.7077. On the basis of this data a mantle origin for the magmas is preferred, with only little contamination by crustal material. The progressive change in the ratio with time is inferred to be the result of changes in the source

material with respect to the degree of melting and phase-equilibrium relationships during partial melting, and also to the increasing addition of material rich in <sup>87</sup>Sr.

Unfortunately, comparable data are not yet available for the igneous rocks of the segments of the Andes which show a well-defined zonation in the metals contained in mineral deposits, and in particular for the segments which contain the tin province. There is however a suggestion, from very limited data, that the rocks of the segments containing the tin belt are enriched in potash relative to rocks of similar age and distance from the trench in the regions to the south. This would appear to correspond with the dip of the present-day Benioff zone, which is much deeper under the segments containing the tin belt than under the regions to the south (Clark et al., 1976).

### 1.3 Mineralization

The distribution of mineral deposits and the metallogeny of various parts of the central Andes have been discussed by numerous workers. Important compilations and interpretations have been made for various parts of the region including the following: central Peru (Peterson, 1965); Bolivia (Ahlfeld, 1967; Ahlfeld and Schneider-Scherbina, 1964; Turneure, 1971); Chile (Ruiz et al., 1965) and Argentina (Stoll, 1964; Angellini et al., 1970). In addition, the metallogeny of the central Andes as a whole has been discussed by Stoll (1965), Sillitoe (1972a, 1976), and Clark et al., (1976). Some of the most important features of the mineralization and metallogeny of the region will be briefly reviewed here, a more detailed discussion of the



geology, mineralization, and geochronology of the Bolivian tin belt is given in later Chapters.

#### 1.3.1. Pre-Andean mineral deposits

Pre-Andean mineral deposits are sparsely distributed and of relatively little economic importance. The only well-developed pre-Andean metallogenic provinces are those of the Eastern Cordillera in northern Argentina, and the Cordillera Real in Bolivia, if the Triassic plutons there are considered to be pre-Andean.

In the Sierras Pampeanas of Argentina there are widespread minor occurrences of tin and tungsten vein mineralization and rare-metal (Be, Li, W, Ta, U) pegmatites associated with the Palaeozoic granitic plutons. Tin and tungsten mineralization developed in both the Upper Ordovician-Lower Devonian and the Mid-Carboniferous plutonic episodes. In central and southern Bolivia the very extensive Palaeozoic terrain of the Eastern Cordillera contains no mineral deposits (or igneous rocks) except those that are attributed to the Andean orogeny. In the north there are important tin-tungsten deposits, and also gold and antimony and occurrences of molybdenum, lithium and beryllium associated with the granitic plutons of the Cordillera Real. The question as to whether these plutons represent the earliest magmatic activity of the Andean orogeny or not has been discussed above. Although they are distinct both in time and space from the mineralization of the Sierras Pampeanas, the deposits do represent a continuation or resurgence of tin metallogeny in the Eastern Cordillera in general, and mark the beginning of tin metallogeny in the Bolivian tin belt in particular.

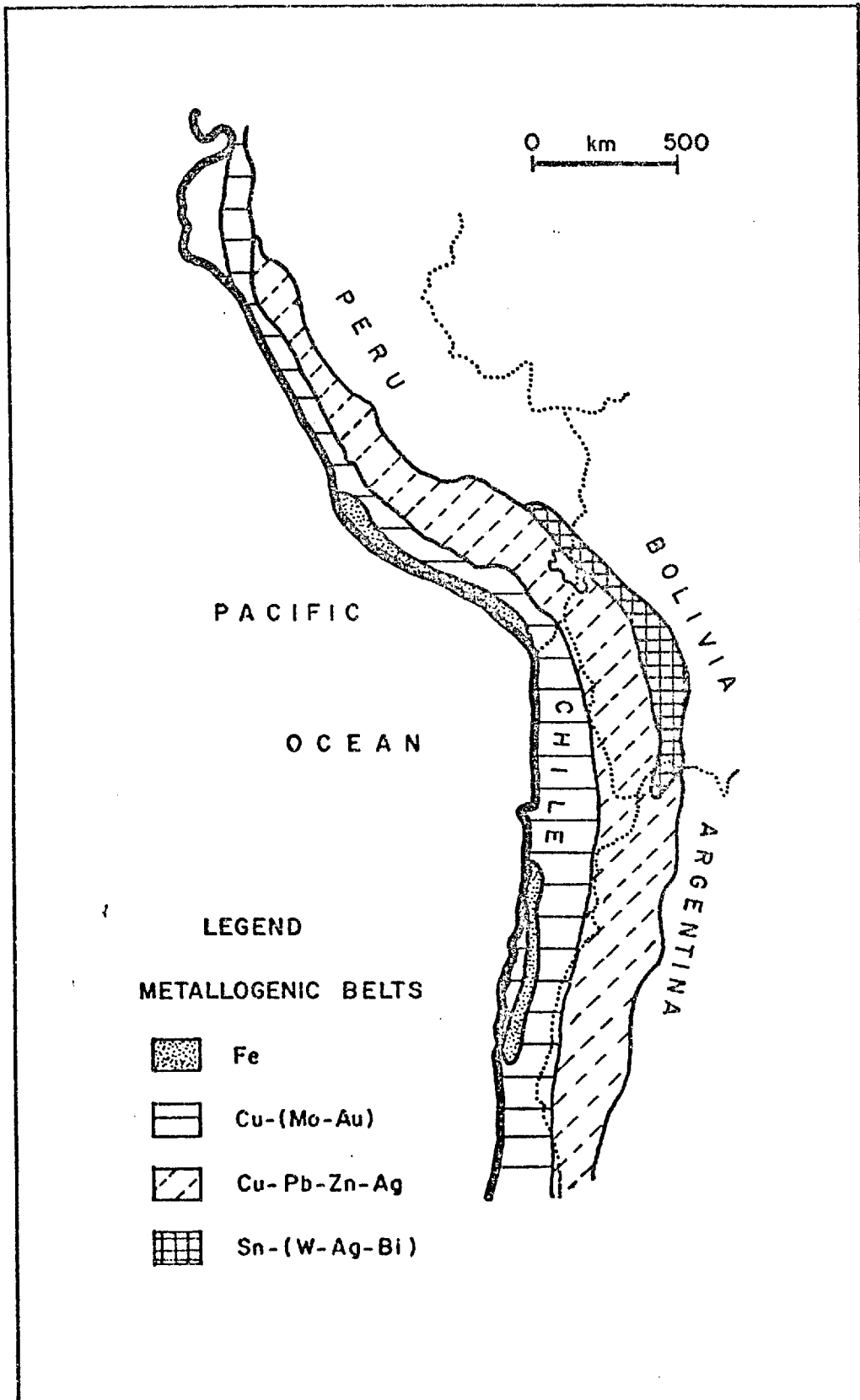
### 1.3.2. Andean mineralization

The distribution of mineralization and the relationships between the metallogeny and the tectonic development of the orogen has been discussed in some detail by Sillitoe (1976), who pointed out that the relatively simple geological evolution of the region, together with the great variety of well exposed mineral deposits, makes this a type-area for the study of continental margin metallogeny along a convergent plate boundary.

The outstanding feature of the distribution of mineralization is the presence of a series of well-defined metallogenic provinces (in which the mineralization is related mainly to igneous activity) which run parallel with the trend of the orogen and correspond broadly with the linear tectonic zones described above. The metal provinces are systematically zoned, with respect to their metal content, across the orogen. The distribution of the metal provinces is shown in Fig. 1.7.

In the most general terms, there is a belt of iron deposits (contact metasomatic) in the coastal zone of Peru and Chile; this is succeeded to the east by a broad belt of copper deposits in the Western Cordillera. There are also some important silver-producing districts within the Western Cordillera. The copper province is succeeded on the east by a copper-lead-zinc-silver province which occupies the eastern flank of the Western Cordillera and the Altiplano, especially in Peru. There is also a province of "red-bed" type copper deposits in the Altiplano. In Bolivia these are succeeded to the east by the tin-tungsten-bismuth-silver province of the Eastern Cordillera (the 'Bolivian tin belt'). In detail, the time-space pattern of mineralization is

FIG. 1.7



METALLOGENIC BELTS OF THE CENTRAL ANDES  
(After SILLITOE, 1976)

much more complex, and reflects regional and local geochemical variations, variations in ore-forming environments, and the effect of variations in post-ore erosion levels. For example, within the general copper province of the Western Cordillera there are a variety of deposit types whose distribution reflects the above factors. They include copper-gold and silver vein deposits which are associated with the Jurassic-Cretaceous batholiths; stratiform disseminated copper deposits associated with volcano-sedimentary sequences of Jurassic, Cretaceous and early Tertiary age; copper-bearing breccia pipes associated with the roofs of Tertiary granodiorite plutons, and the porphyry copper-molybdenum deposits whose ages range from Palaeocene to Pliocene and which are found in association with both small stocks and larger plutons, generally towards the eastern side of the Cordillera.

The distribution of mineralization also reflects the lateral segmentation of the orogen. Thus, the Andean tin-tungsten province is restricted to a sharply-defined section of the Eastern Cordillera, almost entirely in Bolivia, which spans two otherwise recognisable tectonic segments (Sillitoe 1974, 1976; Fig. 1.5). In the regions to the south, the copper province extends eastward into the Eastern Cordillera and Andean tin deposits are absent. Porphyry copper deposits (such as Farellon Negro and Famatina) are found in the Eastern Cordillera in northern Argentina. Other examples of the segmentation of the metallogenic provinces are documented by Sillitoe (1976). Possible mechanisms for the lateral zonation and overall development of the metallogenic provinces are discussed in Chapter 6.

## CHAPTER 2.

GEOLOGY OF THE BOLIVIAN TIN BELT AND SUB-VOLCANIC TIN DEPOSITS2.1. General Geology and Mineralization

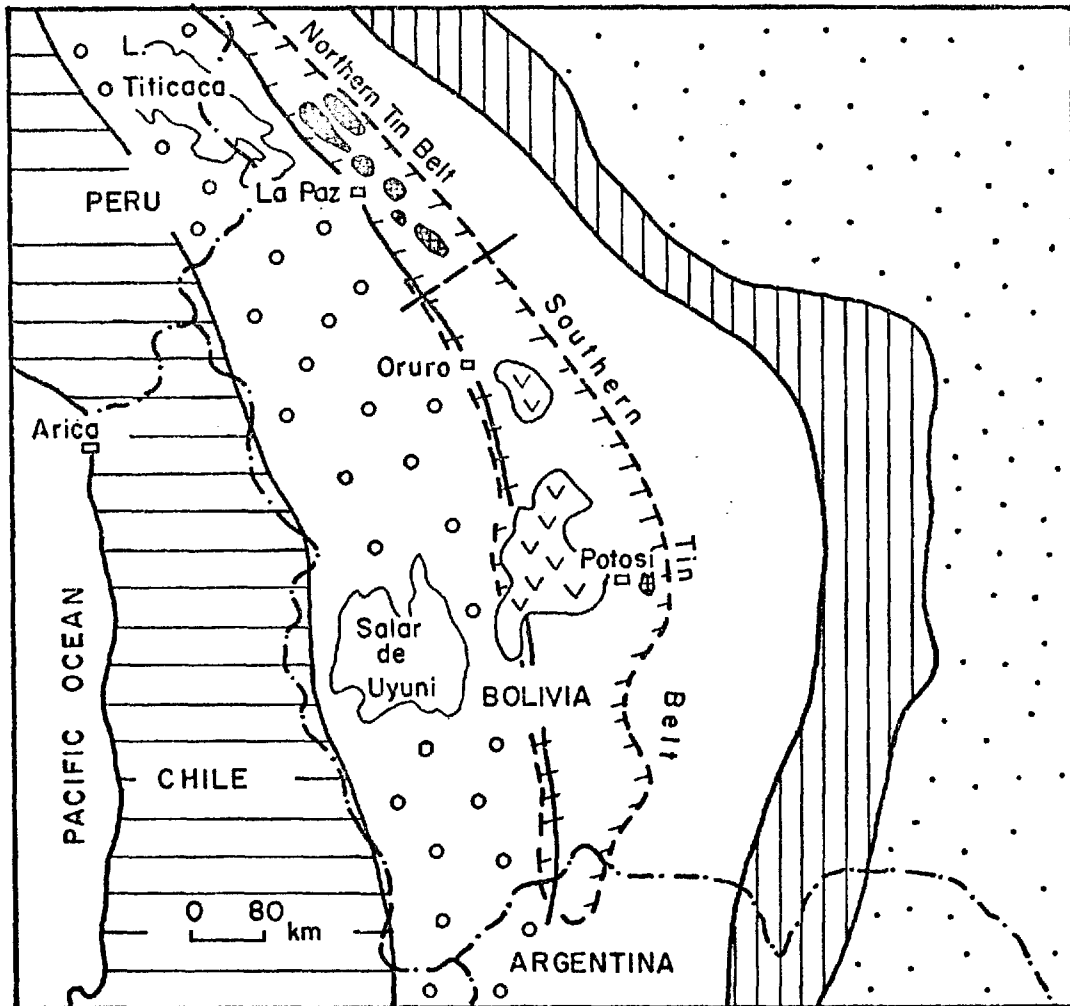
The geological evolution of the central Andes has been outlined in Chapter 1. In this section a more detailed description is given of the geology of the Eastern Cordillera in Bolivia, and in particular the geology of its Andean igneous rocks and associated mineral deposits.

2.1.1. Geology

The Cordillera is an elongated massif lying between the Altiplano intermontane basin to the west, and the Sub-Andean foothill zone to the east (Fig. 2.1). It is made up largely of Lower Palaeozoic sedimentary rocks, mainly shale and sandstone of Ordovician, Silurian and Devonian age. The rocks are strongly folded and faulted but only very weakly metamorphosed. There are a number of synclinal structures containing remnants of the Cretaceous and in some cases Tertiary epicontinental and continental sedimentary rocks. These once probably formed a thin cover over much of the region, but have since been largely removed by erosion.

The important mineral deposits are all associated with Andean igneous rocks although some major vein systems are located partly or entirely in the sedimentary rocks. Local variations in the geology of the sedimentary rocks have important controlling effects on the local distribution of mineralization in some areas (e.g., Turneure and Welker, 1947), but on a regional scale the sedimentary rock types are relatively uniform

FIG.2.I. THE BOLIVIAN TIN BELT



LEGEND

- |  |                        |  |                                 |
|--|------------------------|--|---------------------------------|
|  | WESTERN CORDILLERA     |  | SUB ANDEAN ZONE                 |
|  | ALTIPLANO              |  | CHACO BENI PLAIN                |
|  | EASTERN CORDILLERA     |  | PLUTONS ( Mesozoic - Tertiary ) |
|  | IGNIMBRITE ( Neogene ) |  | LIMITS OF TIN BELT              |

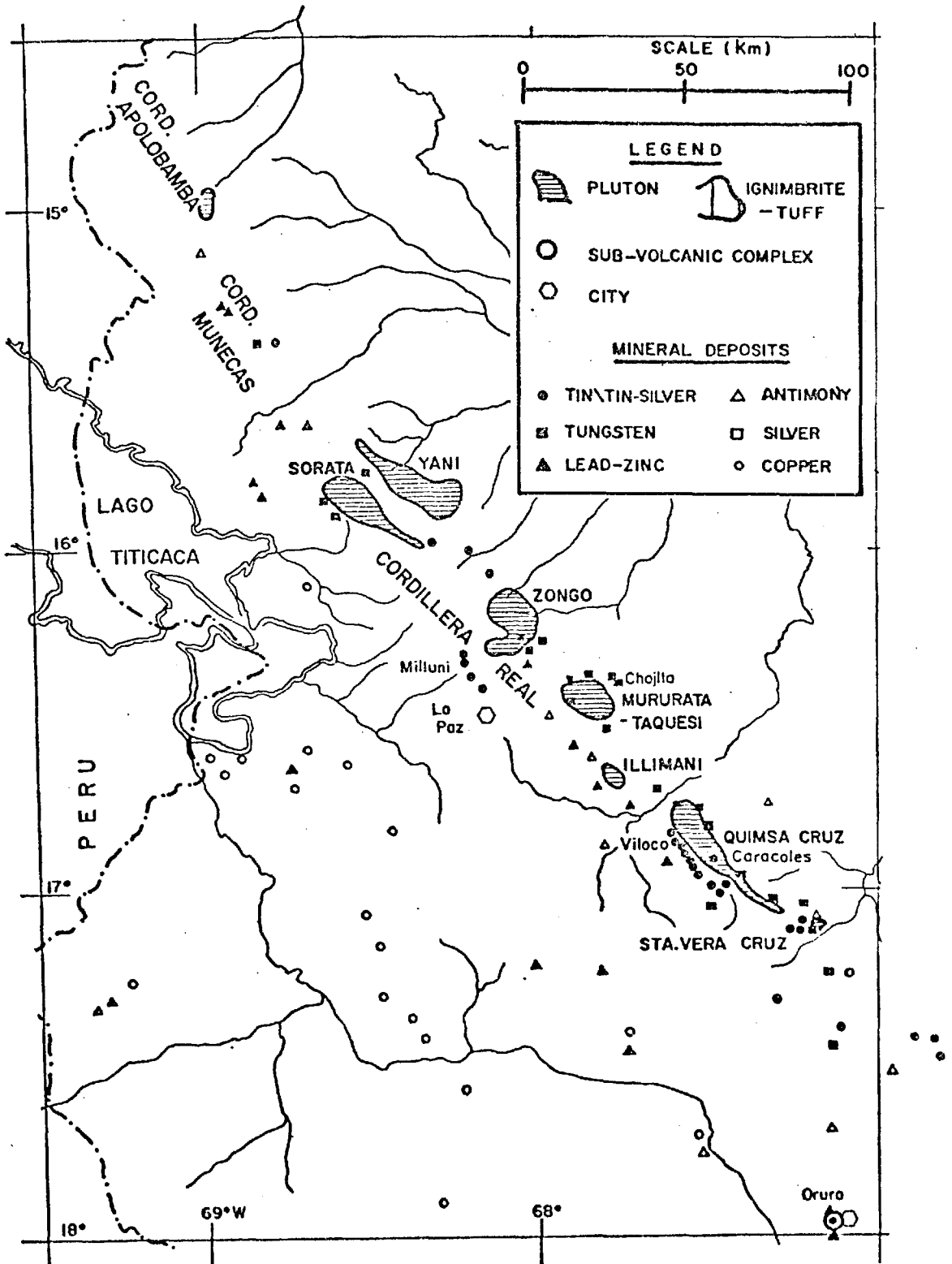
and there are no variations in the type or style of mineralization which can be attributed to regional variations in the geology of the sedimentary rocks.

During the Andean orogeny the Cordillera had a complex history of deformation, igneous intrusion, volcanism and uplift. It is separated from the Altiplano by a well-defined fault zone (the Coniri fault) and from the Sub-Andean zone by a broad complex belt of deformation. The strike of the northern part of the Cordillera is roughly northeast-southwest but in the region between 17 and 18 degrees south latitude the strike changes to north-south. The change corresponds with a somewhat hypothetical transverse tectonic zone known as the Arica Elbow Line (Radelli, 1966; Schlatter and Nederlof, 1966). This line divides the Cordillera into two distinct physiographical sections and probably reflects deep crustal structures, although there is little evidence at the surface for a transverse fault zone (Turneure, 1971). It has exerted no marked influence on the age distribution of Andean igneous activity. The general geology and mineralization of the Cordillera will be discussed in terms of these two sections for convenience, but as discussed further in Chapter 5, there is no distinct geological boundary between them.

#### A. The northern section

In the northern section the Palaeozoic terrain is more elevated and deeply eroded than to the south. The Andean igneous rocks are all plutonic, and comprise a number of batholiths and stocks which form the cores of high, ice-covered mountain massifs. These can be divided into three groups (Fig.2.2).

FIG. 2.2: THE NORTHERN TIN BELT, LOCATION MAP  
 (After AHLFELD and SCHNEIDER-SCHERBINA, 1964)





The northernmost ranges are the Cordilleras de Apolobamba and Munecas. The former contains a quartz monzonite stock of unknown age (Avila, 1975) while the presence of igneous rocks has not been confirmed in the latter.

The next range to the south is the Cordillera Real; it contains from north to south: the batholiths of Yani, Sorata, Zongo (Chucura) and Mururata-Taquesi. The Illimani stock is generally included on physiographic grounds although it is chronologically distinct. The Yani batholith is relatively low lying but the others form very high mountain massifs separated by deep gorges eroded in the Palaeozoic sediments. Potassium-argon ages of 60.5 Ma (Cordani, 1967) and 71 Ma (Robertson, 1974) have been measured for the Yani batholith, but because of the deep level of erosion they cannot be accepted as definitive and are almost certainly uplift or cooling ages. The Sorata, Zongo and Mururata-Taquesi batholiths all give Triassic to Jurassic ages (Clark and Farrar, 1973; Avila, 1975), but the Illimani pluton gives Miocene ages (Cordani, 1967; Robertson, 1974). These plutons are much less deeply eroded, and the K-Ar ages can be accepted with greater confidence.

South of the Illimani stock, and separated from it by the gorge of the La Paz river, is the Cordillera Quimsa Cruz. Its core is a 45 km long batholith which gives Miocene K-Ar ages. Immediately to the south of this there is another small pluton in the Cordillera Santa Vera Cruz which also gives Miocene K-Ar ages, and which marks the southern termination of the northern section of the tin belt.

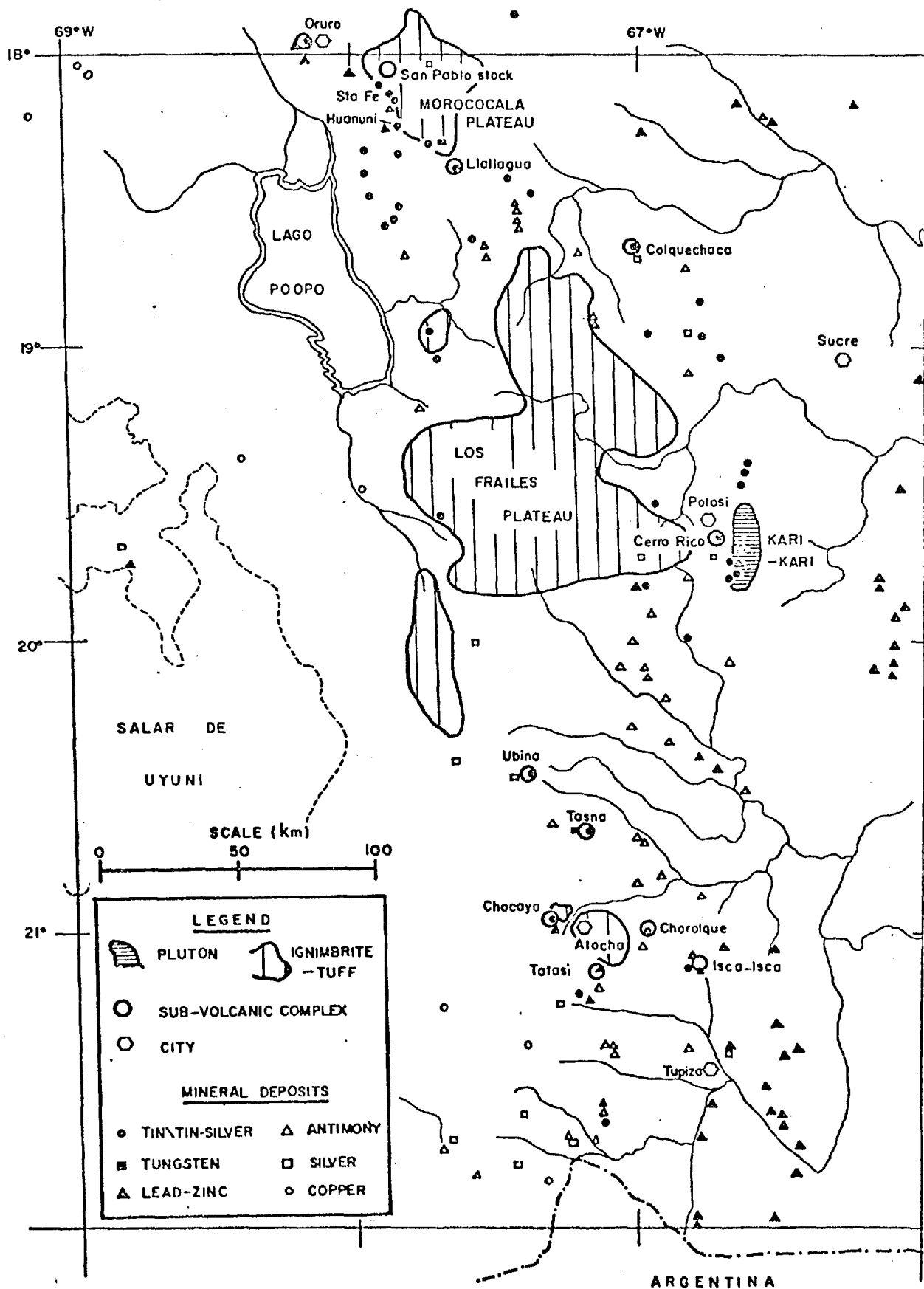
There is little published data on the petrography or

geochemistry of these plutons. They are all composed mainly of granodiorite, adamellite, and tonalite, with biotite as the mafic mineral. There are some more potassic phases with muscovite present, especially in the Yani pluton. The rock textures are both equigranular and coarse porphyritic. The plutons are steep-sided except for their eastern contacts which dip more gently, and they are not interconnected at shallow depth. They have distinct aureoles of contact metamorphism in the surrounding Palaeozoic sediments, and the northernmost batholiths, especially the Yani, are surrounded by regionally metamorphosed terrain (Turneaure and Welker, 1947).

#### B. The southern section

Here the Cordillera is much wider than in the north. The Palaeozoic sedimentary rocks were less strongly elevated, and instead of a single prominent mountain chain, they form a series of broad plateau-like blocks which are separated by river valleys cut less deeply than those which separate the massifs of the northern region. The Andean igneous rocks form small isolated porphyry stocks or larger eruptive complexes. There is also one plutonic body in the southern region, the Kari-Kari batholith near Potosi, and there are extensive sheets of ignimbrite and tuff (Fig. 2.3). The geochronology of igneous activity is discussed in detail in Chapter 5; however, it has long been recognised that the volcanic and sub-volcanic rocks of the southern part of the tin belt are younger than the plutonics of the north, and that the ignimbrites are the youngest of all, and were erupted after a period of erosion had affected the other igneous rocks (Ahlfeld and Branisa, 1960; Ahlfeld, 1967).

FIG. 2.3. THE SOUTHERN TIN BELT, LOCATION MAP  
 (After AHLFELD and SCHNEIDER-SCHERBINA, 1964)



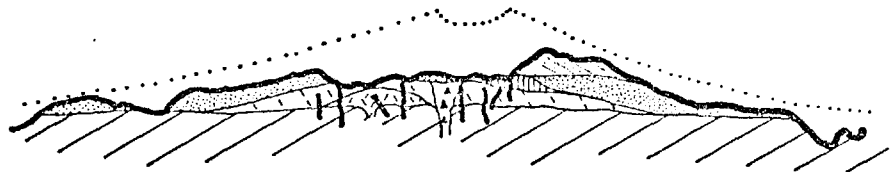
The history of uplift is complex, and several different erosion surfaces have been recognised in the Cordillera (Rutland et al., 1965). There was a very long period of erosion between the folding of the Cretaceous continental and epicontinental sediments and the beginning of igneous activity in the Miocene. The Andean eruptive complexes rest with sharp angular unconformity on the surface which resulted from this period of erosion, but elsewhere it has been destroyed during later uplift, and newer surfaces have developed. Although the chronology of uplift is not well understood, it is probable that the eruptive complexes were formed at very much lower elevations and that most of the uplift which has brought the Cordillera to its present altitude (4000-5000 m) took place later.

The Andean igneous rocks can be divided into three groups:

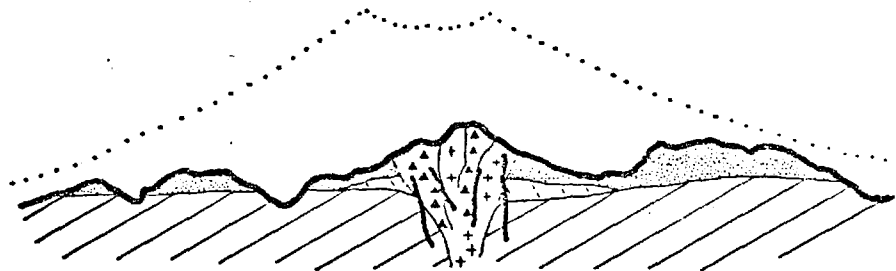
a) Small high-level stocks and eruptive complexes. These are found scattered at intervals down the length of the Cordillera, from Oruro in the north almost to the Argentina border in the south. All of the important tin deposits are associated with these (Fig. 2.3). They range in character from purely volcanic complexes at which no intrusive rocks other than dykes are recognisable, to small stock-like bodies of intrusive porphyry and breccia (Fig. 2.4). The essentially volcanic types, such as Tatasi, Chocaya, and Colquechaca, consist of acid lavas, lava domes, and pyroclastics which rest unconformably on the older sedimentary rocks. They cover tens of square kilometres. The rocks are generally quartz-porphyrines ranging in composition from rhyolite to dacite. They usually have an extensive zone

FIG.2.4. SCHEMATIC CROSS-SECTIONS.

MINERALIZED ERUPTIVE COMPLEXES OF THE SOUTHERN TIN BELT, BOLIVIA.



A EXAMPLES - COLQUECHACA, CHOCAYA, TATASI.



B EXAMPLES - CHOROLQUE, POTOSI, ORURO.

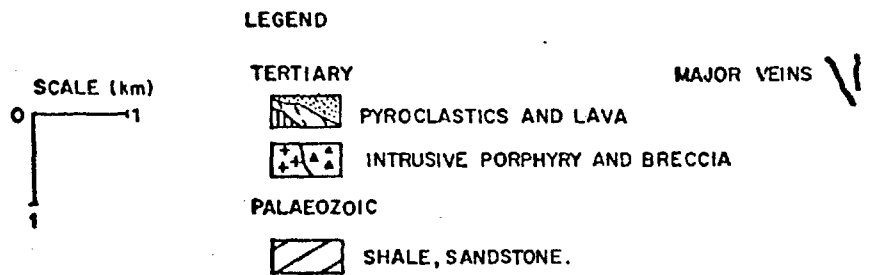
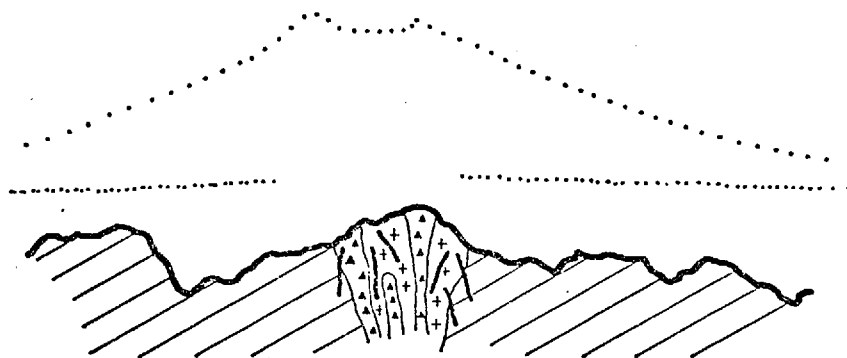
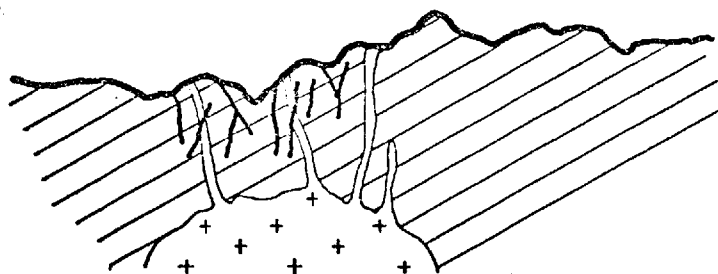


FIG.2.4. CONTINUED



C EXAMPLES - LLALLAGUA, SAN PABLO, ISCA-ISCA,



D EXAMPLES - COLQUIRI, HUANUNI, TASNA.

of hydrothermal alteration in the center, which may measure a kilometre or more in diameter. In other cases, such as Chorolque, Potosi and Oruro, volcanic rocks partly surround and are in contact with a central intrusive stock of porphyry, which apparently fills the vent from which the volcanics were erupted. Erosion has partly removed the overlying volcanic superstructure at these centers. The stocks are typically about one km in diameter at the surface, and conical in vertical section, narrowing with depth. The Cerro Rico stock at Potosi is an extreme example; it narrows downward to form two small dyke-like bodies in the deepest levels of the mine. The stock was emplaced at about the level of the regional erosion surface. The lower part cuts Palaeozoic sedimentary rocks while the upper part is in contact with unfolded Miocene lacustrine sediments, tuff and breccia (Fig. 2.10). Many of the other stock-like bodies were probably emplaced in a similar position, and their characteristic conical shape may be a result of rapid widening of the original vent where it passed upward from the relatively competent folded Palaeozoic sedimentary rocks into poorly consolidated pyroclastics. Most of the stock-like bodies are made up partly or largely of breccia, both igneous and hydrothermal. The original textures and composition of the igneous rocks are commonly obscured by intense pervasive hydrothermal alteration, but where unaltered rock is preserved it is usually a quartz-lattice porphyry. In some cases, for example Llallagua, San Pablo, and Isca-Isca, erosion has completely removed any volcanic superstructure which may have been present, leaving a stock of porphyry and breccia in contact with the older sedimentary rocks (Fig. 2.4).

The Salvadora stock at Llallagua is the most important of these, it contains what has been the most productive of the Bolivian tin deposits. The stock is about one kilometre in diameter at the surface and narrows with depth. The surrounding rocks are Palaeozoic shales and sandstone. The stock is made up of xenolithic and brecciated porphyry. There appear to have been several pulses of porphyry intrusion, and these were followed by explosive hydrothermal brecciation which is an outstanding feature of this and some of the other stocks. A more detailed description of the breccias is given below.

There are a number of localities where only dykes of altered quartz-porphyry are found, cutting the Palaeozoic sedimentary rocks, and without any larger igneous body exposed nearby. Some important mineral deposits are found in this setting, including Huanuni, Tasna, Santa Fe and Morococala. These are probably cases where a larger stock failed to reach the surface before crystallizing completely. There is usually evidence, such as widespread thermal metamorphism or a very extensive vein system, for the existence of a larger igneous body at depth.

b) The Kari-Kari batholith.

This is a complex body of granodiorite porphyry, about 30 km in length, located near Potosi. It is the only relatively plutonic mass in the southern part of the tin belt, although it is undoubtedly a very high-level intrusive and is apparently in contact with its own extrusives in places. It probably owes its exposure to the localized uplift of a block of the Cordillera. It gives a Lower Miocene K-Ar age and, as



discussed in Chapter 5, it was apparently emplaced during a distinct earlier pulse of igneous activity to that which formed the nearby highly mineralized Cerro Rico stock. There are a number of minor tin and base-metal deposits associated with the Kari-Kari pluton.

c) Volcanic rocks not associated with the mineralized eruptive complexes.

These fall into two groups: The volcanics in the Potosi region, such as the Agua Dulce and Canteria formations, and the very extensive ignimbrite sheets of the Morococala and Los Frailes formations (Fig. 2.3). The former are mainly garnet and cordierite-bearing rhyolitic welded tuffs, although andesites are also reported (Turneure, 1960). They are spatially associated with the Kari-Kari batholith, and as discussed in Chapter 5, they have an identical K-Ar age. They are thus closely associated with the emplacement of the batholith and may be its extrusive equivalents. The younger ignimbrites are dacitic in composition. They were probably much more extensive originally, having been partly removed by erosion. At Santa Fe', the Morococala ignimbrite can be seen to unconformably overlie the mineralized vein systems.

### 2.1.2. The mineral deposits

#### A. The metallogenic province

The Eastern Cordillera in Bolivia contains a well-defined metallogenic province which is loosely referred to as the Bolivian tin belt, although large quantities of other metals are also produced including gold, antimony, tungsten, bismuth, copper, lead, zinc, and silver. The ores are epigenetic

hydrothermal, mainly of vein-type, but there is potentially important 'porphyry' tin mineralization as well. In some cases only tin is produced from individual deposits, in others mixed ores are mined.

The province extends from near the Peruvian border in the north, throughout the length of Bolivia, and terminates in northern Argentina (Fig. 2.1). Its western boundary is transitional with a province of tin-free epigenetic lead-zinc-silver-copper deposits which are associated with mainly andesitic igneous rocks in the Altiplano (Ahlfeld, 1967). To the east there are essentially no igneous rocks or mineralization in the eastern part of the Cordillera.

Most of the primary mineral deposits within the province are assumed to be genetically associated with Andean igneous activity, although in some cases there are no exposed igneous rocks in the vicinity of a deposit. In some cases these are vein-type deposits which are assumed to be related to a buried igneous body, but there are also a number of state-bound 'manto-type' deposits in Palaeozoic sedimentary rocks which, it has been suggested, may be fossil placers (Schneider and Lehmann, 1977).

Mineralization is associated both with the plutonic rocks of the northern part of the Cordillera and with the eruptive complexes and small high-level intrusives of the southern part. The age of mineralization thus ranges from Triassic to Upper Miocene. A detailed discussion of age as a factor in the metal zonation and distribution of deposit types is given in Chapter 5. The major features of metal zonation

within the province are as follows:

a) Tungsten occurs predominately in the north, particularly in the Cordillera Real and Quimsa Cruz. There is also gold mineralization associated with the northern plutons.

b) The most important tin deposits are in the central part of the province from the Cordillera Quimsa Cruz to Potosi.

c) The southern part of the province contains a predominance of antimony and lead-zinc deposits. Where tin deposits are present they are also rich in antimony, silver, and lead and zinc.

Superimposed on this regional zonation are more localised zonal patterns which vary in scale from the district-wide zonation of tin-tungsten and antimony around the individual batholiths of the Cordillera Real, to the zonation of metals within individual eruptive centers or veins. As discussed further in Chapter 5, it is probable that the broad regional zonation is partly a function of the regional depth of erosion, while the more localised zonal patterns reflect complex factors in the ore-forming environments around igneous centers, or within individual hydrothermal channelways.

#### B. The mineral deposits of the northern section

The deposits of the northern section are associated with the plutonic igneous rocks (Fig. 2.2). There is little information about the deposits in the Cordillera Apolobamba and Cordillera de Muncas, although both tungsten-tin and lead-zinc mineralization has been found in the latter. The deposits of the Cordillera Real, Quimsa Cruz and Santa Vera Cruz are relatively well known and have been described in some detail (Turneure and

Welker, 1947; Ahlfeld and Schneider-Scherbina, 1964). The Sorata and Yani batholiths are sparsely mineralized and the types of mineralization present are characteristic of a deeper level of formation than the deposits elsewhere in the region. There are some spodumene- and columbite-bearing pegmatites in the Yani batholith, and minor tin, tungsten and molybdenum-bearing veins and pegmatites in the metamorphosed sedimentary rocks near the contacts of both plutons. Farther out, at distances of up to 10 or more km from exposed igneous rocks, there are veins with lead, antimony, and gold mineralization. This zonation of lead and antimony around the batholiths, at considerable distance from the contact, is characteristic of the northern part of the tin belt.

In the remainder of the Cordillera Real there are both tin and tungsten vein deposits within, or close to the contacts of the batholiths. These deposits are very numerous, but with one or two exceptions such as the Milluni and Chojlla mines, they are small. At Milluni the major vein is 1600 m long and 2 m wide. It cuts shales and arenites at a distance of over 4000 m from the nearest granodiorite contact exposed at the surface (part of the Zongo batholith). The mineralization consists of pyrite, fine grained cassiterite, sphalerite, chalcopyrite, and arsenopyrite. Other veins in this region, closer to the intrusive contacts or within the plutons, generally consist of pearly quartz, cassiterite, wolframite and tourmaline, with later chlorite, siderite and sulphides, and the wall-rocks are tourmalinized and chloritized. They are in many respects similar to the tin veins of Cornwall.

At Chojlla the wolframite bearing veins are associated with tongues of greisenized micropegmatitic granite which intruded hornfels and quartzite near the contact of the Mururata-Taquesi batholith. The numerous veins are arranged en-echelon in a zone approximately 300 m long, and have been exploited over a vertical extent of 400 m. They are typically about one m wide, and have a complex mineralogy, dominantly quartz, wolframite, tourmaline and arsenopyrite. In the deep levels the veins were invaded by cassiterite-bearing micropegmatite during the early hydrothermal stage; this was followed throughout the system by a later polymetallic stage of Sn, Bi, Zn, Pb, and Ag mineralization (Ahlfeld and Schneider-Scherbina, 1964).

The Cordillera Quimsa Cruz is the most highly mineralized district of the northern section of the province, with a large number of small deposits scattered round the contacts of the pluton. It also contains the two most important tin deposits of the section, Viloco and Caracoles. The latter is one of the largest and most profitable of the Bolivian tin mines. It is a very extensive complex vein system within a lobe of the Quimsa Cruz granite-granodiorite pluton. The veins contain quartz, cassiterite, sphalerite, chalcopyrite and arsenopyrite with some late carbonates. The wall-rocks are chloritized and kaolinized. The mineral assemblage and wall-rock alteration suggests a moderate temperature of ore deposition, in contrast to Viloco where the veins contain mainly quartz and cassiterite with depositional temperatures of over 400°C (measured from fluid inclusions by Kelly and Turneure, 1970). The Viloco

veins are in hornfelsed shales and sandstones close to the granite contact, and some of the largest of them have been mined over a vertical interval of more than 500 m and a length of 1600 m. Tungsten mineralization is also present around the margins of the Quimsa Cruz batholith, but it is only of minor importance. There does not appear to be a consistent zonal relationship between tin and tungsten with respect to the contacts of the pluton (Turneure and Welker, 1947). There are some small tin vein deposits associated with the granodiorite stock in the Cordillera Santa Vera Cruz, the southernmost pluton of the northern section of the tin belt. They are similar in character to the deposits of the Quimsa Cruz though none are of economic importance.

#### C. The mineral deposits of the southern section

In this section of the tin belt the deposits are mainly associated with the Andean sub-volcanic eruptive complexes which occur scattered down the length of the Cordillera from Oruro southward (Fig. 2.3). Most of the major tin deposits of Bolivia are in this section. Some of the eruptive complexes contain important deposits of silver and lead-zinc with only minor tin (e.g., Colquechaca and Tatasi), and Tasna is a major bismuth producer. There are also a large number of small lead-zinc and antimony deposits in the Palaeozoic rocks which show no obvious relationship to igneous rocks. However, the presence of granodiorite and lamprophyre dykes in the general area where these veins occur suggests that this mineralization is also related to Andean igneous activity. These, and the minor tin and base-metal veins associated with the Kari-Kari pluton, will

not be discussed further.

On the basis of their major metal associations the important deposits can be subdivided into three groups; tin, tin-silver, and tin-zinc (Turneure, 1971). A more fundamental subdivision can be made on the basis of their geological setting, as outlined in section 2.2.1 and Fig. 2.4. This emphasises the relationship between the mineralogy and metal content of the vein ores, and the geological setting in which they occur. Four general types can be recognized.

a) Deposits in essentially volcanic complexes where no intrusive rocks are present: the mineralization is in veins which cut a broad zone of pervasive hydrothermal alteration in the volcanics, and in some cases extend downward into the underlying sedimentary rocks. The ores are sulphide-rich and carry important amounts of silver, lead and zinc, in addition to tin, which may only be present in minor amounts. Disseminated mineralization is not well developed in the zone of alteration. Included in this type are the deposits at Colquechaca, Chocaya, and Tatasi.

b) Deposits in volcanic-intrusive complexes in which erosion has partly removed the volcanic superstructure and exposed the intrusive rocks in the vent: the veins are usually within the intrusive 'stock' but may extend outward into the surrounding volcanic and sedimentary rocks. The vein ores are of predominantly quartz-cassiterite type though with a greater or lesser amount of paragenetically younger sulphides, which may include silver mineralization. In most cases there is widespread disseminated and veinlet sulphide and cassiterite

mineralization in addition to the vein ores. Included in this type are Chorolque (tin only), and Potosi and Oruro which are two of the most important of the tin-silver deposits.

c) Deposits associated with an intrusive stock of porphyry and breccia with no extrusive rocks present: these include Llallagua, the San Pablo stock, and Isca-Isca. The veins are either mainly in the altered stock, as at Llallagua, or mainly external to it, as in the other two cases. The vein mineralization consists of an early quartz-cassiterite stage (with some wolframite at Llallagua and Isca-Isca) followed by sulphide mineralization, predominantly iron sulphides. Tin is generally the only metal present in economic amounts. Disseminated cassiterite and sulphides may be widespread in the altered igneous rocks and in some cases approaches economic grades. Some of the deposits of this type, and the type described in b) above, have been termed 'porphyry tin' deposits (Sillitoe et al., 1975).

d) Deposits in the Palaeozoic sedimentary rocks at which there are no igneous rocks at all, or only minor dykes: these include Colquiri, Huanuni, Santa Fe and Morococala, and Tasna. The type of mineralization in the veins is quite varied. Colquiri has a fluorite -sulphide- cassiterite mineralization rich in sphalerite; at Huanuni only tin is produced from predominantly quartz-cassiterite vein systems; Santa Fe and Morococala are sulphide-cassiterite vein systems in which most of the sulphide is pyrite and only tin is produced; Tasna is sulphide mineralization rich in bismuth and copper with a little tin. In most of these deposits the veins occur within



a wide area of altered and hornfelsed sedimentary rocks; this, together with the presence of dykes and hydrothermal breccia bodies, suggests that there is a larger igneous mass at no great depth.

The distinction between these deposit types rests on the level in the crust at which they formed. The first three types can be considered to represent progressively deeper erosion of sub-volcanic eruptive complexes, although there is no direct evidence that the isolated stocks, such as San Pablo and the Salvadora at Llallagua, ever had a volcanic superstructure. The last type are almost certainly genetically related to high-level plutons which did not reach the surface. This does not imply that any one mineralized system is vertically zoned through the full range of mineralization types, although several do show pronounced vertical zoning (e.g., Potosi) from base-metal and silver sulphide-rich mineralization in the upper parts of the vein system, to quartz-cassiterite in the lower parts. In most cases the vertical range of economic mineralization is relatively limited, and the mineralogical differences between the deposit types reflect differences in the level at which the deposits were formed. Lateral zoning of the mineralization is also pronounced in some cases, and this is discussed further in section 2.3.

## 2.2. Detailed Studies of the Geology and Mineralization of

### Selected Deposits

#### 2.2.1. Introduction

The general geology of many of the sub-volcanic deposits has been described previously. Among the most important of these

are descriptions of Oruro (Campbell, 1942; Chace, 1948; Koslowski and Jaskolski, 1932; Lindgren and Abbott, 1931; Turneure, 1960); Llallagua (Gordon, 1944; Samoyloff, 1934; Turneure, 1935); and Potosi (Evans, 1940; Jaskolski, 1933; Lindgren and Crevelling, 1928; Turneure, 1960). These descriptions have been concerned primarily with the structure and mineralogy of the vein systems, although Turneure (1935, 1960) discussed other aspects, including rock alteration and brecciation, in some detail. Although the mineralization has long been recognized as being typical, indeed providing a 'type example' of ore deposition associated with shallow magmatic activity (Buddington, 1935; Lindgren, 1933; Park and McDairmaid, 1964) little detailed modern work has been done. Considering the economic importance of the deposits their geology is rather poorly known. This is largely due to their geographical and political inaccessibility.

In this section I shall describe the major geological features, and the results of petrographic and geochemical studies of some of the important mineralized eruptive complexes. Except where referred to as having been described by previous workers the observations and interpretations are my own. This is not intended to be an exhaustive description of all aspects of the geology of the deposits, but rather to provide sufficient information, when combined with the fluid inclusion data, on which to base a coherent model of the evolution of the ore-forming systems. The emphasis is on studies of the Chorolque deposit as there is very little previous information about it, and because it has provided some of the most important information gained in this study.

### 2.2.2. Chorolque

#### A. Regional setting

The Chorolque deposit is located in the southernmost part of the tin belt at  $20^{\circ}55'$  south,  $66^{\circ}03'$  west, near the town of Atocha which is on the Bolivia-Argentina railway (Fig. 2.3). Although it is the oldest of all the operating tin mines of Bolivia (production started in 1870), there is no published information on the geology of the deposit apart from an early note by Roberts (1901) and a very brief description by Ahlfeld and Schneider-Scherbina (1964) and my own description in Sillitoe et al., (1975). The deposit produces tin alone, though in the past there has been a very small production of tungsten, bismuth, and lead-zinc ore from small peripheral veins.

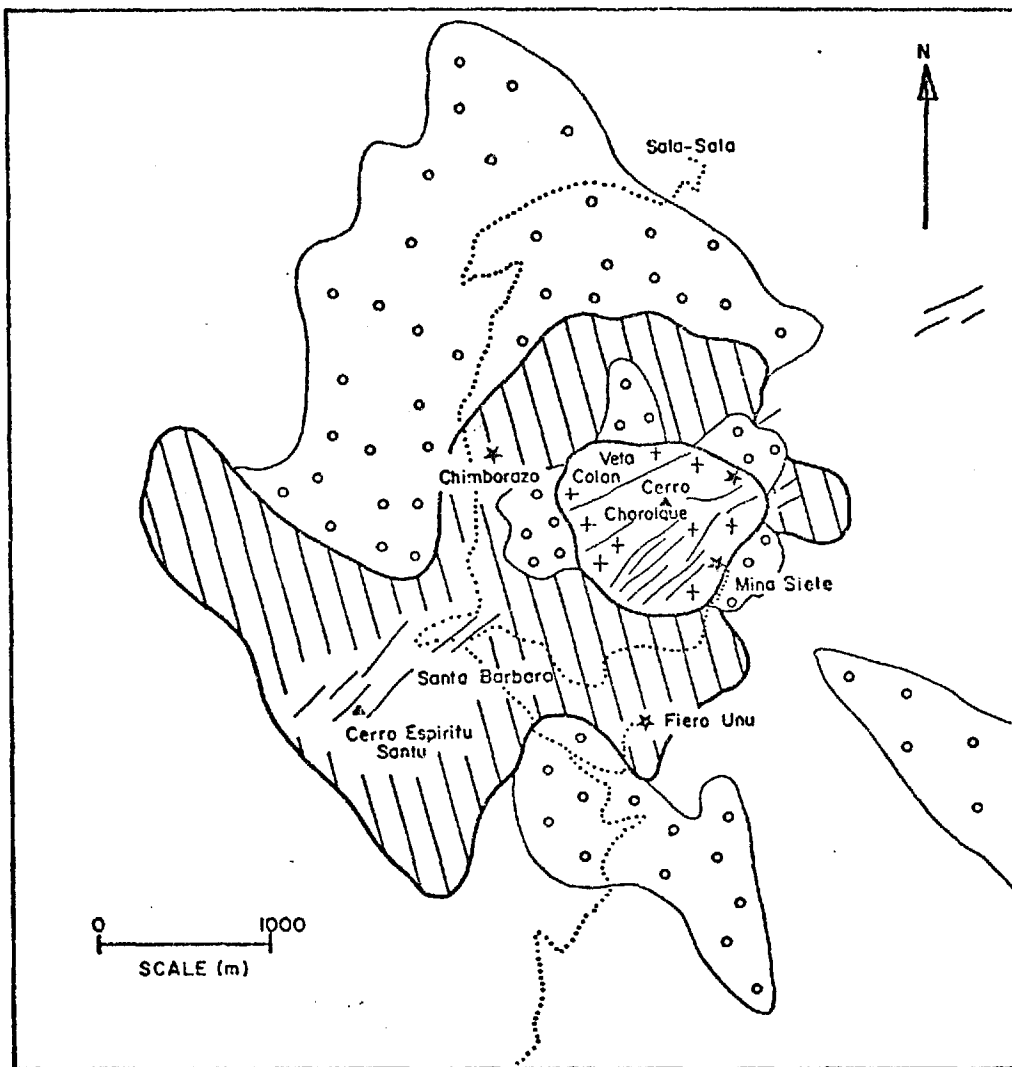
The district is underlain by folded Ordovician shales which were eroded to a relatively flat surface before the beginning of Andean igneous activity, and later elevated to form a high plateau with a present altitude of about 4000 m. Andean eruptive complexes rest on this surface, and they and the Palaeozoic basement rocks have been deeply incised by river valleys. Chorolque is one of a group of six mineralized complexes which occur in this district. Four of these lie on a northwest-southeast line (Ubina, Tasna, Chorolque, Isca-Isca) which is probably related to a deep structural feature. They show some common characteristics in that they are relatively deeply eroded compared with the other two complexes, and have a tin-tungsten-bismuth mineral association. The other two (Chocaya and Tatasi) are relatively weakly eroded volcanic

complexes and their mineralization is a sulphide assemblage rich in silver and lead-zinc with subordinate tin. It seems probable that these two groups of deposits are separated by a major northwest-southeast trending fault along which the northeastern block, containing the more deeply eroded complexes, has been elevated relative to the southwestern block.







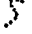
#### B. Rock types

The Chorolque complex consists of a central vent occupied by a mass of porphyry and breccia. It is partly surrounded at the surface by acid pyroclastics and lavas, while beneath these it cuts the Palaeozoic sedimentary rocks. The vent is roughly circular, and about one km in diameter at the surface (Fig. 2.5). It seems to narrow with depth, although its sub-surface shape is poorly defined. It is filled with hard altered rocks which form a very steep triangular peak whose summit is about 5600 m above sea level, and about 1600 m above the unconformity between the Palaeozoic sedimentary rocks and the volcanics flanking the vent (Plate 1). The flanks of the mountain have been deeply eroded by glacial action which produced cirques in which the extrusive igneous rocks have been completely removed, exposing the contact between the vent and the sedimentary rocks. On the ridges between the cirques, the extrusives have been partly preserved, resting unconformably on the underlying Palaeozoic (Fig. 2.6). Surface exposure of the rocks of the vent is excellent, but much of the contact region and the flanking extrusives are covered by moraine. The mine workings are all taking place within the vent at present. There are four main entrance adits at different levels. Two of these enter directly

FIG.2.5. CHOROLQUE, GENERAL GEOLOGY.



**LEGEND**

- |   |                                |
|---|--------------------------------|
| <b>TERTIARY</b>   |                                |
|    | Acid Lavas and Pyroclastics    |
|    | Intrusive Porphyry and breccia |
|    | Main Vein Structures           |
|    | Quaternary Moraine             |
|    | Palaeozoic Sedimentary Rocks   |
|    | Mine Entrance                  |
|  | Road                           |

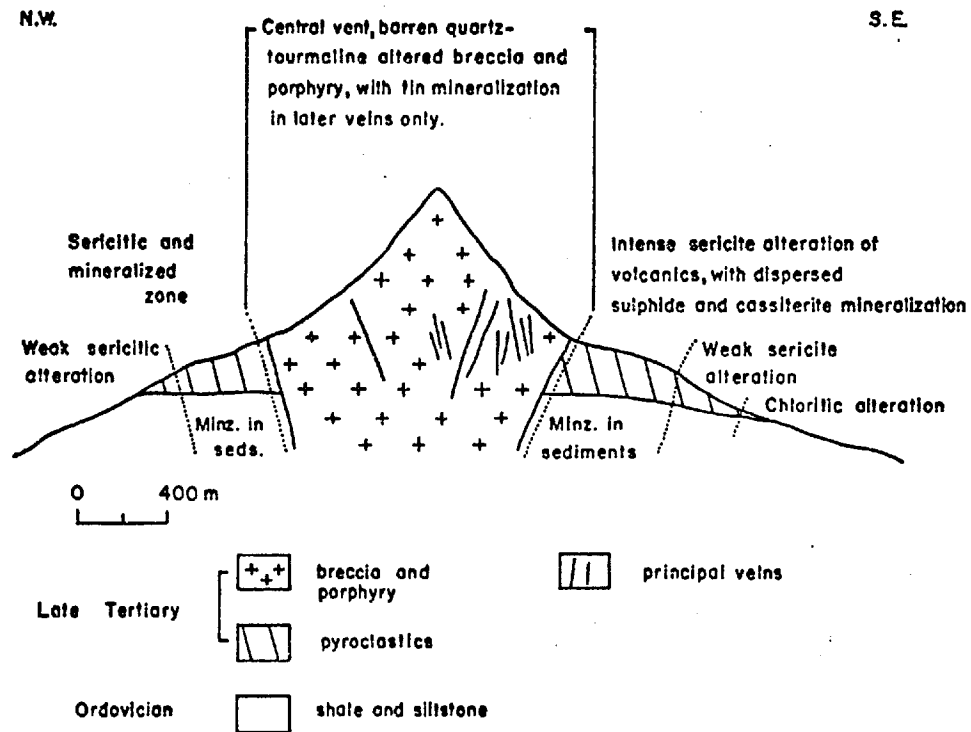


FIG.26. CHOROLQUE, GEOLOGICAL CROSS-SECTION

into the vent rocks; one (the Fiero Unu adit) traverses Palaeozoic sediments underlying the extrusives before entering the vent rocks, while the fourth (Chimborazo adit) traverses extrusive igneous rocks above the unconformity before entering the vent rocks. The Fiero Unu and Chimborazo adits provide excellent continuous exposure of the rocks flanking the vent, and of the contact region itself. Inside the vent there are very extensive mine workings which provide good exposure.

All of the igneous rocks of the complex are altered to a greater or lesser degree. In the case of the rocks filling the vent, their original texture and composition is almost completely obscured. The flanking extrusives have in general retained their primary macro-textures although they have undergone some degree of mineralogical alteration throughout their extent. The alteration is discussed in detail in section 2.3.2.C below.

The extrusives are quartz-porphyrries; they were originally composed of quartz, feldspar, and biotite phenocrysts, in a very fine-grained altered matrix. Lithic fragments, including sedimentary rock, are common. The phenocrysts (especially quartz) are broken into angular fragments. The micro-textures of the matrix are obscured by alteration and weathering, making the distinction between pyroclastics and lavas difficult, but a pyroclastic origin is favoured because of the fragmental textures, uniformity of rock type, and the apparent absence of internal contacts within the extrusive part of the complex. A typical example of relatively unaltered rock is shown in Plate 2A. The approximate mineralogical composition is as follows:

- Quartz phenocrysts, 20%. Broken angular fragments up to 8 mm across.
- Feldspar phenocrysts, 30%. Mainly K-feldspar (sanidine), partly altered and weathered to clay-quartz intergrowth. Some completely altered grains show ghost zoning indicating former plagioclase. Subhedral grains up to 5 mm.
- Biotite phenocrysts, 10%. Lath-shaped pseudomorphs up to 5 mm long. Completely replaced by chlorite, rutile, and opaques.
- Matrix, 40%. Very fine-grained to glassy, dark, cloudy, rich in clay and stained with Fe oxides.
- Accessories Apatite, zircon, occasional cordierite and garnet.

These rocks can be classified as ~~quartz-latites~~, based on the American Geological Institute descriptive classification of igneous rocks.

The rock that fills the central vent is mainly hard, massive, intensely altered breccia. It is composed of angular to subrounded fragments of black or dark grey fine-grained rock, in a pale grey, fine-grained matrix (Plate 2). The fragments range in size from tens of centimetres across down to a few millimetres. They were apparently mainly igneous rock, and they contain large quartz grains, probably relict phenocrysts, set in a matrix of finely intergrown tourmaline and quartz.



Fragments of altered sedimentary rock are also present. The matrix of the breccia is composed of a fine-grained intergrowth of quartz and tourmaline. Relict fine altered rock fragments can often be seen, and there are commonly relict quartz phenocrysts. It is not clear whether the breccia was originally of igneous or explosive hydrothermal origin. Relict igneous quartz phenocrysts are common in the matrix of hydrothermal breccias in some of the other Bolivian deposits, so their presence can not be taken as diagnostic of an originally magmatic breccia matrix. There are, however, parts of the vent which are composed of intensely altered quartz-porphyry with no breccia textures.

The contact between the vent and the surrounding sedimentary rocks is sharp, but the contact with the extrusives is indistinct. It may be a gradational contact which has been further obscured by intense alteration. A few narrow pebble-dykes have been found in the volcanics and sediments around the vent. They are composed of rounded fragments of altered igneous and sedimentary rocks in an altered, clay-rich matrix.

The sedimentary rocks which surround and underlie the complex are shales and siltstones. They are strongly tourmalinized and silicified close to the vent. Elsewhere they have a well-developed cleavage but are otherwise unmetamorphosed.

### C. Alteration types

The hydrothermal alteration which has affected the igneous rocks at Chorolque can be divided into four main types on the basis of the predominant secondary silicate minerals which have been developed. They are gradational with each other, and their

zonal relationships are discussed in section 2.3.2.D. below.

a) Quartz-tourmaline alteration

The rocks that fill the vent are completely altered to a quartz-tourmaline assemblage throughout their entire exposure. The only other minerals which are everywhere present are rutile and accessory zircon. Occasional grains of altered cordierite have been found, and in places there are sulphides and cassiterite (Plate 3).

The proportions of quartz and tourmaline vary somewhat. The darker rocks and breccia fragments are tourmaline-rich relative to the lighter material. In places the rock is almost completely flooded with secondary quartz with little tourmaline, but in general the grain size and textures of the quartz-tourmaline rock vary little except close to the contact with the extrusives. Here there is a gradual decrease in grain size of the secondary quartz-tourmaline intergrowth, the amount of secondary quartz decreases, and the original porphyritic texture of the rock becomes more apparent. The precise position of the contact is impossible to determine. The contact with the sedimentary rocks is sharp, although the intense quartz-tourmaline alteration extends outwards into the sediments for a few tens of metres. No vertical change in the texture or composition of the vent rock is evident although it is exposed over a vertical interval of 2000 m. Its overall uniformity and intensity of alteration is remarkable. The quartz in these rocks occurs in the following forms:

i) Relict igneous phenocrysts. These are usually recognizable even in the most intensely altered rocks. Their shape is outlined

by a zone rich in fluid and solid inclusions which separates them from the surrounding overgrowth of secondary quartz (Plate 3A).

ii) Overgrowths of secondary quartz surrounding phenocrysts. The extent of the secondary overgrowth depends on the intensity of alteration.

iii) Granular intergrowth of anhedral quartz, or intergrown quartz and tourmaline. Where the alteration is intense, i.e., throughout most of the vent, the quartz is relatively coarse-grained and in places has coalesced into large 'lakes'. In the transition zone with the extrusives, the granular quartz is much finer grained, and there is little or no secondary overgrowth in the phenocrysts.

The tourmaline is black in hand specimen, in thin-section it is green to brown and strongly pleochroic, suggesting a schorl composition. It is scattered through the rocks as lath-shaped grains, radiating sprays, or forms a dense intergrowth (Plate 3B). As with quartz, its grain-size varies with the intensity of alteration. Rutile is also common; its distribution is patchy, and clusters and aggregates of grains probably mark former biotite phenocryst sites. In some areas there are also patches of very clear, coarse grained, inclusion-free quartz, intergrown with very fine tourmaline needles. Sulphides are commonly associated with this, and it is probably a later stage of quartz-tourmaline growth which filled open spaces in the altered breccia. The tourmaline in this material is much paler in colour, sometimes almost colourless and non-pleochroic, suggesting a more dravitic composition. Tourmaline alteration extends outward into the sedimentary rocks surrounding the vent.

The amount of introduced quartz seems to be small and is limited to veins and veinlets, but tourmalinization is intense close to the vent, where the rocks are converted to a dense black hornfels.

b) Sericitic alteration

The characteristic mineral of this assemblage is fine-grained white mica (sericite), but secondary tourmaline and minor secondary quartz are almost always present as well. This type of alteration is found in the extrusive rocks surrounding the vent, but not within the vent itself, or in the sedimentary rocks. Where fully developed, it has resulted in the complete conversion of the rocks to an assemblage of quartz (in part residual, in part secondary), sericite, and tourmaline, with accessory rutile, sulphides, zircon and apatite (Plate 3A). Even where mineralogical alteration is complete, the primary porphyritic texture of the rock is partly preserved. Feldspar phenocryst sites are distinguishable as masses of almost pure sericite with a little intergrown quartz and in some cases tourmaline. Biotite phenocrysts are pseudomorphed by sericite and/or tourmaline with much rutile and opaques. The matrix is generally a fine sericite-quartz intergrowth, often with scattered larger tourmaline grains. The relative proportions of tourmaline and sericite are variable and zoned with respect to the vent contact (see below). Of the feldspars, plagioclase was most susceptible to alteration and is usually completely replaced, but unaltered relicts of sanidine are common in the outer part of the sericitic zone. The sericite in these rocks gives sharp muscovite X-ray diffraction peaks. The tourmaline is pale and

weakly or non-pleochroic, suggesting a dravitic composition. The sedimentary rocks underlying the volcanics show little evidence of secondary sericitization.

c) Chloritic alteration

Chloritic alteration affects all of the extrusive rocks beyond the limits of sericitic alteration. It is characterized by the replacement of biotite by chlorite plus rutile. There are no underground exposures of these rocks; surface samples show argillization of the feldspars and matrix, but this is probably a supergene effect. A propylitic alteration assemblage with epidote, albite and carbonate was not developed.

d) Argillic alteration

Argillic alteration of probable hypogene origin is generally not well developed at Chorolque. However, in the Chimborazo adit, there is an extensive zone in the contact region between the vent and the extrusives where the rocks are strongly argillized. They contain much tourmaline as a replacement of biotite and feldspar phenocrysts, some sericite, and much sulphide. The argillization appears to have been superimposed on earlier tourmalinization, and consists of replacement by clay minerals of previously unaltered feldspar phenocrysts and fine-grained rock matrix. It is not clear whether the argillization accompanied the sulphide mineralization, or if the sulphides remained stable during a late-stage argillization of an earlier sericite-tourmaline-sulphide assemblage. The former case seems more probable. Hypogene argillic alteration is also found in the outer parts of the alteration envelopes adjacent to some of the mineralized veins which cut the extrusive

rocks distant from the vent.

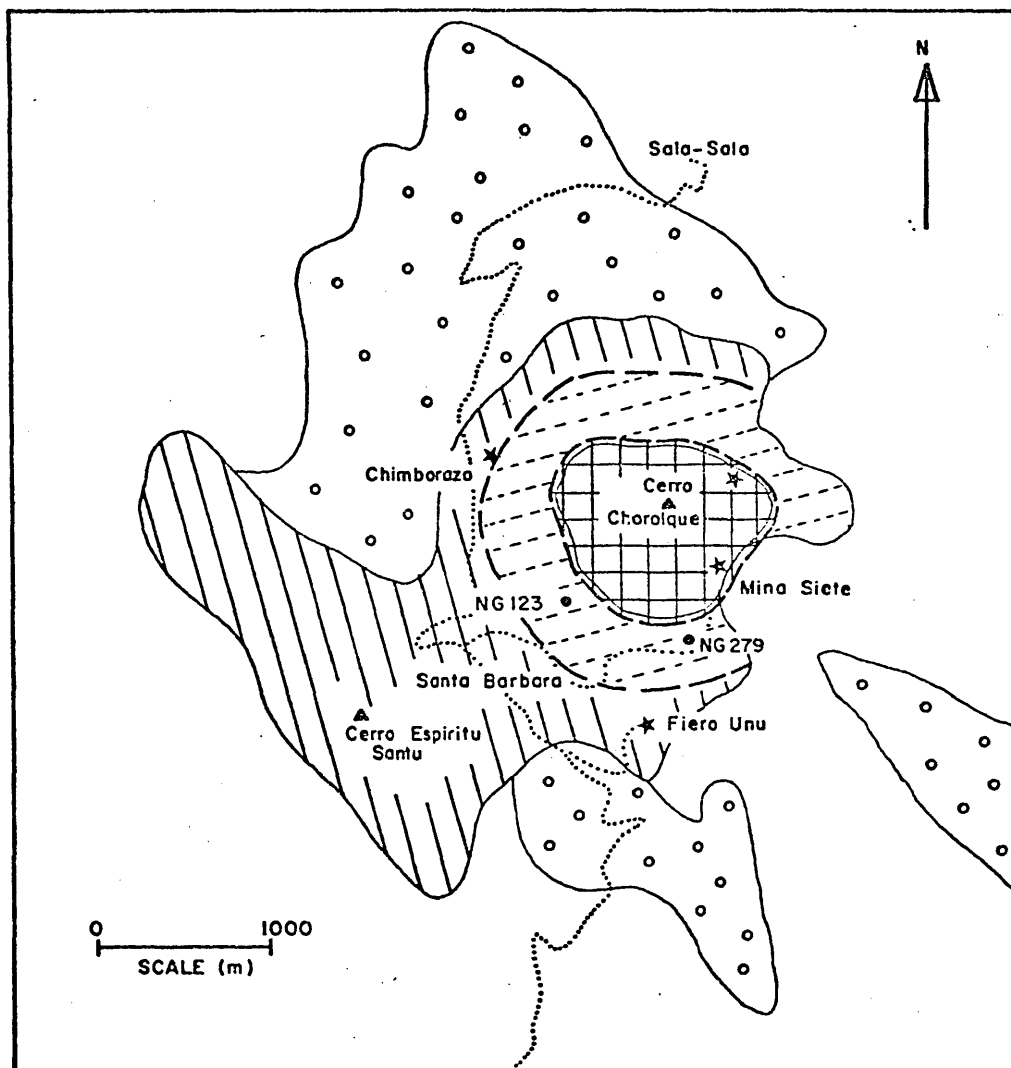
#### D. Alteration zoning

Chorolque has a particularly well-developed lateral zonation of hypogene alteration types. The general zonal pattern is shown in Figs. 2.6 and 2.7. The central vent has undergone intense quartz-tourmaline alteration throughout its entire exposed vertical and horizontal extent. In the surrounding extrusives there is an annular zone of sericitic alteration. At the surface the sericitic zone is best developed over a distance of about 400 m outward from the vent margins. The alteration-zone contacts are transitional, with much tourmaline associated with sericitization near the vent but decreasing outward. Beyond about 400 m from the vent, the intensity of sericitization declines. Up to about 600 m the biotite phenocrysts are sericitized but alteration of feldspar progressively decreases. The transition to chloritic alteration is at about 600 m. Chlorite takes the place of sericite as the alteration product of biotite, and there is little or no hypogene alteration of feldspar beyond the sericitic zone.



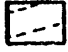





The zonal pattern is best developed in the igneous rocks (Fig. 2.7). In the sedimentary rocks there is very strong tourmalinization close to the vent. Farther out, tourmalinization is associated with sulphide veinlets for a distance of several hundred metres from the contact, but there is little sericitization.

As discussed below, most of the important mineralized veins are within the vent. They do not have distinct alteration envelopes in the quartz-tourmaline altered wall-rocks, although there was some introduction of a new generation of quartz and pale tourmaline. However, on the western side of the complex a

FIG. 2.7. CHOROLQUE, PLAN OF ALTERATION ZONES



## LEGEND

- |   |                                     |   |   |
|---|-------------------------------------|---|---|
|  | Quartz-Tourmaline Alteration Zone   |    | Moraine                                   |
|  | Zone of Strong Sericitic Alteration |    | Palaeozoic Sediments, Generally Unaltered |
|  | Weakly Chloritized Volcanics        |    | Mine Entrance                             |
|   |                                     |  | Road                                      |
|   |                                     |    | K/Ar SAMPLE LOCATION                      |

number of vein structures run outward from the vent, traversing first sericitized and then chloritized extrusives (Fig. 2.5). They have well-developed wall-rock alteration envelopes of several metres width. Where the veins traverse sericitized rocks, the largest of them has a quartz-tourmaline envelope. Where they traverse chloritized rocks they have sericitic and argillic alteration envelopes. These relationships suggest that the pervasive alteration preceded the development of the vein structures, and this is supported by fluid inclusion data which is reported in Chapter 3.

#### E. Mineralization and metal zoning

All production of tin at Chorolque at the present time comes from a system of veins within the quartz-tourmaline altered vent rocks. One or two veins extend beyond the vent into the surrounding extrusives, and there are a number of minor veins farther out, both in the extrusive and sedimentary rocks, which have produced a little tungsten, bismuth, and lead-zinc in the past (Ahlfeld and Schneider-Scherbina, 1964). A generalized plan of the vein system is shown in Fig. 2.5. Most of the veins strike roughly southwest-northeast. In vertical section the veins within the vent dip steeply toward the center. They are generally lodes, one m or less in width, made up of a series of narrow sub-parallel fractures which branch and incorporate slices of wall-rock. In some cases there is only a single major fracture. The vein filling is made up almost entirely of quartz, with volumetrically minor cassiterite. Sulphides are almost completely absent except at the extremities of the veins near the vent contacts. Veins outside the vent are, however, rich in sulphides. There



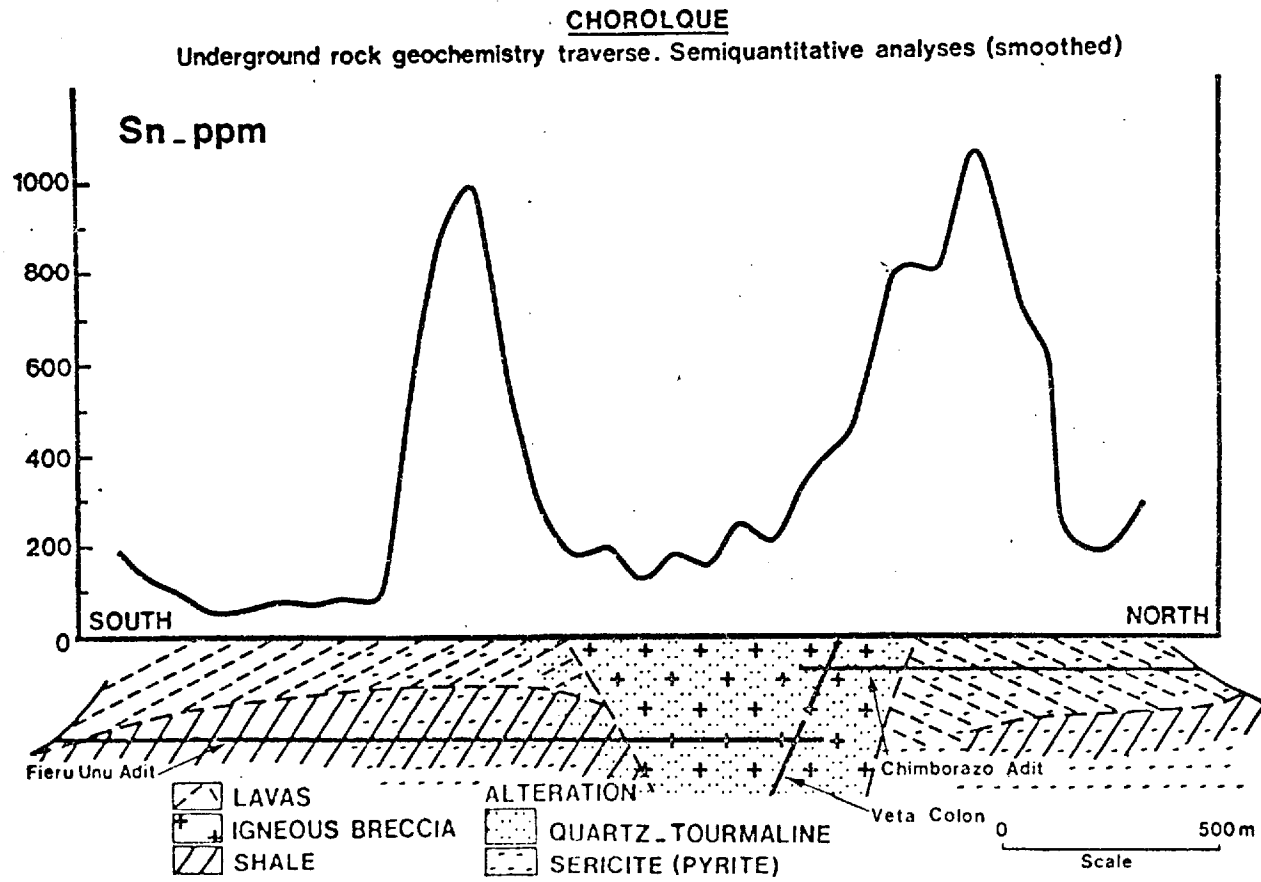
is generally a little late-stage kaolinite. The vein filling was deposited in open fractures, and the textures are commonly crustiform with open vugs remaining. In places there are spectacular drusy cavities lined with large quartz crystals. Cassiterite deposition was clearly late in the paragenetic sequence, and took place after most of the quartz had been deposited. It is black in colour, almost opaque, and very fine grained. A little wolframite is sometimes present, and gold had been reported. The major veins have been exploited over a vertical interval of about 800 m. Many of them do not outcrop, or at least do not contain economic concentrations of cassiterite at the surface. Their downward extension below the lowest mine workings has not been fully explored, but the tin content is reported to decrease, although the vein structures do continue, at least for a distance of 100 m or so. Thus, the main cassiterite-bearing interval of the structures straddles the level of the unconformity between the Palaeozoic sedimentary rocks and the extrusives. In addition to the major veins, there are many minor cassiterite-bearing quartz-filled fractures throughout the vent and some of these are being worked on a small scale almost to the summit of the Cerro, so that the total vertical range of known cassiterite deposition approaches 2000 m.

In the contact region of the vent, and in the surrounding rocks, there are numerous minor veins which contain sulphides. In addition there is strong veinlet and disseminated sulphide mineralization exposed in the sedimentary rocks in the Fiero Unu adit on the south side of the vent, in the altered extrusive rocks in the Chimborazo adit on the north side, and elsewhere at

the surface. Thus sulphide-rich mineralization, including mineralization unrelated to major vein structures, is present in an annular zone around the vent which corresponds roughly with the zone of sericitic alteration. The rocks of the vent itself are almost devoid of sulphides, either disseminated or vein-controlled.

In this study the rocks of the Fiero Unu and Chimborazo adits were systematically sampled by the writer, and the analytical results illustrate the particularly well-developed zonation of metal-sulphide mineralization around the vent. The samples were taken from the walls of the adits at 80 m intervals. Each sample comprises a number of small chips taken at random over an area of a few square metres, adding up to a total weight of 1 to 2 kilograms. The material sampled includes disseminated and veinlet mineralization only. There are no major vein structures in the areas sampled outside the vent, and the vein structures within the vent were deliberately not sampled. The distribution of metals revealed by the sampling is thus considered to be independent of the geometry of any of the major vein structures. The samples were prepared by routine crushing and grinding procedures, with semi-quantitative analysis on the Direct Reading Emission Spectrograph by staff of the Applied Geochemistry Research Group, Imperial College. The data (smoothed by 3-point moving average analysis) is presented in Fig. 2.8. It shows very clearly the way in which disseminated and veinlet mineralization is distributed in the rocks surrounding the vent, and that the quartz-tourmaline altered vent rocks are essentially barren, except where cut by

FIG.2.8A



**CHOROLQUE**

Underground rock geochemistry traverse. Semiquantitative analyses (smoothed)

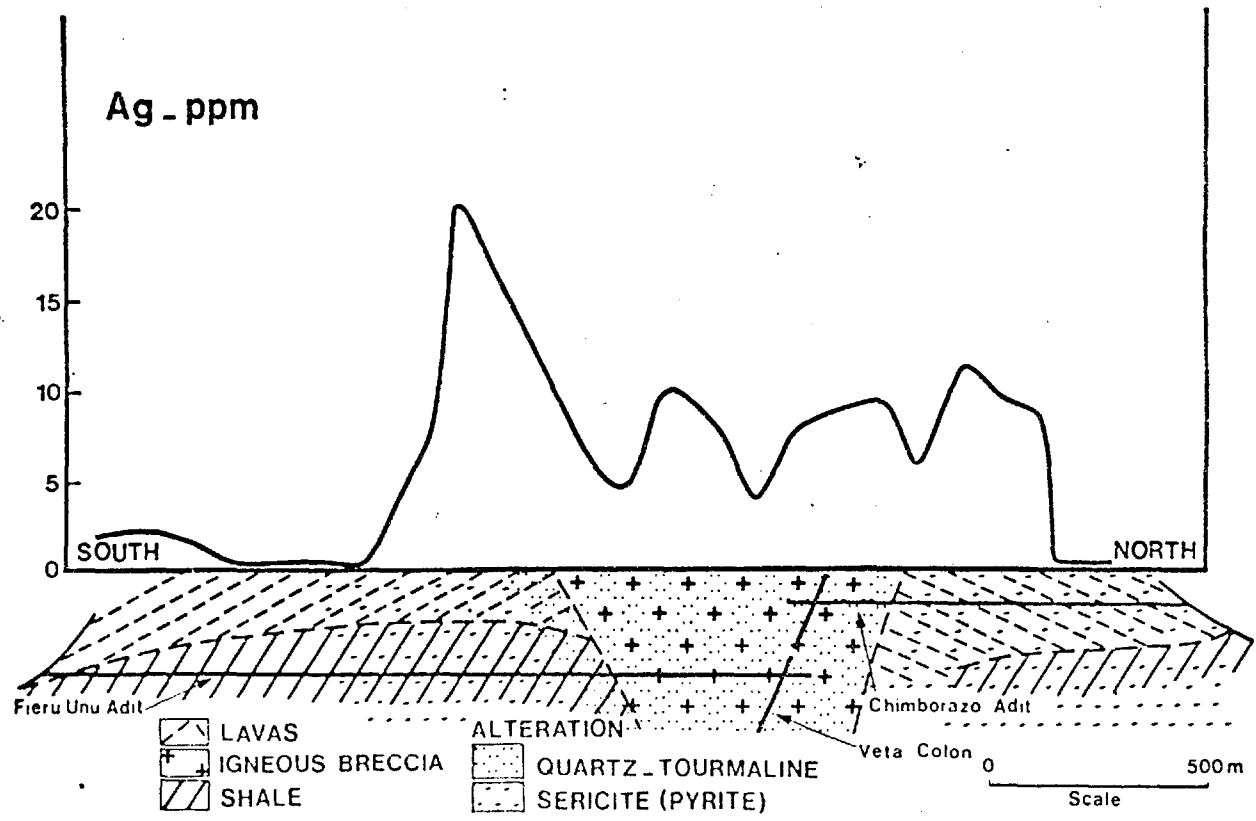


FIG.2.8B

**CHOROLQUE**

Underground rock geochemistry traverse. Semiquantitative analyses (smoothed)

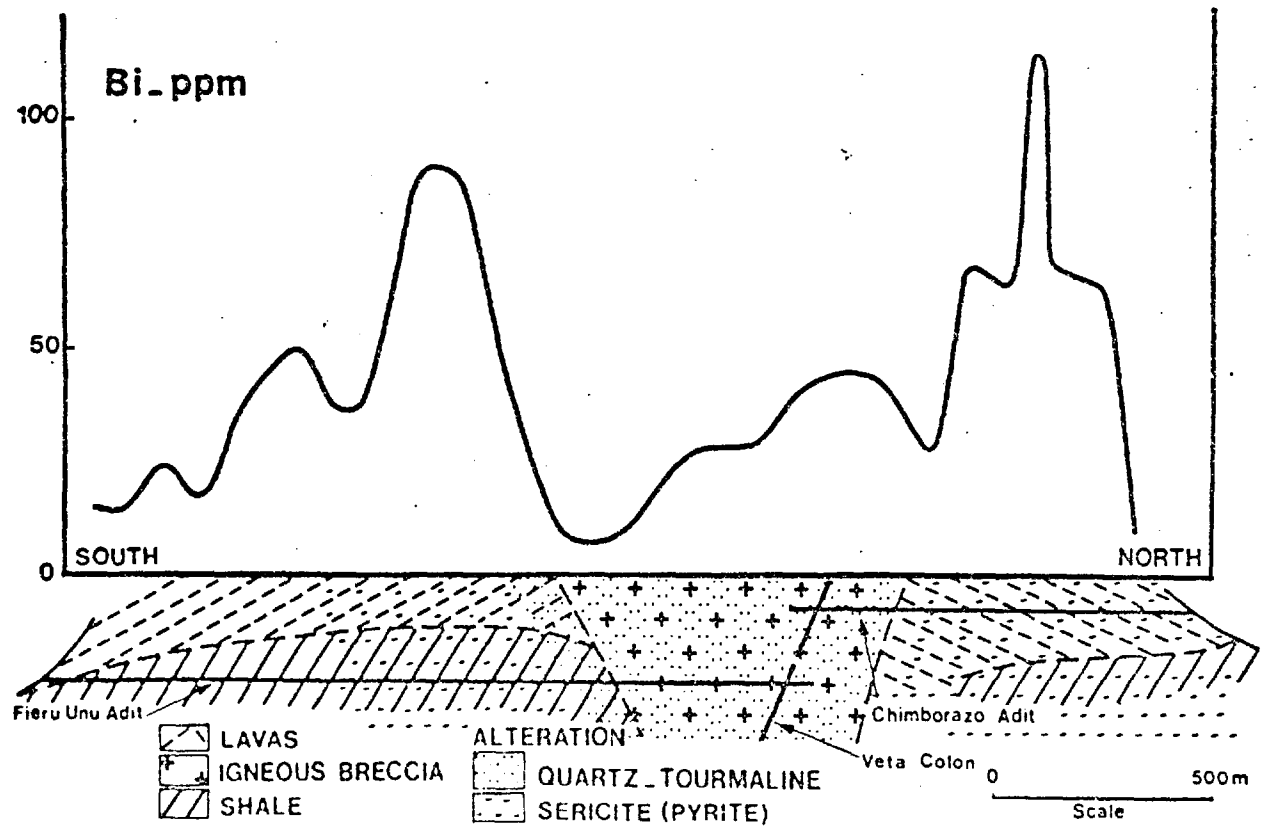


FIG.2.8C

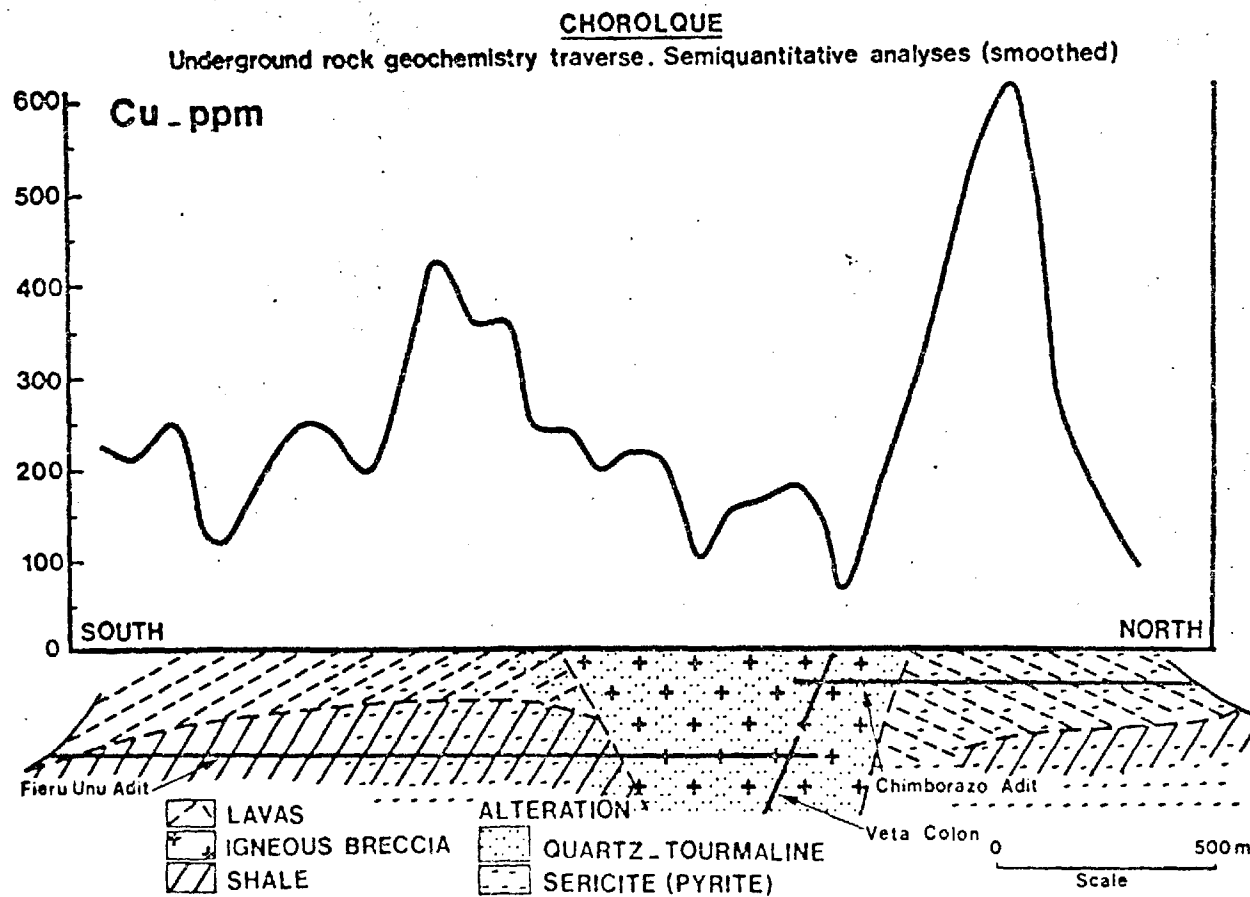


FIG.2.8D

the major vein structures. There was evidently little dispersion of tin within the wall-rocks adjacent to the major veins.

In the peripheral zone of sulphide mineralization, pyrite is the predominant mineral species present, especially in the outer part of the zone at distances of about 200 to 500 m from the vent contact. In the Fiero Unu adit, magnetite and hematite accompany the pyrite in veinlets, breccia zones, and disseminated in the sedimentary rocks beyond 500 m from the contact. Arsenopyrite, pyrrhotite and chalcopyrite increase towards the vent as do the geochemical values for tin, bismuth, lead, zinc and silver. Tin is present as both stannite and cassiterite. Close to the vent contact the metal values and total sulphide content decline sharply. In the Fiero Unu adit on the south side, the intensely tourmalinized rocks in the contact region and the quartz-tourmaline altered vent rocks themselves are virtually barren of sulphides, although in the northern contact region in the Chimborazo adit, the sulphide-rich zone in the extrusives does extend inward into relatively strongly tourmalinized rocks in the contact region.

Where disseminated pyrite is present in the vent rock it is accompanied by clear, inclusion-free quartz intergrown with fine tourmaline needles, similar to that found in the vein margins. This quartz is quite distinct from that of the quartz-tourmaline alteration assemblage, and it and the pyrite appear to have been deposited as later-stage infilling of open spaces in the previously altered vent rocks.

The distribution of mineralization outlined above suggests a distinctly bimodal time-sequence of mineral deposition at

Chorolque. The close association of sulphide mineralization and sericitic alteration in the zone peripheral to the vent suggests that they are contemporaneous. The gradational nature of the alteration inward into the quartz-tourmaline vent rock suggests further that the alteration of the vent, the alteration of the surrounding rocks, and the deposition of the veinlet and disseminated sulphide mineralization were all broadly contemporaneous, and that the absence of dispersed mineralization in the vent reflects unsuitable physico-chemical conditions for ore-mineral deposition in that region during the quartz-tourmaline alteration stage. The major quartz-cassiterite veins cut across this zoned pattern of alteration and mineralization, and thus appear to have begun forming at a somewhat later time when alteration was largely complete. This is born out by the fluid inclusion data which is discussed in Chapter 3. There is no significant relative zonation of metals in the early dispersed mineralization around the vent, and Cu, Sn, Bi, As, Ag, Pb and Zn were all deposited in very much the same region. There is, however, a distinct zonation in the later vein mineralization, with tin giving way outward to tungsten, then bismuth, then lead and zinc, progressively further from the vent.

### 2.2.3. Llallagua

#### A. Regional setting

The geology of the Llallagua deposit has been previously discussed by Turneure (1935) with additional information by Gordon (1944), Samoyloff (1934), Turneure (1960), Ahlfeld and Schneider-Scherbina (1964), and Sillitoe et al., (1975).

The deposit is located at the southern end of the Morococala



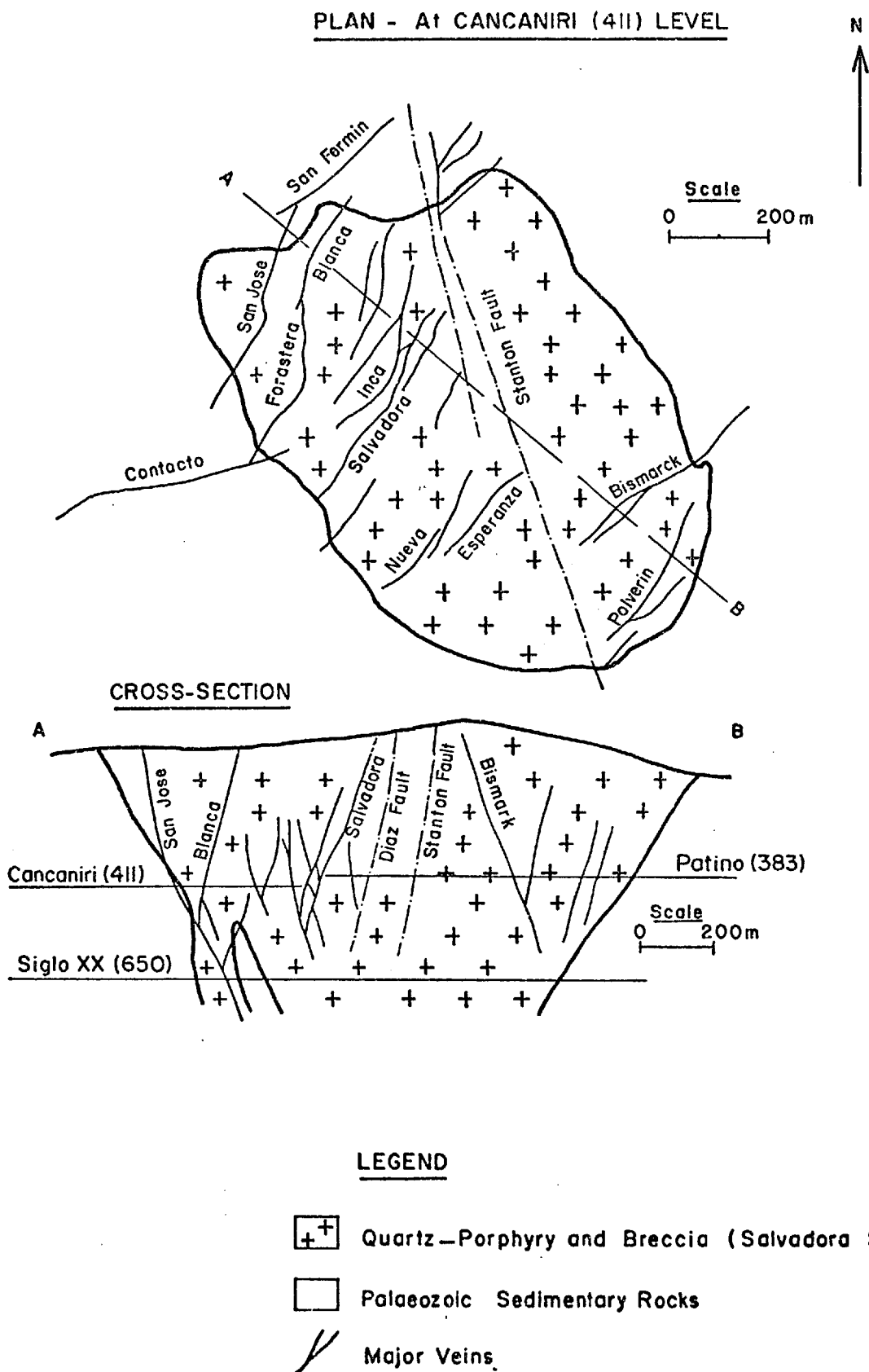
plateau (Fig. 2.3), which is an elevated block of Palaeozoic sedimentary rocks partly overlain by a sheet of ignimbrite. The Palaeozoic rocks are shales, greywacke and quartzite which are strongly folded on northwest-southeast axes. The Llallagua deposit is a complex system of veins, mineralized breccia, and disseminated mineralization within a small isolated porphyry stock (the Salvadora stock). It was intruded into the axis of an overturned anticline in the Silurian-Devonian sediments, and has previously been interpreted as a porphyry-filled volcanic vent from which the volcanic superstructure has been eroded away (Samoyloff, 1934; Turncaure, 1935, 1960). A previous potassium-argon age determination on the stock gave a date of 9.4 Ma (Evernden, 1961). However, the results of a more detailed geochronological study which make up part of this thesis are not consistent with that date, and a Lower Miocene age is preferred, as discussed in Chapter 5. The ignimbrite sheet which overlies much of the Morococala plateau to the north of Llallagua has given ages of 7.8 Ma (Evernden, 1961) and 6.1 Ma (this study) and it is clearly the product of a quite separate igneous event which took place after the region had been substantially eroded.

#### B. Rock types

The Salvadora stock is oval in plan, measuring 1730 by 1050 m at the surface, but it narrows with depth to measure about 1000 by 700 m in the lowest levels of the mine (700 m below surface, Fig. 2.9). The contact with the surrounding sedimentary rocks is sharp. There are a number of porphyry dykes, and also lobes of breccia, extending out into the sedimentary rocks.

# FIG.2.9. LLALLAGUA, THE SALVADORA STOCK

(After Turneure, 1935)



Although strong pervasive hydrothermal alteration has affected the stock almost throughout, the macrotextures of the rocks are relatively well-preserved. Several stages of porphyry intrusion are evident together with very widely developed igneous and hydrothermal breccia. In one or two places almost unaltered porphyry is exposed at the margins of the stock, both at the surface and in the underground workings. The major rock types which make up the stock can be broadly classified as follows; quartz-porphyry, macrocryst porphyry, feldspar porphyry, igneous breccia, hydrothermal breccia. The distinction between the porphyry types is based on texture; compositional variations are less marked.

a) Quartz-porphyry. This is the predominant rock type in the stock, and is easily recognised, even when intensely altered, by the numerous large quartz phenocrysts. There are one or two relatively unaltered underground exposures. A typical description is given below, and the rock can be classified as a quartz-lattice porphyry.

Quartz phenocrysts, 25%.	Rounded, embayed, 2 to 5 mm across.
Plagioclase phenocrysts, 25%.	Subhedral, 2 to 5 mm long, weakly zoned. Oligoclase-andesine composition. Incipient alteration to sericite.
K-feldspar phenocrysts, 20%.	Subhedral to anhedral, 2 to 5 mm long. Very small 2V indicates sanidine.
Biotite phenocrysts, 10%.	Laths, up to 5 mm.
Matrix, 30%	Very fine microcrystalline to almost isotropic glassy material.

Accessory apatite, zircon, cordierite.

Some more potassic varieties are common, in which plagioclase is very much subordinate to K-feldspar.

b) Macrocryst porphyry. This is a distinctive rock type in which the feldspar phenocrysts are very large, commonly 4 to 6 cm long. Quartz phenocrysts (2 to 10 mm) are numerous, K-feldspar seems to predominate over plagioclase, although in most areas the rock is severely altered and the feldspars are completely replaced by sericite, clay and in some cases tourmaline. The composition is probably similar to that of the quartz-porphyry.

c) Feldspar porphyry. This rock type can be distinguished by the scarcity of quartz phenocrysts. It is fine grained, and originally rich in fine (1 to 2 mm) feldspar phenocrysts, although no unaltered exposures have been seen.

d) Igneous breccia. Using the terminology previously applied to the breccias at Llallagua by Sillitoe et al., (1975), igneous breccia can be distinguished from hydrothermal breccia by the nature of the matrix. In hydrothermal breccia the matrix is clastic rock material, while igneous breccias are essentially igneous rocks crowded with xenoliths.

Igneous breccia is widespread in the Salvador stock, a variety of types and textures are present and are gradational with each other. In fact, almost all of the porphyry contains some xenoliths, and the term breccia is applied arbitrarily when the rock is noticeably crowded with them. Breccia composed of predominantly sedimentary fragments in a porphyry matrix is easily recognisable even when the rock is strongly altered. This is common in some areas near the contact of the stock. The matrix is quartz-porphyry, and the quartz phenocrysts are commonly

broken and angular. The fragments are mainly grey, fine-grained argillite, rounded or tabular in shape, and usually no more than a few centimetres across. They sometimes show a parallel alignment probably due to flow, and in some cases they show evidence of corrosion by the matrix. In most cases both sedimentary and igneous rock fragments are present, occasionally igneous fragments alone. In the latter case the breccia texture can be difficult to recognise where the rock has been strongly altered. Typical igneous breccia is illustrated in Plate 4.

e) Hydrothermal breccia. The extent and intensity of hydrothermal brecciation is one of the outstanding features of the Salvadora stock. Large parts of it are made up entirely of this type of breccia, while the remainder contains pipes and irregular masses, and is laced with a network of breccia dykes. They are all undoubtedly earlier than the main stage of fracturing and vein-formation, but there is evidence that some fracturing, alteration and mineralization preceded the brecciation. The hydrothermal breccias display a variety of textural and lithological characteristics, and these are gradational with each other so that a precise classification into distinct types is difficult to make. In a general way, three types can be recognized.

i) Silicified porphyry breccia

In this the fragments are all of the same igneous rock type. The breccia is generally patchy, with unbrecciated areas grading into partly brecciated rock in which the fragments have clearly not moved far, and then into 'channelways' where the fragments are rounded. The matrix is black, fine grained, and

crowded with small rock fragments and quartz grains (which appear to be residual phenocrysts) set in a fine tourmaline intergrowth. The rock fragments are quartz-porphyry, and are almost completely silicified, the tourmaline which cements the matrix penetrates the fractured igneous rock along cracks, and appears to have replaced the edges of the fragments; however, there is no tourmaline within the fragments, suggesting that the rock was silicified prior to brecciation (Plate 5).

ii) Polymict breccia

This is composed of both igneous and sedimentary rock fragments (Plate 6, 7A). They are usually well rounded, and the matrix, although highly altered, has a tuffaceous appearance and is apparently composed of fragmented igneous rock cemented by fine tourmaline (Plate 7B). It includes quartz phenocrysts, in some cases attached to relicts of the parent rock. There are also lath-shaped grains, now composed of fine-grained tourmaline and in some cases rutile, which are suggestive of former biotite and feldspar phenocrysts. In other cases the clastic material is wholly made up of angular to rounded quartz grains cemented by tourmaline (Plate 8A). This latter type can sometimes be seen cross-cutting the former, and there are also fragments of breccia in breccia, indicating a multistage origin. The rock fragments in these breccias are invariably altered. The igneous fragments are generally sericitized, often with disseminated pyrite or pyritic rims. This alteration appears to post-date the brecciation. In some areas silicified igneous fragments are present together with the sericitized ones, and here the silicification was presumably earlier than the brecciation. Late stage kaolinization of sericitized

igneous fragments has also taken place in some areas. In some of the breccia bodies the igneous rock fragments have been completely replaced by quartz and cassiterite resulting in economic ore mineralization, as discussed below. However, this has only taken place in certain specific breccia bodies.

### iii) Black dykes

Turneaure (1935) described the black dykes at Llallagua and recognized their clastic nature. They are narrow, branching bodies generally only 2 to 10 cm wide which penetrate throughout the stock. Their frequency varies from place to place, but they are generally present at intervals of only a few metres. They follow irregular courses rather than well defined planes. They are composed of fine clastic quartz grains cemented with tourmaline, and are clearly the same material as that which forms the matrix of some of the larger hydrothermal breccias (Plate 8B). This material seems to have been formed by the fragmentation, abrasion, and corrosion of igneous rock. A possible mechanism would be the mobilization of brecciated rock in a corrosive hydrothermal fluid, with further abrasion and corrosion during transport. In its most advanced state of development, only the quartz phenocrysts remain, and these would have been injected into fractures as a slurry with tourmaline crystallizing to form the cement.

### C. Alteration

The rock alteration at Llallagua, and the mineralization, have been described in some detail by Turneaure (1935). Silicification, tourmalinization, sericitization, and argillization were the predominant alteration processes. The stock is altered almost throughout, and the distribution of alteration types shows no

relationship to the geometry of the major veins. The alteration assemblages are similar to those described at Chorolque. Neither lateral nor vertical zoning are particularly well displayed. Early quartz-tourmaline alteration is poorly developed, though it is present in the deep levels of the mine. Its distribution is patchy, and it alternates with a tourmaline-sericite assemblage. The greater part of the stock is altered to a tourmaline-sericite assemblage in which the original textures of the rock are relatively well preserved. The proportions of tourmaline and sericite vary widely, but there is a distinct tendency for sericite to increase upward. Argillic alteration is common in some areas near the margins of the stock, and along some late fractures and faults; it is almost certainly hypogene in origin and is found even in the deepest levels of the mine. A later stage of quartz-tourmaline alteration characterized, as at Chorolque, by clear inclusion-free quartz with very fine intergrown tourmaline needles, is also present as a vein-wall alteration in otherwise tourmaline-sericite altered rocks.

#### D. Mineralization

##### a) The veins

The Salvadora stock is cross-cut by a complex system of mineralized veins which together made up one of the biggest and richest tin deposits of the world (Fig. 2.9). The vein mineralization has been studied in some detail by Turneure (1935). He indentified two types. The major veins have dips usually between  $45^{\circ}$  and  $75^{\circ}$  and show gouge, slickensides and brecciation, indicating an origin by shearing stress. Interspersed with these, and in some cases branching off them, is a system of smaller vertical veins of



apparently tensional origin. Both types have a broadly similar strike direction and cut across the contact between the stock and the sedimentary rocks, and across all internal contacts. Mineral deposition in all of the veins seems to have been a broadly continuous process. There is no evidence of well-defined breaks in mineral paragenesis, cross-cutting relationships among veins, or successive opening of veins of different character. The two vein types are apparently contemporaneous and related to the same stress system. There are also some large post-mineral faults which cut across the vein system, with substantial displacements. Turneaure concluded that the vein fracture system was produced by regional stress rather than local stress related to the emplacement of the stock.

The vein mineralization is in the form of fracture fillings. The walls are sharp and there is little or no replacement of the wall-rock by vein material except for a narrow selvage of quartz-tourmaline. The sequence of filling and vein mineralogy is complex, although cassiterite is the only mineral which is commercially recovered. The earliest stage of vein growth consisted of deposition of quartz, cassiterite, bismuthinite and frankeite. This was followed by pyrrhotite deposition and replacement of frankeite by pyrrhotite, then replacement of pyrrhotite by stannite, sphalerite, marcasite, arsenopyrite, pyrite, and siderite. Then came crustification of the earlier mineralization by more sphalerite, pyrite and chalcopyrite, followed by wavellite and supergene limonite, hydrous iron phosphates and covellite (Turneaure, 1935).

b) Disseminated mineralization

In addition to the vein mineralization there is disseminated cassiterite and also sulphide mineralization throughout large areas of the Salvadora stock. This mineralization was mentioned by Turneure (1935), but not investigated in detail. With the progressive exhaustion of the vein tin reserves both at Llallagua and in Bolivia in general, the disseminated 'porphyry tin' mineralization is potentially important (Sillitoe et al., 1975). In this study three types of mineralization were recognized outside the vein structures in the Salvadora stock.

i) Disseminated cassiterite and very fine quartz-cassiterite veinlets.

This type of mineralization is very widespread in the upper levels of the mine where it commonly gives grades of 0.1 to 0.5 percent tin throughout large volumes of rock. The precise distribution of this mineralization is not known although it is clearly not related to the geometry of the veins. Investigations are currently in progress to determine its grade and extent, and the feasibility of mining the whole of the upper part of the stock in an open pit (COMIBOL staff, pers. comm.). The cassiterite is very fine grained. It occurs as isolated grains in the groundmass of sericitized porphyry or as fine grains replacing feldspar and biotite phenocrysts together with sericite and tourmaline. There are also very fine quartz-cassiterite veinlets cutting sericitized porphyry. It is not accompanied by much sulphide mineralization (Plate 9A).

ii) Disseminated sulphide mineralization.

This is widespread in parts of the stock. Its distribution is not well defined but it seems to be best developed in the sericitized porphyry and breccia to the east of the major fault

zone (Stanton-Diaz fault) which transects the stock. Pyrrhotite is the most common mineral in the highly tourmalinized rocks in the deeper levels of the mine. It occurs, with tourmaline, as a replacement of biotite and feldspar phenocrysts (Plate 9B), and is certainly contemporaneous with the earliest alteration. In some areas the pyrrhotite has been replaced by marcasite, and in these rocks there is also disseminated sphalerite, chalcopyrite and stannite. Where the rock alteration is more sericitic, the earliest sulphide is pyrite (Plate 9C).

iii) Cassiterite and sulphide mineralization in certain hydrothermal breccias.

Some of the hydrothermal breccia bodies contain important amounts of cassiterite, and are being mined at present. The most important of these is a pipe-shaped body measuring about 50 m in diameter, located at the western margin of the stock, and known as the 'Clavo San José'. It is typical of the polymict breccias described above. The fragments are of both sedimentary and igneous rock and the matrix is a mixture of fine rock fragments and residual quartz grains cemented with fine tourmaline. This particular breccia differs from most of the others in that many of the igneous rock fragments, both large and small, have been replaced by a relatively coarse intergrowth of quartz and cassiterite. The degree of replacement is not uniform throughout the breccia body. In places there are quartz-tourmaline altered igneous fragments with no cassiterite, in places there are igneous fragments replaced by sericite and clay. The breccia also contains rounded sulphide (pyrrhotite) clasts as well as cross-cutting pyrite veinlets. The presence of pre-breccia pyrrhotite clasts and

quartz-tourmaline altered igneous rock fragments is further evidence that some hydrothermal alteration and mineralization of the stock had taken place before at least some of the breccias were formed. The quartz-cassiterite replacement must have taken place later, and was probably contemporaneous with the development of the vein system.

#### E. Alteration and mineral zoning

The distribution of alteration types in the Salvadora stock has not been studied in detail but it is clear that there is no really well-defined zonal pattern as at Chorolque. Pervasive quartz-tourmaline alteration is only developed in the deepest levels presently exposed, and most of the stock has a tourmaline-sericite assemblage. There does appear to be a fairly distinct predominance of sericite in the upper parts of the stock and of tourmaline in the deeper levels, while argillic alteration is found mainly near the stock margins. Turneaure (1935) noted that a 'pyritic zone' surrounded the central tin-bearing part of the stock. In general, disseminated cassiterite does seem to be best developed in the central and upper part of the stock and has little sulphide associated with it, while sulphides predominate in the outer and deeper regions.

#### 2.2.4 Potosi

The great tin-silver deposit of the Cerro Rico, Potosi, has been described previously, in particular by Lindgren and Crevelling (1928), Turneaure (1960), and Ahlfeld and Schneider-Scherbina (1964). A brief description is given here, mainly summarized from the above accounts, and the regional geology is described in greater

detail in Chapter 5. The Cerro Rico is located just to the south of the city of Potosí (Fig. 2.3).

#### A. Rock types

The ore deposit is a complex vein system associated with a small acid porphyry body, the Cerro Rico stock. The stock intruded the Palaeozoic sedimentary basement rocks of the area and an overlying conglomerate and tuffaceous unit of Miocene age. The stock is oval in plan, measuring about 1711 by 1200 m at the surface. There is a dyke-like offshoot to the north. It is conical in vertical section, narrowing downward to form a dyke about 100 m wide (Fig. 2.10). Below this it divides, and in the lowest level of the mine (300 m below the summit of the Cerro) there are only two narrow porphyry dykes cutting the Ordovician argillites.

The stock is made up of intensely altered porphyry. No remnants of unaltered rock have been found, but the textures are relatively well-preserved, and together with the abundance of relict quartz phenocrysts suggest a quartz-latitude composition. Unlike most of the other mineralized sub-volcanic stocks of the southern tin belt, the Cerro Rico does not contain a significant proportion of breccia, although some small hydrothermal breccia bodies have been found at the margins, and pebble dykes cut the surrounding sedimentary rocks. Turneaure (1960) took the absence of brecciation to indicate that the stock did not represent a volcanic vent. However, the Miocene formations which surround its upper part include tuff beds, and (on the northeastern side) there is a 100 m thick lens of breccia made up of both igneous and sedimentary rock fragments, which is probably of volcanic origin. Together with the characteristic conical shape, this suggests that

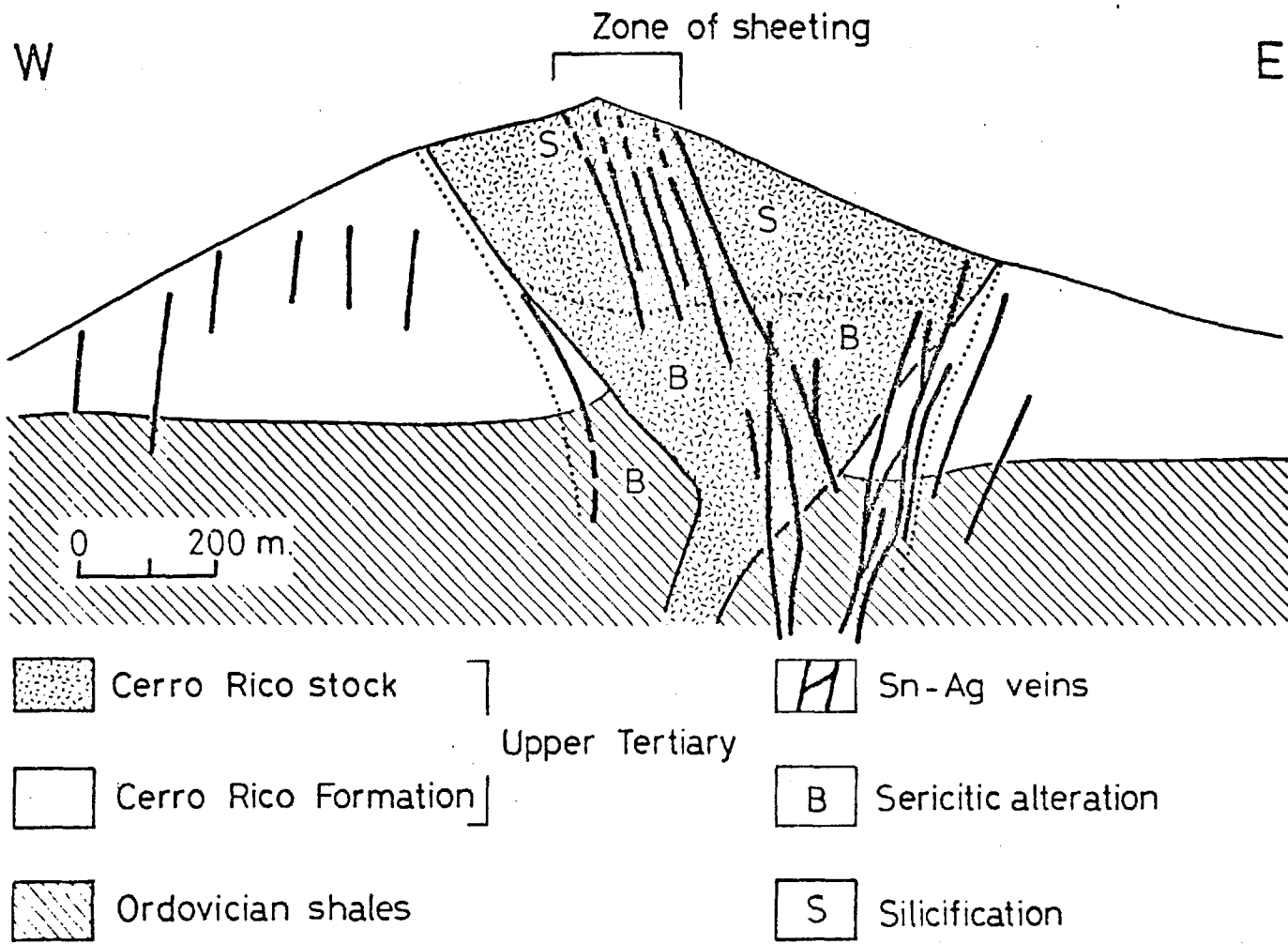


FIG.2.10. POTOSI, THE CERRO RICO STOCK.

the stock did occupy a volcanic vent, although most of the extrusive superstructure has been eroded away (Sillitoe et al., 1975).

#### B. Alteration and mineralization

The Cerro Rico stock is pervasively altered throughout. In the lower part the alteration is sericitic with some clay, but there is little or no tourmaline, although it may be slightly more abundant in the deepest regions. Feldspar and biotite phenocrysts have been replaced by a felty intergrowth of sericite with a little quartz and clay. The primary quartz phenocrysts are preserved and do not show any secondary quartz overgrowths. The amount of clay increases upward. The upper part of the stock is intensely silicified. The entire rock has been replaced by a porous mass of aphanitic silica. The alteration has not been studied in detail, but there does not appear to be any lateral zonation. The sericitic and argillic alteration extends beyond the margins of the stock, and has affected the tuffaceous sediments and breccias at least for some tens of metres from the contact.

The sericitized rocks are strongly pyritized, and there is fine dispersed cassiterite which gives tin grades of over 1000 ppm through large volumes of the stock. The major vein system cuts both the stock and the surrounding sedimentary rocks. The veins strike north to north-northeast and dip steeply. Most of the major veins are within the stock in the upper levels but dip more steeply than the contacts and so pass out into the Palaeozoic sedimentary rocks with depth. In the upper silicified region there is a system of closely spaced parallel veins forming a wide sheeted zone (Fig. 2.10). The major veins are narrow fractures filled with

quartz, cassiterite and sulphides. The earliest mineralization in the deeper levels of the veins is a quartz-cassiterite-pyrite assemblage, it shows some alternation of quartz-rich and pyrite-rich zones with progressive vein growth, and most of the cassiterite was deposited at the earliest stage, against the vein walls, with pyrite predominating in the inner (latest) part. The veins are vuggy, with drusy cavities lined with quartz crystals. The vein system shows strong vertical zoning of mineralization, with quartz and cassiterite decreasing, and sulphides increasing upward. In the middle levels there was a complex sequence of sulphide deposition. A little early quartz-cassiterite-pyrite was followed by a stannite-chalcopyrite stage, then sphalerite-tetrahedrite and then ruby silvers, jamesonite, and boulangierite, with a final open space filling of alunite and clay. In the uppermost levels the silver-rich stages are best developed. There is no well-developed lateral zonation of mineralization, although some minor peripheral veins are rich in lead-zinc with little or no tin.

### 2.2.5. Colquechaca

#### A. Introduction, geological setting

The Colquechaca igneous complex is located 90 km north of the city of Potosi at  $18^{\circ}42'$  south latitude,  $66^{\circ}01'$  west longitude. The only published description of the geology and mineralization is a brief note by Ahlfeld and Schneider-Scherbina (1964). The description of the geology given here is based on observations made during two brief visits, in 1974 and 1975. Although very little fluid inclusion work has been possible on the Colquechaca mineralization because of the absence of suitable transparent minerals, the complex displays a number

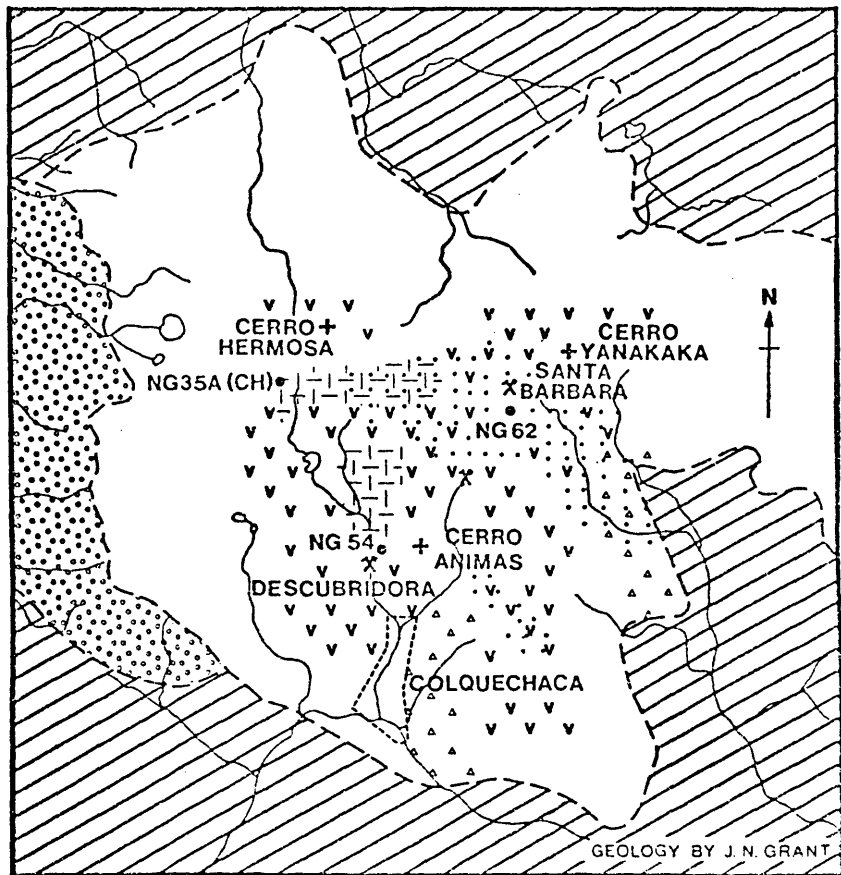


of features which are important in relation to the development of a genetic model for the subvolcanic tin deposits as a whole, and is particularly important with respect to the relationship between the age of the mineralized complexes and their metal content and general characteristics (see Chapter 5).

Ahlfeld and Schneider-Scherbina (1964) described the complex as a 'round dacite stock of approximately 6 km diameter intruding Devonian shales in the crest of an anticline'. However, an alternative interpretation favoured here, is that it is a volcanic complex in which it is doubtful if any intrusive rocks are present (Fig. 2.11). The complex is part of an elevated massif. The volcanics rest unconformably on Devonian shales and have been deeply dissected by glacial erosion. The main part of the complex measures roughly 6 km by 6 km, but there are isolated outliers of volcanics beyond this. The base of the volcanic sequence dips rather steeply southward and this may have been a pre-existing slope rather than due to later tilting. Internal contacts within the volcanics are few and difficult to recognise, but they seem to dip southward in the lower parts while at higher elevations they appear to be horizontal (there is over 1000 m of vertical exposure). The basal part of the complex at its southern margin is made up of a thick volcanic breccia or lahar deposit consisting of mainly sedimentary rock fragments in a tuffaceous matrix.

The geology of the remainder of the complex is rather uniform and consists of thick dacite lavas and pyroclastic units. In the central region there is a coarse-grained porphyritic quartz-latite unit. It appears to have a conformable contact with the overlying dacites and is probably a thick flow, although it is



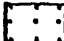

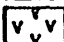

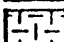

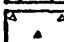



FIG.2.11



**COLQUECHACA VOLCANIC COMPLEX**

0 1000 2000  
Scale (m)

**COLQUECHACA COMPLEX (Tertiary)**

- |   |  |
|---|--|
|  Undifferentiated Volcanics                |  Cretaceous and Palaeozoic Sedimentary Rocks |
|  Zone of Pervasive Hydrothermal Alteration |  Geological Boundary                         |
|  Dacite Lavas                              |  Rivers                                      |
|  Rhyodacite Lavas                          |  Peak   |
|  Volcanic Breccia                          |  K/Ar Sample Location                         |
|  Moraine                                   |  Mine Entrance                                |

possible that it is a semi-conformable intrusive body. Much of the remainder of the complex is made up of fine to medium grained crystal/ash tuffs, with some thick porphyritic lava flows or domes with well-developed columnar jointing in the upper regions (Plate 10A).

#### B. Alteration and mineralization

A poorly-defined zone of pervasive sericitic alteration is present in the central part of the complex. It is elongated in a roughly northwest-southeast direction and measures about 600 m by 2000 m. The alteration is intense in places, and sericite is the predominant secondary mineral, with some clay. There is little tourmaline present. There is weak disseminated sulphide mineralization in this zone, and disseminated cassiterite is also present, giving tin grades of up to 1000 ppm in some surface grab-samples. There are a number of small tin-bearing veins within the alteration zone, striking parallel with its long axis. It is also cross-cut by a number of larger veins. In all cases the vein mineralization is sulphide-rich, and there is little quartz. Tin is present as both cassiterite and stannite. There is usually a narrow envelope of carbonate-bearing argillic alteration adjacent to the veins.

Elsewhere in the complex the volcanics are usually partly chloritized. This low-intensity alteration (consisting essentially of replacement of biotite by chlorite) is not related to mineralization.

There are a number of major vein structures which traverse the complex, mainly outside the zone of pervasive sericitic alteration. They contain massive, quartz-free, sulphide

mineralization consisting of sphalerite, galena and pyrite with some silver minerals. Tin is very weak or absent. They were originally mined for silver in their upper levels, and lead and zinc are still being produced. They have prominent wall-rock alteration envelopes consisting of a clay-sericite-chlorite-carbonate assemblage. These vein structures are faults, and have well-developed breccia textures in which the sulphides form the matrix between rounded fragments of argillized and sericitized igneous rock.

#### 2.2.6. Other deposits

Several other mineralized eruptive complexes were examined briefly, mainly during the collection of samples for the geochronological work described in Chapter 5. In some cases there is a little published data on the geology and mineralization of these complexes, though in general they have never been described in any detail. The brief descriptions given here are based mainly on my field observations, and provide a framework for interpreting the age data as well as emphasizing certain aspects which are important with respect to the genetic considerations discussed in Chapter 6.

##### A. The San Pablo-Morococala area

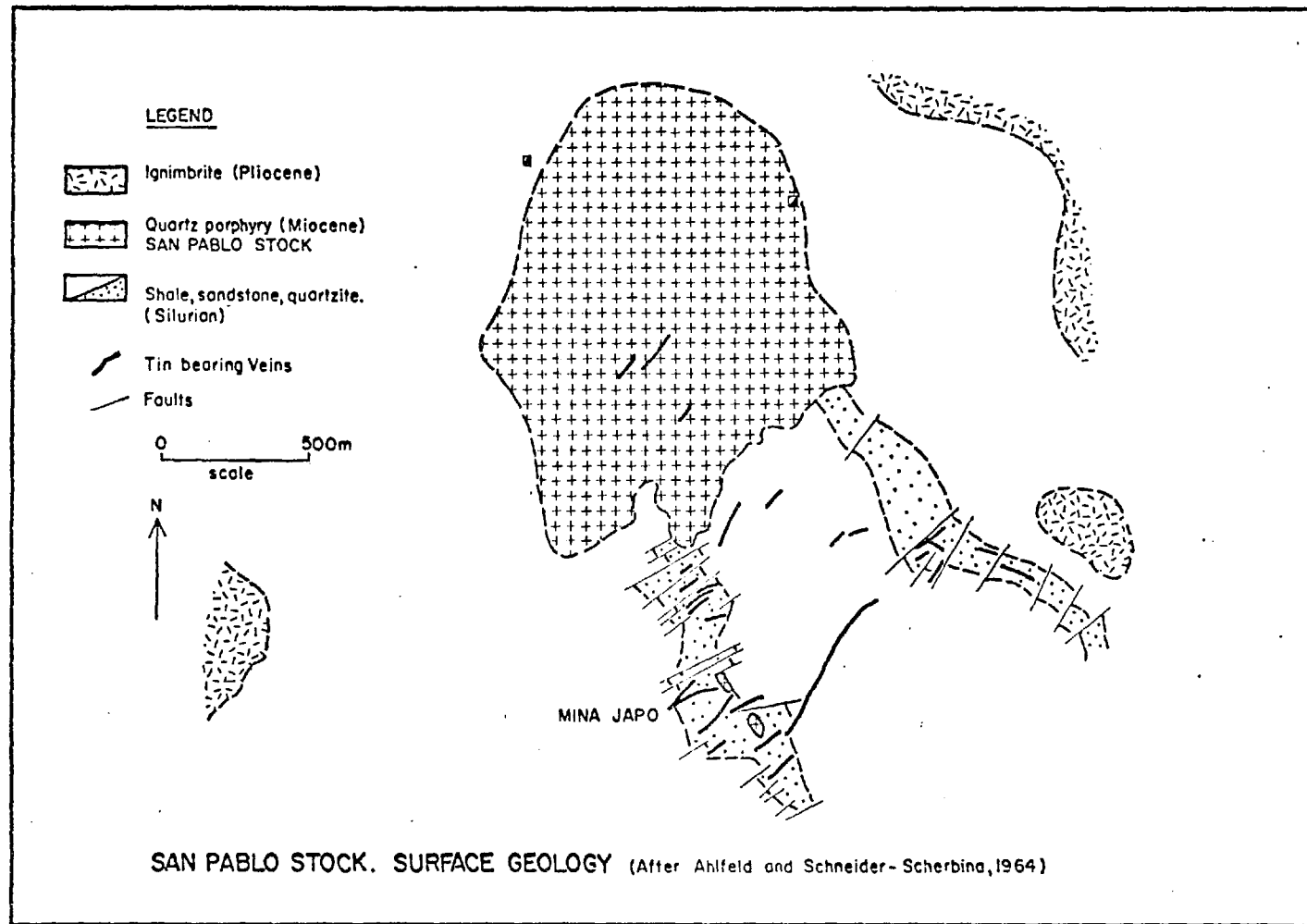
The Morococala plateau is an elevated block of Palaeozoic sedimentary rocks lying immediately to the east of the Altiplano, just southeast of Oruro (Fig. 2.3). The Palaeozoic rocks consist of Silurian and Devonian argillites and quartzites which are tightly folded on northwest trending axes, but are only weakly metamorphosed. They are partly overlain by a thin veneer of dactylic ignimbrite.

There are two main mining areas on the plateau, one around the margins of the San Pablo porphyry stock, and the other at Santa Fe-Morococala. In both cases the mineralization is in veins in the sedimentary rocks, but is associated with intrusive porphyries. The San Pablo area is near the northern end of the plateau. Numerous veins are clustered around a stock of altered quartz-porphyry and breccia. The stock is about 1 km in diameter at the surface (Fig. 2.12). All significant mining activity has taken place outside the stock contacts, and its subsurface shape is unknown at present. The southern part of the stock is made up of coarse hydrothermal breccia consisting of altered igneous and sedimentary rock fragments in a tourmalinized, fragmental matrix. This breccia is very similar to the hydrothermal breccia at Llallagua. The remainder of the stock consists of altered porphyry with patchy brecciation in many areas (Plate 10B).

The rocks are pervasively altered almost throughout the stock. There is a narrow zone near the northern contact where relatively fresh rock has been preserved. It is a typical quartz-lattice porphyry made up of phenocrysts of quartz, sanidine, sodic plagioclase and biotite, in a microgranular quartz-feldspar matrix. The alteration is typical sericite-tourmaline type, with the proportions of sericite and tourmaline varying considerably. A common example is shown in Plate 10C; the feldspar phenocrysts are replaced by black tourmaline, while the remainder of the rock is sericitized. Quartz-tourmaline alteration appears to be absent at the surface and there is no subsurface data available, although deep exploration of the stock is currently in progress.

There are a few minor veins within the stock consisting of

FIG.2.12

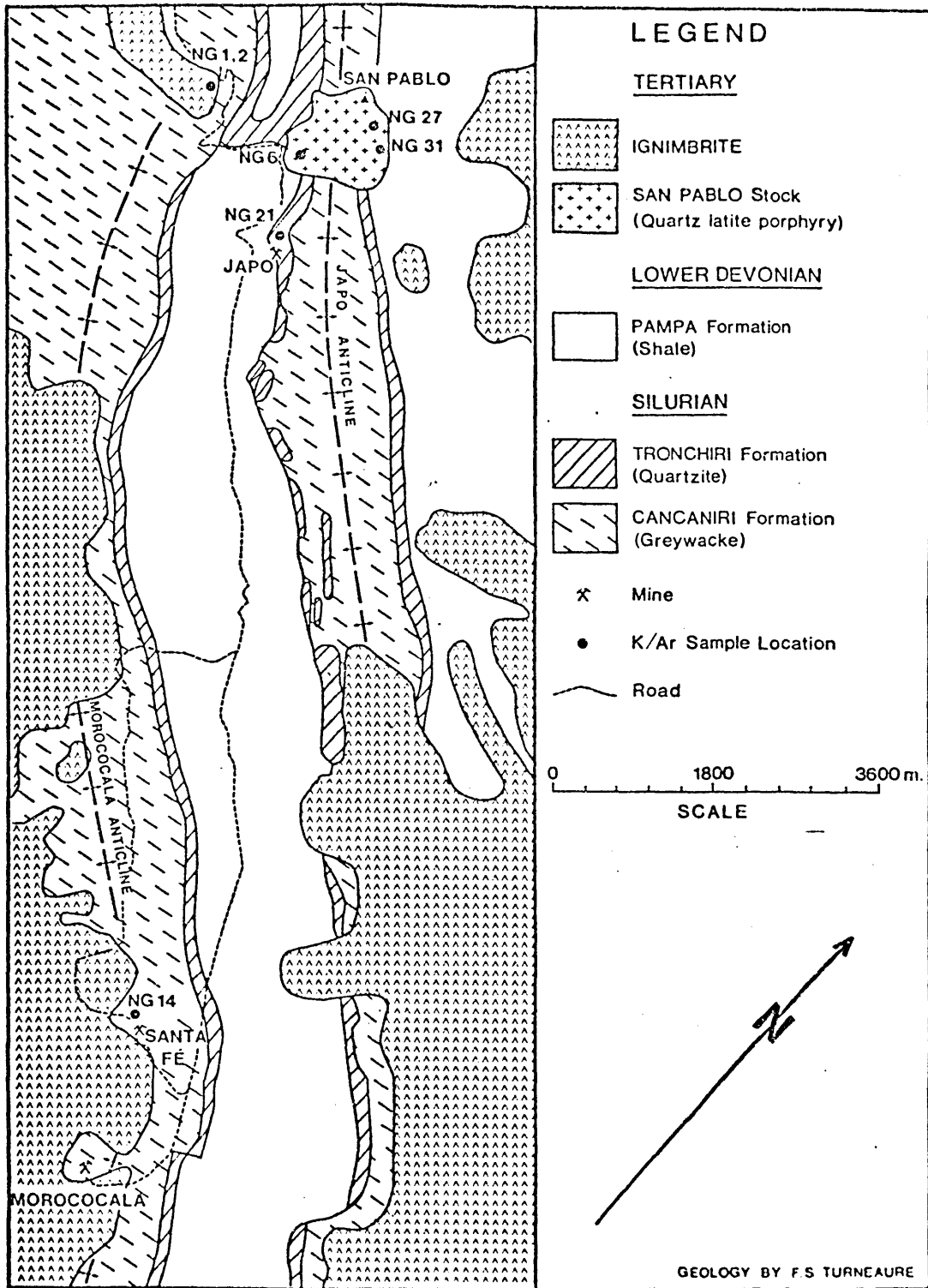


quartz with cassiterite and minor sulphides, and there are some sulphide-rich veins at the stock margins, with pyrite, arsenopyrite, chalcopyrite, bismuthinite, stannite and cassiterite in a chloritic gangue. There is also disseminated cassiterite throughout the altered rocks of the stock. The tin grade is commonly over 1000 ppm in surface grab-samples, but the distribution of this mineralization is not known in detail although it is currently under investigation by the Bolivian State Mining Corporation (COMIBOL). The San Pablo stock offers important potential as a major, low grade, 'porphyry tin' deposit (Sillitoe et al., 1975).

The presently economic mineralization is in sulphide-rich veins in the sedimentary rocks around the stock, the veins are particularly well-developed in a massive, brittle quartzite unit (Fig. 2.12). The Japo mine is the most important. The veins there are narrow sulphide-cassiterite fracture fillings with narrow, argillic wall-rock alteration envelopes and much clay gouge. There are some intensely altered (sericitized and argillized) porphyry dykes in the mine area.

The Santa Fe and Morococala mines are located about 10 km south of the San Pablo stock (Fig. 2.13). The mineralization is in sulphide-rich veins cutting sedimentary rocks (shale and siltstone), and there are also some narrow altered porphyry dykes and hydrothermal breccia dykes and pipes. The sediments in the area containing the mineralized veins are slightly hornfelsed and tourmalinized. The hydrothermal breccia dykes were formed after most of the mineralization had been deposited. In some cases they follow the vein structures, and contain

FIG. 2.13



**SAN PABLO - MOROCOCALE REGION**  
 SURFACE GEOLOGY AND K-Ar SAMPLE LOCATIONS

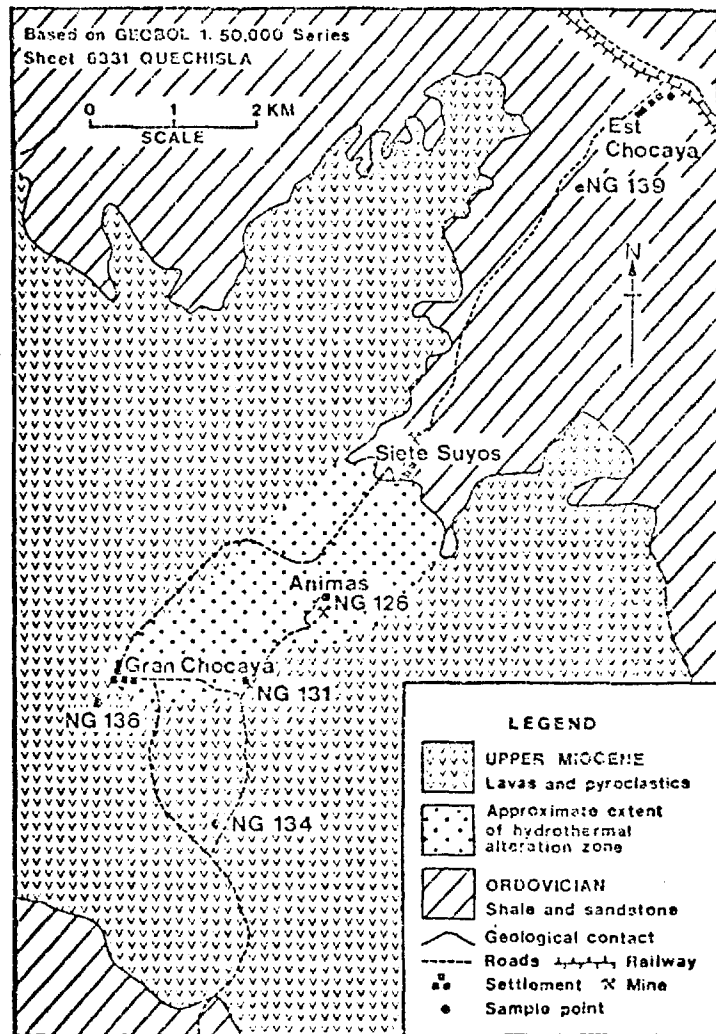


rounded clasts of sulphide and mineralized wall-rock (Plate 11). It seems probable that the mineralization, dykes, breccia pipes and alteration zone are related to a larger igneous body, perhaps a stock, at no great depth beneath the present surface.

#### B. Chocaya

Chocaya is an extensive volcanic complex located in the southern part of the tin belt (Fig. 2.3). It is made up of acid to intermediate (dacitic) lavas, lava domes and pyroclastics, which rest unconformably on folded Ordovician sedimentary rocks. There are no intrusive rocks known, except for some dykes. The predominant rock type is a porphyritic dacite made up of phenocrysts of plagioclase, biotite, lesser hornblende and quartz in a microcrystalline to glassy matrix. There are also extensive areas of more acid tuff and volcanic breccia. There are some lahar deposits on the north-east flank of the complex which may mark the original surface, and if this is the case, the total original thickness of volcanics in the central region would have been of the order of 1000 m, and some of the mineralized veins must have been formed at depths of no more than 500 m below the surface. In the central to north-eastern part of the complex there is an extensive zone of strong hydrothermal alteration which has been deeply eroded by a river system (Fig. 2.14). The mineralized veins are within this zone. The most common alteration types are sericite-carbonate, and argillic assemblages. The former is very widespread throughout the altered zone, while the latter seems to be best developed adjacent to vein structures. At the fringe of the alteration zone chlorite is present as a replacement of the mafics, but in general,

FIG.2.14



### CHOCAYA COMPLEX

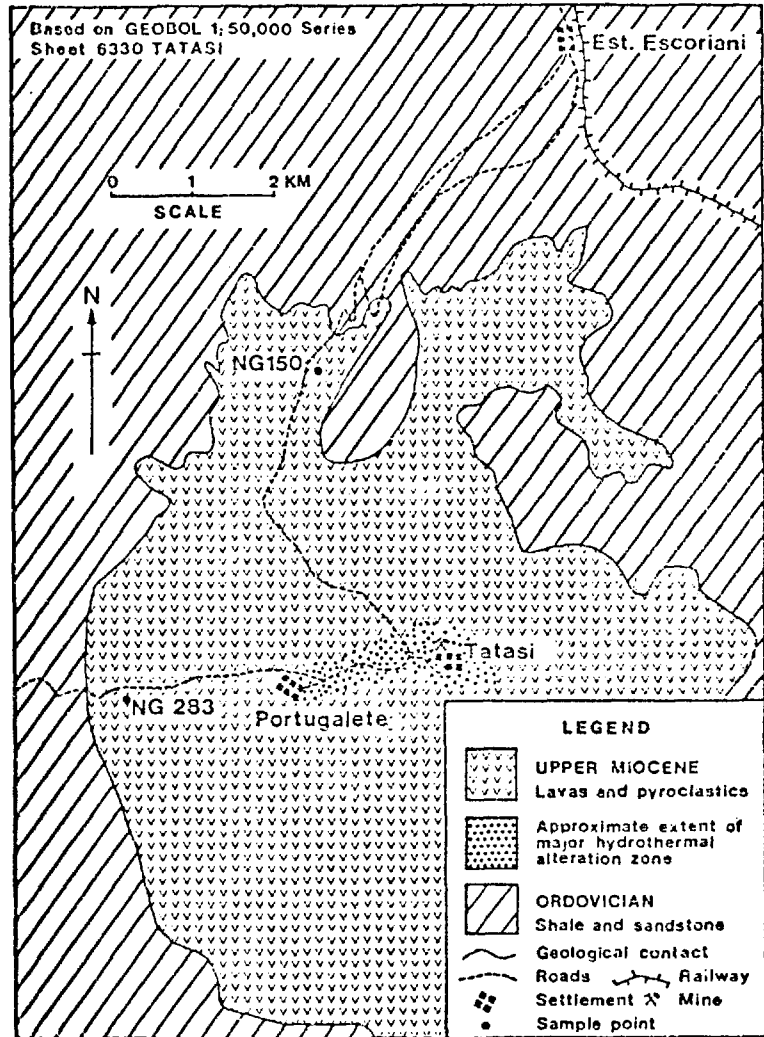
SURFACE GEOLOGY AND K-Ar SAMPLE LOCATIONS

chloritization is not widely developed. There are several clusters of veins within the altered zone, and in some cases they extend downward into the sedimentary rocks below the volcanics. The mineralization is sulphide-rich, with little quartz gangue. There are two types of mineralization, silver-lead-zinc, and sulphide-tin. The latter consists of pyrite, arsenopyrite, chalcopyrite, stannite and cassiterite with numerous subordinate minerals including jamesonite and silver-sulphosalts. The two ore-types are found in different, though adjacent vein structures, and the silver-lead-zinc veins tend to be deeper, and mainly within the underlying sedimentary rocks. There is little or no disseminated mineralization in the altered igneous rocks.

#### C. Tatasi

The Tatasi complex is located to the south of Chocaya, and both are of similar character. The rocks are generally more acid than at Chocaya, and the mineralization is almost entirely silver-lead-zinc, with little tin present. There is a very extensive zone of pervasive hydrothermal alteration with two main clusters of veins within it, at Tatasi and Portugalete (Fig. 2.15). The alteration is strongly argillic with little sericite, and there is no disseminated sulphide or cassiterite mineralization. The vein mineralization is again divided into two types, galena-sphalerite-pyrite with minor silver minerals, and jamesonite-silver mineralization (ruby-silvers and tetrahedrite). As at Chocaya, some of the veins extend down into the underlying sedimentary rocks.

FIG.2.15



**TATASI COMPLEX**

**SURFACE GEOLOGY AND SAMPLE LOCATIONS (K-Ar)**

#### D. Isca-Isca

Isca-Isca is located 40 km north of the town of Tupiza (Fig. 2.3). It is a breccia pipe cutting Palaeozoic shales and siltstones. The breccia is very altered (sericite-tourmaline) and appears to be mainly hydrothermal in origin. It is about 1 km in diameter at the surface. There is no vein mineralization within it, but there are a number of small tin-tungsten-bismuth-copper veins in the sediments close to the contact, and some lead-zinc veins farther out (Ahlfeld and Schneider-Scherbina, 1964). There are no extrusive igneous rocks in the vicinity of the breccia pipes. The grade of disseminated tin in the pipe appears to be low, but it has not been thoroughly investigated.

#### E. Tasna

The Tasna deposit is located 30 km north of Atocha. It consists of numerous scattered veins cutting a large area of tourmalinized and hornfelsed Palaeozoic shales. There are several altered quartz-porphyry dykes in the central part of the altered area. The vein mineralization is sulphide-rich and carries tungsten, bismuth, tin, copper, lead, and silver. There is a poorly-defined zonal arrangement, with tungsten-bearing veins in the central region, bismuth-tin-copper veins farther out and of greatest economic importance, and tin-lead-silver veins beyond (Ahlfeld and Schneider-Scherbina, 1964). The deposit is similar to the Morococala-Santa Fe' and Huanuni deposits in that the ores are entirely in sedimentary rocks and direct evidence of igneous activity is limited to a few acid dykes. The wide extent of the tourmalinized area (15 sq. km) and the even greater

extent of the area containing mineralized veins, suggests that there is a large igneous body at no great depth beneath the present surface.

### 2.3. Discussion

The descriptions of some of the tin deposits given above illustrate the most important features of their geology, and provide a basis for interpreting the fluid inclusion data presented in Chapter 3. The mineralization is a product of high-level acid igneous activity. In many of the deposits there is clear evidence that they were formed by hydrothermal activity associated with the rise of quartz-porphyry magma in the vents of stratovolcanoes, at the closing stages of igneous activity. Two outstanding features of ore-forming hydrothermal systems in this environment are: the development of hydrothermal breccia, and intense widespread rock alteration. These are particularly well-developed at some of the Bolivian sub-volcanic tin deposits, and are discussed in further detail below.

#### 2.3.1. Hydrothermal brecciation

An outstanding feature of the geology of many of the Bolivian sub-volcanic tin deposits is the widespread occurrence of hydrothermal brecciation. In some cases, such as at Isca-Isca and Chorolque, the ore deposits are centered on a major breccia pipe. In other cases, for example Llallagua, the San Pablo stock, and Oruro, breccias make up a significant proportion of the porphyry stocks.

The association between ore mineralization and hydrothermal brecciation is observed in several important types of deposit

throughout the world. In some cases the breccias provided suitable structures for the localization of hydrothermal ore deposition, and the phenomenon of brecciation is an important indicator of the environment in which the hydrothermal fluids were generated. Hydrothermal breccias are particularly well-developed in porphyry copper systems. As with the Bolivian tin deposits, some of these are centered on major breccia pipes, for example, Braden, Chile (Howell and Molloy, 1960; Camus, 1975), and Cananea, Mexico (Velasco, 1966). In other cases the breccias are a subordinate feature of the geology. Many of the porphyry copper deposits of the southwestern U.S. exhibit important breccia development, for example, Bisbee, Arizona (Bryant, 1968), Santa Rita, New Mexico (Rose and Baltosser, 1966), Copper Basin, Arizona (Johnston and Lowell, 1961). Subordinate breccias are also found in porphyry copper deposits in the Andes, for example, Toquepala, Peru (Richard and Courtright, 1958) and Cuajone, Peru (Lacy, 1958), and in the southwest Pacific, for example Yandera, New Guinea (Grant and Nielsen, 1975). Other types of mineralized breccia pipe are widespread in the Andes. Examples include the great polymetallic deposit of Cerro de Pasco, Peru (Petersen, 1965) which is developed within a major breccia pipe, the numerous though generally small copper-gold-tourmaline pipes of Chile (Sillitoe and Sawkins, 1971), and the Bi-Cu mineralized pipe of San Francisco de Los Andes in northern Argentina (Llambias and Malvicini, 1969).

In all cases the breccias are associated with relatively

high-level acid to intermediate intrusive igneous bodies. They are found both in the igneous rocks themselves and in the adjacent wall rocks. In general a distinction can be made between hydrothermal intrusion breccias and hydrothermal collapse breccias (Bryner, 1968). The former are characterized by rounded fragments, sometimes of a variety of rock types, and have a clastic (rock-flour or 'tuffaceous') matrix which fills much of the space between the fragments. Textures indicative of fluidization are common. The latter are made up of angular fragments of the surrounding rock type, and often grade laterally into sheeted fracture zones parallel with the pipe walls. They contain little or no clastic matrix, and are cemented by minerals deposited from solutions which circulated through the breccia after its formation.

Several different mechanisms have been proposed for the formation of hydrothermal breccias. The fundamental requirement is the creation of a void. Where explosive magmatic-hydrothermal action has penetrated through to the surface, producing a diatreme or volcanic vent structure, there is no difficulty in explaining the space problem; however, many important breccia bodies are blind, i.e., do not reach the surface. The various mechanisms by which an initial void might be formed have been reviewed by Mitcham (1974) who favoured a mechanical origin at fault intersections. The void created in this way could then either be the site of collapse brecciation, or could be exploited by upward-streaming hydrothermal fluids, resulting in the formation of intrusion breccia. Such a mechanism undoubtedly has operated in some cases, with a clear relationship existing between faults, joints, and breccias (Mills, 1972). However, many breccia bodies



show no relationship to such structures. The fact that breccia formation often took place during the earliest stage of hydrothermal activity while crystallization of the igneous rocks was continuing, and the tendency of breccias to occur within or just above the tops of high-level plutons, suggests that the hydrothermal fluid itself is primarily responsible for breccia formation.

The corrosive action of hydrothermal fluids has been proposed as a mechanism for breccia formation by Locke (1926), and more recently by Sillitoe and Sawkins (1971). The latter proposed that the copper-bearing tourmaline pipes of Chile were formed by a solution-collapse mechanism. This type of mechanism could operate particularly effectively along pre-existing structures such as faults and joints, with large-scale corrosion and solution of the wall-rocks resulting in a void into which collapse could take place.

An alternative mechanism for the formation of an initial void has been proposed by Norton and Cathles (1973). They suggest that the accumulation of the vapour exolved from a crystallizing magma might be trapped beneath an already crystallized outer rind of a pluton. The void so created would become the site of collapse brecciation, forming a blind pipe, once the surrounding rock had crystallized and fractured, and the initial fluid pressure had been released.

The data of Whitney (1975) indicate the most favourable conditions for breccia development in an initially water-unsaturated quartz-monzonite stock. If the magma rises essentially isothermally, it will evolve a vapour phase only when it reaches a

level at which the confining pressure ( $P$  total) is equal to, or less than, the vapour pressure of dissolved water ( $P_{H_2O}$ ) in the magma. The level at which this would occur depends on the water content, composition, and temperature of the magma. For moderate water contents (3 to 4 weight percent  $H_2O$ ), vapour generation in a quartz-monzonite magma must be restricted to the upper few kilometres (perhaps less than 5 km) of the crust. If a significant amount of vapour is generated fairly rapidly, i.e., during rapid magma ascent, then the pressure of accumulated vapour may be raised above the lithostatic pressure, favouring explosive breccia development at the roof of the stock.

Alternatively, if none of the magma, or only a small part of it, rises to a sufficiently low-pressure region to allow isothermal vapour saturation, then vapour generation will be slow and will proceed with cooling and crystallization of the stock from the margins inward. Under these conditions sufficient vapour accumulation for explosive breccia development is less likely, although continued transport of fresh magma (e.g., by convective rise) into the upper regions could increase the rate at which vapour might accumulate at the top of the pluton.

From this it appears that the type of mechanism envisaged by Norton and Cathles (1973) for the formation of collapse breccia pipes would be favoured in a situation where a large stock rose only a relatively short distance into its vapour saturation field. An outer rind would crystallize (with some vapour generation) and subsequent vapour could accumulate beneath it, perhaps forming large voids. Vapour accumulation would be favoured by convective overturn in the remaining magma.

On the other hand, the rapid rise of magma at shallow depth would favour the type of explosive hydrothermal brecciation which has taken place in the Bolivian complexes. A possible sequence of magmatic fluid generation in these complexes might be as follows: the eruptive complexes were underlain at depth by a large magma chamber. The earliest magma rising from this source was relatively dry. Vapour saturation took place only at very shallow depth, leading to pyroclastic eruption. As the temperature declined in the source, and crystallization preceded,  $P_{H_2O}$  in the upper part of the source magma chamber became closer to saturation. Subsequent pulses of magma rising rapidly in the vent became water saturated at deeper levels than previously. Rapid vapour evolution produced explosive hydrothermal brecciation within the vent, and the magma 'froze' before reaching the surface. Successive pulses of magma resulted in fluctuating fluid pressure in the vent, producing complex patterns of mechanical and hydraulic fracturing and brecciation. As cooling and crystallization of the source magma continued, the level at which vapour generation took place retreated downward. Once the vent was effectively sealed by crystalline magma, and as the temperature of the source magma declined and it became largely crystalline, the rise of magma in the vent ceased. Vapour generation continued in the source magma chamber as a result of cooling, crystallization, and perhaps convective rise of still mobile material from deeper regions. The generation and accumulation of this vapour would take place at a slower rate and under lithostatic pressure too great to allow explosive hydrothermal intrusion brecciation. The fluids would be channeled along fractures, faults and permeable

breccia zones in the overlying vent region.

As described above, the breccias in the Bolivian sub-volcanic tin deposits are predominantly of the intrusion type, with rounded fragments and a substantial proportion of clastic matrix. In some cases, particularly at Llallagua, there is evidence of the corrosive nature of the hydrothermal fluid. The matrix material of the breccias, and the material forming the black dykes, may be composed largely of residual phenocrysts of corroded igneous rock which have been fluidized. The black dykes were apparently formed by the injection of this material along the network of narrow fractures produced both by the mechanical effect of pulsating magma injection and by explosive vapour release. The larger breccias are composed of the same material, together with entrained rock fragments. In some cases they may be diatreme-like structures which reached the surface, in other cases they are blind, and may have originated by solution-collapse with subsequent mobilization during upward streaming of fluid, or simply by exploitation of fracture channelways during fluid release from deeper levels.

The role of meteoric water in breccia formation is difficult to evaluate. An alternative mechanism for the explosive hydrothermal activity for which the breccias are evidence could have been steam explosions produced when hot magma encountered groundwater, or subsequent convective circulation of groundwater through the hot igneous rock (Henley, 1973). However, the hydrothermal brecciation is closely associated with pervasive rock alteration accompanied by sulphide and cassiterite mineralization, for which only a magmatic source seems reasonable, and thus a magmatic fluid-release

mechanism seems most reasonable for the origin of the Bolivian breccias.

### 2.3.2. Hydrothermal alteration

A detailed study of the hydrothermal alteration at these deposits has not been attempted. However, a limited investigation was undertaken because of the importance of alteration in relation to the distribution of mineralization, and as an indicator of the physical and chemical conditions in the hydrothermal systems. The types and distribution of alteration at individual deposits have been described above. The results of some chemical analyses of a suite of typical altered and unaltered rocks are presented here, and discussed in terms of the following generalizations which can be made about the occurrence and distribution of alteration and mineralization.

#### A. Pervasive alteration: types and zoning

Hypogene alteration of igneous rocks involves the replacement of the original minerals by a number of secondary minerals, the most important of which in these deposits are; chlorite, clay minerals, sericite (white mica), tourmaline, and quartz. The intensity of alteration, i.e., the extent to which the primary mineralogy of the rock has been changed, increases with the development of the successive secondary minerals listed, in that order. There is generally a parallel trend towards obliteration of the original rock texture. Notable features of these altered rocks are the virtual absence of minerals such as topaz and fluorite which are commonly found in the alteration assemblages associated with tin deposits elsewhere, and the absence of a feldspar- and biotite-stable alteration assemblage such as that

commonly found in the genetically similar porphyry copper deposits, as well as some tin deposits.

The most common alteration mineral associations found in the igneous rocks are as follows:

a) Chlorite: The replacement of primary biotite by chlorite (plus rutile) is common in the larger eruptive complexes. The other primary minerals of the rock may be virtually unaltered, and this represents the lowest intensity of the distinct alteration types. Chloritization of biotite may be accompanied by partial argillization or sericitization of plagioclase, and thus in some cases it shows a gradational relationship with the other alteration types. Although chloritization is found surrounding zones of more intense alteration, their distribution may be unrelated. At Colquechaca and at Chorolque, for example, the volcanic rocks are chloritized almost throughout the complexes and this alteration probably represents merely a typical response of mafic minerals to burial and fluid circulation in a volcanic pile. It may be essentially unrelated to the mineralizing hydrothermal system, whose more intense alteration effects are superimposed on it. A true propylitic assemblage (chlorite-epidote-albite-carbonate) which typically forms an outermost fringe in the zoned alteration pattern of the porphyry copper systems, is apparently not developed in these deposits; this may be due to the less calcic composition of the rocks.

b) Clay minerals: Argillic alteration is present in a number of different forms in most of these deposits. In some cases it is difficult to distinguish supergene from hypogene argillization. No attempt has been made to study the mineralogy of the argillic

assemblage in detail, though on the basis of optical and very limited X-ray diffraction data the dominant species is kaolinite. Clouding and partial replacement of feldspars and volcanic rock matrix (especially glassy matrix) is common in surface exposures, and this type of alteration is probably supergene. However, in some of the volcanic complexes, especially Tatasi and Chocaya, there is strong pervasive argillization of the volcanics over wide areas, generally coincident with the extent of the mineralized vein system. This alteration is probably mainly hypogene, although there is little disseminated sulphide or cassiterite mineralization associated with it. In these cases there is intense argillization at the walls of the veins, sometimes with a little carbonate, chlorite and sericite accompanying the clay minerals. This type of vein wall-rock alteration is typical of the sulphide-rich, predominantly base-metal and silver veins of Tatasi, Chocaya, and Colquechaca.

The occurrence of widespread argillic alteration in the high-level volcanic complexes only is consistent with its development elsewhere in porphyry-type and other epithermal ore deposits. Argillic and advanced argillic alteration assemblages (Meyer and Hemley, 1967) are normally found in the uppermost levels of such systems in zones peripheral to, or superimposed on, deeper zones of sericitic and other alteration types (e.g., Lowell and Guilbert, 1970; Gustafson and Hunt, 1975; Sillitoe, 1973).

In the more deeply eroded Bolivian deposits, for example at Llallagua, argillic alteration is found as a wall-rock envelope to some of the late-stage veins, fractures and faults, and in

some of the permeable breccias. Clay is also found as a late-stage filling in the mineralized veins of many deposits. This alteration has been superimposed on earlier sericite and tourmaline alteration.

c) Sericite-tourmaline: Sericitic assemblages are the most common and widespread alteration type in the Bolivian sub-volcanic tin deposits, and are present at all of the deposits where there are igneous rocks. In general sericite is accompanied by tourmaline, so that a sericite-tourmaline assemblage is most typical, with some secondary quartz and rutile. The relative proportions of sericite and tourmaline vary widely. The sericitic assemblage grades into a quartz-tourmaline assemblage at Chorolque and Llallagua, while a tourmaline-free, sericite-quartz assemblage is characteristic of much of the Cerro Rico stock at Potosi and is also found in dykes at Japo and Santa Fe'. The sericite in these altered rocks is a well-crystallized, fine flaky white mica. It gives the sharp X-ray diffraction peaks of muscovite. In thin-section the tourmaline is generally green-brown in colour and strongly pleochroic, probably a schorl variety, although some of tourmaline in the sericitized rocks and in the veins is almost colourless and may be dravitic in composition.

Potentially economic concentrations of disseminated and veinlet cassiterite mineralization at Llallagua and the San Pablo stock are associated with a sericite-tourmaline alteration assemblage, and almost all occurrences of this type of alteration probably contain anomalous tin values, often over 1000 ppm. This is the type of mineralization which has led to the 'porphyry-tin' concept (Sillitoe et al., 1975). At Llallagua the disseminated



and veinlet tin values are highest in the upper regions of the stock where sericite is the predominant alteration mineral and tourmaline is subordinate, and the values apparently decrease downward as the amount of tourmaline increases. In the deepest levels of the mine, where tourmaline is the dominant alteration mineral and sericite almost absent, the tin values are very low (below 100 ppm). In the laterally zoned Chorolque system, the sericite-tourmaline alteration zone also contains strong disseminated and veinlet mineralization although much of it is in the sedimentary rocks underlying the altered volcanics. The mineralization is predominantly sulphides, and carries Cu, Bi, Ag, As, Pb, and Zn in addition to Sn. As described in section 2.2.2.E above, the intensity of this mineralization decreases both outward into the chloritic zone and inward into the central zone of quartz-tourmaline alteration, which is essentially barren except where cross-cut by the later major vein structures. Thus in a general way, the distribution of mineralization appears to be sensitive to the sericite/tourmaline ratio in the altered rocks. Strongest mineralization is associated with low-tourmaline alteration.

The association between mineralization and sericitic alteration is typical of many hydrothermal ore deposits in acid to intermediate rocks (Meyer and Hemley, 1967). In many porphyry copper deposits for example, the maximum sulphide deposition accompanied sericitic alteration. The association of tourmaline with white mica is common in tin deposits. Where such minerals as topaz are present, the rocks are often termed greisen. The sericite-tourmaline alteration assemblage in the Bolivian deposits shows both mineralogical and

chemical characteristics which distinguish it from what is normally considered to fall under the term greisen.

d) Quartz-tourmaline: A quartz-tourmaline alteration assemblage occurs in two distinct forms in these deposits. As described below, it is commonly developed as a narrow selvage of wall-rock alteration at the margins of veins of the quartz-cassiterite type. It is also developed as a pervasive alteration unrelated to vein structures, as in the core of the laterally zoned system at Chorólque, and in the deeper levels of the Salvadora stock at Llallagua. The pervasive quartz-tourmaline alteration is the most intense alteration type, with only relict quartz phenocrysts remaining of the original igneous minerals. The primary rock texture is almost completely obscured. A particularly important feature of this pervasive alteration type is that there is essentially no cassiterite or sulphide mineralization associated with it.

#### B. Vein wall-rock alteration

In all of these deposits there is little doubt that the pervasive alteration of the igneous rocks took place at an early stage in the evolution of the hydrothermal system, and pre-dated the formation of the major vein system. By the time that fluid flow had become concentrated in the major vein structures, the igneous rocks must have been, in general, thoroughly altered and were no longer particularly reactive to the hydrothermal fluid. Consequently wall-rock alteration envelopes at the vein margins are only poorly developed, if recognizable at all.

Most veins of the quartz-cassiterite type, for example at Llallagua, and Potosi, have a narrow selvage of quartz-tourmaline alteration, generally only a few centimeters in width. In thin

section this material is quite distinct from the pervasive quartz-tourmaline assemblage; the quartz is clear and almost free of fluid inclusions, and intergrown with very fine almost colourless tourmaline needles.

Fluid inclusion study of this material generally shows that its formation temperature is less than that of the surrounding pervasive alteration assemblage. At Llallagua and Potosi this type of material forms the gangue for the early stages of vein growth as well as a vein selvage, and is intergrown with cassiterite and other ore minerals. At Llallagua it fills vugs (with cassiterite) and has replaced igneous rock fragments in some of the mineralized breccias. At Chorolque, the veins show no alteration selvages against the pervasively quartz-tourmaline altered rocks. However, distinctive lower-temperature quartz-tourmaline material is found, generally accompanied by cassiterite or sulphides, in minor fractures and open spaces in the breccia. Where some of the major veins at Chorolque extend laterally across the outer alteration zones in the volcanics surrounding the vent, they do show well-developed alteration envelopes. In these cases the alteration type at the vein margins is more intense than in the surrounding volcanics, so that veins have quartz-tourmaline alteration selvages where they traverse sericitized volcanics, and sericitic selvages where they traverse chloritized volcanics.

In general, as discussed further in Chapter 3 with respect to fluid inclusion studies, the alteration patterns are consistent with the interpretation that the veins developed later than the pervasive alteration and that vein-related alteration and

mineralization took place at lower temperatures than the pervasive alteration, although there may have been temperature reversals in the outer regions of some systems.

### 2.3.3. The chemistry of some altered and unaltered igneous rocks.

#### A. Introduction

A suite of 14 typical altered and unaltered igneous rocks from various parts of the tin belt were analysed for major, minor, and some trace elements. This was not intended to be an exhaustive study, but was done primarily in order to gain some general information on the major chemical changes which accompanied hydrothermal alteration. No previous data are available on the geochemistry of the igneous rocks of the tin belt, although a major study is currently in progress (Halls, C., Angus, J. and Sillitoe, R., pers. comm.). In addition, semi-quantitative analyses for 13 minor and trace elements were carried out on 39 rocks which had been collected for K-Ar dating. These data provide some information on the distribution of the ore metals in both unaltered and altered rocks.

#### B. The whole-rock analyses

The samples analysed are listed below; petrographic descriptions are given in Appendix 1. The analyses were carried out by X-ray fluorescence spectroscopy by technical staff at the Geology Departments of Imperial College (major and minor elements) and Bedford College (trace elements).

The samples are divided into four groups on the basis of the type and degree of hydrothermal alteration.

Unaltered rocks

NG 487. Llallagua, Salvadora stock. Quartz-lattice porphyry at the stock contact, 650 level, Siglo XX mine.

NG 35Ch. Colquechaca, outcrop south of Cerro Hermosa.

Quartz-lattice porphyry (lava)

NG 75. Kari-Kari pluton, outcrop near Lago Chalviri, Potosi.

Dacite porphyry with partial chloritization of biotite.

NG 150. Tatasi volcanic complex, outcrop on lava flow near the north edge of the complex. Quartz-lattice porphyry.

Sericitized rocks (tourmaline subordinate).

NG 93. Cerro Rico stock, Potosi. Intensely sericitized quartz-porphyry with disseminated pyrite, and very minor tourmaline. Pailaviri Mine, level 0.

NG 123. Chorolque, outcrop above Santa Barbara, on the southwest flank of the Cerro. Intensely sericitized quartz-porphyry (extrusive) with minor tourmaline.

NG 62. Colquechaca, outcrop near Mina Santa Barbara, Yanakaka. Intensely sericitized quartz-porphyry (extrusive), with very minor tourmaline.

NG 38. Llallagua, Salvadora stock. Intensely altered quartz-porphyry, sericite to tourmaline ratio approaching 1 : 1. Catavi mine, level 383.

Tourmaline-sericite altered rocks (tourmaline predominant).

NG 488. Llallagua, Salvadora stock. Intensely altered quartz-porphyry. Tourmaline (fine-grained, almost colourless) is predominant alteration product (with lesser

sericite). Catavi mine, 650 level.

NG 482. Llallagua, Salvadora stock, intensely altered quartz-porphyry, as above. Catavi mine, 650 level.

NG 255. Chorolque, Chimborazo adit, in the contact region between vent rock and flanking extrusives. Intensely altered (tourmaline, sericite, clay) quartz-porphyry.

Quartz-tourmaline alteration.

NG 250. Chorolque, Chimborazo adit. Intensely altered quartz-porphyry breccia of the central vent.

NG 243. Chorolque, Fiero Unu adit. As above.

NG 494. Llallagua, Salvadora stock. "Black dyke" (quartz-tourmaline rock). Catavi Mine, 650 level.

C. Results.

The analytical data for major and minor elements are shown in Table 1. They confirm the quartz-late character of the unaltered rocks from the mineralized eruptive complexes (NG 487, NG 35CH, NG 150). NG 75 is a distinctly more calcic rock, of dacitic composition. It is probably typical of the rocks of the Kari-Kari pluton, which has little significant mineralization associated with it. The unaltered rocks are of sub-alkaline character (calc-alkali series) as defined by Irvine and Baragar (1971). The most notable feature of their major element chemistry is the high alkali content, especially potassium. They are distinctly more potassic than most similar rocks from island arcs and active continental margins, including rocks of similar  $\text{SiO}_2$  content from the Western Cordillera (Myashiro, 1974;

TABLE 1. ALTERED AND UNALTERED ROCKS, MAJOR AND MINOR ELEMENTS

(Weight Percent)

	NG487	NG35CH	NG75	NG150	NG93	NG123	NG62	NG38	NG488	NG482	NG255	NG250	NG243	NG494
SiO <sub>2</sub>	69.35	65.65	61.30	69.80	71.2	74.15	75.7	74.51	75.4	70.51	70.37	70.95	69.55	74.18
TiO <sub>2</sub>	0.51	0.6	0.33	0.49	0.34	0.54	0.6	0.54	0.49	0.5	0.54	0.51	0.48	0.59
Al <sub>2</sub> O <sub>3</sub>	15.15	16.1	19.5	14.95	14.2	15.9	16.41	14.84	14.53	16.01	13.77	13.1	14.95	13.02
Fe <sub>2</sub> O <sub>3</sub>	3.3	3.3	4.05	3.55	5.1	1.44	1.3	1.71	1.43	2.88	3.55	4.1	3.67	2.8
MnO	0.04	0.1	0.04	0.03	0.01	0.01	0.01	0.01	0.01	0.01	0.01	0.01	0.01	0.01
MgO	1.0	1.45	1.05	0.85	0.35	0.82	0.35	0.72	1.02	1.61	0.92	2.16	2.38	1.95
CaO	1.1	1.1	4.2	1.85	0.05	0.03	0.01	0.09	0.05	0.09	0.1	0.31	0.3	0.16
Na <sub>2</sub> O	2.8	3.2	3.0	2.2	0.18	0.22	0.22	0.22	0.22	0.22	0.09	0.18	0.18	0.13
K <sub>2</sub> O	5.0	6.45	4.75	5.80	3.85	4.6	4.94	3.48	3.18	1.72	1.68	0.12	0.1	0.05
P <sub>2</sub> O <sub>5</sub>	0.24	0.3	0.3	0.19	0.31	0.06	0.05	0.19	0.17	0.3	0.18	0.16	0.11	0.11
LOI	1.3	1.13	0.74	0.87	4.46	2.23	2.26	1.8	2.26	1.4	3.83	1.8	1.27	0.57
Total	99.79	99.38	99.27	100.6	100.1	100	102.1	98.11	98.76	95.25	95.04	93.4	93.0	93.57

Means of duplicate analyses by X-ray fluorescence, Geology Dept., Imperial College.

Fig. 2.16). A high potash content is characteristic of 'Andean-type' continental margin volcanics (Jakes and White, 1971, 1972). The particularly high  $K_2O$  content of these rocks is consistent with their position on the inner (continental) side of the orogen, and is in keeping with the results of Clark et al., (1976) who found a progressive increase in the potash content of rocks of similar  $SiO_2$  content along a transect across the Andes from the coast to the Eastern Cordillera at latitude 26 to 29 degrees south, i.e., south of the termination of the tin belt. This progressive increase in  $K_2O$  content of igneous rocks away from the position of the trench has been interpreted as reflecting a progressively deeper level of magma generation along a Benioff zone (Dickinson and Hatherton, 1967). However, the extent to which these magmas are affected by, or are the product of crustal melting is still an open question. At present there are insufficient chemical, and no isotopic data with which to begin evaluating it.

Some trace elements were determined on these rocks and the results are shown in Table 2. The most interesting feature is the high Rb level, which results in low K/Rb ratios. Ratios of less than 150 are characteristic of highly differentiated granitic and pegmatitic magmas (Taylor, 1965), and are commonly found in acid igneous rocks associated with tin deposits (Groves, 1972; Tischendorf, 1977). However, the Sr abundance, Rb/Sr, and Ca/Sr ratios are unexceptional for rocks of this composition, and although less sensitive as indicators, do not suggest particularly extreme fractionation.



FIG. 2.16. ALKALI - SILICA DIAGRAMS  
UNALTERED ROCKS

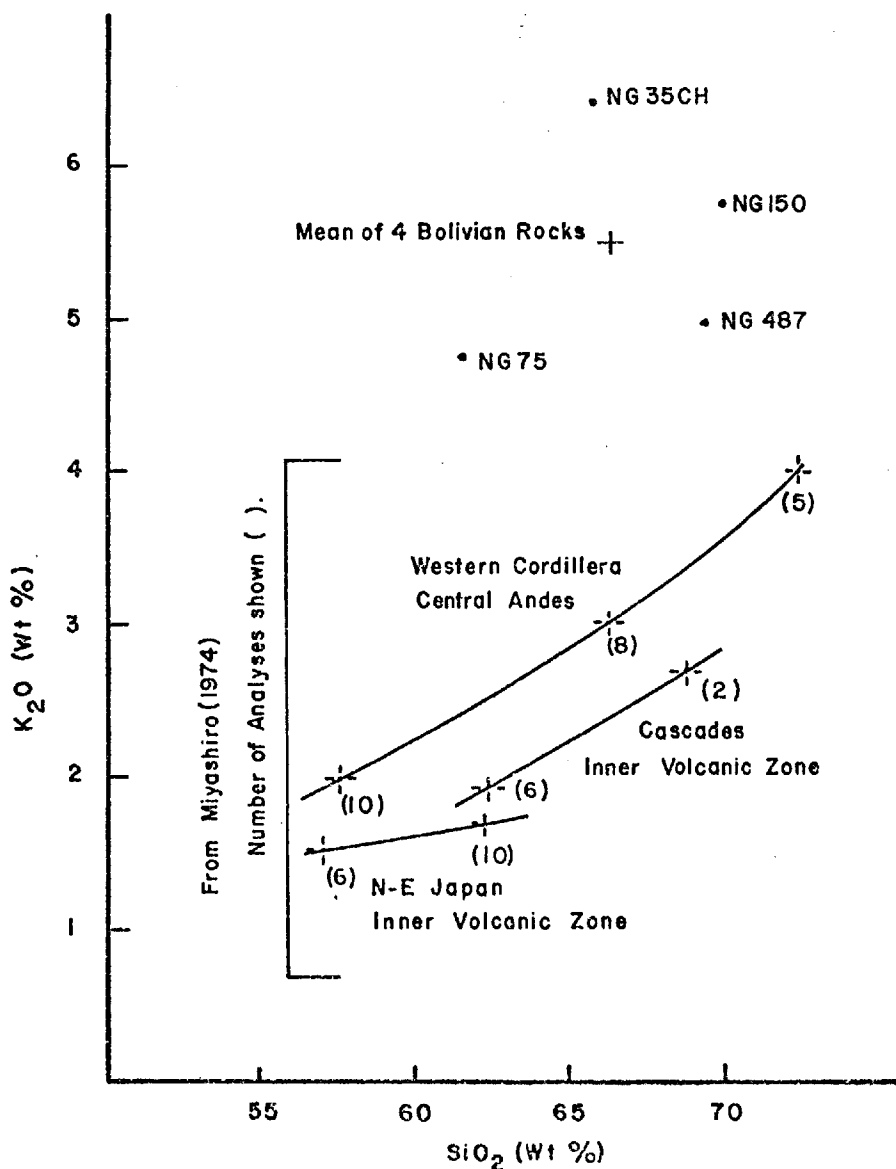
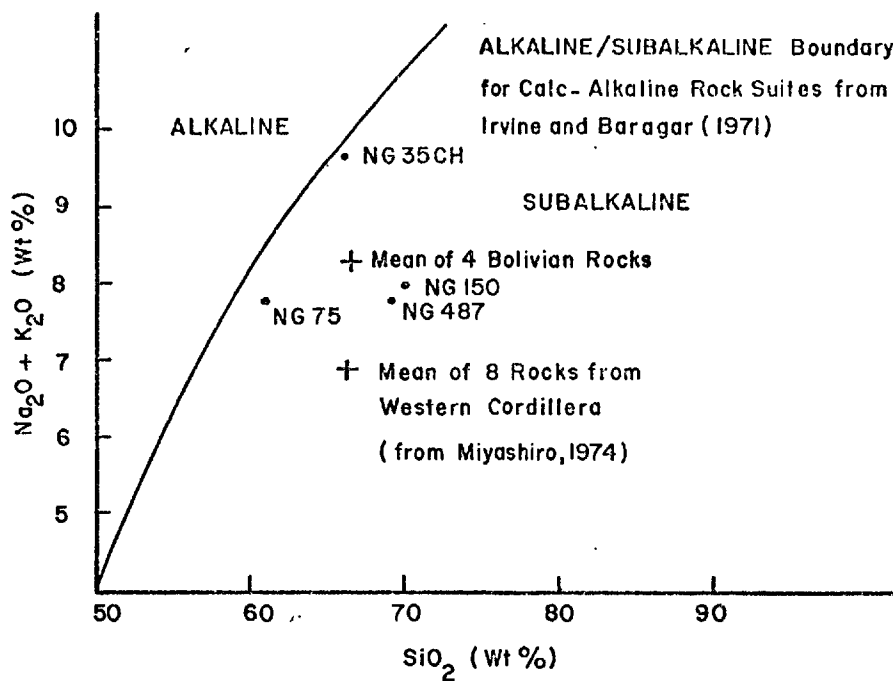


TABLE 2. ALTERED AND UNALTERED ROCKS, TRACE ELEMENTS  
(in ppm)

	NG487	NG35CH	NG75	NG150	NG93	NG123	NG62	NG38	NG488	NG482	NG255	NG250	NG243	NG494
Nb	14	38	35	13	27	17	35	16	16	15	17	20	13	14
Y	17	18	30	22	17	16	4	12	10	17	33	65	12	11
Sr	366	294	588	252	150	12	6	45	17	39	66	28	36	41
Rb	287	309	215	366	380	393	489	307	218	93	51	2	2	4
Zr	141	180	279	135	116	151	201	171	160	150	163	145	152	292
Ti	3447	3609	4035	3369	2175	3370	3170	3061	3200	3244	3750	3633	3423	4294
K/Rb	145	173	215	131										
Rb/Sr	0.78	1.05	0.36	1.45										
Ca/Sr	21	27	51	52										

Means of duplicate analyses by X-ray fluorescence, Geology Dept., Bedford College.

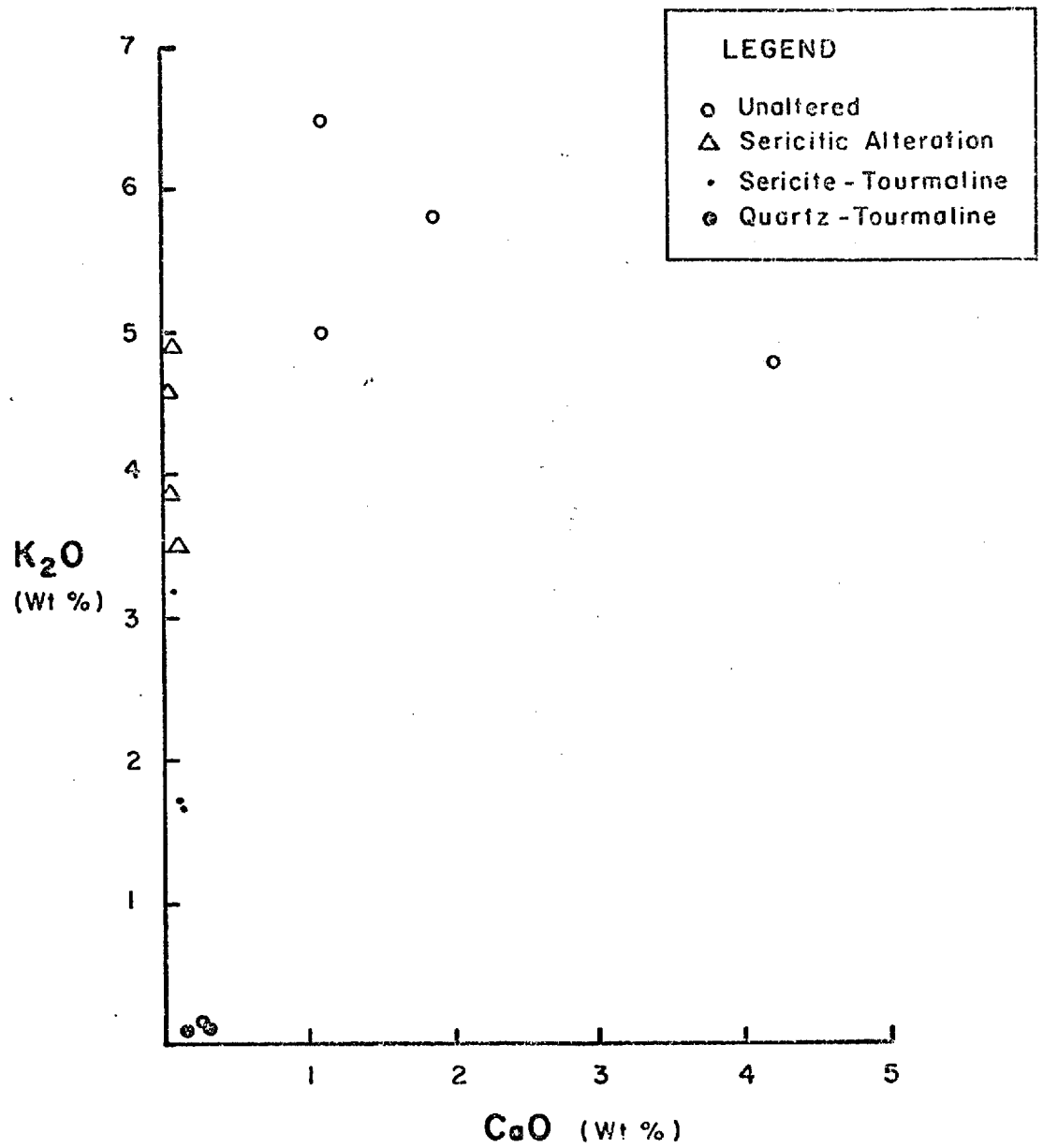
The data obtained in this study are insufficient for a detailed discussion of the petrochemistry.

As discussed above, the hydrothermal alteration of these rocks can, in a general way, be considered to form a continuous progression of increasing mineralogical and textural change. The full sequence is not necessarily developed within a given hydrothermal system, and there are some important differences in the predominant types of alteration developed at different complexes. The generalized sequence of increasing intensity is from chloritic, through sericitic, tourmaline-sericite to quartz-tourmaline assemblages. The fluid inclusion data reported in Chapter 3 suggests that these assemblages were formed at progressively higher temperatures.

The whole-rock analytical data indicate the major chemical changes which accompanied alteration. Most marked is the progressive depletion of Ca, Na, and K. The total  $\text{SiO}_2$  level remains within a fairly narrow range (60-75%) and shows little systematic variation. Plots of  $\text{SiO}_2$  against Mg, Na, and K illustrate the progressive changes (Fig. 2.17). Chloritic and argillic alteration types were not analysed. With sericitic alteration there is an almost complete loss of Ca (Fig. 2.18) and Na, with only partial loss of K. This clearly reflects the early breakdown of plagioclase. With increasing intensity of alteration to the tourmaline-sericite assemblage, the potassium level is further reduced. The quartz-tourmaline assemblage is characterized by almost complete loss of Ca, Na, and K, with a distinct relative enrichment in Mg.



FIG. 2.18. K/Ca VARIATION  
ALTERED AND UNALTERED ROCKS



The ternary indices ACF and AKF were calculated for all rocks from the molecular amounts. Only total iron was determined and is expressed as  $\text{Fe}_2\text{O}_3$  for these calculations. While this is not in keeping with normal petrological methods, the indices are used here purely to illustrate the relative chemical changes which accompanied alteration. They were calculated as follows:

$$\begin{aligned} \text{for ACF,} \quad A &= \text{Al}_2\text{O}_3 - (\text{Na}_2\text{O} + \text{K}_2\text{O}) \\ C &= \text{CaO} \\ F &= \text{MgO} + \text{FeO} + \text{MnO} + 2\text{Fe}_2\text{O}_3 - \text{TiO}_2 \end{aligned}$$

$$\begin{aligned} \text{for AKF,} \quad A &= \text{Al}_2\text{O}_3 - (\text{CaO} + \text{Na}_2\text{O} + \text{K}_2\text{O}) \\ K &= \text{K}_2\text{O} \\ F &= \text{FeO} + \text{MnO} + \text{MgO} + 2\text{Fe}_2\text{O}_3 - \text{TiO}_2 \end{aligned}$$

They are plotted in Figs. 2.19 and 2.20. These indices were originally designed for the study of metamorphic rocks (Barth, 1952). Their application to hydrothermally altered rocks, and the development of the concept of equilibrium 'facies' of hydrothermal alteration in acid to intermediate igneous rocks has been discussed by Creasy (1959), Burnham (1962), Hemley and Jones (1964), and Meyer and Hemley (1967). As with metamorphic rocks, facies of hydrothermal alteration can be theoretically defined by pressure-temperature conditions, and are characterized by particular secondary mineral assemblages and chemistry. In the case of the Bolivian rocks, the ACF and AKF diagrams illustrate a distinctive relative enrichment in alumina and loss in K, Na and Ca with both sericitic and quartz-tourmaline alteration; this is characteristic of sericitic and argillic

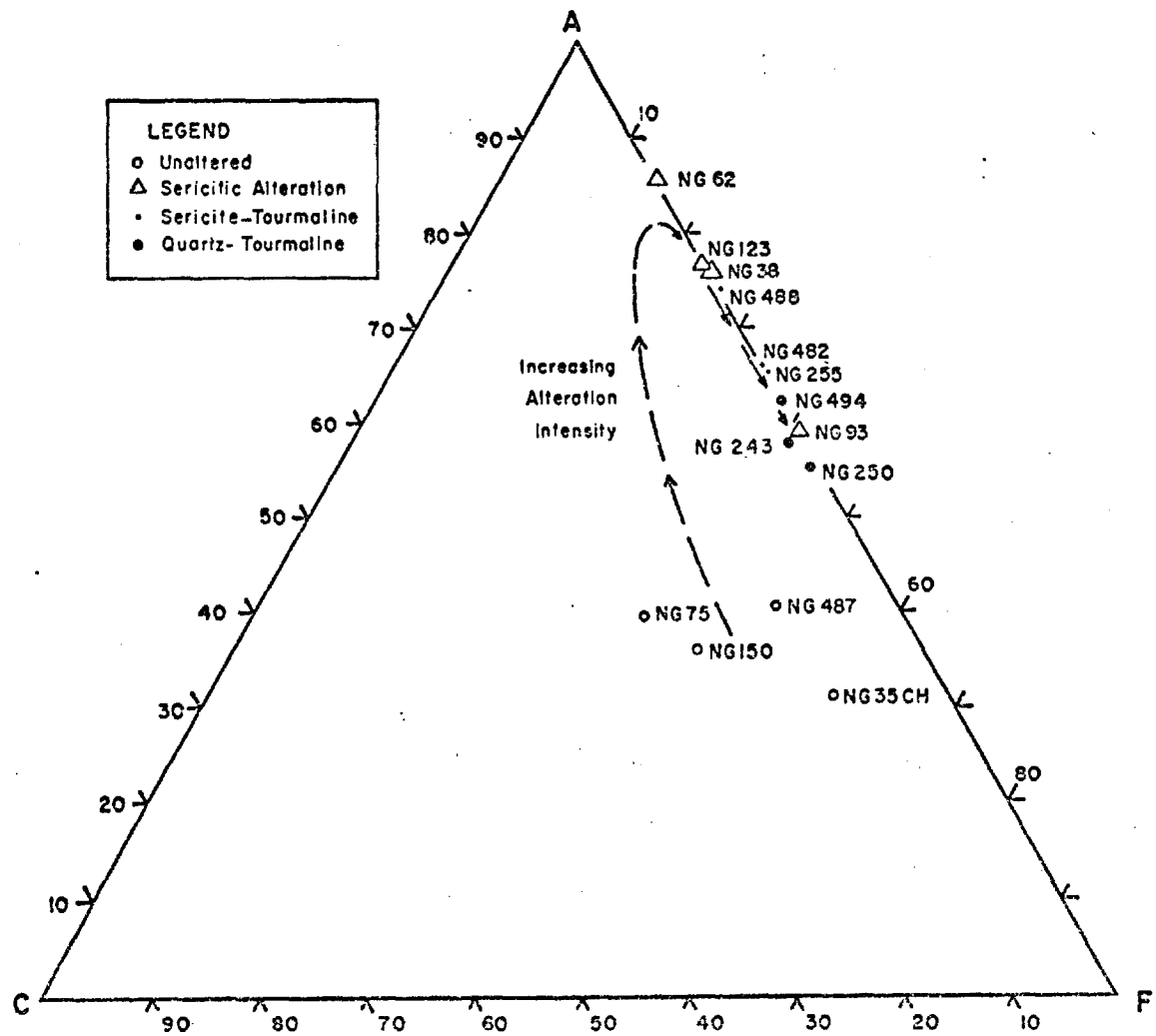
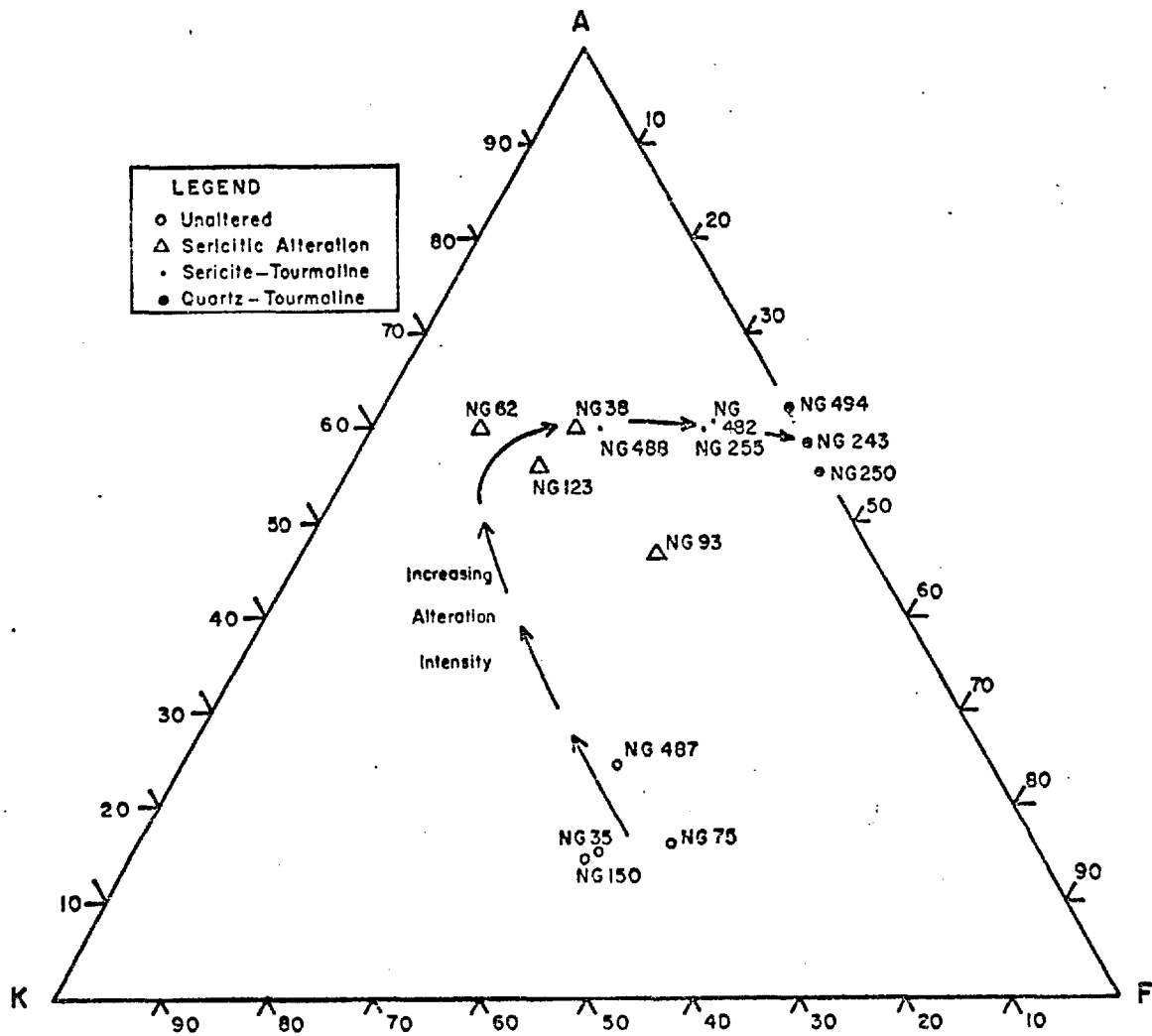


FIG. 2.19. ACF DIAGRAM ALTERED AND UNALTERED ROCKS





alteration assemblages. In hydrothermal systems it is probably unusual for stable equilibrium to be attained, or maintained, since such systems are liable to rapidly fluctuating conditions. Thus the concept of facies of hydrothermal alteration is of limited value, and it is generally better, as has been done here, to discuss alteration in terms of mineral assemblages without any connotation of equilibrium facies. The ACF and AKF diagrams are used here purely to illustrate the composition of the rocks of the different alteration types, and the progressive changes which have taken place with increasing intensity of alteration.

In the Bolivian sub-volcanic eruptive complexes, disseminated tin and base-metal sulphide mineralization (porphyry tin mineralization) is most closely associated with sericitization, and not with the more chemically, mineralogically, and texturally extreme quartz-tourmaline alteration. Uncertainties regarding the stability range of tourmaline and its general significance in alteration assemblages of this type make it difficult to evaluate the overall chemical environment throughout these hydrothermal systems. Sericitization of acid igneous rocks involves hydrogen metasomatism. For the sericitization of K-feldspar the reaction can be written as follows (Meyer and Hemley, 1967)



This implies low pH conditions in the zone of sericitic alteration and mineral deposition. In the porphyry copper

deposits sericitic alteration is also coincident with maximum sulphide deposition (e.g., Lowell and Guilbert, 1970). The inner and deeper zones are characterized by feldspar-stable potassic alteration which took place under conditions of high temperature and near-neutral or slightly alkaline pH (Meyer and Hemley, 1967; Rose, 1970). Thus the outward and upward zonation typically displayed by these deposits, from a low sulphide potassic alteration zone to a high sulphide sericitic alteration zone, reflects decreasing temperature, pH, and  $K^+$  activity. In the Bolivian deposits, the fluid inclusion data discussed in Chapter 3 indicates that the temperature, pressure, and fluid salinity in the inner and deeper zones is closely similar to the inner zones of the porphyry copper deposits. Some aspects of the hydrothermal fluid chemistry are also similar (high K, Na, Cl). Since the data of Smith (1949) indicates that tourmaline is unstable except at near neutral pH at high temperatures, it might be concluded that the quartz-tourmaline alteration in the Bolivian deposits is equivalent to the potassic alteration in the porphyry copper deposits, and that a marked outward decline in both temperature and pH took place and were important in controlling the deposition of disseminated tin and base-metal sulphides, and the development of associated sericitic alteration. However, the complete breakdown of feldspar and the intense leaching of alkalis from the quartz-tourmaline rock suggests that the two systems are not directly comparable. Conditions of alteration may have been relatively acid in the quartz-tourmaline zones, and as illustrated by the ACF and AKF plots, this alteration type may in fact be equivalent to argillic

alteration at high temperature and with high boron activity (Meyer and Hemley, 1967).

#### D. Semi-quantitative analyses

Most of the rocks collected for K-Ar dating, plus a number of other typical altered rocks, were analysed semi-quantitatively by Direct Reading Emission Spectroscopy for the following elements; Cu, Pb, Zn, Ag, Sn, Ti, Ca, Sr, Ba, K, Li, As, Bi, W. The samples can be divided into 3 groups; unaltered (12 samples), sericitized (20 samples), and quartz-tourmalinized (7 samples). The results further illustrate the chemical changes associated with alteration discussed above, and illustrate the general levels and associations of the ore metals in the unaltered and altered rocks. The number of quartz-tourmalinized rocks is small, and almost all come from the same general location (the Chorolque vent). The others come from a number of widely scattered locations throughout the southern tin belt, and comprise a reasonably representative sample of the unaltered and sericitized rocks typical of the mineralized eruptive complexes, although the unaltered group is somewhat biased by a high proportion of samples from the Kari-Kari pluton.

The arithmetic mean values of the elements are shown, for each group, in Table 3. The tin value of the unaltered group (15 ppm) is within the range usually considered to be characteristic of geochemically specialized 'tin-granites' (e.g.,  $30 \pm 15$  ppm, Tischendorf, 1977). The lithium content (153 ppm) is also characteristically high. The data for the major elements are comparable to those of the whole-rock analyses discussed above.

TABLE 3

SEMI-QUANTITATIVE ANALYSES, ALTERED AND UNALTERED ROCKS  
(Mean values in ppm)

	UNALTERED (12)	SERICITIC (20)	QUARTZ-TOURMALINE (7)
Cu	12.9	78.7	243
Pb	26.4	194	67
Zn	112.1	381	136
Ag	0.17	5.8	5.2
Sn	15.0	993	512
Tl	4080	3314	2996
Ca(%)	1.93	0.43	0.6
Sr	425	65	36
Ba	698	252	32
K(%)	4.74	3.26	0.71
Li	153	52	0.4
As	24.0	1033	12330
Bi	1.2	6.1	26

The most important feature is the much higher ore-metal content of the altered rocks. Almost all sericitized rocks in the eruptive complexes contain at least some visible disseminated sulphide mineralization, so the high metal levels in the sericitized groups are not surprising. The metal associations are characteristic of the ores of the region ; tin shows a distinct correlation with silver in particular (Fig. 2.21), its relationship with zinc (and the other base-metals) is less clear (Fig. 2.22). Tungsten was below the detection limit (10 ppm) in all samples. Arsenic and bismuth are well correlated with the other metals in the unaltered rocks, but the data for these elements in the altered rocks are unreliable; there are numerous erratic high values, and the analytical uncertainty is very high.

FIG. 2.21. Sn/Ag VARIATION  
 ALTERED AND UNALTERED ROCKS  
 (Semi-Quantitative Analyses)

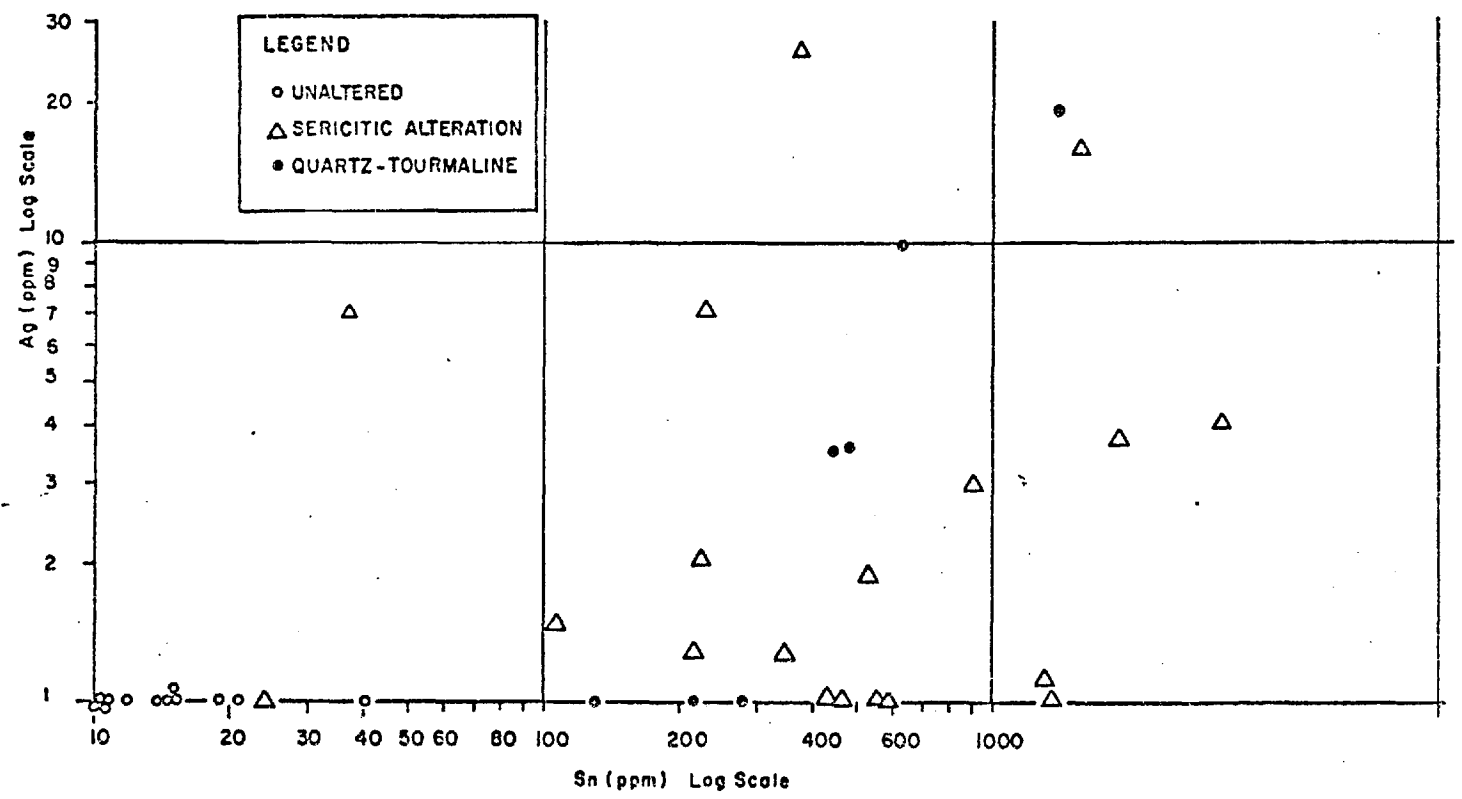
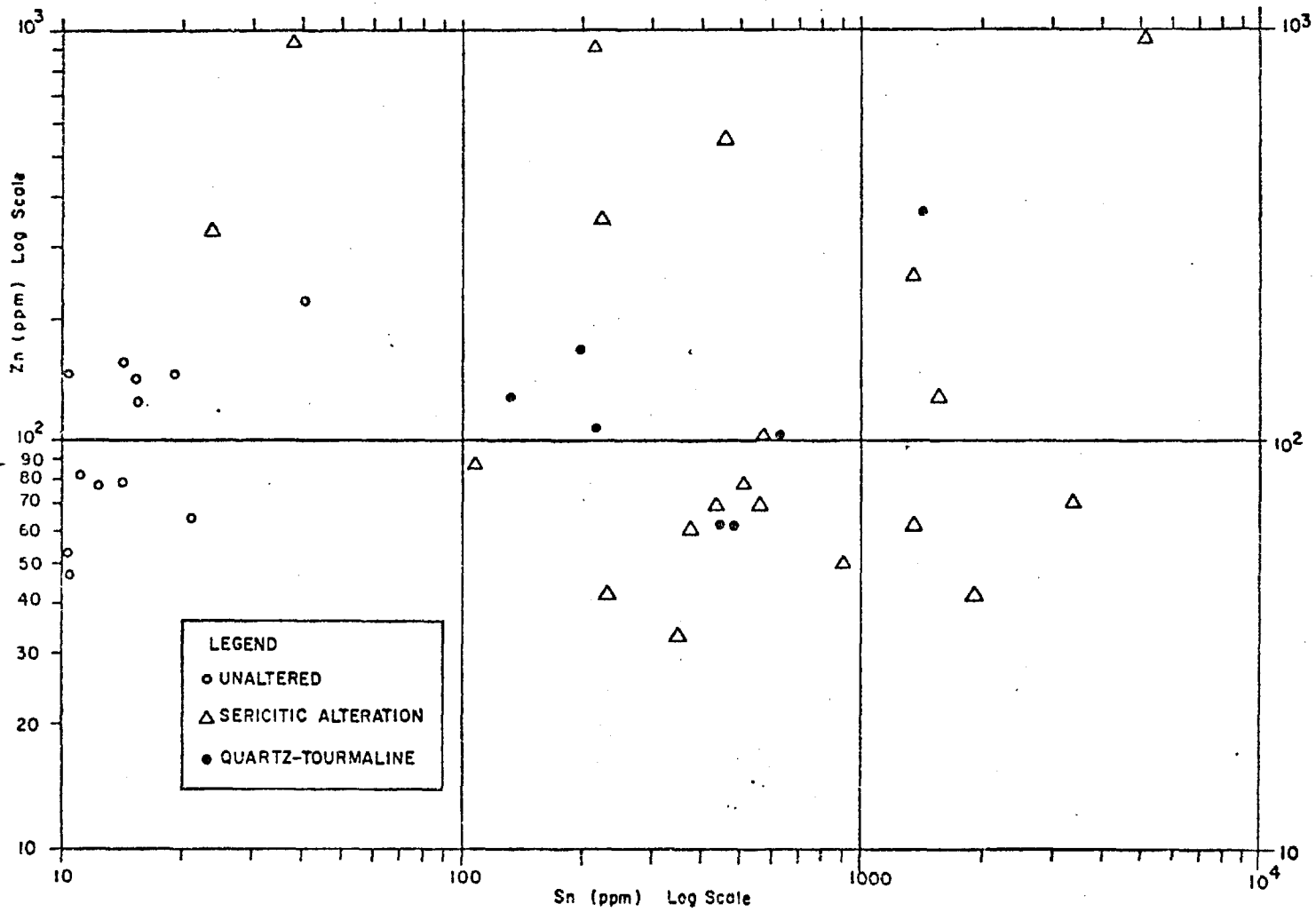


FIG. 2.22. Sn/Zn VARIATION  
 ALTERED AND UNALTERED ROCKS  
 (Semi-Quantitative Analyses)



## CHAPTER 3

FLUID INCLUSION STUDIES3.1. Introduction

The objective of this fluid inclusion study was to provide data on the evolution of the hydrothermal systems which formed the deposits, in terms of the temperature, salinity, and if possible of the chemistry of the ore fluids. The data can be combined with the observed geological features, in particular the distribution of alteration types, the relationship between pervasive alteration and the vein systems, and the zonation and paragenesis of mineral assemblages, and in this way a more complete conceptual model of the overall development of the deposits can be constructed.

The data are also useful in trying to gain a better understanding of the physical and chemical mechanisms of tin transport and deposition in hydrothermal systems.

A previous fluid inclusion study of several Bolivian deposits was made by Kelly and Turneaure (1970). Their work provides an extremely useful survey of the general conditions of temperature and fluid salinity under which the ores have formed. They outlined the range of temperature over which cassiterite was deposited, and the typical decline in fluid temperature and salinity which accompanied the paragenetic sequence of mineral deposition in the vein ores. However, their work was concerned mainly with the tin-tungsten deposits of the northern part of the province, and apart from a few samples from Llallagua, they did not study any of the deposits



discussed here, nor did they attempt to make a comprehensive study of any individual deposit.

### 3.2. Principles of Fluid Inclusion Study

The earliest fluid inclusion studies were made in the 19<sup>th</sup> century. Probably most important was the work of Sorby (1858). He recognized the potential importance of fluid inclusions as a means of studying the thermal and chemical environment of formation of some rocks and ores. He made a number of important experiments which showed that the liquid in fluid inclusions in minerals from veins was an aqueous solution, and that the inclusion fluids in vein quartz, and quartz from granites, contained dissolved sodium and potassium chlorides and sulphates. He described fluid inclusions containing daughter minerals in nepheline from the lavas of Vesuvius. He also deduced that the vapour bubbles normally seen in the inclusions are the result of differential contraction of the fluid and host mineral, and thus that fluid inclusions could be used as geothermometers, and he performed homogenization experiments to obtain information on the formation temperatures of minerals.

Despite this early interest, advances in the study of fluid inclusions proceeded slowly until the 1950's. Since that time there has been an enormous increase in inclusion studies, particularly in the U.S.A. and the U.S.S.R. The method has been applied to a wide range of problems in the geology of ore deposits, petrology, and metamorphic geology, and there is a vast literature on the subject. By far the greatest area of application has been in the study of ore deposits, especially the hydrothermal ore systems. There has been considerable

scepticism in the past (e.g., Krauskopf, 1967) about the validity of the method. However, it is now generally accepted that given suitable material, and allowing for certain fundamental uncertainties, reliable information can be obtained on the temperature and salinity of ore-forming fluids, as well as data on their chemical and isotopic composition. The method is by no means generally applicable to the study of all types of ore deposit, and even with suitable material there are several important areas of uncertainty. The basic principles have previously been described in detail (Roedder, 1967; Smith, 1953; Yermakov, 1965; Deicha, 1955). The most important concepts and areas of uncertainty which bear on the interpretation of fluid inclusion data from ore deposits are discussed briefly below.

#### 3.2.1. Mechanisms of trapping of primary inclusions

Primary fluid inclusions are those which were formed at the time of crystallization of the surrounding portion of the host mineral. The assumption that they represent trapped portions of the fluid from which the mineral grew is fundamental to inclusion studies. Ideally, only primary inclusions would be used in inclusion studies, but this is often not possible. The mechanisms by which primary inclusions are trapped are not well understood, though some important laboratory studies have been done on artificial crystals (Brooks, et al., 1968).

The essential condition which is required for inclusion formation is irregular growth, resulting in depressions and cavities in the crystal face which become sealed over by subsequent growth, trapping a portion of the fluid. This is a

normal condition in natural systems rather than an exceptional one, and natural crystals probably always contain primary inclusions, although they may be sub-microscopic in size (Roedder, 1967). Among the more important probable causes of growth irregularity are : periods of rapid crystal growth, perhaps caused by changes in the degree of supersaturation or rate of flow of the fluid; starvation of nutrient at certain points due to the flow patterns; and changes in the fluid composition. It has been shown ( Shlichta, 1968; Buckley, 1951) that even very minor changes in the trace metal content of fluids can affect the trapping of inclusions in artificially grown crystals. Solid particles can also interfere with growth by starving the crystal face of nutrient at the point of contact, thus producing a cavity if later moved away. Primary inclusions may also be trapped where the growing faces of adjacent crystals intersect.

If the fluid from which a crystal is growing is not homogeneous, the individual primary inclusions may not accurately represent the characteristics of the total fluid. This may be the case, for example, in a boiling fluid, or a fluid containing an immiscible phase such as liquid hydrocarbon in an aqueous hydrothermal fluid, or aqueous saline brines in silicate magma (Roedder, 1967; Roedder and Coombs, 1967). The case of boiling fluids is discussed further below.

### 3.2.2. The distinction between primary, secondary and pseudo-secondary inclusions

Secondary inclusions are those which are formed at some time

after the growth of the mineral grain. They are most commonly formed when a mineral is fractured. Fluid can move into the crack and become trapped during healing of the fracture. With time the irregular portion of fluid trapped in this way will normally become separated into a series of more regularly shaped inclusions which mark the original plane of the fracture. Secondary inclusions may have formed at any time after the crystallization of the mineral, and the physical and chemical conditions of the fluid which fills them may have been radically different from those of the fluid from which the mineral grew. They are therefore not reliable as indicators of the conditions under which the host mineral crystallized. Under some circumstances they may be useful as indicators of the conditions under which secondary changes, such as hydrothermal alteration, have taken place. However extreme care is necessary in attempting to relate secondary inclusions to any given geological event.

Pseudo-secondary inclusions are those which have formed in the same way as secondary ones, i.e., by the filling and rehealing of fractures in the mineral, but they formed before the growth of the mineral was completed. The fracture was sealed off as crystal growth continued, leaving an isolated plane of inclusions which does not extend to the edge of the mineral grain. Clearly these inclusions do give reliable information about a certain stage in the growth of the mineral, although conditions at that stage may have been quite different from those under which the earlier and later-formed parts of the mineral grew.

The distinction between primary, pseudo-secondary and

secondary inclusions can be difficult to make. Numerous criteria have been cited in the literature by which primary inclusions can be identified. These include: large size, regular 'negative crystal' shape, occurrence in free-growing well formed crystals, isolated random distribution, and localization on crystal growth zones. Of these, only the last two are now considered valid (Roedder, 1967). The most useful criteria is the localization of inclusions along recognizable growth zones. This is often applicable in minerals which show a colour zonation along the growth direction, such as some cassiterite, sphalerite and fluorite. However in colourless unzoned minerals it is much more difficult to apply. In such cases negative evidence must be used, and relatively large isolated inclusions which show no planar distribution are generally taken as being of primary origin, while secondary inclusions are easily recognizable because of their planar distribution. Pseudo-secondary inclusions can only dependably be recognized if the planar group can be seen to be truncated by a growth zone. Such positive evidence is generally lacking, but most groups of inclusions which seem to mark healed cleavage planes, and fracture surfaces which do not reach the edge of the mineral grain, are judged to be pseudo-secondary (Roedder, *op. cit.*). The validity of this is borne out by the close correspondence of, for example, the homogenization temperatures of such inclusions with those of others which are judged to be primary.

It can be seen from the above discussion that one of the most fundamental aspects of a fluid inclusion study is dependent on subjective judgement. Each sample or type of sample must be

evaluated on its own merits. Reliable results can only be obtained from the careful study of a rather large amount of material from a given sample. The problem of distinguishing inclusion types is discussed further below in the context of the individual deposits.

### 3.2.3. Leakage and other changes since trapping

Fluid inclusions can leak. Experiments have shown that fluid can be moved both in and out by large pressure gradients (Kennedy, 1950a; Skinner, 1953; McCulloch, 1959). Leakage can result from deformation of the host minerals, both natural in-situ deformation and also that produced during sample preparation procedures. Leakage during homogenization experiments in the heating stage is not uncommon, as a result of strain due to thermal expansion of the host mineral, and especially when there is differential expansion in non-homogeneous mineral samples. In the past the evidence that fluid inclusions can leak has been used as an argument with which to discount the reliability of inclusion studies as a whole. This argument can be rejected. There is considerable evidence that leakage is the exception rather than the rule. The whole question has been discussed in detail by Roedder (1967), and Roedder and Skinner (1968). The main arguments which can be used to show that leakage is not a common phenomenon include the following :

a) the frequently observed systematic relationship between crystal zoning and the temperature and salinity of primary inclusions.

b) Pressure estimates of the contents of inclusions (from

crushing experiments; Roedder, 1967). These often show low pressures in the inclusions even though the host minerals have been under high hydrostatic pressures for millions of years since formation. Conversely, inclusions with high CO<sub>2</sub> pressures are found in minerals which have been at near atmospheric pressure for millions of years.

c) The constancy of phase ratios among a given set of inclusions: leakage will affect the volume ratio of the contraction vapour bubble and liquid. If the ratio is the same for all inclusions of a given generation and type within a mineral, then either leakage affected all of them equally (most unlikely) or no leakage has occurred. This is one of the most important criteria for identifying leakage. It can often be observed that the phase ratios of a group of inclusions are different in those which are very close to the surface of a polished sample, indicating that leakage has taken place during preparation.

d) Experimental evidence that repeated heating to temperatures well above the homogenization temperature does not result in a progressive change in that temperature (Roedder and Skinner, 1968).

It can be concluded that while leakage can and does occur, it can usually be recognized as having taken place. Evidence for natural leakage or leakage induced during sample preparation can usually be evaluated by careful study of the inclusion assemblage in a given sample. Duplication of heating and freezing runs will normally show if leakage has taken place during the experiment. Above all, conclusions must be

drawn from multiple measurements which give consistent results.

The slow diffusion of material directly through the crystal is a more difficult problem to evaluate. There is evidence that hydrogen in particular can diffuse through quartz. This could be a problem with respect to the use of D/H isotope ratios as indicators of fluid origin, because of the probable kinetic isotope fractionation which would result. Hydrogen diffusion could also result in changes in the oxidation state of the fluid after trapping (Roedder, 1972b).

In addition to leakage, a number of other changes can affect inclusions after trapping which may have important consequences for their use in geological studies. The most important of these is necking down, the process by which a single larger inclusion becomes divided up into a series of smaller ones by the process of solution and recrystallization of the walls of the original inclusion (Roedder, 1967). If necking down takes place while the fluid is homogeneous, it will result in no effect on the individual inclusions formed, but if any phase change took place in the original inclusion before necking, such as formation of a contraction vapour bubble, or crystallization of daughter salt, then the homogenization behaviour and composition of the resulting individual inclusions will be changed, and they will give anomalous results. Fortunately inclusions which have been formed by necking of larger inclusions are generally easily recognized. They show non-uniform phase ratios, and characteristic 'tailed off' shapes (Plate 18). Relicts of the fine tubes which once



connected them are often visible. Stranded daughter minerals may be found where high salinity inclusions have necked. The phenomenon of necking seems to be particularly common with inclusions which formed at high temperatures.

#### 3.2.4. Temperature-pressure relationships and the homogenization method of microthermometry

Except in certain particular cases, it is assumed that the contents of fluid inclusions comprised a single homogeneous phase at the time of trapping, that the volume of the inclusion cavity has remained unchanged, and that there was no leakage into or out of the inclusion over geological time and also during sample preparation and experimental heating and cooling. Provided that these assumptions are correct, the physical behaviour of the trapped material during both geological and experimental cooling and reheating depends on the prevailing temperature, the pressure-temperature conditions of trapping, and the composition of the fluid.

Natural fluids of the type trapped in inclusions in minerals of hydrothermal deposits are aqueous solutions containing various concentrations of dissolved salts and gases, the most common of which are NaCl, KCl and CO<sub>2</sub>. Since the overall chemical composition is often unknown or only partly known, the behaviour of trapped inclusion fluids has to be interpreted by reference to certain simple systems whose pressure-temperature-volume relationships are well known experimentally, and whose composition is judged to most closely approximate that of the inclusion fluid under study. In practice there are probably often wide discrepancies between the actual composition of an inclusion

fluid and the composition of the system to which it is referred. However, until more experimental data become available for the behaviour of complex fluids, and until routine analysis of inclusion fluids becomes possible, this situation cannot be resolved. The systems most commonly referred to are :  $H_2O$  (Kennedy, 1950b);  $H_2O - NaCl$  (Lemmlein and Klevtsov, 1961; Sourirajan and Kennedy, 1962);  $CO_2$  (Kennedy, 1954);  $CO_2 - H_2O$  (Malinin, 1959; Khitarov, 1958; Takenouchi and Kennedy, 1964);  $CO_2 - H_2O - NaCl$  (Takenouchi and Kennedy, 1965).

In the case of the Bolivian deposits, no  $CO_2$ -bearing inclusions have been found and the behaviour of the inclusions studied here is interpreted in terms of the system  $H_2O - NaCl$ , although it is clear that in many cases the actual composition of the inclusion fluids is a great deal more complex.

If a homogeneous fluid is trapped in an inclusion cavity above the 2-phase boundary for the system, its density will be controlled by its composition and the P-T conditions at trapping. During cooling, assuming constant volume, the density of the trapped fluid remains constant. As the temperature falls, the pressure inside the inclusion drops; the P-T conditions inside the inclusion follow a constant density path (isochore) until the 2-phase boundary is reached. The fluid then separates into two phases, usually liquid plus vapour, hence forming the familiar contraction vapour bubble which is found in most fluid inclusions.

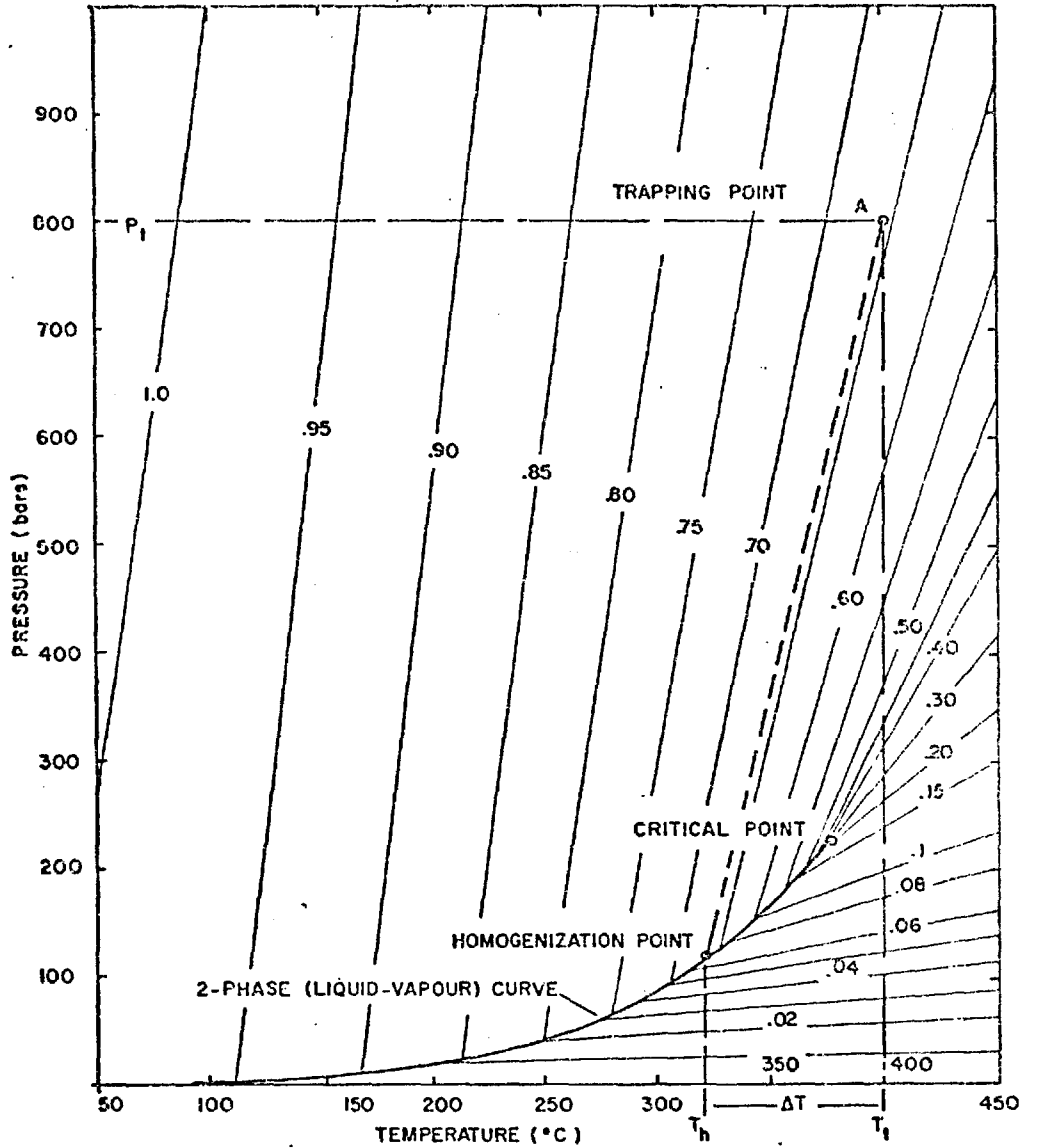
The fluid inclusion method of geothermometry involves reheating inclusions, and measuring the temperature at which the two phases merge into a single phase. This is known as the

homogenization temperature ( $T_h$ ). Homogenization can take place either by contraction and disappearance of the vapour bubble (liquid homogenization), expansion of the vapour bubble until the liquid phase disappears (vapour homogenization), or by sudden fading of the meniscus separating the two phases (critical homogenization). The type of homogenization which takes place depends on the density of the fluid when trapped, hence the degree of filling of the inclusion at room temperature (Roedder, 1967). In most hydrothermal ore systems liquid homogenization is by far the most common, although the other types are sometimes observed in high temperature low pressure deposits.

It is clear from these relationships that  $T_h$  is only equal to the temperature at which the inclusion was trapped ( $T_t$ ) if the P-T conditions of trapping lay on the 2-phase boundary. If the fluid was trapped above the boundary,  $T_t$  differs from  $T_h$  by an amount which is controlled by;  $T_t$ , the pressure under which the fluid was trapped ( $P_t$ ), and the composition of the fluid. This amount is called the pressure correction ( $\Delta T$ ) and it must be added to  $T_h$  to give the true formation temperature  $T_t$ . Thus  $T_h$  is always a minimum temperature for the formation of an inclusion except in the case noted above where the fluid was on the 2-phase boundary when trapped (Roedder, 1967; Ypma, 1963; Touret, 197<sup>7</sup>~~6~~).

The relationships are illustrated in Fig. 3.1 which is a P-T section of the P-V-T diagram for the system  $H_2O$  (Fisher, 1976). The P-T conditions inside an inclusion trapped in the 2-phase region (e.g., at point A where pressure =  $P_t$ , temperature =  $T_t$ ) will, on cooling, follow the appropriate isochore until

FIG.3.1



DENSITY CONTOURS (ISOCORES) ON P-T COORDINATES FOR PURE H<sub>2</sub>O (FROM FISHER, 1976). ILLUSTRATING THE PRESSURE CORRECTION REQUIREMENT FOR FLUID INCLUSIONS TRAPPED ABOVE THE 2-PHASE CURVE.

the 2-phase line is intersected. The temperature at this point is  $T_h$  and (ideally) the fluid will separate into two phases (liquid plus vapour). On further cooling, the P-T conditions follow the 2-phase boundary downward. In microthermometry, the inclusion is heated, the P-T conditions inside follow the 2-phase line upwards until it reaches the intersection of the isochore defined by its density when trapped. This is the homogenization point.  $T_h$  is always measured during heating as inclusions often exhibit phase metastability during cooling, so that phase separation may not actually occur until the temperature is well below  $T_h$ .

The pressure correction  $\Delta T$ , and hence  $T_t$ , can only be determined from  $T_h$  if  $P_t$  and the composition of the fluid can be established, and can reasonably be referred to a system for which the positions of the isochores have been determined.

The magnitude of the pressure correction can be very high. For the system NaCl-H<sub>2</sub>O the corrections have been determined by Lemmlein and Klevtsov (1961), and Potter (1977). The data show that the magnitude of  $\Delta T$  is highly sensitive to the salinity of the fluids at high temperature, though not at low temperature. In dilute fluids, for a given  $P_t$ ,  $\Delta T$  increases rapidly with increasing  $T_h$ , while in highly saline fluids it remains roughly constant. This is illustrated below by the data for 5 weight percent NaCl and 30 weight percent NaCl solutions with  $T_h = 200^\circ\text{C}$  and  $350^\circ\text{C}$ .

1) 5 wt % NaCl

$P_t$ (atm)	$\Delta T$ at $T_h = 200^\circ\text{C}$	$\Delta T$ at $T_h = 350^\circ\text{C}$
250	20	15

750	65	75
1250	105	140
2500	210	295
2) 30 wt % NaCl		
$P_t$ (atm)	$\Delta T$ at $T_h = 200^\circ\text{C}$	$\Delta T$ at $T_h = 350^\circ\text{C}$
250	20	15
750	65	65
750	65	65
1250	110	115
2500	215	235

The most important implications of the pressure correction data are, firstly: between-deposit comparisons of  $T_h$  data can only be meaningful if the pressure at the time of ore deposition can be established and  $\Delta T$  applied where necessary. Pressure corrections can usually be ignored in very shallow ore-forming environments. In the case of within-deposit comparisons it is clear that if the deposit covers a considerable vertical range (hence hydrostatic pressure range), corrections are needed for comparisons between  $T_h$  data for deep and shallow levels, and this is particularly so with dilute fluids giving high  $T_h$  values. Secondly, apparent  $T_h$  fluctuations could be produced by pressure fluctuations during ore deposition at constant temperature and salinity, and fluctuations in salinity could also lead to misinterpretation of  $T_h$  data if not recognized. The former case would be difficult to recognize, since direct evidence of pressure variations in hydrothermal systems is rarely available. It seems likely that considerable pressure fluctuations could take place in magmatic-hydrothermal systems at shallow

depth.

A final important point to be mentioned here is the situation in which the inclusion contents were not homogeneous at the time of trapping. This could arise where suspended solid material was being transported in the fluid, where droplets of an immiscible liquid were present, or where the fluid was boiling. The latter is the most important case in magmatic-hydrothermal deposits. Fluid boiling is now recognised as being a common phenomenon in many hydrothermal ore systems, and is particularly characteristic of the early stages of hydrothermal evolution in 'porphyry' type ore deposits (Roedder, 1977). It is discussed further in the context of the fluid inclusion data for the Chorolque deposit below. If two coexisting phases (liquid plus vapour) are trapped together in a single inclusion, the homogenization temperature will be too high by an amount which depends on the ratio of the actual phases trapped. This can clearly be highly variable, and the inclusion assemblage will give a range of  $T_h$  values, in which the minimum will most closely approach the true  $T_h$  value.

As discussed above, no pressure correction is required for a boiling fluid since the P-T conditions lay on the 2-phase boundary when the inclusions were trapped. If the fluid salinity can be determined, then the trapping pressure can be estimated from the data for the appropriate system. This is essentially the only way in which pressure can be directly estimated from inclusion data, thus the recognition of boiling conditions in an inclusion assemblage is very important. The fact that boiling has not taken place in a fluid of known salinity also places limits

on the minimum pressure at which inclusions must have been trapped (Haas, 1971).

### 3.2.5. Fluid salinity, depression of freezing point, and daughter minerals

The dissolved salt content of natural hydrothermal fluids varies widely, and is a very important factor in considerations of ore-transport and deposition. It is also necessary to be able to estimate the fluid salinity in order to be able to apply the pressure corrections to homogenization temperature data. Inclusion fluid salinity can be estimated by comparison with a simple system whose behavior has been determined experimentally. The system  $H_2O-NaCl$  is normally used since  $NaCl$  is the dominant salt present in most inclusion fluids (Roedder, 1972b). Inclusion fluid salinities are normally expressed as equivalent weight percent  $NaCl$ ; although there may be no direct evidence that the fluid is in fact essentially, or even approximately, an  $H_2O-NaCl$  solution. This introduces considerable uncertainty into fluid inclusion salinity data in some cases, which will only be resolved when analysis of inclusion fluids is routinely possible, and when more experimental data become available for complex systems.

The salinity of unsaturated inclusion fluids is estimated by measuring the freezing point in a microscope freezing stage, and comparing this with the known freezing points of solutions of various  $NaCl$  content.

If the fluids have become saturated during cooling, they will contain salt crystals, usually termed daughter minerals. The most common, often the only, daughter mineral present in inclusions



from ore deposits is NaCl. The maximum solubility of NaCl in H<sub>2</sub>O at room temperature is approximately 26 weight percent, so the absence of halite daughter minerals indicates that fluid salinity is below this level and it can only be measured by freezing experiments. If halite is present, the salinity can be estimated from the solution temperature of the halite daughter salt, since the temperature-solubility relationships of NaCl in H<sub>2</sub>O have been established (Keevil, 1942).

Daughter minerals are of great importance in fluid inclusion studies since, if they can be identified, they provide important information on the composition of the fluid. A very large number of different daughter minerals have been found in inclusions from ore deposits, especially high-temperature magmatic-hydrothermal deposits. They include halides, sulphates, carbonates, silicates, sulphides and borates. In some cases, ten or more different minerals have been found in a single inclusion. Halides, particularly NaCl and KCl, are the most common and are usually readily identified. Others may be difficult or impossible to identify, and many fluid inclusion studies report unidentified daughter minerals. The occurrence of daughter minerals in general, and many of the techniques used to identify them, have been described by Roedder (1972b). The occurrence of daughter minerals in the Bolivian deposits and the identification techniques used are described in detail in later sections.

Certain solid mineral grains present in inclusions may be material which was in suspension in the fluid when trapped. These are not true daughter minerals. They can usually be recognised by their erratic occurrence within a co-genetic inclusion population,

and their failure to dissolve on prolonged heating at the homogenization temperature.

### 3.2.6. The composition of fluid inclusions

Determination of the chemical composition of inclusion fluids is an important way of obtaining information on the chemistry of ore transport and deposition. Complete analysis is rarely possible because of the very small volume of fluid available; however, a large amount of partial analytical data is now available for many types of ore deposit. Numerous analytical methods have been applied. Most involve the opening (by crushing) of numerous inclusions in a relatively large (several gm) sample. This introduces uncertainties as to whether all of the fluid analysed was obtained from inclusions of the same type and generation, since most minerals contain several generations of inclusions related to successive growth stages and later fracturing and rehealing. The most common methods which have been applied are : Crushing in vacuum for gas analysis by mass spectrometry or chromatography, and crushing followed by water or acid leaching followed by analysis of the leachate, usually by atomic absorption spectrophotometry. This latter method has been widely used for determining the major cations or cation ratios. Other methods of analysis which have been used include; wet chemical, specific ion electrodes, emission spectrometry, and x-ray fluorescence techniques. Analysis of single inclusions is much more difficult, except in the case of the rare giant inclusion which are occasionally found, for example in some vein fluorite or minerals in pegmatites. In general, single inclusion analysis has only been

applied where solid daughter minerals are present in the inclusion, and physical analytical techniques, such as X-ray diffractometry or electron probe microanalysis, can be applied.

The results show that hydrothermal ore fluids are aqueous solutions of widely varying chemistry and concentration. Perhaps the single most consistent feature is the almost ubiquitous presence of chloride salts, although a wide range of other salts and gases have also been found. Gases include  $\text{CO}_2$ ,  $\text{H}_2\text{S}$ ,  $\text{SO}_2$ ,  $\text{NH}_4$ ,  $\text{CH}_4$ . The most common elements in solution are Na, K, Ca, Fe, Si, as well as Cl; but S, F, B, Mg, and Mn are often detected also. Determination of the ore metals is particularly difficult because their concentration is often very low, although in some deposits surprisingly high concentrations of metal have been found, for example values of over 1000 ppm Cu in inclusions from porphyry copper deposits are common. There is much literature on fluid inclusion analysis, a large proportion of it from Russia. Good reviews are those of Roedder (1972b, and 1968, 1969, 1970a, 1971, 1972a). The chemical aspect is perhaps the most important area in fluid inclusion research at present, but the complete analysis of inclusion fluids is still far from being routinely possible. The analytical methods which were applied in this study are discussed in detail in the following section.

### 3.3. Experimental Methods

The methods of fluid inclusion microthermometry are basically simple, and well known. In this study, standard techniques were used such as have been described by Roedder (1962, 1963, 1972b);

Kelly and Turneure (1970); Poty et al., (1976). The methods used for the determination of homogenization temperatures and freezing points are outlined briefly below, while the analytical methods which were used are described in more detail.

### 3.3.1. Sample preparation

Most aspects of fluid inclusion study depend initially on transmitted light microscopy. Since it is desirable to be able to routinely study inclusions as small as 10 micron diameter, good optical characteristics are essential. Thin, doubly polished plates of the sample mineral are used. The optimum thickness depends on the mineral. For quartz, which was used almost exclusively in this study, a thickness of approximately 0.5 mm was found to be best. The process of cutting, grinding and polishing the specimen can cause disruption, heating, and in some cases leakage in inclusions which are close to the surface, so a thickness of much less than 0.5 mm was found unsuitable. With greater thicknesses, absorption and refraction begin to cause problems, especially in freezing operations. The specimens were either individual quartz crystals prised out of vuggy vein material, slices or chips of massive vein quartz, rock slices, or individual quartz phenocrysts separated from altered rock after coarse crushing. They were mounted in a casting resin, ground down on both sides, mounted in a holder so that one side could be polished, and reversed for polishing the other side. Initial optical examination was usually made with the specimens still mounted in resin. They were released by dissolving the resin in chloroform for use in the microscope heating and freezing stages, or for analytical procedures.

### 3.3.2. Homogenization temperature determination

Homogenization temperatures were measured using a Leitz Model 1350 heating stage mounted on a Leitz Ortholux petrographic microscope. The stage is capable of temperatures up to 1350°C. It is heated electrically via a rheostat which allows sensitive temperature control. Temperature is recorded with a Pt-Rh-Pt thermocouple connected to a chart recorder. The thermocouple is in contact with a sapphire plate on which the sample rests in the sample chamber of the stage, i.e., the temperature recorded is the temperature of the base of the sample. The chart recorder was calibrated using solids of known melting point. Repeated measurements indicated a (one standard deviation) uncertainty of approximately  $\pm 0.02$  mv on the calibration curve, i.e., approximately  $\pm 2.0^\circ\text{C}$  over the whole range, since the calibration is essentially linear (Fig. 3.2). The chart recorder performance was monitored regularly by applying known voltages and checking the recorder deflections. It is concluded that the instrumental and calibration errors are small when compared with the uncertainty resulting from the thermal gradient within the sample material, and observational uncertainties due to poor optical quality of much sample material.

Thermal gradients are a major problem with the Leitz heating stage, particularly at high temperature. The gradients were estimated by comparing the apparent melting temperatures of the standard melting-point substances when they were placed on the sample holder, and on top of doubly polished quartz specimens of 1.0 mm and 1.8 mm thickness. The calibration curves are shown in Fig. 3.2. For a 1.0 mm thick sample plate there is a temperature

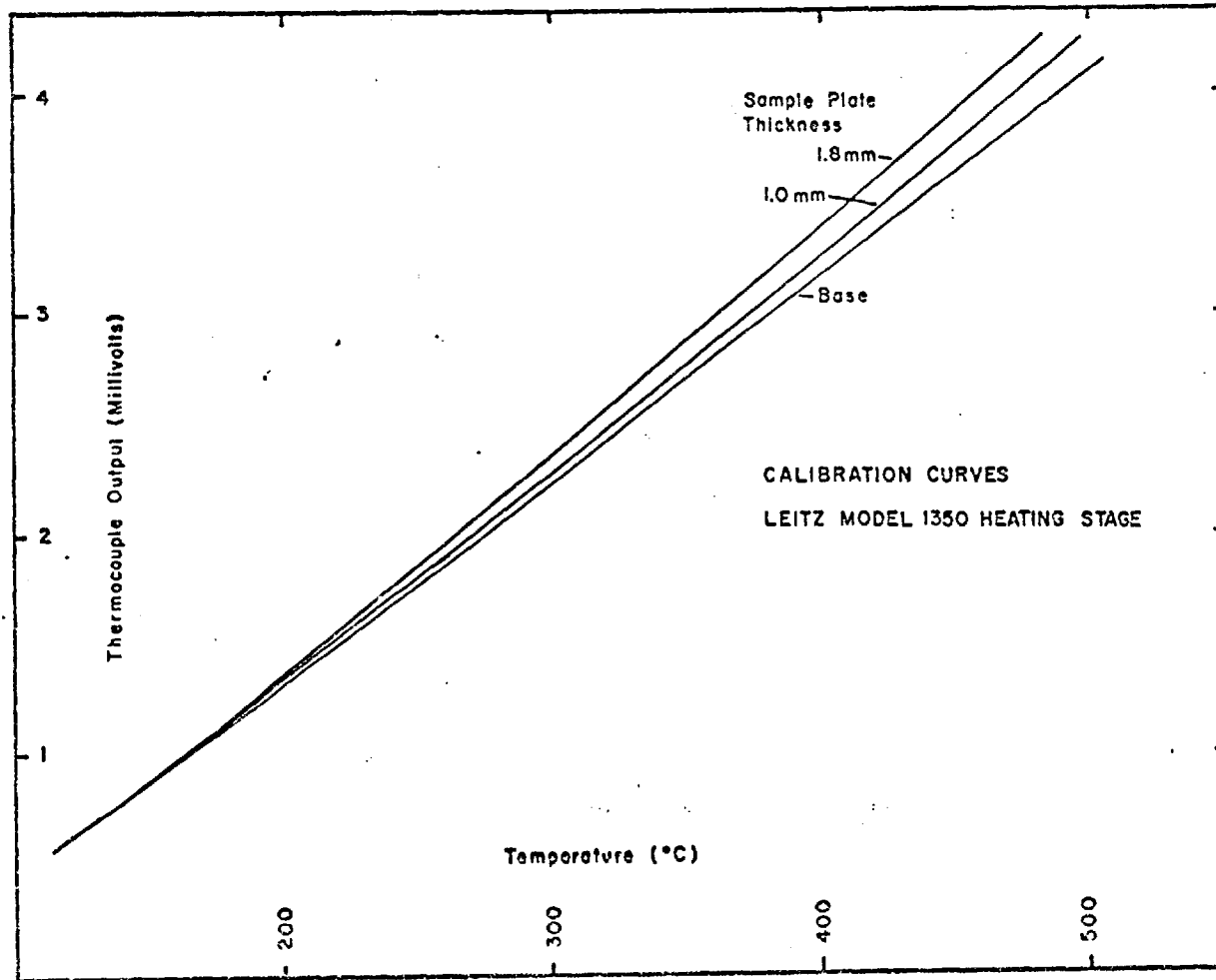


FIG. 3.2

difference of about  $18^{\circ}\text{C}$  between the base and top when the base is at  $500^{\circ}\text{C}$ . The difference is less at lower temperatures. In practice the differences are less severe than this, since most specimens were closer to 0.5 mm in thickness, and the inclusions used are well below the upper surface. The actual temperatures quoted here are the mid-point between the baseplate and 1.0 mm thickness calibration curves for a given millivolt reading on the recorder.

In practice meaningful conclusions can only be drawn from the  $T_h$  data for numerous inclusions of the same type and generation in the same sample. The quality of  $T_h$  data is dependent on the optical quality of the specimen and the size of the inclusions present. This means that there may be substantial uncertainties in the  $T_h$  measurements in poor samples, where homogenization is difficult to observe, and this uncertainty may be much greater than the calibration and thermal gradient uncertainty. The operating procedure used in this study was to measure numerous inclusions for each sample, using several different specimens from the same sample. Each specimen was only run once in the heating stage, and then discarded. In some cases several individual inclusions could be observed in one run, in other cases only a single inclusion was measured. The  $T_h$  value was normally checked by allowing the specimen to cool until phase separation occurred and then reheated to  $T_h$ . The data for some samples consist of very limited numbers of  $T_h$  determinations on optically poor material, with substantial errors on individual determinations expected. Much of the spread in values in the data is a result of this, although other factors such as necking and fluid boiling

are also involved.

Some sample material proved to be completely unusable because of the absence of any inclusions large enough to study. This is a problem which is not often mentioned in reports of fluid inclusion studies, though it must be common. In some of the Bolivian deposits it was found that the quartz of certain vein growth stages is so milky (due to extremely small inclusions) as to be almost opaque, and completely lacking in inclusions large enough to work with. In other growth stages the quartz is clear, but virtually free from any inclusions at all. The latter is particularly the case in the quartz most closely associated with cassiterite, and has made definition of the conditions of cassiterite deposition difficult to define in some deposits.

### 3.3.3. Freezing temperature determinations

Freezing temperatures were only measured on a few samples in this study. The reasons for this were as follows. 1) Most of the material studied (especially from Chorolque) contained only highly saline inclusions for which the fluid salinity could be determined from the solution temperatures of the daughter minerals. 2) Freezing measurements had already been made for the Llallagua deposit (Kelly and Turneaure, 1970). 3) Much of the material under study was unsuitable for freezing work either because of poor optical quality or because the fluids were metastable at very low temperatures and did not freeze. 4) A suitable instrument for freezing measurements was not initially available.

Such work as was done was carried out mainly on a freezing stage constructed at the Royal School of Mines, London. It consisted of a cylinder of asbestos with a lower window, baffles



to circulate and mix the incoming cold gas, a glass sample holder plate, and an upper (plastic) window, mounted on a Vickers petrographic microscope. Dry nitrogen gas is passed through a coiled copper tube immersed in liquid nitrogen and then into the stage. The temperature is controlled by regulating the rate of flow of the gas. Temperatures of at least  $-50^{\circ}\text{C}$  were achieved. The temperature was read directly with a thermometer whose bulb was adjacent to the sample inside the stage. Calibration using fluid inclusions of known freezing point indicated that there were considerable thermal gradients inside the stage, so in its existing form it was not suitable for detailed work. Some additional data was later obtained using a highly accurate CHAIXMECA dual purpose heating/freezing stage (Poty et al., 1976) at Billiton Research, Arnhem, The Netherlands.

The operating procedure with both stages was first to freeze the inclusions by rapid cooling (to  $-180^{\circ}\text{C}$  in six minutes with the CHAIXMECA). The temperature was then allowed to rise slowly, while melting of the ice was observed. Great care is necessary when the ice is almost completely melted, to ensure that the true last melting temperature is recorded. Successive periods of re-cooling, observation of the re-growth of the ice, further warming, etc, are necessary in order to accurately determine the freezing point. The measured temperature is then referred to the known freezing point depression data for  $\text{H}_2\text{O}-\text{NaCl}$  solutions.

#### 3.3.4. Analytical procedures

No attempt has been made in this study to carry out a comprehensive investigation of the chemistry of the inclusion fluids. Such an investigation would be a long-term project in

itself. However, early in the work it became apparent that the high-temperature fluid associated with the quartz-tourmaline alteration at Chorolque was unusual. It is an exceptionally highly saline brine, and the daughter mineral assemblage includes a number of important phases which suggested that the composition differed substantially from the NaCl- and KCl-dominated brines which are commonly found in inclusions from the early stages of mineralization at other magmatic-hydrothermal deposits, such as the porphyry copper deposits. This fluid is considered to be of particular importance because the geological relationships indicate that it might be a primary magmatic fluid by which the tin and other metals were initially introduced into the hydrothermal system. Qualitative analytical work was carried out in order to identify the major chemical components of this fluid. The methods used are outlined here, and the results are described in Section 3.4.1 (E).

#### A. Non-destructive tests of daughter minerals

A number of important optical observations can be made on unknown daughter minerals. They include crystal form, twinning, measurement of interfacial angles, birefringence, length-sign, colour, and refractive index relative to the inclusion fluid, host mineral, or neighboring daughter minerals. Combined with observations of the behaviour of the daughter minerals during heating, these can often serve to identify some of the commonest phases including (in this case) NaCl and KCl.

#### B. On-stage optical and chemical tests on extracted daughter minerals

The daughter minerals contained in inclusions can be released

by crushing fragments of the mineral in oil under the microscope. Microscope crushing stages have been specially designed for this purpose (Roedder, 1970b), but an equally good method is to crush by hand with the sample in oil (of refractive index equal to that of the host mineral) between two glass microscope slides. Opening an inclusion is relatively simple, but finding and separating the daughter minerals from the mass of fragments of host mineral which are also produced is a difficult and tedious task unless they are particularly large.

A number of daughter minerals were isolated in this way, enabling further optical and some chemical tests to be carried out. The refractive indices of daughter minerals can sometimes be determined by successive immersion in standard oils, provided a solvent can be found which will remove the oils without dissolving the daughter salt. The problem of handling the minute grain through successive immersions and cleanings is considerable.

Attempts were also made to carry out some simple chemical tests, in particular the test for sulphate involving solution in HCl and addition of BaCl to give a white precipitate ( $\text{BaSO}_4$ ). A test for iron was also attempted, by dissolving the daughter salt in HCl and adding potassium ferricyanide to give a blue colour in the presence of iron. Although some useful results were in fact obtained, and one of the major unknown daughter salts was first identified as an iron compound in this way, the handling problems were found to be so severe that these methods were abandoned in favour of X-ray methods as described below.

### C. Electron probe microanalysis

A simple method of obtaining qualitative information on the

non-volatile constituents of inclusion fluids, using an electron microprobe, has been described by Eadington (1974) and was used in this study as a first analytical step. The method involves choosing an inclusion which is as close as possible to a surface of a polished mineral sample plate. The sample is placed in the heating microscope stage and heated beyond the homogenization temperature until sudden leakage, or bursting, takes place. The non-volatile constituents of the fluid condense on the surface of the sample, forming a well-defined halo of solid material around the crater, or point of leakage. This halo can then be analyzed using conventional EPMA methods.

Several inclusions were studied in this way using a Cambridge 'Geoscan' EPMA. A number of major constituent elements of the fluids were detected, although the results are purely qualitative because of the complete lack of control over the behaviour of the fluid once it leaks out of the inclusion. In practice it was found that, given the qualitative nature of the experiment, a more satisfactory method was to examine and analyse the halo of condensed material using a scanning electron microscope (SEM) equipped with solid state X-ray detector as described below. This is a much more rapid method, giving virtually instant analytical data instead of the long scanning time necessary with the crystal spectrometers on the EPMA.

#### D. The scanning electron microscope.

The use of the SEM equipped with x-ray detector is rather new in the study of fluid inclusions. Although the form of inclusion cavities have previously been investigated (Deicha and Sella, 1962), the identification of daughter minerals by this

method has not been widely attempted. Current research using this method has been reported by Metzger et al., (1977), who used it to identify daughter minerals in inclusions in quartz and fluorite from some mineral deposits, and calcite from a carbonate, in the U.S.A. Le Bel (1976) has obtained spectacular imagery, and identified numerous daughters from inclusions in vein quartz from a Peruvian porphyry copper deposit.

In this study of the Bolivian deposits, the method was used as a means of identifying some of the daughter salts in the very highly saline inclusion fluids from Chorolque. For SEM work, the inclusion contents have to be exposed to the electron beam, i.e., the inclusions have to be opened. The samples were mostly prepared by selecting a suitable group of inclusions (generally a plane of pseudo-secondary inclusions) by microscopic examination of a doubly polished quartz plate. This was then manually cracked into pieces, and those which had a new surface which traversed the inclusion group were mounted with the new face roughly parallel to the surface of the mount. In some cases it was desirable to use rough unpolished mineral fragments. These were selected under the optical microscope while immersed in oil, then cleaned in acetone. Once dry the inclusions could no longer be seen under the microscope, so the grains were cracked manually (between glass slides) and fragments chosen more or less at random and mounted as above. The use of thin polished plates was found to be preferable because they are much easier to crack. This resulted in a smoother new surface (making location and observation of the inclusions in the SEM easier) and less disturbance of the daughter salts. An attempt was also made to use fragments which

had been cracked in immersion oil. In this way a more precise selection of suitable inclusions could be made before mounting, but the fragments had to be first cleaned of oil. It was found that most of the daughter salts were soluble in whichever cleaning solvent was used, and those which were not tended to fall out of the inclusion cavity during washing, so this method was abandoned. The mounted specimens were carbon coated before loading in the SEM. Gold would be preferable as a coating medium for optimum image resolution, but it interferes with the analytical procedure.

The instrument used was a Cambridge Instruments A2 SEM, equipped with an Ortec solid state X-ray detector (energy dispersive) connected to a Northern Instruments multichannel analyser. Most of the inclusions studied were in the 10 to 30 micron size range. It was found that, with suitably oriented specimens, good resolution could be obtained at magnifications of 1500 to 2000. The instrument gives a spectacular view of the opened inclusion cavity and its contents. Analysis is carried out by means of a finely focused high energy electron beam which can be directed at any point on the specimen surface, or scanned over any desired area. The procedure is very rapid. The energy spectrum produced is displayed almost instantaneously by the multichannel analyser, and the elements present are identified by their characteristic X-ray energies.

Several serious problems were encountered in the application of this method; they can be classified as follows:

- 1.) Problems inherent in the type of material being studied. It was found that the high-salinity inclusions contained daughter salts which were deliquescent on exposure to air. These salts

lost their crystalline form on opening, and although they presumably lost the excess water under vacuum in the instrument, they did not regain their original well-defined crystal form. This meant that although it was still possible to obtain analytical information from the rather formless lumps of material seen in the opened inclusions, it was often difficult to be at all precise in relating this to any particular salt which could be observed optically in the unopened inclusion.

2.) Problems caused by sample preparation procedures. The mechanical cracking procedure can produce considerable disturbance of the daughter minerals. In some cases mineral grains may fall out of the inclusion cavity, although in general it seems that the wetting effect of the inclusion fluid keeps the daughter minerals in place. In a tubular inclusion containing multiple daughter minerals, it is obvious that a fracture which splits the inclusion in half will expose different daughter minerals in each half to the electron beam. It is necessary to examine numerous inclusions of the same family in order to get information on the overall daughter mineral population and hence fluid chemistry. Pumping the specimens down under vacuum may also affect the daughter minerals. They may be forced out of the inclusion cavity by the escape of the liquid phase trapped behind them.

3.) Problems inherent in the instrument. The orientation of the samples in the instrument can be a problem, especially for X-ray analysis. The surface on which the inclusions are exposed must face towards the X-ray detector. It is often impossible to get analytical data from within deep inclusions because insufficient

x-rays escape. It is also likely that scattered electrons produce x-ray emission from objects adjacent to the one under direct bombardment. Thus there may be some uncertainty about the precise location of some of the elements recorded by the analyser. The detection limits are relatively poor because of these problems, so the method is not particularly suitable for investigating the ore metal content of inclusions as the concentration levels are commonly rather low. Quantitative work with inclusions is impossible, since the response varies according to the configuration of the exposed surface; nevertheless the method has proved to be extremely useful both as a means of identifying individual daughter minerals, and in gaining information on the general composition of high salinity inclusion fluids.

#### E. Crushing and leaching

Crushing and leaching techniques have been rather widely used in the study of both dilute and highly saline inclusion fluids. Both limited chemical data, such as sodium to potassium ratio measurements, as well as more complete analyses, have been obtained by these methods. Roedder (1958), and Roedder et al., (1963) have described in detail methods of extracting and analysing inclusion fluids by crushing and leaching. Similar methods have been used in numerous other studies (see reviews by Roedder, 1972a and 1972b). The procedures generally involve first cleaning the sample material by boiling in nitric acid and de-ionized water, followed by electrolysis or ion-exchange procedures to remove all surface contamination. The sample is then crushed, usually in a ball-mill, and leached with water or



acids. The leachate is then separated from the crushed residue by centrifuging, filtering, or by electrodyalisis through semi-permeable membranes, and analyzed usually by atomic absorption spectrophotometry. The potential for contamination is enormous, and reliable results can only be obtained by the most careful procedures with suitable equipment.

In this study a very limited number of analyses were carried out using crude methods. The objective was to try to estimate the ratios, principally of Fe, Na, and K in the fluids from Chorolque, as a check on the composition of the highly saline inclusion fluids and to see if the ratios changed significantly during the progressive decrease in salinity which accompanied vein growth.

The method used was as follows: the samples (including an inclusion-free quartz blank) of about 10 gm each of quartz, crushed to -10 + 60 mesh, were boiled for 3 hours in concentrated  $\text{HNO}_3$ , rinsed and boiled again in de-ionized water for 3 hours. They were then electrolytically cleaned in cells made from pyrex glass 'U' tubes with platinum electrodes, attached in parallel to a 100 volt DC source. The procedure was to change the de-ionized water in each cell approximately every 12 hours and monitor the conductivity at the end of each period. Cleaning was judged to be complete when there was negligible conductivity rise at the end of several water changes; this occurred after about three or four days. The samples were then dried; ten grams of each sample were then crushed for 20 minutes in a pre-cleaned agate mortar with addition of 30 ml of de-ionized water. The slurry was filtered, and analysed by atomic absorption

spectrophotometry for Fe, Na, K, Mg and Li. The results are purely qualitative. No attempt has been made to estimate the volume of inclusion fluid which was extracted, and the data are considered only in terms of element ratios.

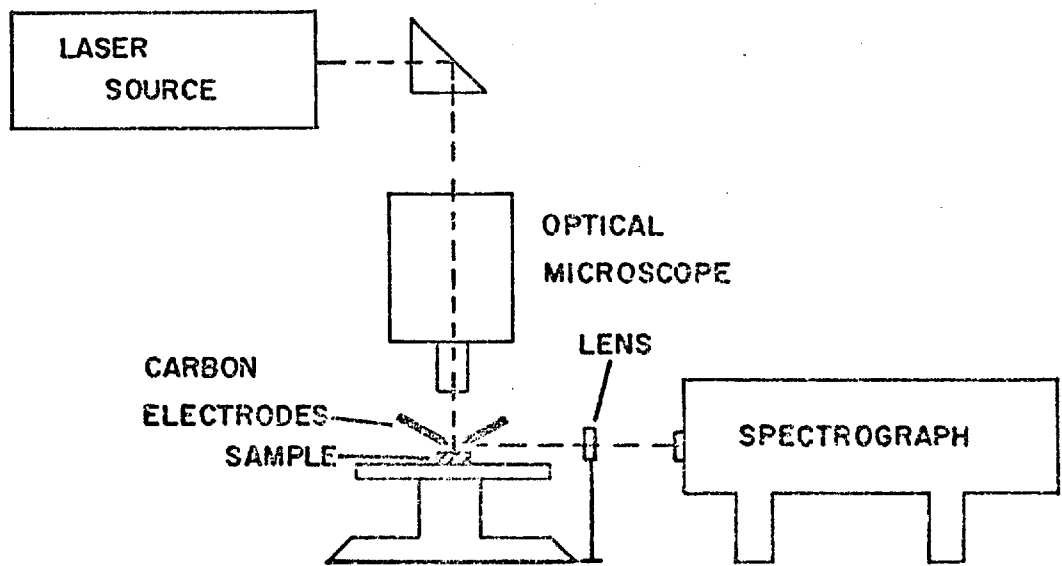
#### F. Laser microprobe analysis

The laser microprobe is an analytical tool which, in theory, is ideally suited to fluid inclusion work. It offers the possibility of being able to provide rapid and rather complete analysis of individual inclusions without the need for prior opening, extraction, and hence likely contamination of the fluid.

The principles of the laser microprobe have been described by Moenke and Moenke (1968). It has been applied to a number of analytical problems with particular success, including analysis of the trace-metal content of minerals.

A finely focused pulse of laser light is fired onto the surface of the sample through an optical microscope (Fig. 3.3). Provided the sample is not transparent to the wavelength used, the laser pulse vaporises a portion of the sample, penetrating some distance below the surface by creating a micro-crater. A plume of vaporized (ionized) sample material is produced, which is further excited by means of a synchronized DC spark. The resulting atomic emission spectrum is analysed with a suitable optical spectrograph. The sensitivity of the method is very high, possibly better than that of EPMA in some materials (Eremin, 1975). For qualitative work the method is rapid and simple. No special sample preparation is required, in fact unpolished surfaces are better, and there are no rigid

FIG. 3.3



LASER MICROPROBE  
SCHEMATIC DIAGRAM

geometrical requirements. The instrument operates in air, no vacuum pumping is required. There are however formidable problems with calibration and accuracy in quantitative work because of the difficulty in controlling the amount of sample material which is vaporized per shot. Under ideal conditions in work with metals, crater sizes as small as 10 micron diameter by 20 micron deep have been obtained.

In fluid inclusion analysis, the objective is to use a single laser pulse to burn a crater down through the host mineral to an unopened inclusion and to vaporize the contents of the inclusion which then form part of the plume and can be analysed. Very little work appears to have been done with this method to date although Tsui et al., (1975) used a Jarrel-Ash Mark II laser microprobe to analyse inclusion fluids in quartz from several ore deposits. They calibrated the instrument by analysing fluids of known composition trapped in holes in fused silica glass plates. They report detection limits of  $3 \times 10^{-10}$  gm for Cu, Mn, Ca and Mg;  $1 \times 10^{-9}$  gm for Fe; and  $3 \times 10^{-8}$  gm for Na. They measured the concentration ratios of all of the major cations except K, and combined this with salinity data from freezing stage measurements to obtain approximate element concentrations.

The work reported here was carried out using a Zeiss LMA-1 laser microprobe, at the Physics Department, University of St Andrews. It was done mainly on an experimental basis, to test the applicability of the method. The amount of time available with the instrument was limited, and no attempt was made to calibrate it for quantitative work. This instrument has been described in detail by Moenke and Moenke (1968). It employs a

ruby rod (Cr-doped) resonator which produces laser light at a wavelength of  $6943 \text{ \AA}$ . The laser source is mounted on what is essentially a normal optical microscope which can be used in both transmitted and reflected light modes for sample location. The laser pulse is fired through, and focussed by, the microscope objective lens. Under normal operating conditions, using the Zeiss reflecting objective (40/0.50, f6.3 mm), the theoretical diameter of the laser pulse is 1.4 microns.

Secondary cross-excitation of the plume is produced by a DC spark fired between carbon electrodes. The electrode gap and relative positions can be adjusted as required. The spark is synchronized by increasing the voltage across the electrodes gradually until sparking occurs without the laser being fired. The electrode voltage is then set at a value just below the breakdown voltage. When the laser is fired, the plume of sample material reduces the resistance of the air between the electrodes so that a synchronized spark automatically fires. The spectrograph used for analysis was a Zeiss Q-24 optical prism instrument which operates over the wavelength range 2000 to  $5500 \text{ \AA}$ .

The major problem encountered in this work is that the ruby resonator produces laser light in the visible wavelength region, and consequently optically transparent minerals such as quartz, and dilute inclusion fluids, are relatively transparent to the laser pulse and do not absorb enough energy to produce cratering. The amount of energy absorbed depends on the amount of impurities in the quartz. It was almost impossible to achieve cratering in clear quartz containing dilute 2-phase liquid plus vapour inclusions. Highly saline fluid inclusions containing numerous

daughter salts did absorb laser energy and satisfactory craters could be produced within this type of material.

The operating variables which can be altered to change the energy and characteristics of the laser pulse, and hence crater size and shape, are as follows :

a) Flash tube voltage: The initial energy input to the ruby resonator is provided by a xenon flash tube. The output can be varied, and in practice it was found necessary to operate at 1.9 kv which is near the maximum obtainable.

b) Q-Switch setting: Q-switching is a means of delaying the spontaneous emission of laser radiation from the resonator until a maximum number of chrome atoms have reached the correct excitation state from which spontaneous emission occurs. The LMA-1 is equipped with a passive Q-switch, which consists of 4 cells containing dye solutions of different strength. They can be placed in the light path in the resonator, where they absorb some of the early energy emission and thus allow a greater build-up of energy in the ruby rod before spontaneous emission takes place. The effect of Q-switching is to increase the power density of the laser pulse at the sample surface, but to decrease the pulse life. These characteristics in turn affect the cratering ability of the energy pulse. According to Moenke and Moenke (op. cit.) the smallest diameter, deepest craters are obtained in metals without Q-switching, but it was found that no cratering of quartz could be achieved without the Q-switch set to produce maximum effect.

c) Diaphragm setting: The instrument has a diaphragm in the light path. This was found to reduce the power obtained without

decreasing the crater size and so was operated in the wide open position.

d) Objective lens magnification and focus: The laser was normally fired through the highest power lens available (40/0.50) as this gives the smallest pulse diameter and hence should give the narrowest crater. Careful focusing on the inclusion is necessary for best results. In practice the crater diameter is much larger than the calculated diameter of the focused pulse, and is affected by properties of the sample such as thermal conductivity, reflectivity, surface quality and transmission characteristics. The best cratering results were obtained by operating with Q-switched laser and high flash-tube voltage, on highly saline inclusions containing numerous daughter salts (Plate 12). Excellent results were also obtained in experimental tests on subsurface microscopic grains of opaque minerals (e.g., Plate 13). The best crater diameter to depth ratios obtained were about 3 : 1. This is nowhere near as good as the results which have been obtained in metals, where ratios of 1 : 2 or 1 : 3 have been reported (Moenke and Moenke, *op. cit.*). In quartz, much of the cratering effect seems to be the product of mechanical fracturing which produces large irregular craters (Plate 14). These do have, however, a narrow "burn hole" in the center (see Plate 13) and most of the ejected quartz was presumably in solid form and not included in the vapour plume. With clear quartz containing dilute fluid inclusions it was generally found to be impossible to crater the surface at all. The use of laser energy at some different wavelength to that used here may be necessary to get better results.

### 3.4. Results

#### 3.4.1. Chorolque

##### A. Material studied

The fluid inclusion study of the Chorolque deposit was carried out entirely on inclusions in quartz. No other suitable minerals are present; the cassiterite is almost opaque, and very fine grained. Three different types of quartz were studied.

1) Quartz from the pervasive quartz-tourmaline altered rocks of the central vent. This included both relict quartz phenocrysts and secondary quartz, especially overgrowths on phenocrysts. The inclusions in this material are clearly secondary with respect to the phenocrysts, but mainly primary with respect to the secondary overgrowths.

2) Vein quartz, mainly from the major veins cutting the vent rocks, but also from the veins in the surrounding sedimentary rocks. The vein quartz can be broadly divided into two growth stages; pre-cassiterite, and with-cassiterite. Pre-cassiterite quartz accounts for most of the material in the veins. The distinction between pre-cassiterite quartz and quartz accompanying cassiterite is difficult to make as there was no break in deposition between the growth stages and, in most cases, the growth of individual quartz crystals has spanned almost the entire period of mineral deposition in the veins. Most cassiterite deposition appears to have taken place after the deposition of almost all quartz and it is intergrown with, or overgrown on, the free-growing terminations of quartz crystals in vuggy open spaces in the veins. Thus the interpretation of the fluid inclusion data with respect to the conditions under which cassiterite was deposited is rather subjective and imprecise,



although there is no doubt at all that the cassiterite is late in the overall depositional sequence.

3) Quartz phenocrysts from the sericitized volcanics. These contain secondary inclusions which are interpreted as having been formed during the hydrothermal alteration of the volcanics.

#### B. Classification of inclusion types

The fluid inclusions in the Chorolque quartz can be classified into six types, on the basis of the assemblage of liquid, vapour, and solid phases which fill them. The classification also applies to the other deposits included in this study.

Type I. These are two-phase, liquid plus vapour filled inclusions. They often also contain a very small opaque daughter mineral grain which is sometimes roughly equidimensional, sometimes needle or sword shaped, and apparently non-magnetic. This type of inclusion has been found as either primary, pseudo-secondary or secondary inclusions in all of the material studied, but they are particularly common as secondary inclusions in the vein quartz. Typical examples are shown in Plate 15.

Type II. These are three-phase (liquid plus vapour plus daughter mineral) inclusions in which the daughter is a fine, acicular, weakly birefringent mineral usually forming a group of radiating or matted needles, sometimes faintly greenish in colour. They are found as primary, pseudo-secondary or secondary inclusions especially in vein quartz. The amount of the characteristic daughter mineral is variable. They sometimes also contain an opaque daughter mineral; they are always closely

associated with Type I inclusions. Typical examples are shown in Plate 16.

Type III. These are three-phase, liquid plus vapour plus daughter mineral inclusions. The daughter mineral is a clear, colourless, cube-shaped isotropic salt with a refractive index very close to that of quartz. These properties suggest that it is halite (NaCl). These are found as primary, pseudo-secondary and secondary inclusions, especially in the vein quartz and quartz phenocrysts in the sericitized volcanics. They do not contain the acicular daughter mineral characteristic of Type II inclusions, but they may contain an opaque phase as in Types I and II (Plate 17).

Type IV. These are three-phase, liquid plus vapour plus daughter mineral filled inclusions in which there are two or more transparent daughter minerals. They always contain a halite cube plus one, two or three additional daughter minerals, and always have a clearly distinguishable liquid phase in addition to a contraction vapour bubble. A very small opaque phase may be present, but the acicular mineral which is characteristic of Type II inclusions is not present. The identity of the other daughter minerals is discussed below. These are found as primary and pseudo-secondary inclusions in vein quartz and occasionally as secondary inclusions in the quartz phenocrysts in the sericitized volcanics and in the quartz of the quartz-tourmaline altered vent rocks. Typical examples are shown in Plate 18.

Type V. These are two-phase or single-phase inclusions which are almost or completely filled with vapour. They occur as rounded primary inclusions in the secondary quartz in the

quartz-tourmaline altered vent rocks and, less commonly, as pseudo-secondary inclusions in the early vein quartz. They are almost exclusively associated with Type VI inclusions. Examples are illustrated in Plates 19 and 20.

Type VI. These are three-phase inclusions (liquid plus vapour plus solid daughter minerals). They are so packed with daughter minerals that the liquid phase is virtually indistinguishable, and the vapour bubble is often distorted (Plate 20). At least eight different daughter salts can sometimes be distinguished in these inclusions, although they usually overlap each other to such an extent that distinction is difficult or impossible. The identity of some of the daughter minerals is discussed below. These are found as primary and pseudo-secondary inclusions co-existing with Type V inclusions in the quartz-tourmaline rock of the central vent. They are also present in the earliest vein quartz of some (Veta Colon), though not all, of the major veins. In this material they are larger and easier to study than in the quartz-tourmaline rock; examples are shown in Plate 21.

Most of these inclusion types are gradational with each other; for example the distinction between Types VI and IV is made on the basis of whether or not there is a clearly visible liquid phase present, although the dominant daughter salts are the same in each. However, the distinction is important because the two types are mainly found in different material, and the Type VI inclusions are particularly associated with Type V inclusions, which is not the case for Type IV. Types IV and III are gradational also, the distinction depending on whether there

are one or two daughter minerals present (only halite in Type III). In fact, Types I, II, IV, and VI apparently represent a continuous progressive increase in the salinity of the inclusion fluid. Type V inclusions are not gradational with any other of the types; they do not show any significant variation in the liquid to vapour ratio.

#### C. Distribution of inclusion types

The inclusion types described above are systematically distributed with respect to some of the important geological features of the Chorolque complex.

1) The quartz-tourmaline alteration zone of the central vent. The secondary quartz of this rock contains primary inclusions of Types VI and V, and the relict quartz phenocrysts contain the same inclusion types in planes cutting across them. Other types are rare, and are usually clearly secondary in origin. The Type VI and V inclusions are generally very small (5-10 micron), very numerous, and occur intimately associated with each other and with generally random distribution (Plate 19). They are also found clustered around the margins of relict phenocrysts, and in planes (healed fractures) traversing the relict phenocrysts.

There is no doubt that both these inclusion types are primary with respect to the growth of the secondary quartz. They were trapped simultaneously during the hydrothermal alteration of the vent rocks, and their co-existence indicates that the fluid which accomplished the alteration was two-phase, consisting of a very highly saline brine and a co-existing low density vapour. Assuming that the vapour which fills the Type V inclusions is water, this indicates that the hydrothermal fluid was either a

boiling liquid or condensing vapour during much of the time in which alteration took place.

2) The veins. The quartz in the veins contains inclusions of all types, although Type VI inclusions have only been found in one of the veins which have been studied (Veta Colon) and Type V inclusions are rare. The distribution of inclusion types in the quartz in the major veins shows a well-defined progression from high to low salinity as vein growth progressed. In the case of the Veta Colon, which is the largest of all the vein structures, the quartz closest to the walls of the vein contains pseudo-secondary Type VI inclusions and occasional planes of Type V inclusions. The two types have been trapped separately. In the other veins the earliest quartz contains Type IV inclusions, and Type VI inclusions are absent. There are occasional planes of Type V inclusions. In some of the material studied, a gradual decline in the salinity of the Type IV inclusions can be observed from the base towards the tip of individual crystals, marked by a decrease in the number and size of the daughter salts present. Type III inclusions are found as pseudo-secondary planar groups closer to the crystal terminations than Type IV inclusions. They are generally not very numerous, and are completely absent in some material. Type II and I inclusions are found as pseudo-secondary and primary inclusions in the apical and outermost region of vein quartz crystals, where the quartz is sometimes intergrown with, or overgrown by cassiterite. Type I inclusions in particular are also found as secondary inclusions in planes (healed fractures) which cross-cut all parts of the vein quartz. In some very small veins filled with a quartz-cassiterite intergrowth,

the vein quartz only contains Types I and II inclusions, although it is overgrown on quartz-tourmaline altered wall-rock in which the quartz is crowded with Types VI and V inclusions.

3) The altered igneous rocks surrounding the vent. The only mineral in these rocks which is suitable for inclusion studies is primary igneous quartz. The quartz phenocrysts contain primary glass inclusions, but as would be expected, the only liquid inclusions are of secondary origin. In the chloritic alteration zone fluid inclusions are virtually absent. However, in the sericite-tourmaline zone closer to the vent, the quartz phenocrysts contain numerous planes of secondary fluid inclusions. These include separate planes of Types I, II, III, and IV inclusions apparently identical to those in the veins although they are generally small and difficult to observe (Plate 22). This suggests that these secondary inclusions were formed during the alteration of the rocks, and so can give useful information on the conditions in the hydrothermal system in this zone peripheral to the vent.

#### D. Temperature and salinity data

The homogenization temperature and fluid salinity data for each inclusion group measured per run in the heating stage are shown in Table 4. These are plotted in Fig. 3.4, in which the horizontal axis (time) gives only a generalized indication of the relative age relationships of the alteration and vein-growth stages. The individual inclusion group measurements are plotted in order of decreasing mean homogenization temperature, not in a detailed time sequence. The data are plotted in this way in order to emphasize the close correlations which exist between the

TABLE 4  
Chorolque: Fluid Inclusion Homogenization Temperature  
and Salinity Data

Sample	No. <sup>1</sup> Tested	Type	Class. <sup>2</sup>	T <sub>h</sub> Range (°C)	T <sub>h</sub> Mean (°C)	T <sub>soln.</sub> <sup>3</sup> (°C)	Salinity <sup>4</sup>
NG 242. Altered (quartz- tourmaline) vent rock. Pieru Unu adit.	5	VI	PS/P	628-810	715		
	1	"	"		798		
	2	"	"	677-678	678		
	2	"	"	715-716	716		
	9	"	"	444-637	550	359	43
	1	"	"		532		
	2	"	"	811-816	813	421	48
NG 115. Altered (quartz- tourmaline) vent rock. At Veta 18, 8-level.	7	VI	PS	427-760	595		
	5	IV	"	489-582	525	411	46
	2	"	P	319-320	320	290	37
	6	VI	P/PS	445-512	481	430	50
	3	"	PS	416-457	436		
	1	"	"		822		
	3	"	"	531-561	552	535	60
	4	"	"	497-577	533		
NG 112. Altered (quartz- tourmaline) vent rock. At Veta 4, 8-level.	3	VI	PS	536-563	552		
	4	"	"	498-577	533		
NG 261. Altered (quartz- tourmaline) vent rock. Surface, Cerro Chorolque summit.	10	IV	PS	395-517	440	390	45
	7	"	"	366-476	412	360	43
	4	"	"	400-494	442	296	38
	5	"	"	348-425	368	290	37
NG 507. Vein quartz, at outer edge of Veta Colon, 13-level.	7	VI	PS	503-552	541		
	5	"	"	488-528	506	325	40
	20	"	"	473-477	475	470	53
	9	IV	"	368-441	393	320	39
	5	"	"	364-396	383	350	40
	6	"	"	324-364	347	300	38
	5	III	"	340-354	347	243	34
	4	"	"	324-372	350	228	33
	4	"	"	221-242	230	165	31
	12	II	"	308-313	311		
	5	I	"	208-296	286		

1. Number of inclusions tested per heating run.
2. Inclusion classification: P=primary, S=secondary, PS=pseudo-secondary.
3. Solution temperature of last-melting daughter mineral (normally halite).
4. Fluid salinity in equivalent weight percent NaCl.

TABLE 4. Continued

Sample	No. <sup>1</sup> Tested	Type	Class. <sup>2</sup>	T <sub>h</sub> Range (°C)	T <sub>h</sub> Mean (°C)	T <sub>soln.</sub> <sup>3</sup> (°C)	Salinity <sup>4</sup>
NG 277. Vein quartz, pre- cassiterite and intergrown with cassiterite. From east end, Veta Colon.	8	IV	PS	390-408	398	348	41
	10	"	"	338-375	360		
	15	"	"	353-359	357	316	39
	3	"	"	344-363	355	325	40
	8	"	"	325-372	355	306	38
	3	I	"		290		
	2	"	"		288		
	1	II	"		281		15
	13	"	"	286-306	296		
	12	I	"	278-292	282		
	5	"	"	268-302	275		
	14	"	"	266-281	272		
	5	"	"	252-311	287		
	2	II	"	235-238	236		
6	I	S	163-194	183		3	
NG 121. Early vein quartz, intergrown with cassiterite. Veta Colon, 17-level.	3	IV	PS	347-353	349	258	37
	5	III	"	346-357	353	270	36
	6	I	"	297-333	313		
	9	II	"	275-309	291		
	3	"	"	235-281	250		
NG 273. Quartz from small vein at east side of the vent.	9	IV	PS	327-351	336	274	36
	2	I	"	283-284	284		
	12	II	"	261-288	277		
	7	"	"	220-300	273		
NG 112. Quartz intergrown with cassiterite, Veta 4, 8-level.	28	II	PS	269-309	269		16
NG 251. Quartz intergrown with cassiterite, small vein near Cerro Chorolque summit.	6	I	PS	289-301	294		14
	1	"	P		282		
	6	"	PS	201-305	262		
	5	"	"	273-282	270		
	4	II	"	239-282	269		



TABLE 4. Continued

Sample	No. Tested <sup>1</sup>	Type	Class. <sup>2</sup>	T <sub>h</sub> Range (°C)	T <sub>h</sub> Mean (°C)	T <sub>soln.</sub> (°C) <sup>3</sup>	Salinity <sup>4</sup>
NG 123.	10	I	S	352-386	375		
Igneous quartz	10	"	"	365-385	375		
phenocrysts, from	3	"	"		376		
sericitized volcanics,	4	III	"		365		
Mina Siete road.	6	I	"		365		
	4	"	"	353-364	361		
	1	III	"		342	190	31
	5	"	"		332	170	30

CHOROLQUE, FLUID INCLUSION HOMOGENIZATION TEMPERATURE DATA.

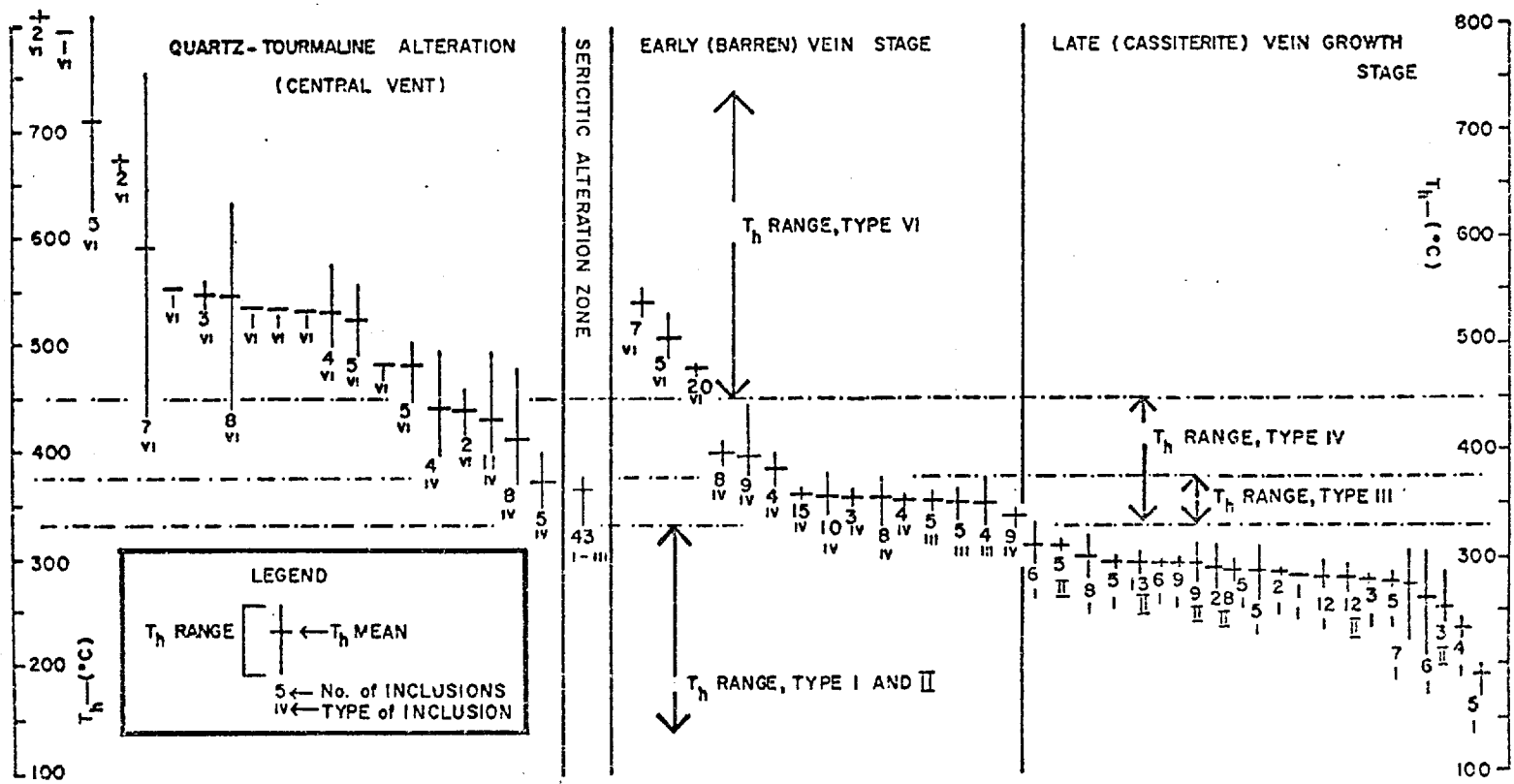


FIG. 3.4

temperature ranges and inclusion types (and hence salinity), and the progressive alteration and vein growth stages. This is summarized in Fig. 3.5. There is a wide spread in the  $T_h$  values within individual samples of the early alteration quartz, compared with the later vein quartz. This is probably due partly to differential trapping of the liquid and vapour phases in the boiling fluid. Part of the spread may also be due to unrecognized necking of the inclusions, which is more common in high-temperature material.

The geological relationships discussed in Chapter 2 indicate that the early quartz-tourmaline alteration of the vent, and the sericitic alteration of the surrounding rocks, were essentially contemporaneous. The inclusion data indicate that temperatures in the vent ranged from approximately  $600^{\circ}\text{C}$  down to  $350^{\circ}\text{C}$  during quartz-tourmaline alteration. Most samples gave values between  $500^{\circ}\text{C}$  and  $400^{\circ}\text{C}$ .

The data for the sericitized volcanics peripheral to the vent (NG 123) is subject to great uncertainty, since only secondary inclusions can be used. Temperatures in the range of  $400^{\circ}\text{C}$  to  $300^{\circ}\text{C}$  are indicated, and the fluid salinity is much lower than in the vent rocks. There are some vapour-phase inclusions in this material also, so the fluid evidently did boil, at least intermittently. The formation temperature of the dispersed sulphide and cassiterite mineralization in the sericitized volcanics and underlying sedimentary rocks has not been determined, as no suitable material was found. The data for NG 123 probably indicates the upper temperature limit for alteration peripheral to the vent, but mineral deposition may

CHOROLQUE — INNER ALTERATION ZONE AND THE VEINS  
 SCHEMATIC DIAGRAM — FLUID TEMPERATURE/SALINITY EVOLUTION WITH TIME

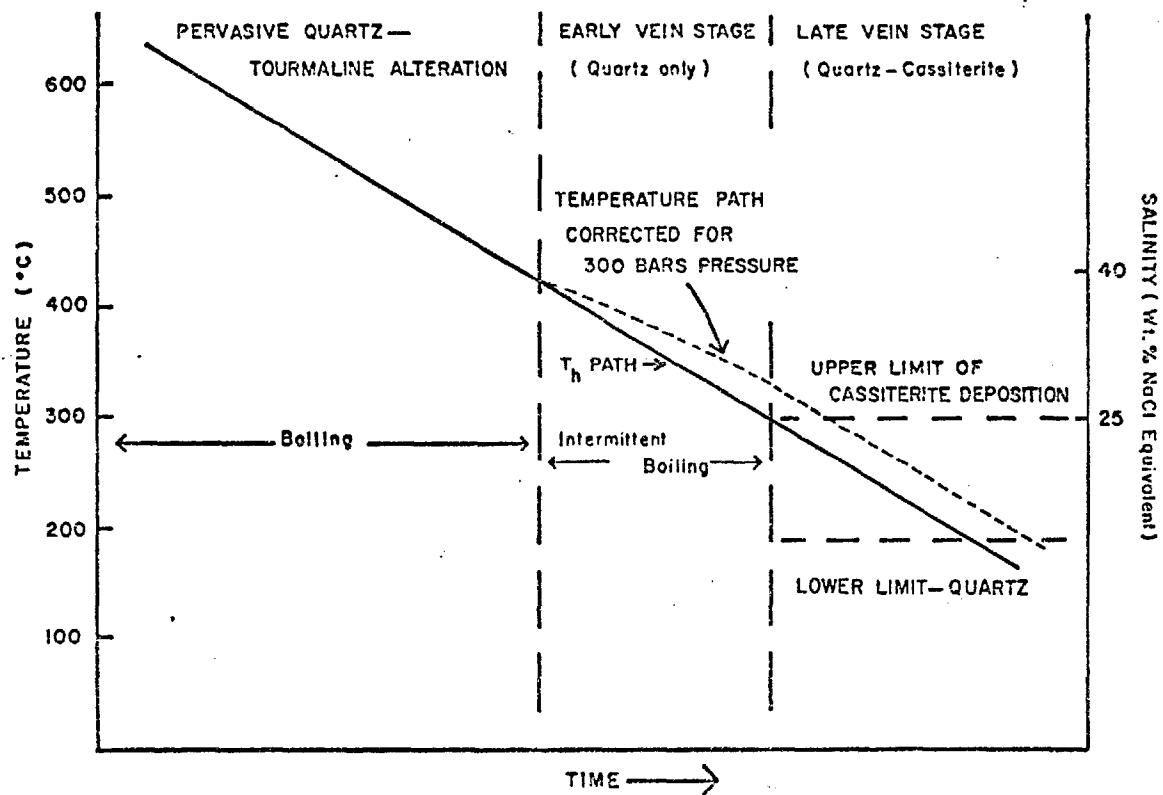


FIG. 3.5

have taken place at considerably lower temperatures. In other Bolivian deposits relatively low temperatures are indicated for sulphide-rich mineralization. A rather steep temperature-salinity gradient outward from the vent seems probable.

The geological data also indicate that the major vein system began to form after the pervasive alteration of the vent and surrounding rocks. The fluid inclusion data indicate that, in the case of the Veta Colon (which is the largest of the vein structures) the fluid conditions during the earliest stage of vein growth were essentially the same as in the surrounding quartz-tourmaline altered rocks. There are co-existing primary and pseudo-secondary Type VI and V inclusions, and the temperature was above  $450^{\circ}\text{C}$ . This suggests that the beginning of vein formation and pervasive alteration were at least partly contemporaneous. In the other veins there is a distinct temperature and salinity difference between fluids in the earliest vein quartz and in the surrounding rocks, supporting the geological evidence for the somewhat later formation of the veins. The data show a progressive decline in temperature and salinity during vein growth. The last quartz deposition took place at temperatures in the region of  $250^{\circ}$  and with fluid salinity as low as 10 equivalent weight percent NaCl. Of particular importance is the evidence that all cassiterite deposition took place at relatively low temperatures ( $T_h$  below  $300^{\circ}\text{C}$ ) and from a relatively dilute solution. No significant cassiterite or sulphide deposition took place from the high-temperature, highly saline fluid during the alteration of the vent rocks and early stages of vein growth.

The need for a pressure correction has been discussed above. The inclusion assemblage in the quartz-tourmaline vent rocks indicates that the fluid was on the 2-phase boundary so no pressure correction is required for the  $T_h$  measurements; the data for these fluids can be used to estimate the maximum confining pressure which would have allowed the fluids to boil, using the vapour-pressure data for the NaCl-H<sub>2</sub>O system (Sourirajan and Kennedy, 1962). This then gives the maximum depth at which the deposit could have formed, provided some estimate can be made of the likely pressure gradient. Taking the minimum salinity at which boiling took place as 40 equivalent weight percent NaCl, and a temperature of 450°C, gives a vapour pressure of approximately 300 bars. The depth at which this pressure would obtain is difficult to estimate. Assuming a lithostatic pressure gradient of approximately 300 bars/km would give a maximum depth of 1 km. However, if the pressure was essentially hydrostatic, the depth could be considerably greater. Extrapolation of Haas's (1971) data for NaCl-H<sub>2</sub>O solutions indicates that a 40 percent NaCl solution at 450°C would boil at approximately 2 km depth. This assumes uniform salinity with depth. If the salinity of the hydrostatic column was non-uniform with depth, dilute at shallow depth and increasing in salinity downwards, the maximum depth at which boiling could take place would be greater than 2 km. This seems to be a likely situation in natural systems. In a breccia pipe such as the Chorolque vent, the fluid pressure must have exceeded the lithostatic load pressure for brecciation to have taken place (assuming the brecciation is in fact due to explosive hydrothermal activity) and it seems likely that the pressure in the

fluid may have continued to remain above the purely hydrostatic level during the early alteration. Thus it seems reasonable to assume a depth of between 1 and 2 km for the samples taken in the lower mine levels, and this is consistent with the general geological setting. The effect of adding a correction for 300 bars pressure, using the data of Lemmlein and Klevtsov (1961) is shown in Fig. 3.5, which illustrates the general trends in fluid temperature and salinity during alteration and vein growth at Chorolque.

#### E. Chemical data

##### 1) Daughter mineral identification.

The daughter mineral population in Type VI inclusions is very complex. At room temperature the mineral grains commonly overlap with each other so that individuals are often difficult to distinguish optically (Plate 20). During heating runs, at least eight different daughters have been observed.

In the earliest vein quartz of the Veta Colon there are primary and pseudo-secondary Type VI inclusions which are larger and easier to study than those in the quartz-tourmaline altered rocks. They contain at least 6 daughter minerals and most of the identification work was done using this material. The dominant phases present (volumetrically) are a cubic isotropic mineral with refractive index very close to that of quartz, and a rhomb-shaped strongly birefringent mineral which is faintly greenish in colour and is sometimes twinned (Plate 23). The latter has a low solution temperature and commonly shows signs of having been partially dissolved and re-crystallized, apparently during sample preparation. These two salts are present in all Type VI

and IV inclusions. In the latter they may be the only daughters present, while in the former they are accompanied by numerous other salts. On the basis of its optical properties the cubic salt was identified as halite (NaCl), and this was confirmed by analytical work with the SEM.

An initial attempt to identify the rhombic birefringent mineral was made by crushing specimens containing relatively large Type VI inclusions in oil, and physical separation of the daughter mineral grains followed by tests for refractive index, and simple chemical tests. Although the technique was found to be impractical, one or two grains of this daughter mineral were successfully separated. It was found that the salt turned a yellow-brown colour and became deliquescent on exposure to air, and is soluble in acetone and alcohol, though not in  $\text{CCl}_4$ . Attempts to determine its refractive index by successive immersions in standard oils were not successful, but a simple test for iron using hydrochloric acid and potassium ferricyanide gave positive results. Some preliminary data on the overall composition of the Type VI inclusions was obtained by decrepitating selected inclusions in the heating stage and analysing the resulting condensate by EPMA, as described above. This confirmed the high Fe content of the inclusions, and Na, K, Cl and S were also detected.

The most useful data was gained using the SEM. Numerous Type VI and Type IV inclusions were examined in this way. Using the electron beam to probe individual grains it was possible to identify the presence of discrete K-Cl, Na-Cl and Fe-Cl salts. It was generally not possible to relate individual



grains seen in the SEM with those observed under the optical microscope because of the deliquescence and distortion which took place on opening. However, considering its optical properties as well, there is little doubt that the rhomb-shaped birefringent salt is a hydrous iron chloride, probably  $\text{FeCl}_2 \cdot 2\text{H}_2\text{O}$ . This has previously been identified as a daughter mineral in pegmatite quartz from Russia (Roedder, 1972b) and in vein quartz from a porphyry copper deposit in Peru (Le Bel, 1976).

It has not been possible to positively identify any of the other daughter salts in the Type IV and VI inclusions (apart from halite). The SEM work revealed substantial amounts of potassium in the Type VI inclusions. Sylvite is common as a daughter mineral in high temperature magmatic-hydrothermal deposits. An isotropic salt, with very low solution temperature and high relief relative to halite, is present in these inclusions and this may be sylvite ( $\text{KCl}$ ). The SEM frequently showed K occurring together with Na (and Cl) suggesting a mixed Na-K chloride salt, although this may also have been due to electron scattering from adjacent grains. Sulphur was detected in some of the inclusions studied (though not all), and usually in conjunction with Ca. A small rhombic highly birefringent salt which is very slow to dissolve on heating may be anhydrite ( $\text{CaSO}_4$ ). In some of the inclusions studied, a small grain giving the characteristic X-rays of iron alone was found, and this may be the opaque daughter, which is most probably an iron oxide. No silicate daughter minerals were positively identified, the characteristic X-rays for silicon were commonly recorded, but in most cases apparently came from quartz fragments

which had fallen into the inclusion cavity on opening, or from the walls of the inclusion.

The acicular birefringent daughter mineral which is characteristic of Type II inclusions is most probably dawsonite ( $\text{NaAlCO}_3(\text{OH})_2$ ). This has been found as a daughter in inclusions from many hydrothermal mineral deposits, and seems to be common in relatively low-temperature, dilute inclusions (Coveney and Kelly, 1971; Rye and Sawkins, 1974; Metzger et al., 1977).

## 2) General chemical data.

Some general data on the major element composition of the high salinity inclusions were obtained using the SEM. An attempt was also made to investigate some of the major cation ratios using the crushing and leaching method, and a little information was also obtained during experiments to test the usefulness of a laser microprobe in fluid inclusion analysis.

All of the data reported here concern the composition of the liquid phase, or solid daughter salts which have crystallized from what was a liquid phase at the time of trapping. The gaseous phase present in all of these inclusions at room temperature apparently consists essentially of  $\text{H}_2\text{O}$  vapour. Tests performed by crushing inclusion-bearing material in oil showed that none of the inclusion types in any of the deposits contained compressed gasses. There is no evidence that any of the inclusions contain significant amounts of  $\text{CO}_2$ . No liquid  $\text{CO}_2$ , or  $\text{CO}_2$ - $\text{H}_2\text{O}$  hydrate was observed during freezing tests. Several typical samples from the Chorolque and Llallagua altered rocks and veins were crushed under vacuum for extraction of the

inclusion fluid and isotopic analysis of the  $H_2O$  (described in Chapter 4). Attempts were made to separate any  $CO_2$  which might be present from the  $H_2O$  vapour by selective freezing in the vacuum line. The amounts of  $CO_2$  collected were unmeasurably small. The absence of  $CO_2$  in inclusions from any of the Bolivian tin deposit which they studied was also noted by Kelly and Turneaure (1970).

a) The scanning electron microscope data.

Numerous Type IV and VI inclusions were examined, mainly in early vein quartz from the Veta Colon. Typical aspects of opened inclusion cavities are shown in Plates 24 to 27.

Plate 24A shows a fractured sample surface at low magnification. A group of Type VI inclusion cavities are visible, together with daughter salt material which shows no crystalline form, and appears to have been extruded out of the inclusion cavities. This is probably the result of deliquescence of the salts on exposure to air when the sample was cracked open. Plate 24B shows one of these inclusions at higher magnification. The image resolution is very poor, but it can be seen that the daughter salts have lost their crystalline form. Cl, K and Fe are the only elements detected, and detailed study with the electron probe shows that most of the material gives X-rays of K and Cl only.

Plate 25A shows an inclusion cavity with relatively undisturbed daughter minerals inside. The X-ray data for two points are shown. One gives high Fe and Cl with minor Na, K, and Mn. The Na and K responses may come from adjacent grains excited by scattered electrons. The other gives high Na, K, and

Cl, with little Fe. This is fairly typical of the sort of data which can be obtained from inclusions of this type. The return of X-rays from within the inclusion cavity is weak, and the discrimination between individual grains is poor because of scattering effects. Plate 25B shows two adjacent inclusion cavities containing remnants of Na-K-Cl and Fe-Cl daughter salts. Plate 26A shows a single Type VI inclusion cavity crowded with daughter mineral grains. The image resolution is poor, but the X-ray data obtained by scanning the electron probe over the entire cavity shows that S is present in addition to Na, K and Cl.

Plate 26B shows a deep inclusion cavity containing distinct Na-Cl and Fe-Cl daughter minerals, together with numerous quartz fragments.

Plate 27 shows a sulphur bearing inclusion. Individual grains give characteristic X-rays for Fe-Cl-Na, and Fe-S-K-Cl although both spectra are probably composite due to scattering. Small amounts of Ca and P are also present.

In conclusion, the total list of elements identified in the Type IV and VI inclusions by this method is as follows :

Fe, Na, K, Mn, Ca, P, S, and Cl.

Although no quantitative information can be obtained, it seems probable that the relative proportions of Na and K are not far from equal, that Fe is a major component, and that Cl is greatly in excess of S. Many of the inclusions in fact gave no response for S, while it was consistently detected in other groups of inclusions. This suggests that the composition is variable among different generations of primary and pseudo-secondary inclusions within the alteration and early vein stages.

No metals were detected other than Fe and Mn, and the method is unsuitable for the detection of trace amounts of metal, as the sensitivity is often low because of orientation and scattering effects. Sn would be difficult to detect in any case, as its main X-ray energy lines overlap with those of K which is usually present in substantial amounts. The method has, however, been used to identify chalcopyrite as a daughter mineral in fluid inclusions from porphyry copper deposits (Le Bel, 1976).

b) Data from crushing and leaching.

An attempt was made to measure the major cation ratios in the inclusion fluids by crushing suitable sample material, leaching with de-ionized water, and analysing the leachate by atomic absorption spectrometry. The method of cleaning and preparing the samples has been described above. The samples used were as follows:

NG 507. Early vein quartz from the Veta Colon containing a high density of primary and pseudo-secondary Type VI inclusions.

NG 121. Vein quartz from the intermediate growth stage of the Veta Colon containing Type IV and III inclusions, with some Type II and I inclusions also.

NG 273. Late-stage quartz (associated with cassiterite) containing only Type II and I inclusions.

Also run were a sample of inclusion-free quartz, and a sample of de-ionized water which had been stirred in the agate mortar for 20 minutes and then passed through the filter paper.

Equal amounts of each sample (10 gm) were crushed in equal

amounts of de-ionized water (20 ml); however, the concentration of inclusions in each sample is not equal, so the analytical results are not directly comparable and only the ratios are meaningful. The results are shown in Table 5.

Considering the crudeness of this experiment, the only conclusion which can be drawn is that the data support the observations made with respect to the daughter mineral population, that the Na/K ratio of the hydrothermal fluid increased with decreasing salinity and temperature. This is in keeping with the normally observed trend in magmatic-hydrothermal systems. The Na/K ratio of less than 2 is somewhat low compared with values obtained during experimental water-rhyolite reaction at similar temperatures (Ellis, 1967). However, the extreme salinity and high K content of the early Chorolque fluids may be related to the particularly intense alkali depletion of the wall-rocks which accompanied the pervasive quartz-tourmaline alteration. The Na/K atomic ratio in the early Chorolque fluids (1.7) is comparable to the Na/K atomic ratio (0.85) in unaltered rhyodacite from Llallagua, which was probably similar to the original unaltered quartz-porphyry at Chorolque.

c) Laser microprobe data.

The methods used, and some of the problems which were encountered in attempting to use a laser microprobe for fluid inclusion analysis have been described above. In addition to samples from Chorolque, some highly saline inclusions from mineralized quartz veins from the Panguna porphyry copper deposit, Papua-New Guinea, and from quartz from a greisen zone (Bostraze) in the Lands End Granite, Cornwall, were analysed for comparison.

TABLE 5

Data from Crushing Experiment.  
 Analytical Results Expressed as Atomic Ratios.

Sample	Na/K	Na/Fe	K/Fe	Na/Ca
NG 507 A	1.70	1.41	0.83	11.30
NG 507 B	1.70	1.70	1.01	12.17
NG 121	2.42	2.51	0.85	6.09
NG 273	3.25	3.59	1.10	12.17
Brazil Quartz	3.16	-	-	4.87
Blank	2.87	-	-	-

The results are shown in Table 6, which summarizes the data from numerous individual inclusion analyses. The spectrograph used operates in the ultraviolet (2000 Å to 5500 Å) range, so only a limited number of elements could be detected, mainly the metals. The data confirm the high iron concentration in the Chorolque Type VI inclusions, and indicate the presence of several other elements which have not been detected by other methods. Most important is the indicated presence of tin and boron in the Chorolque samples, but their absence in the Panguna samples. Boron, but no tin was detected in the material from Cornwall.

Although the work demonstrates the potential usefulness of the method, particularly in the detection of low metal concentrations, there are many serious problems, and a great deal of work would be required before more reliable and quantitative results could be obtained.

### 3.4.2. Llallagua

#### A. Previous investigations

Previous geological investigations of the Llallagua deposit by Turneure (1935) have been discussed in Chapter 2. In their general study of the tin and tungsten deposits of the Bolivian Tin belt, Kelly and Turneure (1970) studied some samples of tin vein material from Llallagua. Their work indicated the general temperature and salinity conditions of cassiterite deposition in the veins. They measured homogenization temperatures in excess of 400°C in both early vein quartz and cassiterite, and found limited evidence of fluid boiling during cassiterite deposition. Freezing temperature measurements indicated that fluid salinity in the veins fluctuated between approximately 5 and 25 equivalent



TABLE 6

## Laser Microprobe Qualitative Results

Element	Spectral Line (Å)	Chorolque, Bolivia	Bostraze, Cornwall	Panguna New Guinea
Fe	Many	XXX	XX	XX
Mn	2949	XX	XX	XX
	2939	XX	XX	XX
	2933	XX	XX	XX
B	2496.7	XX	XX	
	2497.7	XX	XX	
Al	3082	XX		XX
	3092	XX		XX
Ca	3158.9			XX
	3179.3	XX		XX
Ti	3190	XX	XX	XX
	3249.4	XX	XX	XX
	3337	X		
Cu	3247.5	XX	XX	XX
	3272.9	XX		
W <sup>1</sup>	2444	XX	XX	XX
	2452	XX	XX	XX
	2533.6	XX	XX	XX
K <sup>2</sup>	3446	X	X	X
Sn	2840	X		
	3262	X		

XXX - Strong Response

XX - Weak Response

X - Tentative Response

1 - Probably due to contamination

2 - Beyond optimum range of Spectrograph.

weight percent NaCl.

Additional work was carried out in this study in order to get more information on the fluid conditions during vein formation, and to relate this to fluid conditions during alteration of the stock and formation of the breccia pipes.

#### B. Material studied

Only quartz was studied. As at Chorolque the cassiterite now being mined is very dark in colour, and fine grained. Three types of quartz were studied; primary igneous quartz phenocrysts from altered (mainly sericitized) rocks, vein quartz, and quartz (intergrown with cassiterite) which replaces rock fragments in one of the hydrothermal breccia bodies. Unlike the situation at Chorolque, cassiterite and sulphides were deposited in association with the pervasive alteration of the stock, and cassiterite deposition took place in the earliest stages of vein growth. The later stages are dominated by sulphide mineralization. There is little quartz-tourmaline alteration exposed in the present mine workings at Llallagua, and where it is present (in the deepest levels) the secondary quartz is too fine grained to be usable for inclusion studies. The locations of the samples used are indicated in Table 7.

#### C. Classification, and distribution of inclusion types

The classification of inclusion types which was established for Chorolque is also applicable to Llallagua. The vast majority of inclusions which were found in all of the material studied are of Type I. They occur as primary, pseudo-secondary and secondary inclusions in the vein quartz, and breccia-replacement quartz, and as secondary inclusions in the quartz phenocrysts.

TABLE 7

Llallagua: Fluid Inclusion Homogenization Temperature  
and Salinity Data.

Sample	No. Tested <sup>1</sup>	Type	Class. <sup>2</sup>	T <sub>h</sub> Range (°C)	T <sub>h</sub> Mean (°C)	T <sub>soln.</sub> <sup>3</sup> (°C)	Salinity <sup>4</sup>
NG 495. Quartz phenocrysts, sericitized porphyry, 650-level.	2	I	S	458-461	460		
	2	"	"	375-378	376		
	2	"	"	460	460		
	2	"	"	376-404	390		
	1	"	"		372		
NG 467. Quartz phenocryst, sericitized porphyry, 685-level.	1	IV	PS		460	370	44
NG 41. Quartz phenocrysts, sericitized porphyry, 383-level.	5	I	S	351-359	357		
	2	"	"		352		
NG 39. Quartz phenocrysts, sericitized porphyry, 383-level.	6	I	S	283-339	319		
	3	"	"	334-361	343		
NG 44. Quartz phenocrysts, sericitized porphyry, surface.	15	I	S	296-312	303		
	1	"	"		295		
	2	"	"	290-295	293		
	4	IV	"		294	240	34
	3	I	"		294		
	1	"	"		288		
	1	"	"		288		
	1	"	"		288		
	2	IV	"		286		
	1	"	"		280	150	30
	3	I	"	265-270	268		
1	IV	"		240	118	28	
NG 36. Quartz-cassiterite intergrowth, Clavo San Jose, 551-level.	1	I	PS		398		
	1	"	"		396		
	4	"	"	364-375	369		
	1	"	"		368		
	1	"	"		360		
	1	"	"		361		
	7	"	"	343-356	353		
	1	"	"		351		
	1	"	"		342		
	3	"	"	320-352	333		
	2	"	"	326-337	332		
1	"	"		330			

1. Number of inclusions tested per heating run.
2. Inclusion classification: P=primary, S=secondary, PS=pseudosecondary.
3. Solution temperature of last-melting daughter mineral (halite).
4. Fluid salinity in equivalent weight percent NaCl.

TABLE 7. Continued

Sample	No. <sup>1</sup> Tested	Type	Class. <sup>2</sup>	T <sub>h</sub> range (°C)	T <sub>h</sub> Mean (°C)	T <sub>50%<sup>3</sup></sub> (°C)	Salinity <sup>4</sup>
NG 37. Quartz, early vein stage. Veta Bismarck, 383-level.	10	I	PS	367-391	386		
	7	"	"	382-387	385		
	3	"	"		383		
	8	"	"	377-385	380		
	10	"	"	375-382	380		
	3	"	"		374		
	10	"	"	352-388	366		
	6	"	"	450-358	354		
3	"	"	357-365	361			
NG 458A. Small quartz vein, San Miguel shaft, 530-level.	5	I	PS	356-398	388		
	11	"	"	348-370	364		
	5	"	"	171-182	174		
NG 458B. Quartz, early vein stage. Veta Esperanza, 530-level.	5	I	PS	349-362	357		
	2	"	"	344-355	350		
NG 460. Early vein quartz, with cassiterite. Veta Uno A, 530-level.	7	I	PS	372-380	376		
	7	"	"	365-384	375		
	8	"	"	341-382	365		
NG 32. Early vein quartz, with cassiterite. Veta San Jose, 586- level.	10	I	PS	364-385	380		
	5	"	"	378-379	379		
	6	"	"	369-384	372		
	7	"	"	362-368	364		
	6	"	"	251-266	257		
6	"	"	254-260	257			
NG 456. Early vein quartz, with cassiterite. Veta Esperanza, 530-level.	5	I	PS	344-363	357		
	4	"	"		320		
NG 495. Small quartz vein, with cassiterite. 650-level.	4	I	PS	300-348	325		
	2	"	"	310-313	312		
NG 467. Vein quartz, with cassiterite. Veta San Fermin, 685-level.	3	I	PS	312-325	325		
	1	"	"		320		
	4	"	"	320-325	322		18

TABLE 7. Continued

Sample	No. <sup>1</sup> Tested	Type	Class. <sup>2</sup>	T <sub>h</sub> range (°C)	T <sub>h</sub> Mean (°C)	T <sub>soln.</sub> <sup>3</sup> (°C)	Salinity <sup>4</sup>
NG 32A. Vein quartz with cassiterite. Veta San Jose, 586-level.	5	I	PS	382-389	384		12
	5	"	"	363-374	369		
	2	"	"	363-365	364		
	13	"	"	325-322	329		
	6	"	"	320-326	322		
	3	"	"	315-332	322		
	2	"	"	307-309	308		
	1	"	"		280		
	6	"	"	278-281	280		
	11	"	"	263-291	279		
	10	"	"		249		
	6	"	"	225-247	240		
	6	"	"	235-244	239		
	5	"	"	232-233	233		
	3	"	"	183-204	192		
3	"	"	144-152	149		5	
NG 32B. Vein quartz with cassiterite. Veta San Jose, 586-level.	13	I	PS	362-383	374		
	7	"	"	362-391	373		
	10	"	"	363-380	371		
	7	"	"	361-369	363		
	2	"	"	337-339	338		
	1	"	"		316		
	5	"	"	241-311	280		
	5	"	"	239-230	263		
	3	"	"	254-267	259		
	2	"	"	221-240	231		
	3	"	"	158-192	174		
	3	"	"	143-182	158		
	4	"	"	159-181	173		

Occasional Type II inclusions with a bladed or acicular weakly birefringent daughter mineral (probably dawsonite) were found, but they are much less common than at Chorolque. Type III and IV inclusions (secondary) were found in some quartz phenocrysts (Plate 28). They are very small and difficult to observe, and are not common. They were only found in tourmaline-rich altered rocks from the deepest mine levels. Type V (vapour) inclusions are common in the quartz phenocrysts as secondary inclusions and are also present (though not common) in the early vein quartz. No Type III or IV inclusions were found in the Llallagua vein or breccia-pipe material.

#### D. Temperature data

The homogenization temperature data are shown in Table 7 and Figs. 3.6 and 3.7. Little freezing work was done. The fluid salinity was below 26 equivalent weight percent NaCl during the alteration of the stock, except perhaps at the very deepest levels of the present mine workings, where occasional more highly saline inclusions have been found (Plate 28).

As described in Chapter 2, the pattern of alteration in the Salvadora stock is unrelated to the geometry of the vein system. Alteration appears to have followed development of the breccia pipes, and to have preceded and to some extent overlapped with development of the vein system. The inclusion data indicate that fluid conditions during alteration were closely similar, in terms of temperature and salinity, to conditions during early vein growth. This is particularly significant, since cassiterite deposition also took place during both alteration and early vein stages.

**LLALLAGUA, FLUID INCLUSION HOMOGENIZATION TEMPERATURE DATA.**

ALL TYPE I/II, PerPS INCLUSIONS- EXCEPT WHERE SPECIFIED

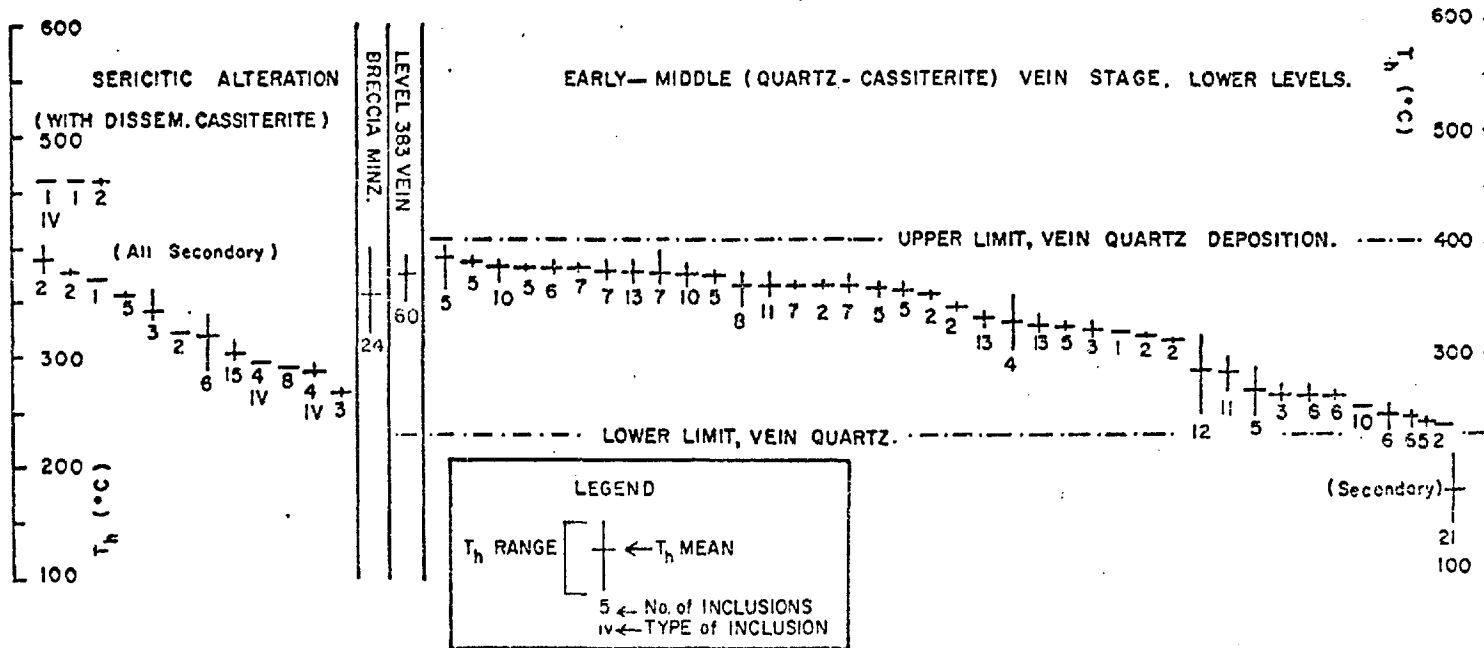


FIG. 3.6

LLALLAGUA — SERICITIC ALTERATION ZONE AND THE VEINS  
 SCHEMATIC DIAGRAM — TEMPERATURE / SALINITY EVOLUTION WITH TIME

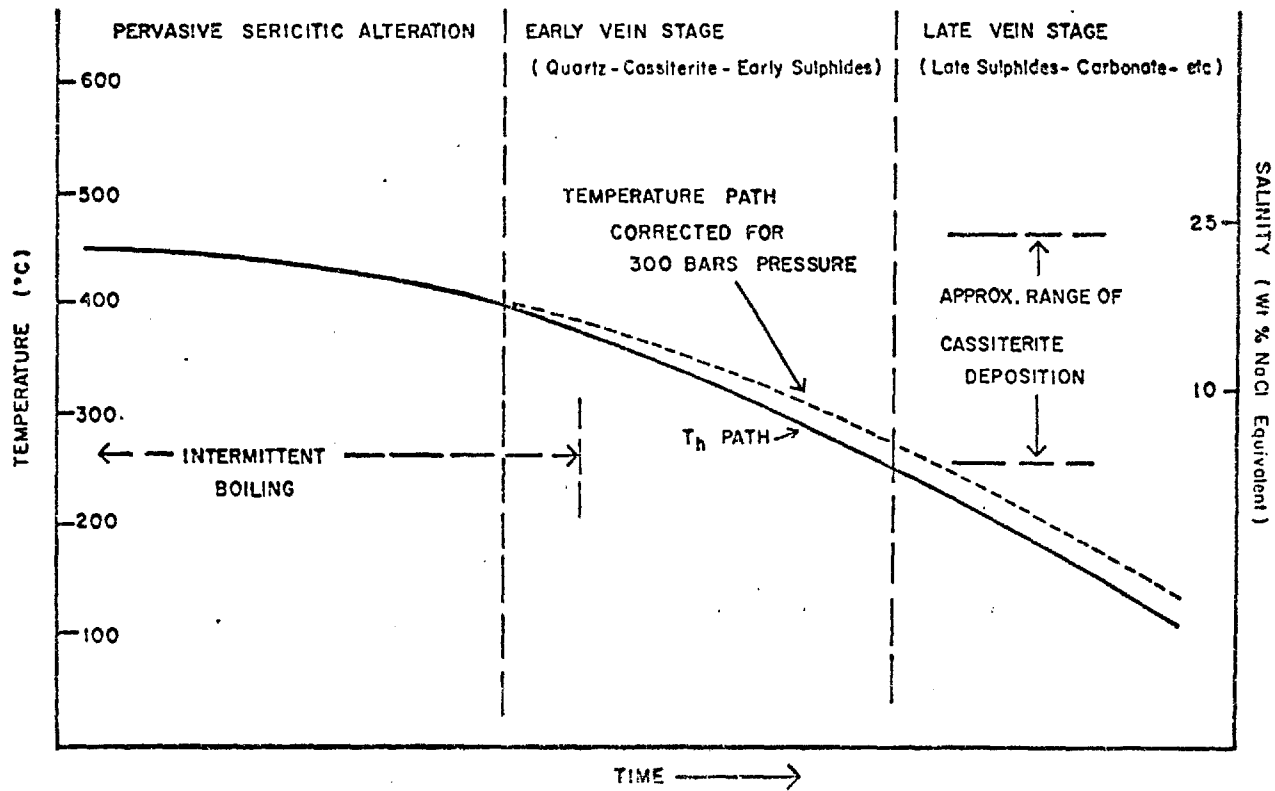


FIG.3.7



The data suggest that alteration took place at temperatures in general below  $400^{\circ}\text{C}$ . There are very numerous vapour phase (secondary) inclusions in some of the quartz phenocrysts, and occasional inclusions with a very high vapour to liquid ratio which homogenize in the vapour phase at temperatures near  $450^{\circ}\text{C}$ . It is possible that these represent an early higher-temperature condition, perhaps associated with the brecciation, when the system was vapour-dominated at that level. Insufficient work has been done to evaluate this.

The material from one of the breccia bodies (Ng 36) gave homogenization temperatures for secondary quartz replacing breccia fragments which are similar to those of the early vein stage (approximately  $350^{\circ}\text{C}$ ). It appears that the secondary quartz and cassiterite in the breccia were deposited by vein-stage fluids moving through the consolidated but still permeable pipe, and give no information as to the conditions of formation of the breccia. There is no evidence for boiling during deposition of this mineralization in the breccia.

The early vein stage quartz, with intergrown cassiterite, was deposited at between  $350^{\circ}\text{C}$  and  $400^{\circ}\text{C}$ . There is some evidence for boiling in the form of separate pseudo-secondary planes of vapour-filled inclusions, but these are not common. The freezing data of Kelly and Turneaure (1970) indicated fluid salinities as low as 5 to 10 equivalent weight percent NaCl for the early vein fluids. The later stages of vein growth, with much sulphide mineralization, took place at temperatures down to  $250^{\circ}\text{C}$ ; and the final stages, of sulphide-barite-fluorite-siderite mineralization, were probably

deposited at temperatures below this.

The salinity and temperature data for the early vein fluid provide some limitations on the possible depth at the time of ore deposition. Taking a temperature of  $375^{\circ}\text{C}$ , the maximum depth to which boiling could take place, assuming a hydrostatic pressure gradient, can be estimated by extrapolating the data of Haas (1971). Assuming a uniform fluid salinity of 25 equivalent weight percent NaCl, which is the maximum likely figure, gives a depth of about 2200 m. Assuming 5 percent salinity gives about 3000 m depth. The evidence for boiling during the vein stage is limited, and it may have been associated with only occasional temperature and pressure fluctuations. It appears that the fluid in general did not boil, but that it was close to the boiling curve. Assuming a salinity in general well below 25 percent, and a hydrostatic gradient, a depth in the range 2500 to 3000 m seems probable. This is a maximum likely depth range since a higher pressure gradient (e.g., partly lithostatic) would imply lesser depths. The data indicate a maximum likely hydrostatic pressure during ore deposition at the lower mine levels of around 200 bars. As an illustration, the effect on the homogenization temperatures of a 300 bar pressure correction is shown in Fig. 3.7 (data from Lemmlein and Klevtsov, 1961).

### 3.4.3. Potosi

#### A. Material studied and inclusion types

A limited study of the Potosi deposit was carried out, mainly on material from the veins. There was no previous fluid inclusion data for this deposit which is the most important

of the tin-silver deposits of Bolivia. Quartz is the only mineral which was found suitable for inclusion studies; as with the other deposits, the cassiterite is too dark and fine grained. Both vein quartz and quartz phenocrysts from the pervasively sericitized rocks were examined. In general the material is difficult to work with; the inclusions are very small, and much of the vein quartz is very clear and inclusion-free.

Four samples (NG 88, 89, 90, 91) are from veins from the deepest level at present being developed (Pailaviri-10, elevation 3900 m). Here the veins are narrow (less than 1 m width) almost vertical lodes made up of several narrow fractures cutting Palaeozoic siltstones. The mineralization is a simple open-space filling consisting of cassiterite and quartz with a little pyrite. Most of the cassiterite was deposited early, immediately adjacent to the vein walls, but deposition continued almost throughout vein growth. The individual fractures are vuggy, often with free-growing quartz crystals in the center.

Two samples (NG 294 and NG 295) are from the mid-upper levels of the vein system (Level Caracoles-70). Here the veins cut the altered igneous rock of the Cerro Rico stock. They are similar in form to the deep veins, i.e., lodes made up of multiple narrow fractures, and also narrow breccia lodes. The mineralization is sulphide-rich with much less quartz than at depth, and there is a late-stage filling of kaolinite and alunite.

As described in Chapter 2, the igneous rocks of the Cerro Rico stock are pervasively sericitized, except in the upper levels where argillic and siliceous alteration is developed.

Two samples of sericitized quartz-porphyry were studied (NG 93 and NG 94). The rocks are typical intensely sericitized quartz-porphyry containing much disseminated pyrite, and have a high tin content (over 1000 ppm).

The inclusions can be classified as at Chorolque and Llallagua. Only Type I (liquid plus vapour) inclusions were found in the veins. They generally contain a minute opaque daughter, and occasionally a trace of the acicular birefringent daughter (dawsonite) which has been found in the other deposits. The vast majority of the (secondary) inclusions in the igneous quartz phenocrysts are Type I inclusions also, however a few groups of Type III (halite-bearing) and Type IV (multiple daughter) inclusions were also found. They are extremely small and difficult to observe, but the Type IV inclusions contain a halite cube plus a rhombic birefringent salt as at Chorolque and Llallagua (Plate 29). Type V inclusions are not present, and this may be significant considering the virtual absence of hydrothermal brecciation within the Cerro Rico stock.

#### B. Results

The homogenization temperature data are shown in Table 8 and Fig. 3.7. Some of the early deep-level vein material gives  $T_h$  values well above  $300^{\circ}\text{C}$ , while late-stage temperatures are as low as  $190^{\circ}\text{C}$ . The maximum temperatures for the middle-upper level material is lower than for the deep-level material, indicating a vertical temperature gradient in the vein system. Assuming that the early quartz deposition was contemporaneous in the lower and upper levels, the temperature gradient could have been as high as  $100^{\circ}\text{C}$  over 400 m.

TABLE 8

Potosi: Fluid Inclusion Homogenization Temperature  
and Salinity Data.

Sample	No. <sup>1</sup> Tested	Type	Class. <sup>2</sup>	T <sub>h</sub> Range (°C)	T <sub>h</sub> Mean (°C)	T <sub>soln.</sub> <sup>3</sup> (°C)	Salinity <sup>4</sup>
NG 93 and 94. Quartz phenocrysts, sericitized porphyry, Pailaviri -10 level.	5	III	S	286-323	310	224	33
	5	"	"	282-289	287		
	1	"	"		285		
	3	"	"		280		
	3	"	"		272		
	1	"	"		270		
	1	"	"		264		
	5	"	"	252-275	263		
	3	"	"	258-266	262		
	1	"	"		255		
	1	"	"		242		
1	IV	"		240			
NG 89. Vein quartz, with cassiterite. Veta Bolivar-2, Pailaviri -10 level.	1	I/II	P		292		
	5	"	"	278-292	285		
	5	"	"	270-285	280		
	3	"	"	268-280	276		
	1	"	"		260		
	1	"	"		244		
	1	"	"		220		
	5	"	"	188-216	200		
	3	"	"		192		
	4	"	PS	168-212	190		
NG 90. Vein quartz, with cassiterite. Veta Bolivar Nueve, level Pailaviri -10.	1	I/II	PS		339		
	1	"	"		329		
	1	"	"		329		
	5	"	"	313-335	326		
	2	"	"	308-321	315		
3	"	"	306-316	312			
NG 295. Vein quartz with cassiterite. Veta Bolivar-2, level Caracoles -70.	4	I/II	P	269-281	275		
	2	"	"	272-273	273		
	3	"	"	266-276	269		
	4	"	"	267-271	269		
NG 294. As above, Veta Bolivar 1, level Caracoles -70.	4	I/II	PS	238-248	244		
	3	"	"	224-264	243		
	5	"	"	224-266	240		
	3	"	"	234-238	237		
4	"	"	194-246	224			

1. Number of inclusions tested per heating run.
2. Inclusion classification: P=primary, S=secondary, PS=pseudosecondary.
3. Solution temperature of last-melting daughter mineral (halite).
4. Fluid salinity in equivalent weight percent NaCl.

POTOSI, FLUID INCLUSION HOMOGENIZATION TEMPERATURE DATA.

ALL TYPE I/II INCLUSIONS Except Where Specified.

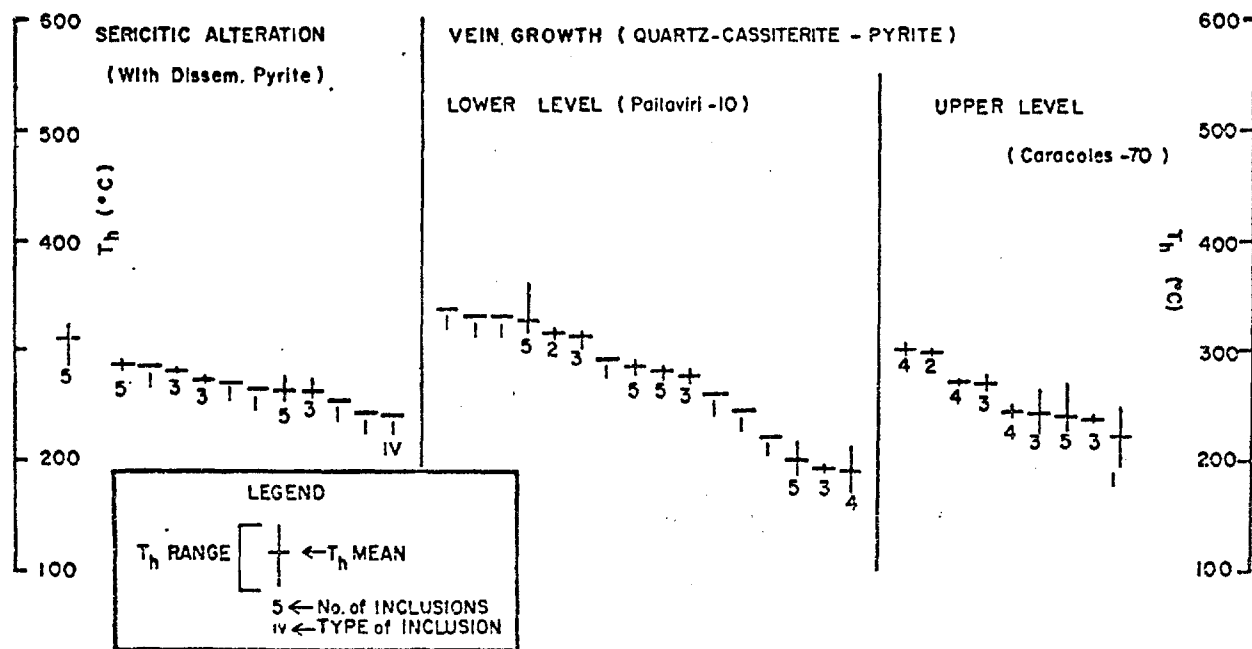


FIG. 3.8

The inclusion temperatures in the altered rocks are generally below those of the early vein quartz. Since the phenocryst inclusions are secondary, this is not reliable evidence that the vein temperatures did in fact ever exceed the temperature in the altered rocks; the phenocrysts might not have trapped secondary inclusions while the temperature was higher. In general the data are insufficient to draw detailed conclusions on the relative alteration stage and vein stage temperatures. However, there is no evidence that the alteration temperature was much different from that of the main vein stage. The pressure correction can not be estimated with any confidence since boiling is not indicated and the fluid salinity has not been determined. However it is clearly very small. The fluid inclusion data are consistent with a minimum depth of 600 meters for the lowest level samples taking  $300^{\circ}\text{C}$  as the temperature and 26 equivalent weight percent NaCl as the maximum possible salinity. A greater minimum depth would be indicated if the salinity is lower, e.g., 1000 meters at 5 percent NaCl (Haas, 1971). Although not definitive, the inclusion data are thus compatible with the geological evidence for a shallow depth.

As at Llallagua, deposition of tin and sulphide mineralization took place both throughout the sericitized parts of the stock as well as in the veins. The inclusion evidence suggests that fluid conditions were similar during the alteration of the stock and the main vein growth stage. Alteration probably began before the opening of the vein system, as the pattern of alteration is unrelated to the geometry of the vein system.

In contrast to Chorolque, fluid conditions in the veins were initially similar to those in the altered rocks, with cassiterite deposition spanning sericitic alteration and the main vein filling stage over a temperature interval from 300°C down to 250°C. Mineral deposition in the veins continued as the temperature decreased further, and base-metal and silver mineralization were deposited in the late stages and at the highest levels. This mineralization is not found in the altered rocks of the stock, indicating that during the late stages of hydrothermal activity, the mineralizing fluid was confined to the vein channelways.

#### 3.4.4. Other deposits

A very limited amount of data were obtained from 3 other deposits: Colquechaca, Chocaya, and Huanuni; the results are shown in Table 9. These were visited primarily in order to collect material for the K-Ar dating work described in Chapter 5, and a detailed fluid inclusion study was not intended.

The geology of Colquechaca and Chocaya have been outlined in Chapter 2. The vein mineralization in both cases is sulphide-rich, and there is very little quartz, so that detailed fluid inclusion study is not possible. Cassiterite, where present, is very fine grained and sphalerite is very dark.

Sample NG 61 is from a sphalerite-pyrite vein, carrying some cassiterite, which cuts the upper part of the Colquechaca complex. The volcanic rocks at the vein margins are strongly sericitized and argillized. There are occasional quartz crystals intergrown with the sphalerite, and the fluid inclusion data were



TABLE 9

## Miscellaneous Fluid Inclusion Homogenization Temperature Data.

Sample	No. Tested	Class. <sup>1</sup>	Type	T <sub>h</sub> Range (°C)	T <sub>h</sub> Mean (°C)
NG 61. Quartz intergrown with sulphides and cassiterite, Veta Invidiosa, Yanakaka, Colquechaca.	21	PS	I	236-360	290
NG 140. Quartz intergrown with galena-sphalerite. Veta Burton, Chocaya.	15 3	PS "	I "	185-240 206-239	205 228
NG 299. Quartz intergrown with cassiterite, Veta Keller, Huanuni.	14	PS	I	387-412	397

1. Inclusion classification: P=primary, S=secondary, PS=pseudosecondary.

obtained from these. Only Type I liquid plus vapour inclusions were found, and no salinity measurements were made. Sample NG 140 is from the Veta Burton, level 661, Mina Animas, Chocaya. This is a galena-sphalerite vein with little quartz which cuts the Palaeozoic sedimentary rocks beneath the volcanic rocks of the complex. Again, only Type I inclusions were found. These two samples illustrate the relatively low temperatures and salinities at which the sulphide-rich vein ores of the volcanic complexes were deposited.

In contrast, the Huanuni sample (NG 299) is from a quartz-cassiterite vein. The deposit is a complex vein system in Palaeozoic sedimentary rocks. The only direct evidence of igneous activity in the vicinity are some altered quartz-porphry dykes. On geological grounds the deposit appears to be deeper than the others, and probably related to an intrusive body which did not reach the surface. The vein quartz, intergrown with cassiterite, contains primary co-existing vapour and 2-phase liquid plus vapour inclusions (Plate 30). No daughter mineral-bearing inclusions were found. The 2-phase inclusions homogenize in the liquid phase at temperatures close to  $400^{\circ}\text{C}$ . Cassiterite deposition at Huanuni took place from a boiling, high temperature, relatively dilute (less than 26 equivalent weight percent NaCl) fluid. This is in contrast to the quartz-cassiterite vein mineralization at Chorolque where, although vein quartz deposition began at similar temperatures (above  $400^{\circ}\text{C}$ ) and the early fluid was boiling, the salinity of the early fluid was very high, and no cassiterite deposition took place until the salinity was below 26 equivalent weight percent NaCl, the

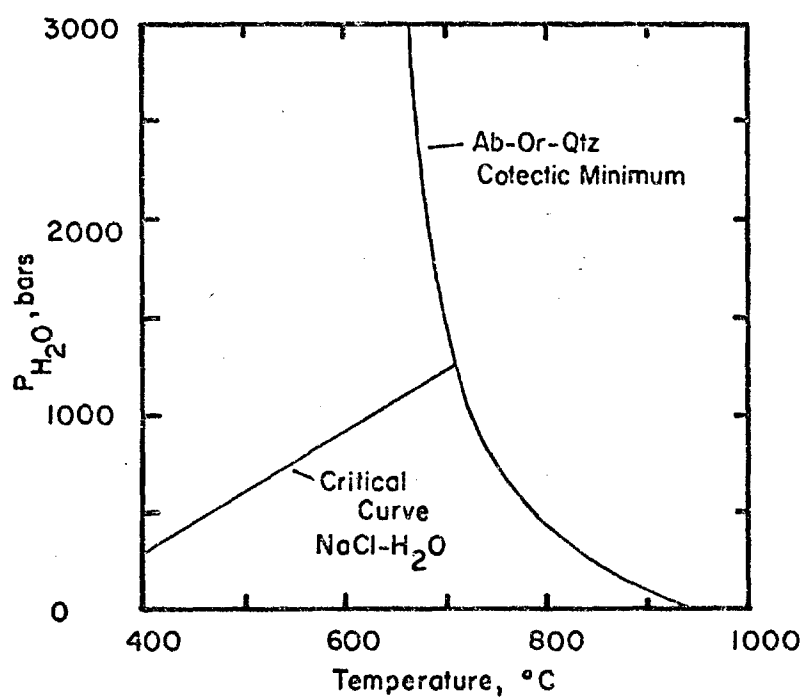
temperature had fallen to below  $300^{\circ}\text{C}$ , and boiling had ceased.

### 3.5. Discussion

The brecciated rocks of the Chorolque vent were altered to a quartz-tourmaline rock by a high-temperature 2-phase fluid consisting of a highly saline liquid and a low-density vapour. The data for the system  $\text{NaCl-H}_2\text{O}$  indicate that this is the expected behaviour for an aqueous fluid separating from an acid magma at shallow depth. The critical curve for the  $\text{NaCl-H}_2\text{O}$  system is shown together with the minimum melting curve for granite in Fig. 3.9. (Holland, 1967; Sheppard, 1977a). An aqueous fluid separating from an acid magma at temperatures below about  $700^{\circ}\text{C}$  and at pressures less than about 1200 bars would separate into a highly saline aqueous brine (greater than 50 equivalent weight percent  $\text{NaCl}$ ) and a separate low-density vapour phase. The ratio of brine to vapour would depend on the weight relationships of  $\text{H}_2\text{O}$  to soluble salts in the magma (Fournier, 1972). Fluids of this type have been described from the high-temperature alteration zones of numerous porphyry copper deposits (Roedder, 1971b; Nash and Theodore, 1971; Nash and Cunningham, 1974; Moore and Nash, 1974) and in several cases have been shown to be of magmatic origin on the grounds of their stable isotope characteristics (Sheppard, 1977a). The highly saline phase is typically rich in  $\text{NaCl}$  and  $\text{KCl}$ .

The highly saline fluid (Type VI inclusions) at Chorolque co-existed with a low-density vapour phase and has been shown to be rich in  $\text{NaCl}$  and  $\text{KCl}$ , and also  $\text{Fe}$  chloride. It thus has

FIG. 3.9



Relationship between the critical curve for NaCl-H<sub>2</sub>O and the melting curve of granite (after Holland, 1967 and Sourirajan and Kennedy, 1962)

many of the characteristics which would be expected of a magmatic fluid under the indicated conditions of temperature and pressure. However, the rocks of the Chorolque vent are strongly depleted in Na and K, and so it is possible that the highly saline fluid could have been derived by loss of alkalies during rock alteration, to a fluid of other than magmatic derivation, with the salinity perhaps increased by the effects of boiling. The results of a limited stable isotope study designed to investigate the origin of the fluid are discussed in the following chapter.

Little or no cassiterite or sulphide mineralization was deposited in the Chorolque vent from the early high-temperature fluid. It is likely, and there is supporting evidence from the inclusion fluid chemical data, that most if not all of the metals and sulphur were in solution in the fluid, but remained in solution until fluid temperature and salinity declined.

Mineralization was deposited both in the altered (sericitized) rocks peripheral to the vent, and in the later vein structures which cut the vent. The fluid inclusion data indicate that in both cases the temperature and salinity were much lower than during the early quartz-tourmaline alteration stage, and that cassiterite deposition took place after the fluid had stopped boiling.

At Llallagua, the exposed levels of the Salvadora stock are sericitized and carry disseminated cassiterite and sulphide mineralization, and the stock is cut by a mineralized vein system. In the deepest levels the alteration is tourmaline-rich,

and sericitization dies out. The mineralization in the vein structures extends downward into the tourmalinized rocks for a short distance only. The fluid inclusion data indicate that in contrast to Chorolque, the fluid conditions during sericitic alteration and disseminated ore mineral deposition, and main vein stage mineral deposition, were similar. The fluid was high-temperature but dilute (less than 26 equivalent weight percent NaCl), and boiling did take place during cassiterite deposition although it had ceased before the main sulphide deposition stage in the veins. There is limited fluid inclusion evidence that the tourmaline-rich alteration at depth, which is barren of disseminated mineralization, was associated with a highly saline boiling brine similar to that which formed the quartz-tourmaline alteration at Chorolque.

Thus the two deposits show comparable zonal relationships of alteration and mineralization. At Llallagua the zonation is vertical. A deep tourmaline-rich alteration zone is barren of ore mineralization (it contains a little pyrrhotite). It was probably developed under high-temperature, high-salinity boiling fluid conditions, although fluid inclusion evidence is limited. It is overlain by a sericitic zone containing disseminated mineralization and cut by a mineralized vein system. Both alteration and disseminated and early vein mineral deposition took place under similar moderate-temperature and dilute fluid conditions. At Chorolque the zonation is lateral (concentric). The inner (vent) quartz-tourmaline zone is barren of mineralization, and formed under high-temperature and high-salinity, boiling fluid conditions. It

is surrounded laterally by a mineralized sericitic zone which formed under distinctly lower temperature and salinity conditions. The barren core is cross-cut by mineralized veins, but ore deposition did not begin in the veins until fluid temperature and salinity conditions were much lower than those at which the tourmaline-rich alteration developed, and are similar to those of the sericitic zone.

The mechanical effects of boiling have been mentioned in Chapter 2 with respect to the origin of the hydrothermal breccias, and have been discussed in detail by Phillips (1973). The fluid inclusion data reported here do not provide any direct evidence as to the mechanism of formation of the breccias. They do show however, that fluid boiling took place throughout the highly brecciated Llallagua stock and Chorolque vent during post-breccia alteration at least, but apparently did not take place in the Cerro Rico stock which is essentially unbrecciated. Only a limited amount of material from the Cerro Rico stock has been studied, so the evidence against fluid boiling is not conclusive.

Zonal relationships of alteration and mineralization in hydrothermal deposits are controlled by several interrelated factors including changes in fluid temperature, pressure, salinity, pH and oxidation state (e.g., Barnes, 1975; Helgeson, 1970). Boiling could be an effective mechanism for ore deposition since it would decrease the fluid temperature and increase pH by loss of volatile acids ( $\text{CO}_2$ ,  $\text{H}_2\text{S}$ ,  $\text{HCl}$ ,  $\text{HF}$ ) in the vapour phase. Both effects would favour deposition of metals which are in aqueous solution as chloride complexes

(Helgeson, *op. cit.*). It has been invoked as a primary cause of ore deposition in numerous relatively near-surface hydrothermal deposits, and Turneaure (1960) suggested that the location of 'bonanza' ore-shoots in the Llallagua veins were controlled by the interval over which boiling was taking place. The fluid inclusion data presented here do not support a simple causative relationship between boiling and ore deposition. At Chorolque, almost all mineralization (except quartz) was deposited after boiling had ceased. At Llallagua, the period of at least intermittent boiling did coincide with deposition of ore mineralization but there is also evidence that much mineralization, including cassiterite ore, was not deposited from a boiling fluid. There is no evidence for boiling in the material studied from the rich Potosi veins, but some of the very rich cassiterite ore in the Huanuni veins was certainly deposited from a boiling fluid. It does seem that boiling may contribute to the deposition of particularly rich cassiterite ore, but it is certainly not a requirement for ore deposition in these systems.

The low-density vapour phase of a high-temperature two-phase aqueous fluid of magmatic origin would contain other volatiles in addition to  $H_2O$ , including  $H_2S$ ,  $HCl$  and  $HF$ . This vapour would move outward and upward, and condense to form an acid liquid of moderate salinity and lower temperature. Sericitic alteration indicates low pH conditions, and is characteristically associated with maximum sulphide deposition in many hydrothermal deposits including the Bolivian sub-volcanic tin deposits. It could be suggested that the zonal



relationships of alteration and mineralization at these deposits are simply related to a single boiling fluid. The zones of sericitic alteration and dispersed mineralization might have formed from a condensed vapour phase which had migrated upward and outward from the high-temperature inner and deeper regions of a magmatic-hydrothermal system. This implies, however, that the metals were carried in the vapour phase. There is evidence that significant amounts of some metals can be transported in sub-critical aqueous vapour although it is not clear if this is true of tin. A more complex mechanism, perhaps more likely, could involve the outward and upward mixing of the high-temperature boiling fluid with a cooler fluid, perhaps meteoric or formation water from the surrounding rocks. The metals could be transported outward and upward in solution in the highly saline liquid phase, which would become progressively diluted and cooled. Mineral deposition would take place in the zone of mixing because of temperature and salinity decrease and changes in pH and the availability of oxygen and reduced sulphur. These same factors would apply to mineral deposition in the veins. The fluid inclusion data, especially for Chorolque, show that substantial temperature and salinity decline did take place before cassiterite and sulphide mineral deposition began. The physical and chemical controls on the deposition of cassiterite are not well established, and the mechanism by which tin is transported in hydrothermal solutions is not clear. The close association of cassiterite with base-metal sulphide minerals indicates that the conditions under which

they are transported and deposited are similar. The presence of sulphur and iron in the brine phase of the early fluid at Chorolque has been demonstrated, and tin and copper have also been tentatively identified. The controlling effect of temperature decline on sulphide deposition is well documented (e.g., Holland, 1965; Barton and Skinner, 1967; Helgeson, 1970; Barnes, 1975). The importance of a high chloride concentration in extracting and transporting metals from magma and rocks by a hydrothermal fluid has also been demonstrated (Holland, 1972) and there is no doubt about the high chloride content of the early brines in the Chorolque system. The effect of salinity decrease in precipitating chalcopyrite has been documented (Crerar and Barnes, 1976) and this can be expected to apply in general to the other base metal sulphides and probably cassiterite also.

The direction of pH change in the Bolivian deposits is not altogether clear. Such data as is available (Smith, 1949) indicates that tourmaline is only stable at near-neutral pH at high temperature. Thus, the quartz-tourmaline alteration of the vent rocks at Chorolque and the deep levels of the Salvadora stock at Llallagua might be regarded as equivalent to the zone of potash metasomatism which is characteristic of the inner, high-temperature alteration zone of the porphyry copper deposits. The temperature of formation and general fluid conditions are very similar. In the porphyry copper deposits, the surrounding sericitic zone indicates an initial decrease in pH outwards (Rose, 1970). In the Bolivian deposits the destruction of feldspars and extreme leaching of alkalis which accompanied

quartz-tourmaline alteration indicates more acid conditions in the highest-temperature regions, so the comparison may not be valid.

In conclusion, the initial hydrothermal activity at these deposits was highly explosive, resulting in widespread breccia development. The early post-breccia fluid, represented by the inclusion fluid in the quartz-tourmaline altered vent rock at Chorolque, was at high temperature (over 500°C) and comprised two separate co-existing phases, a low-density vapour and a highly saline brine rich in Na, K and Fe chlorides. This fluid has many of the characteristics expected of a primary magmatic hydrothermal fluid separating from an acid magma at low pressure, although other modes of origin are also possible. Intense pervasive hydrothermal alteration took place in the vent area where the fluids were streaming upward. Quartz-tourmaline alteration developed in the highest temperature and salinity regions, exposed only at Chorolque and the deepest levels at Llallagua. No ore mineral deposition took place under those conditions. Sericitic alteration, which is peripheral to the quartz-tourmaline zone at Chorolque, vertically above it at Llallagua, and developed throughout the lower and middle regions of the Cerro Rico stock at Potosi, is associated with lower fluid temperatures and salinities. In all of the deposits studied, ore mineral deposition began only when temperature and salinity had fallen to the range in which sericitic alteration was taking place (mainly 250-350°C, less than 26 equivalent weight percent NaCl salinity). Probable causes of ore deposition include the documented decline in fluid

temperature and salinity, and also probable changes in pH, and increasingly oxidizing conditions. All of these may be related to the incorporation of dilute meteoric water into a convecting hydrothermal system, which could explain the observed lateral and vertical zoning of alteration and mineralization, including the extreme acid leaching which is characteristic of the highest levels of the eruptive complexes. The model concepts are discussed in more detail in Chapter 6.

## C H A P T E R 4

OXYGEN AND HYDROGEN ISOTOPE STUDY4.1. Introduction

The processes which concentrate tin into the most highly specialized end-members of a differentiating granitoid magma series are relatively well understood. However, the mechanisms and processes by which tin is transferred to, transported in, and deposited from a hydrothermal fluid are not well understood. Part of the solution to these problems lies in determining the origin of the fluids during the various stages of evolution of the hydrothermal system.

Oxygen and hydrogen isotope studies provide one of the more powerful methods for distinguishing between waters of different origin; e.g., magmatic, meteoric, formation, or sea water etc. The principles and application of this approach have been reviewed by Taylor (1974) and Sheppard (1977a).

In regions where the isotopic characteristics of magmatic and meteoric water can be differentiated, these studies have shown that in the sub-volcanic porphyry copper-molybdenum type ore-forming systems magmatic waters were associated with the earliest and highest temperature alteration (K-silicate alteration) and sulphide deposition processes. These took place in the inner, deeper parts of the systems, largely within an intrusive igneous rock-mass. A meteoric-hydrothermal convective system operated in the surrounding country rocks, and progressively collapsed inward on the magmatic-hydrothermal

system as temperature and magmatic fluid supply declined. The strength of the meteoric convective system critically affects the rate of cooling of the intrusive mass. Physical-chemical gradients are particularly large in the zone of mixing between magmatic and meteoric fluids, and ore-mineral precipitation is concentrated in that zone.

The close geological similarities between some of the sub-volcanic tin deposits of Bolivia and typical porphyry copper deposits suggests a similar origin (Sillitoe et al., 1975). The supporting evidence of the fluid inclusion studies is described in Chapter 3. However, as pointed out in Chapter 2, the type of rock alteration associated with the early stages of fluid evolution in the Bolivian deposits is different from that in the porphyry copper deposits. This reconnaissance stable isotope study was carried out to test if the distinction between magmatic and meteoric waters is possible in the Bolivian setting and, if possible, to set some constraints on the origin of the fluids which were responsible for tin transport and deposition at the several stages during the evolution of these systems.

#### 4.2. Principles

The general principles of oxygen and hydrogen isotope geochemistry have been described in detail, for example, by Epstein and Mayeda (1953), Hoefs (1973), Sheppard (1977a) and Taylor (1967, 1968, 1974, 1977). Only a brief discussion of the principles most relevant to the Bolivian problem are presented here.

The light elements such as hydrogen, carbon, oxygen and

sulphur have stable isotopes whose composition or ratios vary in natural materials. The isotopes are partitioned among the different phases, often in a systematic way, because of equilibrium or kinetic isotope fractionation processes. The fractionation of isotopes between two species X and Y are described in terms of the fractionation factor  $\alpha$  where

$$\alpha_{x-y} = \frac{R_x}{R_y}$$

and  $R_x$  is, for example, the D/H or  $^{18}\text{O}/^{16}\text{O}$  ratio in species X and  $R_y$  is the same isotope ratio in species Y. In the present context,  $\alpha$  often closely approximates to the equilibrium isotope fractionation and is temperature dependent. Kinetic isotope fractionations, which arise because the different isotopes of an element react at different rates, are not considered here.

The isotopic data are presented as deviations of the relevant isotopic ratio from that ratio in an arbitrary standard. The conventional notation is as follows :

$$\delta_{\text{sample}} \text{ (in per mil, } \text{‰}) = \left[ \frac{R_{\text{sample}}}{R_{\text{standard}}} - 1 \right] 1000$$

where, for oxygen,  $\delta = \delta^{18}\text{O}$  and  $R = ^{18}\text{O}/^{16}\text{O}$

for hydrogen,  $\delta = \delta\text{D}$  and  $R = \text{D}/\text{H}$

For both oxygen and hydrogen, the standard is Standard Mean Ocean Water or SMOW. Since  $\delta_{\text{standard}}$  is equal to 0, the  $\delta_{\text{sample}}$  values are either positive (enriched in the heavy isotope) or negative (depleted in the heavy isotope) relative to the standard. For small differences in  $\delta$  between two minerals or species, it can be shown that

$$1000 \ln \alpha_{x-y} = \delta_x - \delta_y$$

which gives a relationship between the measured isotopic composition of two species X and Y,  $\delta_x$  and  $\delta_y$ , and the fractionation factor  $\alpha_{x-y}$ .

Waters of different origin have characteristic hydrogen and oxygen isotopic compositions (Fig. 4.1). Sea waters have a very restricted range of compositions. Present-day meteoric waters (rain, rivers, snow etc) have a very wide range of isotopic compositions but lie about a straight line, the meteoric water line. This reflects the fractionation processes for both hydrogen and oxygen isotopes during vapour-liquid condensation. The isotopic composition of a meteoric water is related through this to the latitude, altitude, and previous path history of the clouds.

Magmatic water is defined as an aqueous fluid (of whatever ultimate origin) that has thoroughly exchanged or equilibrated isotopically with a silicate magma. Primary magmatic waters have compositions in the range  $\delta D$  -40 to -80 ‰,  $\delta^{18}O$  + 5.5 to + 9.5 ‰, based on the isotopic composition of 'normal' igneous rocks. Thus the isotopic compositions of unmodified meteoric waters are distinct from primary magmatic waters (Fig. 4.1) although some meteoric waters have  $\delta D$  values within the magmatic water range. Because rocks are normally strongly enriched in  $^{18}O$  relative to meteoric waters, in a hydrothermal system isotopic exchange can take place between the water and rock resulting in a shift towards higher  $\delta^{18}O$  values in the water. The  $\delta D$  value of the water is normally unaffected since the rock contains so little hydrogen. The magnitude of the  $\delta^{18}O$  shift depends on the water : rock ratio, and can be used to



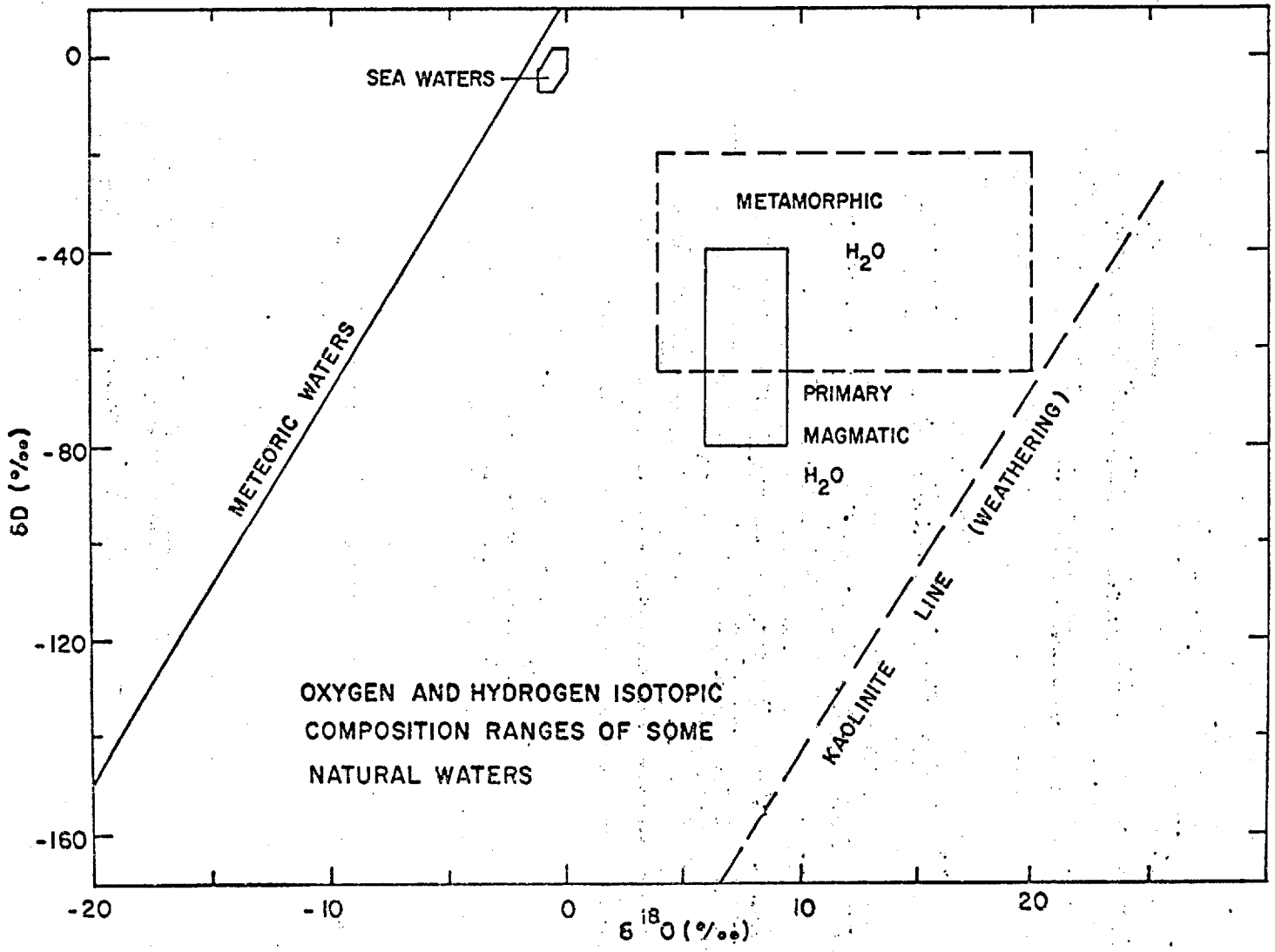


FIG. 4.1

estimate that ratio . In regions where meteoric waters have  $\delta D$  values within the primary magmatic water range a meteoric hydrothermal water which undergoes an " $^{18}O$  -shift" can acquire an isotopic composition indistinguishable from that of magmatic water.

#### 4.3. Analytical Methods

The isotopic analyses reported here were carried out in the laboratories of Dr. S.M.F. Sheppard at the Scottish Universities Research and Reactor Center, East Kilbride. The methods used are those given in Sheppard (1977b) for mineral and water samples, and in Rye and O'Neil (1968) for fluid inclusions. Oxygen was extracted from minerals using bromine pentafluoride and the resulting  $O_2$  gas converted to  $CO_2$  for mass spectrometric analysis (Clayton and Mayeda, 1963). Water samples (for oxygen) were equilibrated with  $CO_2$  at  $25^\circ C$  and the  $CO_2$  subsequently analysed (Epstein and Mayeda, 1953). For hydrogen, absorbed water was first removed from the minerals by heating the sample at temperatures up to  $200^\circ C$  under vacuum. Then the mineral was completely dehydrated under vacuum at temperatures up to  $1500^\circ C$  and the resulting  $H_2O$  (with any  $H_2$ ) was passed through a hot uranium tube to give  $H_2$  gas for mass spectrometric analysis (Bigeleisen et al., 1952).

Fluid inclusion samples were analysed for  $H_2O/CO_2$  ratio and hydrogen isotope composition. The samples, consisting of 20 to 30 gm of vein quartz chips, were pre-heated at  $150^\circ C$  for 24 hours under vacuum to remove any absorbed water. This was carried out with the sample in a stainless steel tube

(previously vacuum-tested) attached to a vacuum line. The sample tube was closed off using the stop-cock, and crushed in a vice to pulverise the sample and release the inclusion fluid. It was then connected to the hydrogen vacuum line where the released water, after separating off the non-condensable gases and any  $\text{CO}_2$ , was passed through the uranium furnace to give  $\text{H}_2$  gas. Because of the presence of hydrous daughter salts in the most highly saline inclusions, the samples were heated while the water was being removed. Both non-condensable gases and  $\text{CO}_2$  were present in trace quantities only, and the amount of  $\text{CO}_2$  was too small to recover for analysis. The sample material which was selected for the fluid inclusion analyses were divided into two unequal amounts and separate crushings and extractions performed.

There are many possible problems associated with the analysis of fluid inclusions. Because the amount of mineral material required for crushing is quite large, the single greatest difficulty is in ensuring that all of the inclusions which are analysed are of the same type and generation. Most vein minerals contain several types and generations, and great care and attention was given to the problem of sample selection and preparation. The similarity in the isotopic analyses of the sample pairs suggests that a reasonable separation of inclusion types was attained, and that problems associated with the dehydration of hydrous daughter minerals were not important. Oxygen isotope ratios of the fluids were not measured because of the exchange problems between fluid and oxygen-bearing host mineral (Rye and O'Neil, 1968).

Isotopic analyses were performed on McKinney-Nier type double-collector mass-spectrometers. The analytical error for oxygen is  $\pm 0.1$  to  $0.2$  per mil and for hydrogen is  $\pm 1$  to  $2$  per mil. All isotopic compositions are reported as  $\delta$  values or per mil deviations from SMOW.

The oxygen isotope compositions and some hydrogen isotope compositions of the fluids were calculated from isotopically analysed minerals using temperatures based on the fluid inclusion homogenization data. The mineral-water fractionation data summarised by Taylor (1974) was used.

#### 4.4. Samples Studied and Results

The samples analysed are divided into six types as follows:

1.) Present day meteoric waters. Three samples were analysed, of which two (NGW 3 and NGW 5) were from permanent-flowing surface rivers and the third (NGW 2) was from a thermal spring at Llallagua. The spring water was at about  $60^{\circ}\text{C}$  and near-neutral pH where it emerged. NGW 3 was from the Cotagaita River near Chorolque, and NGW 5 was from a stream between Potosi and Colquechaca. The precipitation in both cases had probably fallen mainly as snow; the region is arid, cold, and at an altitude of 4000 to 5000 m above sea level.

2.) Kaolinite from a tin vein, Llallagua mine. Clay forms a late-stage in-filling of open spaces in many of the tin veins at Llallagua and most of the other deposits. This sample (NG 32) was from the San José vein on 586 level. A small amount of pyrite is closely associated with the clay, but it is not clear from the textural relationships if the clay is hypogene, or supergene, in origin. The sample material

was checked by X-ray diffractometry, and gave the single broad peak of moderately well-ordered kaolinite group. As discussed previously, much of the uplift of the Eastern Cordillera is believed to have taken place in the Pliocene. Since the age of the Llallagua deposit is approximately 20 Ma (see Chapter 5), the mineralization was probably formed at a much lower elevation than its present position. Since the isotopic composition of meteoric water is highly sensitive to altitude and topography, it is likely that the meteoric water at Llallagua at the time of ore deposition had a significantly different isotopic composition to that of the present day waters. The importance of this clay sample is that it may indicate the isotopic composition of the local meteoric waters during the latest stages of the evolution of the deposit. Previous isotopic studies of kaolinite associated with hypogene argillic rock alteration in hydrothermal systems (e.g., Sheppard et al., 1969) have shown that the hydrothermal fluids responsible for the clay alteration were undoubtedly heated meteoric water, hence the clay mineral data can be used to determine the isotopic composition of the local meteoric water at the time of argillic alteration.

3.) Sericite. Two samples of hypogene alteration sericite were analysed, one from the central, intensely sericitized region of the Salvadora stock at Llallagua (NG 38), and one from altered volcanics in the zone of sericitization peripheral to the central vent at Chorolque (NG 123). In both cases the sericite is well crystallized, gives sharp muscovite XRD peaks, and has formed mainly as a replacement of feldspar phenocrysts. Samples were prepared by heavy liquid separation

to remove tourmaline and quartz.

4.) Tin vein material (inclusion fluid and quartz).

Two samples of inclusion-rich quartz from tin veins at Llallagua were analysed (NG 37, NG 467). They are typical vein quartz material, intergrown with cassiterite, from the main cassiterite deposition stage of vein growth. The quartz is rich in dilute (non-daughter mineral bearing) fluid inclusions giving homogenization temperatures of 380°C (NG 37) and 350°C (NG 467). The specimens for hydrogen isotopic analysis of inclusion fluids were hand-picked under the microscope to obtain material free from secondary inclusions. The fluids were extracted as described above, and  $\delta D$  determined;  $\delta^{18}O$  was determined on the host quartz.

5.) High-temperature early alteration stage fluids and quartz. One sample (NG 507) of the highly saline, high-temperature fluid from the core of the Chorolque system was analysed. The specimen is from the margins of the Veta Colon and represents the earliest stage of vein growth. The temperature and salinity are the same as in the surrounding vent rocks. Vein quartz was used because it was found impossible to separate suitable material, free from secondary inclusions and intergrown tourmaline, from the altered quartz-tourmaline rock. The sample quartz pre-dated the cassiterite deposition stage of the veins, and was rich in Type VI inclusions giving homogenization temperatures of 450°C, and with salinities of over 50 equivalent weight percent NaCl.

6.) Four other samples were run as follows : a) two samples of biotite from unaltered igneous rocks (NG 487 and NG 498),

these were run to confirm the composition of magmatic water in these rocks in case of any peculiarities; b) one sample of tourmaline (NG 122) from the quartz-tourmaline alteration zone at Chorolque. There is no data on tourmaline-water D/H fractionation, and this sample was analysed to set a limit on the isotopic properties of this important alteration mineral; c) one sample of apparently unaltered shale from near Chorolque. The oxygen isotopic composition (whole-rock) of the shale was determined because, as discussed below, the vein quartz at both Chorolque and Llallagua was found to be particularly  $^{18}\text{O}$  rich; a possible explanation for this is through isotopic exchange between the hydrothermal fluid and the shales.

The analytical results are shown in Table 10, and are plotted in Fig. 4.2. Also shown for reference are the meteoric water line and the kaolinite line. The latter gives the isotopic composition of kaolinites formed by surface weathering. It reflects the isotopic variation of meteoric waters since it is defined by the equilibrium isotopic fractionations between kaolinite and the local meteoric water at essentially uniform temperatures (Savin and Epstein, 1970). Some data from other mineral deposits in the central Andean region are also shown for comparison. These are from studies of the Casapalca Ag-Pb-Zn-Cu deposit in Peru (Rye and Sawkins, 1974), the Pasto Bueno tungsten deposit, Peru (Landis and Rye, 1974), and the El Salvador porphyry copper deposit, Chile (Sheppard and Gustafson, 1976).

TABLE 10. Results of Isotopic Analyses <sup>1</sup>

Sample	Material	Location and Description	$\delta D$ ‰	$\delta^{18}O$ ‰
NGW 3	Water <sup>2</sup>	Cotagaita River	-91 $\pm$ 1 (2)	-11.5 (1)
NGW 5	Water <sup>2</sup>	Stream, north of Potosi	-95 $\pm$ 2 (2)	-12.2 (1)
NGW 2	Water <sup>2</sup>	Llallagua, hot spring (60°C)	-113 $\pm$ 1(2)	-15.0 (1)
NG 32	Kaolinite	Llallagua, late clay fill in tin vein	-102 $\pm$ 3(2)	12.8 $\pm$ 0.2 (2)
NG 38	Sericite	Llallagua, sericitized porphyry	-77 $\pm$ 2 (3)	13.8 $\pm$ 0.2 (2)
NG 123	Sericite	Chorolque, sericitized porphyry	-70 $\pm$ 1 (2)	13.7 $\pm$ 0.2 (3)
NG 37	Quartz, fluid	Llallagua, barren section of tin vein	-81 $\pm$ 7 (2)	15.3 $\pm$ 0.2 (2)
NG 467	Quartz, fluid	Llallagua, mineralized deep tin vein	-74 $\pm$ 4 (2)	14.7 $\pm$ 0.1 (2)
NG 507	Quartz, fluid	Chorolque, quartz tour- maline alteration-stage quartz	-76 $\pm$ 1 (2)	12.2 $\pm$ 0.2 (3)
NG 487	Biotite	Llallagua, unaltered porphyry	-97 $\pm$ 1 (2)	7.8 $\pm$ 0.1 (2)
NG 498	Biotite	Kari-Kari pluton, unaltered granodiorite	-85 (1)	6.9 $\pm$ 0.1 (2)
NG 122	Tourmaline	Chorolque, altered vent rock	-61 $\pm$ 0 (2)	-
NG 225	Shale	Chorolque, unaltered	-66 (1)	13.1 $\pm$ 0.3 (2)

1. Mean values of  $\delta D$  and  $\delta^{18}O$  with number of determinations per sample shown in brackets. SMOW scale.

2. Collected September 1975.



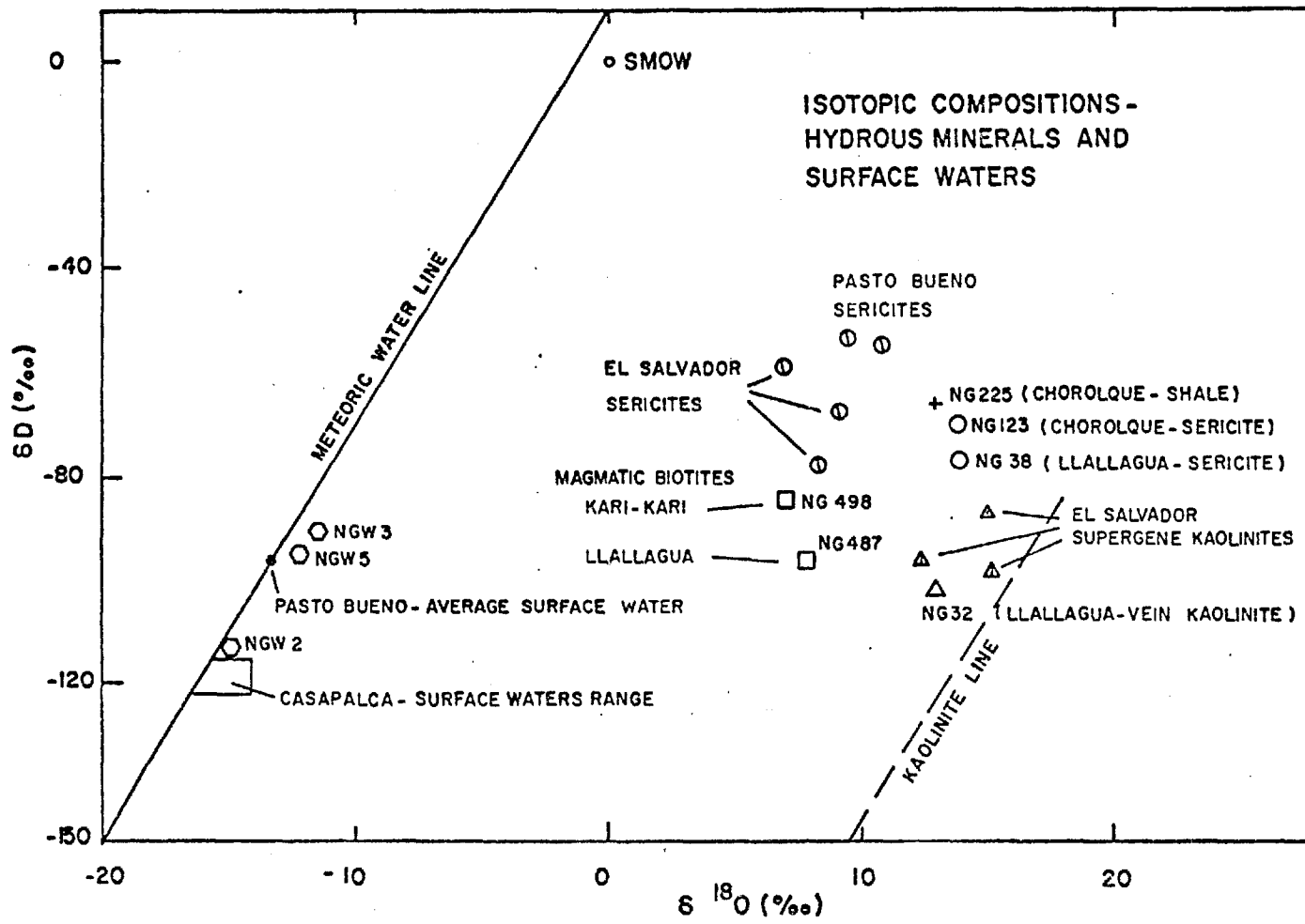


FIG.4.2

#### 4.5. Discussion

The calculated isotopic composition of the fluids associated with the alteration and vein minerals are shown in Table 11, together with the fluid inclusion temperatures and isotopic fractionations used in the calculations. The fluid data are plotted in Fig. 4.3, together with some of the Casapalca, Pasto Bueno and El Salvador data.

##### 4.5.1. Surface water data

The three Bolivian surface water samples plot close to the meteoric water line. The two stream samples are closely similar to the Pasto Bueno present-day surface waters which are derived from precipitation at a similar altitude (about 4000 m). The Casapalca surface waters are isotopically somewhat lighter, reflecting their derivation from snow-fall at higher altitude (5000 m). The reason for the distinctly different composition of the Llallagua spring water is not clear. It may reflect local topographic and climatic conditions which can result in pronounced isotopic effects through their influence on the precipitation history of the local airstream.

Of particular importance is the difference between these present-day waters and the range of meteoric water compositions, marked 'El Salvador Lower Tertiary Groundwater' in Fig. 4.3. The El Salvador deposit lies in the Western Cordillera of Chile at a much lower elevation (2000 to 3000 m) than the Bolivian deposits. The isotopic composition of the local groundwater at El Salvador at the time of mineralization has been calculated from the oxygen and hydrogen isotopic composition of kaolinite of a late-stage argillic alteration assemblage

TABLE 11. Calculated Isotopic Composition of Fluids

Sample	Remarks	Estimated temp, °C	Fractionations <sup>1</sup> (1000 ln α)		Calculated H <sub>2</sub> O per mil	
			D/H	<sup>18</sup> O/ <sup>16</sup> O	δD	δ <sup>18</sup> O
NG 498	Magmatic	700	-20	-3.6	-65	10.5
NG 487	Magmatic	700	-20	-3.6	-77	11.4
NG 507	Earliest (qtz -tourm) altn.	450	-	+3	-76 <sup>2</sup>	9.2
NG 467	Early vein (cassiterite) stage	350	-	+6	-74 <sup>2</sup>	8.7
NG 37	Early vein	380	-	+5	-81 <sup>2</sup>	10.3
NG 123	Peripheral sericitic alteration	300	-30	+3.3	-40	10.4
NG 38	Pervasive sericitic alteration	300	-30	+3.3	-47	10.5
NG 32	Late vein	200	-18	+6	-84	6.8

1. From Taylor (1974)

2. Measured.

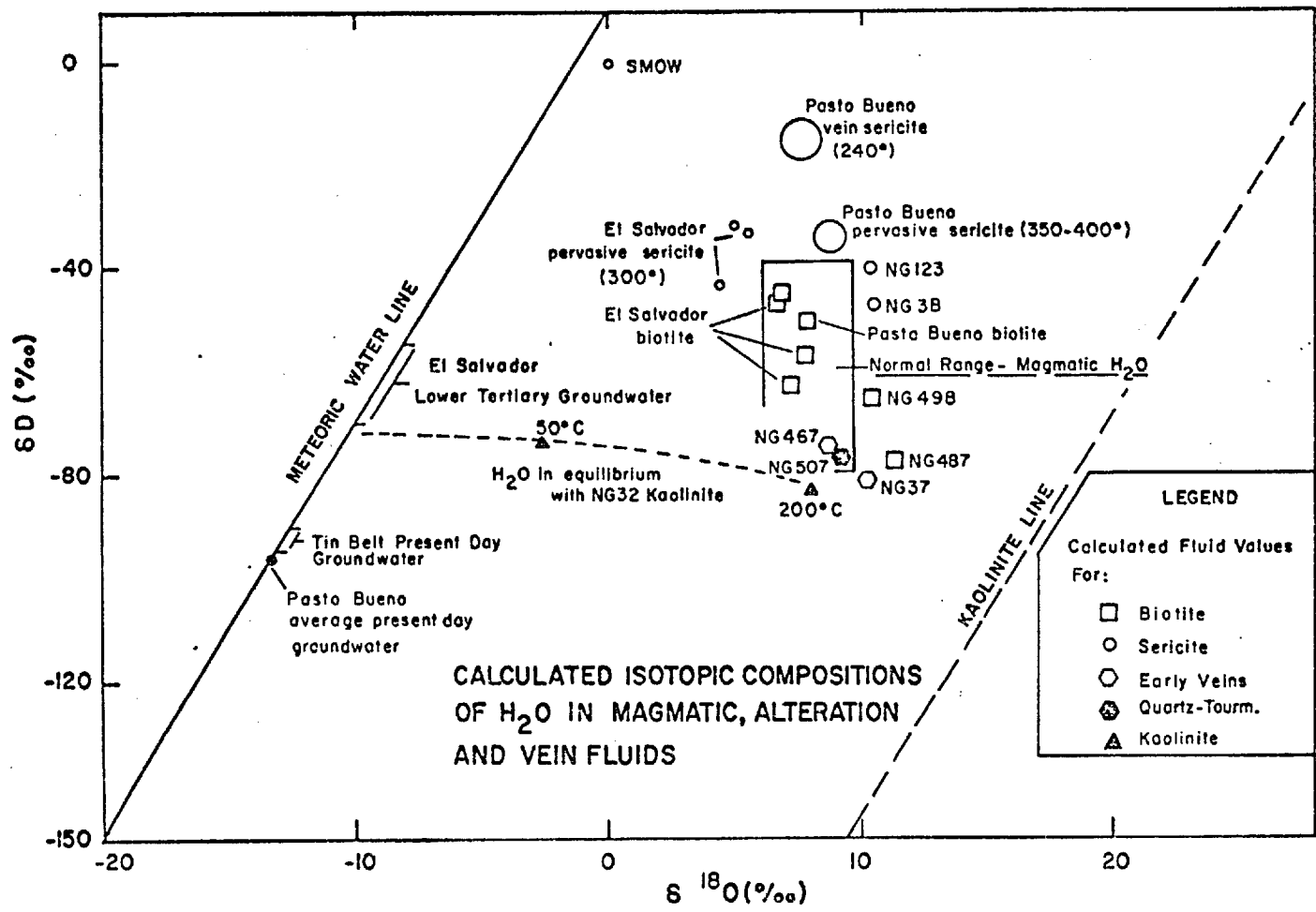


FIG. 4.3

(Sheppard and Gustafson, 1976). As noted above, the data from numerous other porphyry deposits show that the water responsible for these late-stage alteration effects is local groundwater. It seems reasonable to postulate that the El Salvador Lower Tertiary groundwater gives a guide to the isotopic composition of the groundwater at the Bolivian deposits at the time they were formed (mid-Tertiary) since at that time the Eastern Cordillera was at a much lower elevation, prior to the mainly Pliocene uplift. If this was the case, then the meteoric water at the Bolivian deposits had a  $\delta D$  value within the range of normal magmatic waters.

#### 4.5.2. Clay data

The calculated composition range of water which would have been in isotopic equilibrium with the single clay sample (NG 32) is shown in Fig. 4.3 for a range of temperature from 200°C to 25°C. At the low-temperature end, the composition lies close to the meteoric water composition indicated by the El Salvador groundwater, while the kaolinite itself plots close to the supergene (weathering) kaolinite line. This suggests that a supergene origin could be possible. However, as noted above, the clay is from a deep vein, and is intimately associated with sulphides, so a hypogene origin is also possible on geologic grounds. The formation temperature is difficult to estimate. The clay post-dates quartz crystals which have minimum fluid inclusion temperatures of about 200°C. This provides an upper limit. At this temperature the fluid composition falls near the composition range of normal magmatic waters; however it seems more reasonable to suggest

that the formation temperature was lower, and that the fluid was meteoric water which had been enriched in  $^{18}\text{O}$  by exchange with the surrounding rocks. This would still indicate that the local meteoric water at the time of alteration had a  $\delta\text{D}$  value within the normal magmatic water range.

#### 4.5.3. Biotite data

The two analysed biotites (NG 498 and 487) have isotopic compositions which are essentially normal for magmatic biotites, although their  $\delta^{18}\text{O}$  values are slightly heavier than most reported magmatic biotites from other porphyry-type deposits (Sheppard et al., 1971), and the calculated water composition lies outside the "normal" range for magmatic water. Unusually heavy oxygen has been found in a number of calc-alkaline granitic rocks, including the Cornubian batholith in S.W. England, and some granites in eastern Australia (Sheppard, 1977b; O'Neill and Chappell, 1977), both of which have tin mineralization associated with them. The most likely explanation for the heavy oxygen in these rocks is that either the magma incorporated or exchanged with large volumes of sedimentary rocks, which are characteristically enriched in  $^{18}\text{O}$  (especially shales), or were formed largely by the melting of such rocks. In this context a single sample of shale from the Chorolque region (NG 225) gave  $\delta^{18}\text{O} = +13.1\text{‰}$ . It is not yet clear if heavy oxygen is a characteristic of tin-bearing magmas in general.

The calculated water values for the biotites are based on a  $-20\text{‰}$  fractionation for D/H and  $-3.6\text{‰}$  for  $^{18}\text{O}/^{16}\text{O}$  at  $700^\circ\text{C}$ . It has been shown experimentally (Suzuoki and Epstein, 1976) that the biotite- $\text{H}_2\text{O}$  fractionation for hydrogen is

sensitive to the composition of the biotite. The compositions of these biotites have not been determined, and the value used is for a phlogopite composition and gives a minimum fractionation.  $\delta D$  for both is within the normal range of magmatic water.

#### 4.5.4. Quartz-tourmaline alteration and vein data

The isotopic composition of the fluid associated with the early, high-temperature alteration of the igneous rocks of the Chorolque vent is given by the data for sample NG 507. The  $\delta^{18}O$  value of the (hydrothermal) quartz is  $+12.2^{\circ}/\text{oo}$ , close to that of the surrounding shales. The fluid composition plots within the range of normal magmatic waters for both  $\delta D$  and  $\delta^{18}O$ . As discussed in Chapter 3, the fluid inclusion data show that this is a high-temperature, 2-phase fluid consisting of separate co-existing ultra-saline liquid and low density vapour. The predicted nature of a magmatic aqueous phase separating from a magma in the sub-critical region of the  $H_2O$ -NaCl system is just such a 2-phase fluid as this (Fournier, 1972). Similar fluids have been found in the inner, deeper regions of many porphyry copper deposits and have been shown on isotopic grounds to be of magmatic origin. Thus, although the  $\delta D$  value for the NG 507 fluid is within both the magmatic water range and close to the estimated value of the local meteoric water at the time of mineralization, a magmatic origin is preferred. The  $\delta^{18}O$  shift required for meteoric water to attain this composition ( $+10^{\circ}/\text{oo}$ ) is greater than that which has been measured in most natural geothermal systems (Taylor, 1974) and would imply an extremely low water to rock

ratio. This seems unlikely considering the intense pervasive alteration and the brecciated nature of the vent rocks.

The two vein fluid samples (NG 467 and NG 37) are lower temperature, much lower salinity (less than 26 equivalent weight percent NaCl) single phase (liquid) fluids. Both are from Llallagua, where the high-temperature 2-phase fluid inclusions of NG 507 type, and associated pervasive quartz-tourmaline alteration, are found only in the deepest levels, below the part of the stock containing the major vein structures and the pervasive sericitic alteration and disseminated mineralization. The inclusion evidence suggests that the early vein growth stage (with cassiterite) represented by these samples was roughly contemporaneous or slightly younger than the pervasive alteration of the stock. The isotopic compositions of the two vein fluids plot close to that of NG 507, despite the difference in temperature and the radical difference in salinity. If these fluid types are isotopically similar because they are of similar origin, the salinity variation must be explained by some mechanism which would not change the isotopic composition. Alternatively, if the fluids are different, for example if the dilute vein fluids are meteoric water, then the similarity of their  $\delta^{18}\text{O}$  values must be explained. In the first case, it is possible that the dilute vein fluids might be the condensed low-density vapour from the deeper parts of the system where boiling was taking place. At present there are no fractionation data available between liquid and vapour in 'boiling' brine solutions to either support or eliminate this possibility.



In the second case, the  $\delta^{18}\text{O}$  shift again implies a low water to rock ratio, which seems unlikely in an open vein system. A dominantly magmatic origin is preferred, considering the geological and hydrological evidence.

#### 4.5.5. Sericite data

The calculated isotopic compositions of the fluids responsible for sericitic alteration at both Chorolque (NG 123) and Llallagua (NG 38) show strong deuterium enrichment relative to the quartz-tourmaline alteration (Chorolque) and early vein fluids (Llallagua). Deuterium enrichment of fluids associated with sericitic alteration is also a feature of the data from Pasto Bueno and El Salvador.

There are several possible explanations, involving either a fluid of different  $\delta\text{D}$ , or some process of deuterium enrichment. There is also the possibility that the D/H fractionation data for sericite- $\text{H}_2\text{O}$  (used here) are substantially different, and so not correctly applicable, to sericite-brine fractionations (Sheppard, pers.com.). The following are possible reasons for the deuterium-rich fluid associated with sericitization.

a) The fluid is of different origin to the early alteration and vein fluid. The most likely fluid to be present in the outer and upper regions of these hydrothermal systems is meteoric water. The available evidence, presented above, is that the local meteoric water at the time of mineralization had  $\delta\text{D}$  values 20 to 30 ‰ lighter than the calculated sericite waters. The evidence for the isotopic composition of the meteoric water is far from conclusive, and there is a possibility that the meteoric water was in fact heavier during the

earliest stages of alteration, particularly since there is considerable uncertainty as to the precise elevation and topographic conditions in the Eastern Cordillera at the time of mineralization. The problem with this explanation is that  $\delta D$  values of -40 to -50 ‰ for meteoric water are not compatible with the late-stage kaolinite data (NG 32) unless considerable uplift took place between these two stages of alteration. The possibility that the fluid associated with sericitization is evolved meteoric water is discussed below.

Landis and Rye (1974) have suggested that the comparable deuterium enrichment of the fluid associated with sericitic alteration at Pasto Bueno is due to the incorporation of D-rich metamorphic water. The meteoric waters at Pasto Bueno at the time of mineralization appear to have been extremely deuterium depleted (as low as -140 ‰), so the magnitude of the difference between the meteoric and sericite waters is much greater than in the Bolivian deposits. It seems rather unlikely that a significant volume of metamorphic water would be present at shallow level in the Eastern Cordillera of Bolivia, considering the lack of metamorphism of the rocks, and the fact that the last significant period of deformation prior to igneous activity took place in the Cretaceous.

b) The fluid associated with sericitization was either meteoric water or was of similar isotopic composition to vein fluid, and has evolved to its calculated isotopic composition by some process of deuterium enrichment. There are several possible mechanisms, and these have been discussed by Landis and Rye (op. cit.) and Sheppard and Gustafson (1976).

The vein fluids could have become enriched in deuterium, without significant change in  $\delta^{18}\text{O}$ , by isotopic fractionation between  $\text{H}_2\text{O}$  and hydrogen, with escape of hydrogen from the system; by  $\text{H}_2\text{O}-\text{H}_2\text{S}$  fractionation; or by boiling ( $\text{H}_2\text{O}_{\text{liquid}}-\text{H}_2\text{O}_{\text{vapour}}$  fractionation), although the latter is probably not effective because the fractionation is negligible except at low temperatures. Loss of hydrogen has been invoked by Gustafson and Hunt (1975) to explain the highly oxidized state of sulphur in the El Salvador deposit. The  $\text{H}_2\text{O}-\text{H}_2$  equilibrium D/H fractionation is substantial at high temperature, and would lead to D enrichment in  $\text{H}_2\text{O}$ . An  $\text{H}_2\text{O}-\text{H}_2\text{S}$  fractionation mechanism might also be effective, with loss of  $\text{H}_2\text{S}$  from the system.

Another possibility is that the fluids associated with sericitization were meteoric water which had undergone both  $\delta^{18}\text{O}$  shift and  $\delta\text{D}$  shift. Deuterium enrichment is found in meteoric fluids involved in acid 'hot-spring' geothermal systems, because of kinetic isotope effects associated with steam evaporation. The Bolivian eruptive complexes which have not been deeply eroded all have very extensive argillic alteration zones which have developed in relatively low temperature, acid, hydrothermal systems in the volcanic superstructure of the complexes. This type of hot-spring system may have overlain all of the important deposits at the time of their formation, and it is possible that significant volumes of meteoric water were isotopically modified in this way before being drawn down into the deeper regions where sericitic alteration took place. The isotopic composition of

fluids modified in this way lie along a line with slope 3.

The Bolivian data are compatible with this.

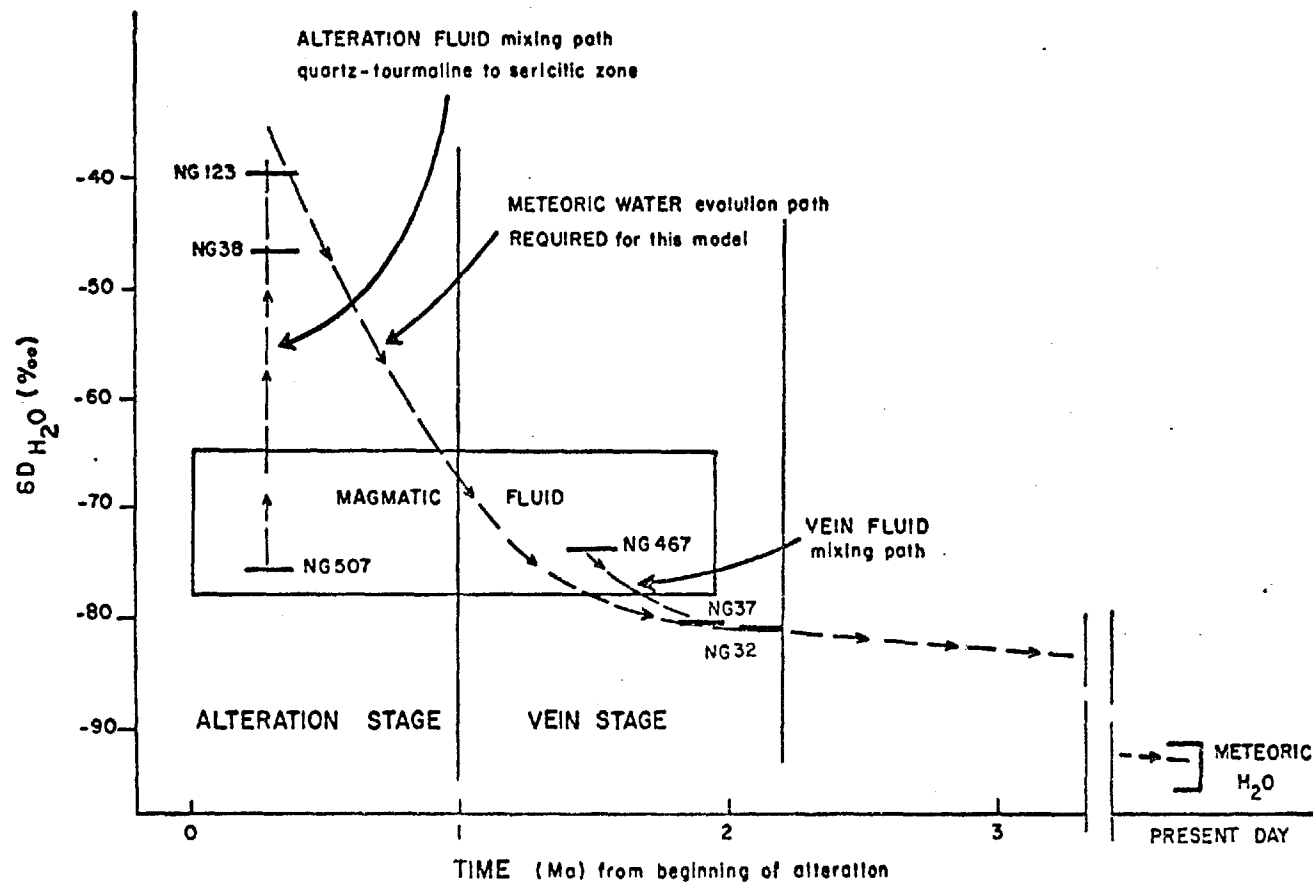
#### 4.6. Conclusions

The isotopic composition of the local meteoric water at the time of mineralization appears to have had  $\delta D$  within the range of normal magmatic waters, making the distinction between these two water types difficult. Because of this, and partly because there are insufficient analyses, the isotopic data presented here are not definitive in tracing the evolution of the fluids in the systems under study. However, a number of important points emerge. The data are consistent with a magmatic origin for the early high-temperature fluid associated with the quartz-tourmaline alteration of the Chorolque vent, and this is the preferred interpretation on geological and fluid inclusion grounds. The isotopic data are also consistent with a magmatic origin for the early (tin deposition) stage of vein fluids. This conclusion is important, since the fluid inclusion data show that these fluids are of substantially different temperature, and especially salinity, to the quartz-tourmaline alteration fluid. It is also geologically reasonable, since it is believed that the high-level eruptive complexes are underlain by much larger igneous bodies which must have supplied much of the ore mineralization via the vein channels. The origin of the fluids associated with sericitization can not be determined decisively. They are isotopically distinct from the quartz-tourmaline alteration and early vein fluids. They could be evolved magmatic or meteoric water, or possibly but less likely, metamorphic water. The late-stage vein

kaolinite was deposited from either a low-temperature hydrothermal fluid of meteoric origin, or else is a product of supergene weathering and was transported into the vein systems by downward percolating groundwater.

These conclusions are summarised diagrammatically in Fig. 4.4 and 4.5. In these, the  $\delta D$  data for the two separate deposits (Llallagua and Chorolque) are combined to give a generalized evolutionary scheme for the hydrothermal systems, based on the assumption that the fluid associated with sericitization was meteoric water. In Fig. 4.4, possible mixing paths for the alteration and vein fluids are shown, with the assumption that the late-stage vein kaolinite is of meteoric-hydrothermal origin and was deposited at a temperature of about  $200^{\circ}\text{C}$  shortly after the main stage of vein mineralization. The difference in  $\delta D$  between the two Llallagua vein samples is taken as being significant and reflects incorporation of meteoric water into the vein fluid, which was initially of magmatic origin. This model requires that  $\delta D$  of meteoric water changes from approximately  $-40^{\circ}/\text{oo}$  to  $-80^{\circ}/\text{oo}$  during the life-span of the hydrothermal systems. The most plausible mechanism for such a change is regional uplift. There is no doubt that major uplift has taken place between the time of formation of the deposits and the present, but it seems unlikely that the greater part of it, which would probably be required to explain a  $40^{\circ}/\text{oo}$  change in  $\delta D$ , would have taken place in the limited time indicated. There is no direct evidence as to the life-span of the hydrothermal systems. However, it seems unreasonable to postulate more than a short

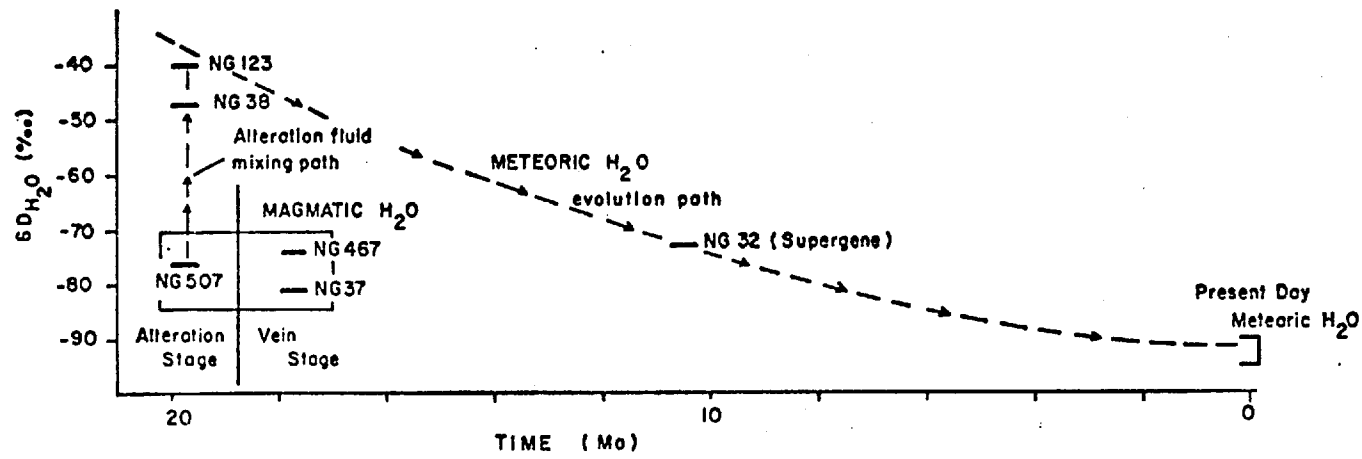
**SCHEMATIC DIAGRAM - POSSIBLE EVOLUTION PATHS OF FLUIDS  $\delta\text{H}_2\text{O}$**



**FIG. 4.4**

FIG. 4.5

SCHMATIC DIAGRAM - POSSIBLE EVOLUTION PATHS OF FLUIDS  $\delta\text{H}_2\text{O}$



time between pervasive alteration and the main vein-stage at least.

A more satisfactory model is shown in Fig. 4.5. In this it is assumed that the fluid associated with sericitization was meteoric water, that the difference between the two vein samples is either not significant or represents a reverse trend to that indicated in Fig. 4.4, and that the clay was deposited at a much later time and is perhaps of supergene origin. This allows a much greater time-span for the postulated change in  $\delta D$  of the local meteoric water. In this model, deep, inner quartz-tourmaline alteration is associated with a high-temperature magmatic fluid. This mixes outward and upward with meteoric water which is dominant in the zones of sericitization. As the veins develop they continue to tap magmatic fluid from a deep source (pluton). Gradual mixing of vein fluid with meteoric water would be likely, but has not been tested adequately here. The clay fill is much younger, possibly supergene, and deposited from meteoric water strongly depleted in D relative to earlier meteoric water due to uplift. The  $\delta D$  of this clay-depositing fluid approaches that of present-day meteoric water.

This is the preferred model, and is most consistent with the geological and fluid inclusion evidence, although considerable further work is required to fully test its validity.



## CHAPTER 5

A GEOCHRONOLOGICAL STUDY OF THE SOUTHERN  
PART OF THE BOLIVIAN TIN BELT

5.1. Introduction

A total of 41 rocks were dated by the potassium-argon method. The samples were collected by the writer at several of the major mineralized eruptive complexes of the southern part of the tin belt, as well as from a number of rock units unrelated to mineralization. The analyses were carried out by the writer in the Isotope Geology laboratory of the Institute of Geological Sciences (I G S), London.

The objective of the study is to provide a general chronological framework for the Andean igneous rocks and associated mineral deposits in the southern part of the Bolivian tin belt. The data provide a chronological link between the batholiths of the northern tin belt, and the volcanic and sub-volcanic centres to the south of Oruro. The approximate age of mineralization at several of the major mining centres has been determined, and the data reveal some distinct age groupings. The approximate length of time involved in the formation of some of the mineralized igneous complexes has also been measured.

5.2. Previous Geochronological Data

The geochronology of the batholiths of the northern tin belt is currently under investigation (Robertson, 1974; Clark et al., 1976). Reviews of the available data have been

given by Clark and Farrar (1973) and by Avila (1975). The K-Ar dates which have been reported range from Triassic to Lower Miocene in age. The batholiths of the Cordillera Real give mainly Triassic to Jurassic ages while the more southerly Illimani, Quimsa Cruz and Santa Vera Cruz plutons give Lower Miocene dates, the youngest being 22.8 Ma for a sample from the Santa Vera Cruz (Cordani, 1967).

In the southern tin belt it has long been recognised that many of the eruptive centers are of Tertiary age. Volcanic rocks can be seen to unconformably overlies Cretaceous sediments at a number of localities, and the Cerro Rico stock at Potosi cuts plant-bearing tuff beds containing a flora classified as Late Pliocene (Berry, 1937) or Miocene (Steinmann, 1922). From this a general Miocene or Pliocene age has previously been applied to all of the igneous rocks of the region (Turneure, 1960).

Prior to this study, only a limited number of radiometric age determinations had been carried out on igneous rocks of the southern part of the tin belt (Evernden, 1961; Clark and Farrar, 1973; Evernden et al., 1977). These provided firm data on the age of the Kari-Kari batholith and Agua Dulce - Mondragon lavas of the Potosi region (20-22 Ma), and indicated a late Miocene (7.3 Ma) age for the post-mineral ignimbrites of the Los Frailes formation. They provide little information on the age of the mineralized eruptive complexes, although a date of 9.4 Ma was reported for the Salvadora stock at Llallagua. This was of particular significance. As noted above, the southern plutons of the northern tin belt have given Lower Miocene ages, the youngest of which is

22.8 Ma. Thus a time break of over 10 Ma was indicated between the emplacement of the igneous rocks and associated mineralization of the southern end of the northern tin belt, and the emplacement of the mineralized eruptive complex at Llallagua, near the northern end of the southern tin belt.

These data were used by Ahlfeld (1967) to propose three episodes of mineralization in the tin belt as a whole.

He recognised a Mesozoic stage associated with the batholiths of the Cordillera Real; a Lower Miocene stage associated with the southermost plutons of the northern tin belt, in which he included the minor mineralization associated with the Kari-Kari batholith near Potosi; and he ascribed all of the sub-volcanic mineralization of the central and southern parts of the belt to a distinct younger (Upper Miocene-Pliocene) stage.

The new ages determined in the present study do not support Ahlfeld's subdivision. In particular it has not been found possible to confirm Evernden's (1961) Upper Miocene age of 9.4 Ma for the Salvadora stock and a much older, Lower Miocene, age is preferred, the implications of which are discussed below.

### 5.3. Location and Description of Samples

In this study rocks from the following areas have been dated; the San Pablo (Morococala) stock and Japo and Santa Fé mines; the Salvadora stock, Llallagua; the Colquechaca eruptive complex; the Potosi region, including the Cerro Rico stock; and the mineralized eruptive complexes of Chocaya, Tatasi, Chorolque and Tasna. The samples can be divided into two groups:

- a) From intrusive and volcanic units directly associated with mineralization: these include mineralized intrusive porphyries forming small stocks, such as the San Pablo, Salvadora (Llallagua) and Cerro Rico stocks; porphyry dykes associated with ore-veins in sedimentary rocks, such as at Japo, Santa Fé and Tasna mines; and lavas and pyroclastics of the mineralized volcanic complexes such as Colquechaca, Chocaya, Chorolque, and Tatasi. In all cases the rocks are quartz-porphyries. Unaltered, they are generally of quartz-latitude composition and composed of quartz, sanidine, sodic plagioclase, and biotite phenocrysts in a microcrystalline or glassy matrix. Many of these rock units have been hydrothermally altered; the common alteration types are tourmalinization, sericitization, argillization, and chloritization. Where possible both unaltered and altered samples from the same unit have been dated.
- b) Volcanic and intrusive rocks which are not directly associated with mineralization: these include the post-mineral ignimbrite formations of the Morococala and Los Frailes regions; the Kari-Kari granodiorite pluton and volcanic formations of the Potosi region; and the rhyolitic tuff of the Atocha region. A limited number of samples from these units have been dated, but no attempt was made to investigate their chronology in detail.

#### 5.4. The Principles of the Potassium-Argon Method of Age Determination

The principles and techniques of the K-Ar method are well

known and have been exhaustively described in several texts, including those of Dalrymple and Lanphere (1969) and York and Farquhar (1972). Some of the most important points are discussed briefly below.

#### 5.4.1. The K-Ar age equation

The method rests on the fundamental property of radioactive decay, i.e., that decay is a statistical process in which the number of atoms of a radioactive element which decay in unit time is proportional to the number of atoms of that element which are present

$$-\frac{dN}{dt} = \lambda N$$

where  $N$  is the number of atoms present and  $\lambda$  is the decay constant, which expresses the probability that an atom will decay in unit time. From this is derived the basic radioactive decay formula

$$N = N_0 e^{-\lambda t}$$

where  $N_0$  is the initial number of radioactive atoms present, and  $N$  is the number remaining at time  $t$ .

This equation cannot be used for dating since  $N_0$  cannot be determined without first knowing  $t$ . However, in a closed system in which neither parent nor daughter atoms are lost or gained except by the decay process itself, the decrease in the number of parent atoms must be equal to the increase in the number of daughter atoms. If  $P$  is the number of parent atoms and  $D$  the number of daughter atoms

$$\frac{dD}{dt} = -\frac{dP}{dt}$$

and at any given time

$$P_0 = P + D$$

where  $P_0$  is the original number of parent atoms. Substituting

this into the basic radioactive decay equation gives

$$D = P(e^{\lambda t} - 1)$$

from which  $t$  may be found without knowing  $P_0$ .

$$t = \frac{1}{\lambda} \log_e \left( \frac{D}{P} + 1 \right)$$

In this equation it is assumed that all of the daughter atoms are the product of radioactive decay of the parent  $P$  in the closed system. If, however, some atoms of the daughter nuclide were incorporated into the system at the time of its formation, they must be subtracted from  $D$ , and the equation becomes

$$t = \frac{1}{\lambda} \log_e \frac{D_t - D_0}{P} + 1$$

where  $D_t$  is the total number of atoms of  $D$  at time  $t$  and  $D_0$  is the number of atoms of  $D$  incorporated into the system at its initiation. This is called the General Age Equation.

For potassium-argon dating this requires modification since  $^{40}\text{K}$  undergoes branching decay to both  $^{40}\text{Ca}$  and  $^{40}\text{Ar}$ . The decay of  $^{40}\text{K}$  to  $^{40}\text{Ar}$  is by electron capture with gamma-ray emission; this accounts for about 11% of the total  $^{40}\text{K}$  decay, and the decay constant  $\lambda_\epsilon$  has a value of  $0.585 \times 10^{-10}/\text{yr}$ . The decay to  $^{40}\text{Ca}$  is by  $\beta^-$  emission and the decay constant  $\lambda_\beta$  has a value of  $4.72 \times 10^{-10}/\text{yr}$ . There are some uncertainties here, both in the values of the measured decay constants and in the fact that a very small proportion of the  $^{40}\text{K}$  decay takes place by other processes, however for young rocks these are insignificant compared with experimental uncertainties and can be ignored.

For the branching decay of  $^{40}\text{K}$ , the age equation can be written

$$^{40}\text{Ar}_{\text{rad}} + ^{40}\text{Ca}_{\text{rad}} = ^{40}\text{K} \left[ e^{(\lambda_\epsilon + \lambda_\beta)t} - 1 \right]$$

where the subscript rad indicates the radiogenic nuclide produced by decay within the closed system. For K-Ar age calculations this becomes

$${}^{40}\text{Ar}_{\text{rad}} = {}^{40}\text{K} \frac{\lambda_{\epsilon}}{\lambda_{\epsilon} + \lambda_{\beta}} \left[ e^{(\lambda_{\epsilon} + \lambda_{\beta})t} - 1 \right]$$

Solving for t gives the K-Ar age equation

$$t = \frac{1}{\lambda_{\epsilon} + \lambda_{\beta}} \log_e \left[ \frac{{}^{40}\text{Ar}_{\text{rad}}}{{}^{40}\text{K}} \cdot \left( \frac{\lambda_{\epsilon} + \lambda_{\beta}}{\lambda_{\epsilon}} \right) + 1 \right]$$

substituting the values of the decay constants gives

$$t = 1.885 \times 10^9 \cdot \log_e \left[ 9.068 \cdot \frac{{}^{40}\text{Ar}_{\text{rad}}}{{}^{40}\text{K}} + 1 \right]$$

thus the age t can be calculated from the experimental determination of the amounts of  ${}^{40}\text{Ar}_{\text{rad}}$  and  ${}^{40}\text{K}$  in a suitable rock or mineral sample.

In practice it is not necessary to measure the abundance of the  ${}^{40}\text{K}$  isotope in samples being dated since the ratio  ${}^{40}\text{K}/\text{K}_{\text{total}}$  is constant in all geological materials. It is necessary only to determine  $\text{K}_{\text{total}}$ , then  ${}^{40}\text{K}$  is calculated from the isotopic ratio. The value normally used is  ${}^{40}\text{K}/\text{K} = 0.0119$  atom percent. This equation involves only radiogenic  ${}^{40}\text{Ar}$  which is produced by decay of  ${}^{40}\text{K}$  in the closed mineral or rock system. It does not account for any  ${}^{40}\text{Ar}$  which might be incorporated at crystallization. It also requires correction for the small amount of atmospheric  ${}^{40}\text{Ar}$  which can not be excluded from the measuring system, as discussed in section 5.5 below. The equation embodies three fundamental assumptions.

- 1) That the decay constants have remained unchanged over geologic time.
- 2) That no  ${}^{40}\text{Ar}$  was present at the time of crystallization of the rock or mineral.

- 3) That the system has remained closed to loss or gain of both parent and daughter nuclides since crystallization.

In the case of 1), it has been shown that although the decay constant for some radioactive transformations can be affected by the chemical and physical environment, in the case of the decay of  $^{40}\text{K}$ , there is no significant variation in  $\lambda$  with environment, and it can be assumed that it has been constant over geological time (Dalrymple and Lanphere, 1969). The others are discussed below.

#### 5.4.2. Extraneous argon

If  $^{40}\text{Ar}$  is incorporated into a rock or mineral at the time of crystallization, its potassium-argon age will be too great. This can come about in two ways: firstly, where gaseous  $^{40}\text{Ar}$  is present in the environment of crystallization and becomes incorporated in the crystal lattice or perhaps trapped in fluid inclusions. This is called excess argon. Secondly, where older,  $^{40}\text{Ar}$ -bearing mineral grains are incorporated into a rock, or where  $^{40}\text{Ar}$  from pre-metamorphic decay of  $^{40}\text{K}$  is retained during a metamorphic event. This is called inherited argon. The latter is only likely to occur under rather special circumstances which are relatively easy to identify. Excess argon is more difficult to identify, and its presence can only be firmly established if the rock or mineral can be reliably dated by some other method.

Since potassium is present virtually throughout the earth's crust, and probably the upper mantle as well, the production of  $^{40}\text{Ar}$  from decay of  $^{40}\text{K}$  must have been going on throughout geological time. This is the source of excess argon in minerals. It has been found in a variety of rocks,



especially those which have formed in a high gas-pressure environment, such as kimberlites, pegmatites, and submarine lavas. Virtually all minerals could contain excess argon since crystals are normally imperfect, and so may be able to contain the argon atom even though they may not have suitable sites in their ideal lattice. This is born out by experimental studies which have shown its presence, in certain cases, in all of the minerals which are normally considered useful for K-Ar work, and many others as well (Damon and Kulp, 1958).

In practice, erroneous K-Ar age measurements resulting from excess argon are rare. It has most frequently been encountered in minerals having extremely low potassium contents since in these, the ratio of excess argon to  $^{40}\text{Ar}_{\text{rad}}$ , and hence the error on the age, is likely to be high even when the amount of excess argon is extremely small. This is particularly the case in young rocks.

In the present study there was some question as to whether tourmaline, which is common in many of the altered rocks, might contain excess argon. Damon and Kulp (1958) recorded large amounts of excess argon in tourmaline, but it is not known if this is a common feature of the mineral. Because of this uncertainty, it was decided to remove tourmaline from the samples to be dated. One tourmaline-rich sample was dated (NG 279) and did give a substantially older age than a separate, tourmaline-free sample from the same rock unit. Another possible case of extraneous argon is NG 6. This is a sample of altered (tourmaline-sericite) hydrothermal breccia, part of the San Pablo stock. It gave an anomalously old age

(older than an unaltered sample of the stock) which might be due to excess argon or perhaps inherited argon in older rock-fragments present in the breccia.

One way in which to evaluate the possibility of extraneous argon in a group of samples from the same rock unit is to plot the concentration values of  $^{40}\text{Ar}$  against K. This should give a straight line passing through the origin for samples of the same age (since the age equation is a straight-line relationship). If extraneous argon is present, the line will not pass through the origin, since the ideal  $^{40}\text{Ar}/\text{K}$  relationship will not obtain (e.g., Fyles et al., 1973).

In the present study insufficient samples from any individual rock unit were dated for this test to be applied. However, in areas where a number of different rock units give similar ages such as San Pablo-Morococala; the Salvadora stock, Lallagua; and the Potosi region, the  $^{40}\text{Ar}/\text{K}$  relationships are close to ideal (see section 5.7) suggesting that extraneous argon is not generally present. This does not exclude the possibility of its occurrence in some individual samples such as the two mentioned above, but apart from these there is no reason to suspect that extraneous argon is a source of error in any of the rocks dated in this study.

#### 5.4.3. Argon loss

The validity of the K-Ar dating method depends on the ability of potassium-bearing minerals to retain the radiogenic  $^{40}\text{Ar}$  produced within them. The very large amount of work which has been done using the method has demonstrated beyond doubt that, under suitable conditions, certain minerals do

completely retain their argon. However, it has also been shown that all minerals are subject to argon loss as a result of post-crystallization disturbances (mainly thermal) and further, that some potassium-bearing minerals do not retain argon completely even when undisturbed.

The argon-retentivity of various common K-bearing minerals has been investigated in detail (e.g., Hart, 1964; Hanson and Gast, 1967; Aldrich et al., 1965). The most widely used minerals for dating igneous rocks are biotite and muscovite, hornblende, plagioclase and sanidine. Orthoclase and microcline have been found to be unreliable, they apparently lose argon during lattice changes which accompany exsolution, and thus lose argon even when undisturbed (Dalrymple and Lanphere, 1969). A number of other minerals have been used, including feldspathoids, lepidolite and pyroxene; and it has also been shown that in suitable rocks, mineral separation is not necessary and the whole rock can be analysed provided it does not contain any K-bearing, non-argon retentive materials such as orthoclase, microcline or volcanic glass. Most of the dates reported here for unaltered rocks were measured on biotite, which is abundant in all of the igneous rocks of the region. A few were also measured on sanidine. Hornblende is present in some of the dacite rocks but in general it is very fine grained and difficult to separate, and commonly altered to chlorite. Numerous rocks were also dated which have undergone intense hydrothermal alteration. Of the secondary minerals produced, only sericite (fine-grained muscovite) is considered reliable for K-Ar dating, so the altered rocks were dated by analysis

of sericite mineral concentrates, or whole-rock analysis of intensely sericitized rocks. Both biotite and muscovite have been very extensively used in K-Ar age determination. Although both appear to be more susceptible to argon diffusion at elevated temperatures than hornblende, they both retain argon completely at low temperature.

Several factors can result in argon loss from minerals. Consideration of these is essential in evaluating the geological significance and reliability of K-Ar ages. The most important are thermal effects such as reheating by igneous intrusion or metamorphism, and mineralogical changes during weathering and hydrothermal alteration.

#### A. Thermal disturbance

Both laboratory diffusion studies and the results of numerous geochronological studies have shown that argon diffuses out of all minerals above a certain temperature, termed the blocking temperature. Argon loss results in ages which are too young, and for this reason K-Ar ages are usually referred to as apparent ages and generally represent a minimum possible age. For biotite, the blocking temperature for argon diffusion appears to be in the region of 200°C.

There are two consequences of this in dating igneous rocks. The first is that during crystallization and cooling, the K-bearing minerals will not begin to retain argon until they have cooled to some temperature well below their crystallization temperature. This is a particular problem in the dating of plutonic rocks which crystallize and cool slowly, at depth. The time-span between crystallization of a pluton and its cooling to the temperature at which argon diffusion ceases completely

can be long. The K-Ar age will be the age at which the blocking temperature was reached, not the emplacement age.

In volcanics and high-level intrusives such as those dated here, this effect is not a problem since there is no doubt that the time-span between solidification of the rocks and cooling to the blocking temperature for argon diffusion is insignificant compared with the age of the rock.

The second consequence of argon diffusion is that ages can be disturbed by thermal events subsequent to the original cooling of the rock. Among the common causes are regional metamorphism, renewed igneous activity, and heat generated by tectonic deformation. An important aspect of this type of age disturbance is that it can either be partial, in which case only part of the argon is lost from minerals; or it can be complete, in which all of the argon is lost. In the latter case the K-Ar age will be the age of the disturbing event itself and thus may provide useful geological information. In the former case the K-Ar age will have no relationship to any geological event.

There are a number of ways in which the thermal disturbance of K-Ar ages can be recognised and evaluated. The most direct and satisfactory is to date the same rocks by another method which is not subject to the same disturbance, such as the whole-rock Rb-Sr isochron method. This approach can provide much information on both primary igneous events and subsequent thermal disturbances. It does, however, require rather comprehensive study of a large number of samples, and a good understanding of the overall geological relationships.

A good example is the work of Bignell and Snelling (1977) in the granite provinces of the Malayan peninsula.

Evaluation of individual or limited numbers of K-Ar dates is more difficult. Confidence can be improved by dating 2 or more minerals from the same rock. Since different minerals are not equally susceptible to argon loss, concordant mineral ages are an indication that loss has not occurred. This is particularly the case if one mineral is hornblende since it seems to be considerably more resistant than micas and feldspars, whose behaviour is rather similar (Aldrich et al., 1965).

In the present study only single minerals were dated from individual samples, and no ages have been determined by other methods. Confidence in the accuracy of the results is provided by the concordancy of ages of different samples from the same, or related, rock units. The only recognised disturbing event is the hydrothermal alteration which is associated with mineralization at all of the eruptive complexes.

#### B. Hydrothermal alteration

Any process which results in the breakdown of an original mineral lattice will result in disturbance of the K-Ar age. Complete alteration, i.e., complete replacement of a primary potassium-bearing mineral by a new mineral species, will result in complete argon loss. In this case the K-Ar age of a new K-bearing mineral will be the age of alteration provided that no  $^{40}\text{Ar}$  was incorporated into the new mineral at the time of alteration, the system cooled rapidly if alteration took place above the blocking temperature, and there were no subsequent disturbing events.

The dating of altered rocks is important in the geochronological study of mineral deposits since in many cases the mineralization itself cannot be dated directly, and associated altered rocks provide the only suitable material for age determination.

There are three particular questions which arise in the K-Ar dating of altered rocks. These are : a) is a new K-bearing mineral formed which is suitable for dating?, b) is excess argon from the primary mineral incorporated in the new mineral during the alteration process?, c) is the alteration complete, so that no remnant of the primary K-bearing mineral remains which could contribute inherited argon to the material being dated?. Of the minerals commonly formed as products of hydrothermal alteration, especially of igneous rocks, the most suitable for K-Ar dating are the micas biotite, muscovite, and sericite. Biotite is common as an alteration product only in certain types of high-temperature mineral deposits (especially the porphyry copper deposits), muscovite is particularly common in certain alteration mineral assemblages associated with tin deposits in granites (greisen), while sericite (fine-grained muscovite) is common as an alteration mineral in many deposit types. Of the other common K-bearing alteration minerals, chlorite and clay minerals have both been used (e.g., Ineson and Mitchell, 1972, 1974). The reliability of chlorite is still in doubt (Snelling, pers. comm.). Of the clay minerals, illite is probably reliable for K-Ar dating. However, the argillic alteration associated with mineral deposits is rarely mineralogically simple, and many of the clays, although capable of carrying significant K, have not been shown to be reliable in

retaining argon. The same is true of tourmaline, as noted above. In the present study only sericite was used in the dating of altered rocks, and it gave results which are, in general, reasonable and consistent.

The question of excess argon in secondary minerals has not been investigated in detail. However, since most hydrothermal alteration associated with mineralization takes place in relatively low-pressure conditions (especially sericitization, which is characteristic of rather high-level ore-forming systems), it seems unlikely that this would be a problem. Rather high argon contents have been reported in some fluid inclusions from mineral deposits (Roedder, 1972b) and this could have implications in the dating of altered rocks by the whole-rock method. In the present study two of the altered samples gave anomalous results which could perhaps be attributed to excess argon, as discussed above, but there is no evidence that it is generally present in the sericite used here.

The question of the completeness of alteration is particularly important. Incomplete alteration will lead to erroneous K-Ar ages, unless all radiogenic argon was completely lost from the primary mineral at the time of alteration. Clearly this is not likely to be the case in relatively low-temperature hydrothermal systems. Also, if the primary potassic mineral (or glass) is not argon-retentive at low temperature, as in the case of orthoclase or microcline, then erroneous results will also be obtained. Sericitization usually takes place at temperatures in the region of 300°C (e.g., Rose, 1970; Sheppard



et al., 1971). In the case of the Bolivian deposits this is above the blocking temperature for one of the primary minerals commonly replaced (biotite) but probably below the blocking temperature for the other (sanidine; see Dalrymple and Lanphere, 1969). For this reason, great care was taken to ensure that no primary feldspar remnants were present in the material which was analysed.

Apart from hydrothermal alteration associated with mineralization, many igneous rocks are affected by weak alteration associated with meteoric water interaction during cooling, or burial in a volcanic pile. This commonly results in partial or complete replacement of mafic minerals by chlorite. This can render biotite and hornblende unsuitable for K-Ar dating since even where alteration is complete, chlorite may not be a reliable argon-retainer. In the present study no age determinations were carried out on biotite which showed more than minor chloritization; even this may have been responsible for the considerable spread of ages among certain samples from the Kari-Kari pluton (see Section 5.7).

The effects of weathering can be considered equivalent to hydrothermal alteration at low temperature; although in some cases it appears to affect the K and  $^{40}\text{Ar}$  contents of minerals in proportion, and satisfactory results have been obtained from partially weathered minerals (Dalrymple and Lanphere, 1969). Despite this, in the present study the weathered outer skin was removed from all surface samples.

## 5.5. Experimental Methods

### 5.5.1. Sample preparation

Each sample collected in the field consisted of several

pieces of rock totalling 1 to 2 kg weight. In the case of surface samples, the weathered outer skin was chipped off. The rocks were all examined in thin-section before any mineral separation was carried out. Those supposedly fresh rocks which showed significant chloritization of biotite were discarded, as were hydrothermally altered rocks not rich in sericite. The altered samples were examined carefully for relict feldspar, and those which appeared totally altered were checked by X-ray diffraction. The samples chosen for dating were washed in de-ionized water, crushed in a jaw-crusher, ground to a suitable size for liberation of the desired minerals and sieved to give a narrow grain-size range for mineral separation (usually - 240, +125 micron). Separation of biotite and sericite were carried out using conventional magnetic and heavy-liquid techniques. Intensely sericitized rocks free of tourmaline were treated with heavy liquids to remove sulphide minerals, which would have created problems in the argon-extraction procedure. They are thus slightly modified whole-rock samples. In general approximately 10 gm of mineral concentrate or sulphide-free whole-rock were prepared for each sample.

#### 5.5.2. Analytical methods

##### A. Potassium analysis

Potassium determinations were carried out as follows. Between 1000 and 2000 mg of each sample were weighed out into platinum crucibles, then dissolved in hydrofluoric-perchloric acid mixture and evaporated to dryness. The residue was dissolved in de-ionized water, a known amount of lithium

added in solution as an internal standard, and the mixture made up to a standard volume with de-ionized water. This solution was then analysed for potassium by flame photometry using an EEL 170 digital flame photometer. All samples were analysed in duplicate, the results were discarded and the sample re-analysed if the K values differed by more than + 1% of their mean value. International and IGS standard mineral samples were analysed after approximately every 10 samples.

#### B. Argon isotopic analysis

The isotope dilution methods of radiogenic  $^{40}\text{Ar}$  determination used at the IGS have been described briefly by Bignell and Snelling (1977) and are similar to those described by Dalrymple and Lanphere (1969).

The sample material is weighed into a molybdenum foil crucible. The crucible is placed in a holder within a glass bulb in the sample fusion section of the apparatus, which can hold 3 samples at a time. The fusion section is connected via valves to the mass spectrometer, the  $^{38}\text{Ar}$  tracer (spike) reservoir, and a high-vacuum pump, and is opened to the atmosphere during sample loading. The fusion section is pumped out for 15 hours after loading. During this the samples and entire fusion section are heated to about  $50^{\circ}\text{C}$  to assist removal of atmospheric argon from the system. The fusion section is then isolated from the pump and checked for leaks. The  $^{38}\text{Ar}$  spike is metered from the reservoir via a standard volume valve and admitted to the fusion section. The sample is then fused using an electromagnetic induction coil placed around the glass bulb. The sample is held at a high temperature for

several minutes to ensure complete gas extraction. All non-inert gases are removed from the sample gas mixture by freezing (condensables) in a liquid nitrogen cold-trap, and absorption on titanium sponge. Part of the remaining gas is then finally cleaned with a Zr-Al getter pump before admission to the mass spectrometer. The instrument used is an AEI MS-10, operated in the static mode. The beam strengths for the  $^{36}\text{Ar}$ ,  $^{38}\text{Ar}$ , and  $^{40}\text{Ar}$  isotopes are measured, and from these the isotope ratios and volumes are calculated using the known volume of the  $^{38}\text{Ar}$  tracer. Since it is not possible to exclude all air from the extraction and measuring system, some atmospheric  $^{40}\text{Ar}$  is always present as a component of the total  $^{40}\text{Ar}$  measured in the mass spectrometer. This amount has to be determined, and subtracted from the total  $^{40}\text{Ar}$  to give the volume of radiogenic  $^{40}\text{Ar}$ . From this, and the  $^{40}\text{K}$  value, the age of the sample can be calculated as described in section 5.4.1. Details of the methods of obtaining the volume of the  $^{38}\text{Ar}$  tracer, and of calculating the corrected volume of radiogenic  $^{40}\text{Ar}$  are given in Appendix II.

#### 5.6. Precision and Resolution

The potassium-argon age is given by the following equation:

$$t = \frac{1}{\lambda_{\epsilon} + \lambda_{\beta}} \ln \left[ 1 + \frac{\lambda_{\epsilon} + \lambda_{\beta}}{\lambda_{\epsilon}} \cdot \frac{{}^{40}\text{Ar}(\text{rad})}{{}^{40}\text{K}} \right]$$

where the decay constants  $\lambda_{\epsilon}$  and  $\lambda_{\beta}$  have values of  $0.585 \cdot 10^{-10} \text{ yr}^{-1}$  and  $4.72 \cdot 10^{-10} \text{ yr}^{-1}$  respectively and

$$\frac{{}^{40}\text{Ar}(\text{rad})}{{}^{40}\text{K}} = 1.466 \cdot 10^{-3} \frac{\text{nl } {}^{40}\text{Ar}(\text{rad}) \text{ per gm}}{\% \text{ K}}$$

The volume of radiogenic  $^{40}\text{Ar}$  in nanoliters per gram is given by

$$\text{Spike volume} \times \left[ \frac{40}{38} M - \frac{40}{36} A \cdot \left( \frac{36}{38} M - \frac{36}{38} S \right) \right] \times \frac{1}{\text{sample weight}}$$

where spike volume is the volume of  $^{38}\text{Ar}$  used as an isotopic tracer and

$$40/38 M = \text{measured } ^{40}\text{Ar}/^{38}\text{Ar} \text{ ratio}$$

$$36/38 M = \text{measured } ^{36}\text{Ar}/^{38}\text{Ar} \text{ ratio}$$

$$36/38 S = ^{36}\text{Ar}/^{38}\text{Ar} \text{ ratio of the spike, (isotopic tracer)}$$

$$= 0.000056$$

$$40/36 A = \text{Atmospheric ratio of } ^{40}\text{Ar}/^{36}\text{Ar} = 296$$

(see Appendix II)

For young samples such as those considered here, the error in the age is given by the square root of the sum of the squares of analytical errors in the potassium and argon determinations. As all the potassium determinations were done in duplicate, the data can be combined to give a pooled standard error. The samples have been divided into two groups. The biotites (26 samples), give a pooled standard deviation of  $0.56 \cdot 10^{-3}$  gmK/gm. Their average potassium value is 6.62% giving an error of  $\pm 0.85\%$ . The whole rock and sericite samples (13) give a pooled standard deviation of  $0.33 \cdot 10^{-3}$  gmK/g. Their average potassium value is 3.46%, giving an error of  $\pm 0.95\%$ .

The error in the argon content must be estimated by combining the errors in the spike volume and in the expression.

$$R = \left[ \frac{40}{38} M - \frac{40}{36} A \cdot \left( \frac{36}{38} M - \frac{36}{38} S \right) \right]$$

The spike was metered from a reservoir system from which the volume of successive spikes decreases exponentially. Repeated

calibrations of this system indicate an error of about  $\pm 1\%$ .

The expression R takes into account the correction necessitated by the presence of some non-radiogenic (mainly atmospheric)  $^{40}\text{Ar}$  in the total  $^{40}\text{Ar}$  which is measured in the mass spectrometer. This results in a degree of error enhancement which is a function of the fractional amount of non-radiogenic  $^{40}\text{Ar}$ . To an adequate degree of approximation the fractional error in R is given by

$$\sigma R = \frac{\sqrt{x^2 + \left(\frac{A}{T}\right)^2 \cdot y^2}}{1 - \frac{A}{T}}$$

where x is the fractional error in the ratio  $^{40}\text{Ar}/^{38}\text{Ar}_M$

y is the fractional error in the ratio  $^{36}\text{Ar}/^{38}\text{Ar}_M$

and A/T is the fractional amount of atmospheric  $^{40}\text{Ar}$  in the total  $^{40}\text{Ar}$  (Baker et al., 1967).

In the present investigation the mean values of x and y were  $\pm 0.08$  and  $\pm 0.51$  respectively, and A/T varies from 0.14 to 0.84, giving a range of R from  $\pm 0.125\%$  to  $\pm 2.724\%$ . By adopting  $\pm 1\%$  as the error on the potassium determinations and  $\pm 1\%$  as the error on the spike volume this gives an error range on the age determinations of from  $\pm 1.4\%$  to  $\pm 3.1\%$ .

Basically the errors quoted for the ages reported here have been calculated as indicated above. That they are realistic estimates can be assessed in part by the errors indicated by replicate argon analyses. A total of seventeen samples were analysed for  $^{40}\text{Ar}_{\text{rad}}$  in duplicate. Ten biotite samples gave  $^{40}\text{Ar}_{\text{rad}}$  contents ranging from 3.02 nl/gm to 6.11 nl/gm, mean 4.55 nl/gm. The pooled standard deviation is 0.0175 nl/gm or 2.36% of the mean. Seven whole-rock samples gave  $^{40}\text{Ar}_{\text{rad}}$  ranging from 1.23 nl/gm to 2.77 nl/gm,

mean 2.02 nl/gm. The pooled standard deviation is 0.0373 nl/gm or 1.84% of the mean. Adopting a standard error on the duplicate argon determinations of  $\pm 2.5\%$  and on potassium determinations of  $\pm 1\%$  gives an error on the age of  $\pm 2.7\%$ , which is in agreement with the range of errors obtained by combining the error on R, the spike volume and the potassium analysis. This indicates that the latter method is indeed valid. Consideration of the errors on the ages reported in Table 12 indicates a typical value of about  $\pm 2\%$ . Adopting this value we can calculate a critical value which must be exceeded if we are to say with 95% confidence that there is a real difference between the calculated ages of any two samples with an age difference  $(\bar{x}_1 - \bar{x}_2)$ . Dalrymple and Lanphere (1969) quote the following equation (after Mc Intyre, 1963).

$$\text{C.V. (Critical Value)} = 1.96 \left( \frac{\sigma_1^2}{n_1} + \frac{\sigma_2^2}{n_2} \right)^{\frac{1}{2}}$$

where  $\sigma_1$  and  $\sigma_2$  are the standard deviations of the respective ages  $\bar{x}_1$  and  $\bar{x}_2$ , and  $n_1$  and  $n_2$  are the numbers of age determinations made on each sample. If only single ages have been determined and  $\sigma$  is taken as 2%, the critical value becomes 5.5%. If we take a more cautious view of the data and adopt 2.7% as the average standard deviation the critical value becomes 7.5%. In terms of the ages of the samples analysed during this investigation the critical values when comparing single determinations are as follows :

<u>Age</u>	<u><math>\sigma = 2\%</math></u>	<u><math>\sigma = 2.7\%</math></u>
20 Ma	1.1 Ma	1.5 Ma

<u>Age</u>	<u><math>\sigma = 2\%</math></u>	<u><math>\sigma = 2.7\%</math></u>
16 Ma	0.9 Ma	1.2 Ma
13 Ma	0.7 Ma	1.0 Ma
6 Ma	0.3 Ma	0.5 Ma

### 5.7. Results

The analytical results are summarized in Table 12 and are discussed below.

#### 5.7.1. San Pablo-Morococala region

This lies just to the south of Oruro (Figure 2.3). It is an elevated plateau made up of folded Silurian-Devonian sedimentary rocks. During the Tertiary these were intruded by small porphyry bodies and later overlain by an extensive sheet of dacitic ignimbrite (Morococala formation) which makes up much of the present land surface. The geology of the San Pablo-Morococala area and locations of the dated samples are shown in Fig. 2.13. Tin mineralization is found at a number of localities, mostly in veins in the Palaeozoic sedimentary rocks, though in close association with the porphyries. The most important mines are Japo, at the southern margin of the San Pablo stock, and the Santa Fé and Morococala mines which are adjacent to each other about 10 km to the southeast. Quartz-porphyry dykes are exposed underground in the Santa Fé mine.

The San Pablo stock is composed of quartz-lattice porphyry which has undergone intense hydrothermal alteration (sericitization and tourmalinization). Some patches of relatively fresh rock were preserved in a narrow zone at the northern contact.



TABLE 12

## POTASSIUM-ARGON AGE DATA.

Sample No.	Rock Type	Material Dated	$\lambda_{K^2}$	$\lambda_{Ar}^{40}$ Atmos	Vol $^{40}Ar_{rad}$ ml gm <sup>-1</sup>	Calculated Age (Ma) <sup>3</sup>
(a) SAN PABLO-MOROCOCALA REGION.						
NG1	Dacite (ignimbrite)	Biotite	7.16	35	1.75	6.1 ± 0.11
Repeat				50	1.72	6.0 ± 0.13
NG2	Dacite (ignimbrite)	Biotite	6.61	58	1.65	6.2 ± 0.13
NG6	Quartz-latite porph (breccia). Altered.	Sericite	3.98	42	3.86	24.1 ± 0.44
NG27	Quartz-latite porph Altered	Sericite	4.51	39	3.56	19.7 ± 0.35
NG31	Quartz-latite porph	K-Feldspar (Sanidine)	10.98	14	10.02	22.7 ± 0.40
NG21	Altered porphyry			68	3.24	20.0 ± 0.44
Repeat	dyke, (Japo Mine)	whole-rock	4.03	61	3.48	21.5 ± 0.43
NG14	Altered porphyry			56	2.63	19.5 ± 0.38
Repeat	dyke, (Santa Fe)	whole-rock	1.36	30	2.70	20.1 ± 0.36
(b) LLALLAGUA, THE SALVADORA STOCK.						
NG487	Quartz-latite			36	4.85	21.1 ± 0.38
Repeat	porphyry	Biotite	5.73	40	4.65	20.3 ± 0.38
NG38	Altered porphyry	Whole-rock	3.35	35	2.70	20.1 ± 0.36
NG45	Quartz-latite porphyry	K-Feldspar (Sanidine)	10.77	18	8.69	20.1 ± 0.35
NG44	Altered porphyry	Whole-rock	2.58	38	2.13	20.6 ± 0.38

1. Constants used:  $\lambda_{\beta} = 4.72 \times 10^{-10} \text{ yr}^{-1}$ ;  $\lambda_{\gamma} = 0.585 \times 10^{-10} \text{ yr}^{-1}$ ;  $^{40}K/K = 0.0119 \text{ atom. } \%$
2. Mean of duplicate analyses.
3. Errors at one standard deviation.

TABLE 12 Continued

(c) POTOSI REGION.

Sample No.	Rock Type	Material Dated	K	$V^{40}\text{Ar}_{\text{atmos}}$	$Vb^{40}\text{Ar}_{\text{rad}} \text{ nl gm}^{-1}$	Calculated Age (Ma)
NG68	Dacite ignimbrite	Biotite	6.96	53	2.02	$7.3 \pm 0.23$
Repeat	(Fm Los Trailles)			58	2.03	$7.3 \pm 0.17$
NG71	Rhyolite (Ihuakachi)	Biotite	7.38	52	3.44	$11.7 \pm 0.22$
NG93	Altered Porphyry	whole-rock	3.58	68	1.85	$12.9 \pm 0.32$
Repeat	(Cerro Rico)			63	1.95	$13.6 \pm 0.33$
NG94	Altered Porphyry	whole-rock	3.30	47	1.81	$13.7 \pm 0.26$
Repeat	(Cerro Rico)			50	1.82	$13.8 \pm 0.30$
NG73	Rhyodacite Porphyry (Kari-Kari)	Biotite	5.69	39	4.59	$20.1 \pm 0.34$
NG75	Rhyodacite Porphyry (Kari-Kari)	Biotite	6.78	27	5.61	$20.6 \pm 0.33$
NG75A	Rhyodacite Porphyry (Kari-Kari)	Biotite	6.42	35	5.60	$21.7 \pm 0.36$
Repeat				38	5.37	$20.9 \pm 0.28$
NG75B	Rhyodacite Porphyry (Kari-Kari)	Biotite	6.97	37	5.91	$21.1 \pm 0.26$
NG80	Rhyodacite Porphyry (Kari-Kari)	Biotite	4.31	51	3.59	$20.8 \pm 0.39$
NG83	Granodiorite (Kari-Kari)	Biotite	6.03	32	5.01	$20.7 \pm 0.34$
NG78	Rhyodacite tuff	Biotite	5.61	36	4.61	$20.5 \pm 0.34$
Repeat	(Agua Dulce fm.)			28	4.67	$20.8 \pm 0.36$
NG79	Rhyodacite tuff (Agua Dulce fm.)	Biotite	7.22	24	5.91	$20.4 \pm 0.32$
NG96	Rhyodacite tuff	Biotite	7.12	39	6.11	$21.4 \pm 0.36$
Repeat	(Canteria fm.)			36	6.09	$21.1 \pm 0.38$
NG97	Rhyodacite tuff (Canteria fm.)	Biotite	7.40	24	6.11	$20.6 \pm 0.33$
NG97A	Rhyodacite tuff (Canteria fm.)	Biotite	7.10	38	6.05	$21.2 \pm 0.36$
NG98	Rhyodacite tuff (Canteria fm.)	Biotite	7.42	35	6.19	$20.8 \pm 0.34$

TABLE 12 Continued

(d) COICUECHACA.

Sample No.	Rock Type	Material Dated	K	$^{40}\text{Ar}_{\text{atmos}}$	$\text{Vol } ^{40}\text{Ar}_{\text{rad}} \text{ nl gm}^{-1}$	Calculated Age (Ma) $\pm$
NG35A (CH)	Quartz-lattice	Biotite	6.20	46	5.49	22.1 $\pm$ 0.42
NG54	Quartz-lattice Lava	Biotite	6.75	36	5.67	20.9 $\pm$ 0.35
NG62	Altered lava	whole-rock	4.51	28	3.83	21.2 $\pm$ 0.37

(e) CHOCAYA VOLCANIC COMPLEX.

NG134	Rhyodacite Lava	Biotite	7.36	31	3.98	13.5 $\pm$ 0.22
Repeat				34	4.13	14.0 $\pm$ 0.26
NG131	Rhyodacite Lava	Biotite	5.05	44	2.70	13.3 $\pm$ 0.24
NG136	Rhyodacite Lava	Biotite	5.82	41	3.02	13.0 $\pm$ 0.23
Repeat				29	3.09	13.3 $\pm$ 0.23
NG126	Rhyodacite Lava (Altered)	whole-rock	3.60	49	1.75	12.2 $\pm$ 0.24

(f) CHORLOQUE.

NG123	Rhyodacite	whole-rock	4.34	22	2.71	15.6 $\pm$ 0.27
Repeat	Lava, (Altered)			40	2.76	15.9 $\pm$ 0.30
NG279	Rhyodacite Lava, (Altered)	whole-rock	1.91	83	1.37	17.9 $\pm$ 0.65

(g) TATASI.

NG283	Rhyodacite Lava	Biotite	7.73	29	4.64	15.0 $\pm$ 0.24
Repeat				41	4.83	15.6 $\pm$ 0.29
NG150	Rhyodacite Lava	Biotite	7.51	30	4.57	15.2 $\pm$ 0.25
Repeat				38	4.50	14.9 $\pm$ 0.27

(h) TASNA.

NG281	Quartz-porphry dyke. Altered	Whole rock	1.94	51	1.23	15.8 $\pm$ 0.31
Repeat				52	1.25	16.1 $\pm$ 0.31

TABLE 12 Continued

(1) OCHUPEN, (ATOCHA TUFF UNIT).

Sample No.	Rock Type	Material Dated	K	$^{40}\text{Ar}/\text{Atmos}$	$\text{Vol } ^{40}\text{Ar}_{\text{rad}} \text{ ml gm}^{-1}$	Calculated Age (Ma) <sup>1</sup>
NG99	Rhyodacite tuff	Biotite	7.29	33	4.79	$16.4 \pm 0.27$
Repeat	Chorolque road			26	4.77	$16.3 \pm 0.31$
NG139	Rhyodacite tuff Atocha-Chocaya road	Biotite	6.49	41	4.36	$16.8 \pm 0.32$

The southern part of the stock consists of hydrothermal breccia made up of fragments of altered igneous and sedimentary rocks in a fine, granular tourmalinized matrix. The porphyry dykes at Santa Fe and Japo mines are completely sericitized. All these altered rocks contain disseminated sulphides and cassiterite. The age of the San Pablo stock is indicated by the data from samples NG 6, NG 27, and NG 31. The sanidine date of  $22.7 \pm 0.4$  Ma (NG 31) is perhaps the best estimate of the minimum age of emplacement of the stock. The greater age of  $24.1 \pm 0.4$  Ma (NG 6) should be regarded with suspicion as the rock is a polymict breccia which may contain older material. Sericitized porphyry (NG 27) gave an age of  $19.7 \pm 0.35$  Ma, suggesting a resolvable time difference between the emplacement of the stock and the completion of pervasive hydrothermal alteration. This view is supported by the unweighted mean age of  $20.8 \pm 0.4$  Ma (NG 21) for the altered dyke in the Japo mine adjacent to the stock. On geological grounds it is reasonable to assume that the alteration of the stock and the adjacent dykes, and the formation of the mineral veins, are all part of the same extended hydrothermal event. The alteration age of the dyke is not resolvable (using the critical value for a 2.7% standard error on the ages) from the alteration age of the stock, but both are significantly younger than the sanidine date for the emplacement of the stock. The mineralized veins in the Japo mine formed at the same time, or slightly later than the main stage of alteration of the stock and dykes, so there appears to be a resolvable time difference of over 1 Ma between

the emplacement of the stock and the deposition of the mineralization in the veins.

The unweighted mean age of duplicate analyses of a sample (NG 14) of the altered dyke in the Santa Fé mine is 19.8  $\pm$  0.5 Ma, which indicates that igneous activity and mineralization in the Santa Fé and Morococala mines was essentially contemporaneous with that of the San Pablo-Japo area.

The data are plotted diagrammatically in Fig. 5.1A, and the  $^{40}\text{Ar}/\text{K}$  diagram is shown in Fig. 5.1B. The least-squares regression line gives an age of 23.7 Ma (from the slope), but this is not really meaningful since both altered and unaltered samples are involved in the calculation.

Samples NG 1 and NG 2 are from the Morococala formation ignimbrite. Their age of about 6 Ma indicates the long time-span which separated the intrusion of the mineralized porphyries and the eruption of the ignimbrite sheet which covers much of the area.

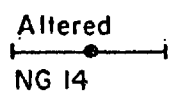
#### 5.7.2. Llallagua, the Salvadora stock

The Salvadora stock is an isolated body of about 1 km diameter which intrudes the Silurian-Devonian sedimentary rocks just to the south of the Morococala plateau. It was probably the vent of a volcano whose superstructure has been completely eroded away. It is made up of intensely altered porphyry laced with irregular patches and dykes of hydrothermal breccia. Relatively unaltered quartz-lattice porphyry was preserved at the contact of the stock in some areas. The alteration products are sericite, tourmaline, quartz, and clay minerals, with disseminated sulphides and cassiterite.

FIG. 5-1. SAN PABLO - MOROCOCALA. K/Ar DATA

A. APPARENT AGE RELATIONSHIPS

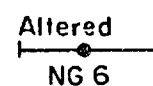
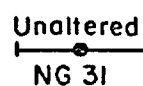
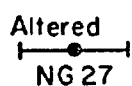
DYKE - SANTA FE MINE



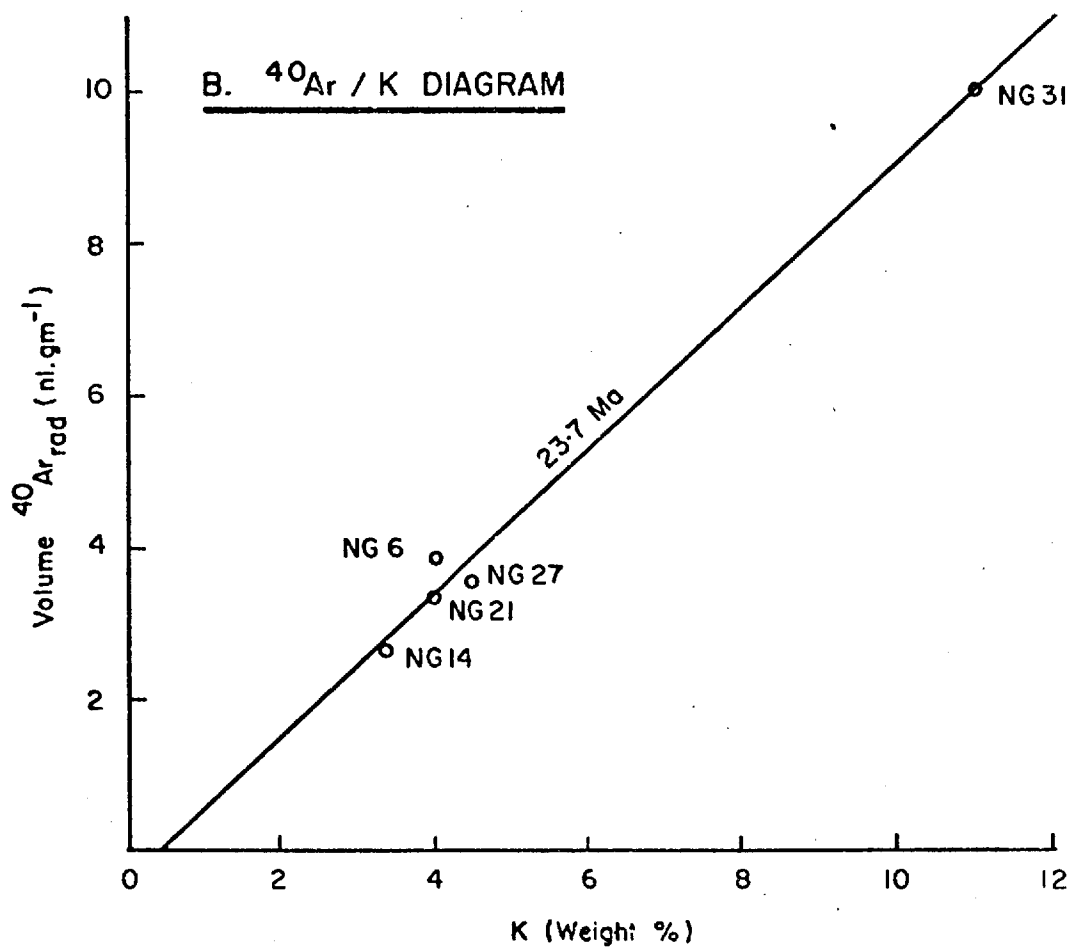
DYKE - JAPO MINE



SAN PABLO STOCK



18 19 20 21 22 23 24  
AGE (Ma)



The stock is cut by a system of rich tin-bearing veins, some of which extend out into the surrounding sedimentary rocks.

Four samples of the stock from widely differing locations were dated. Two are whole-rock samples of sericitized porphyry; NG 38 is from level 383, Salvadora section of the mine and NG 44 is from the surface. One (NG 45), is a sanidine concentrate from a relatively unaltered dyke-like off-shoot of the stock at the surface. One is a biotite concentrate (NG 487) from almost unaltered porphyry near the margin of the stock on the 650 level, Siglo XX section of the mine.

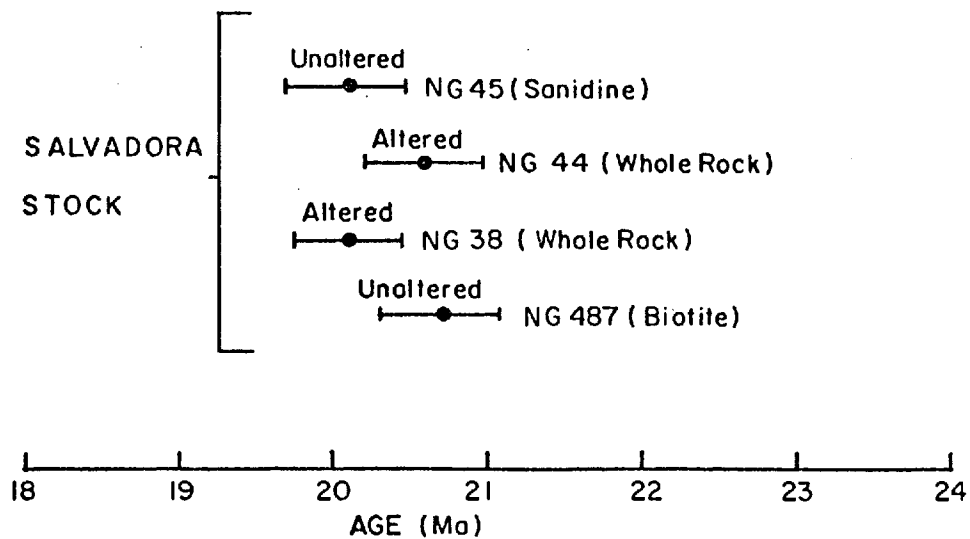
The ages of these differ by less than one million years, and give an unweighted mean of  $20.5 \pm 0.4$  Ma. There is no resolvable difference between the ages of altered and unaltered samples. This indicates that either the time difference between the emplacement of the stock and the completion of pervasive alteration was too short to be resolved by this method, or else that the temperature of the unaltered rocks remained above the blocking temperature for argon diffusion while the remainder of the stock was being altered, even though little or no mineralogical change took place. The concordancy of the ages of these four samples indicates that a date of a little over 20 Ma is a reliable estimate of the minimum age of emplacement of the stock, and is a good estimate of the age of alteration and mineral deposition at Llallagua. This date is preferred to the previously published age of 9.4 Ma (Evernden, 1961; Evernden et al., 1977), although the reason for the lack of agreement is not known.

The data are plotted diagrammatically in Fig. 5.2A and the

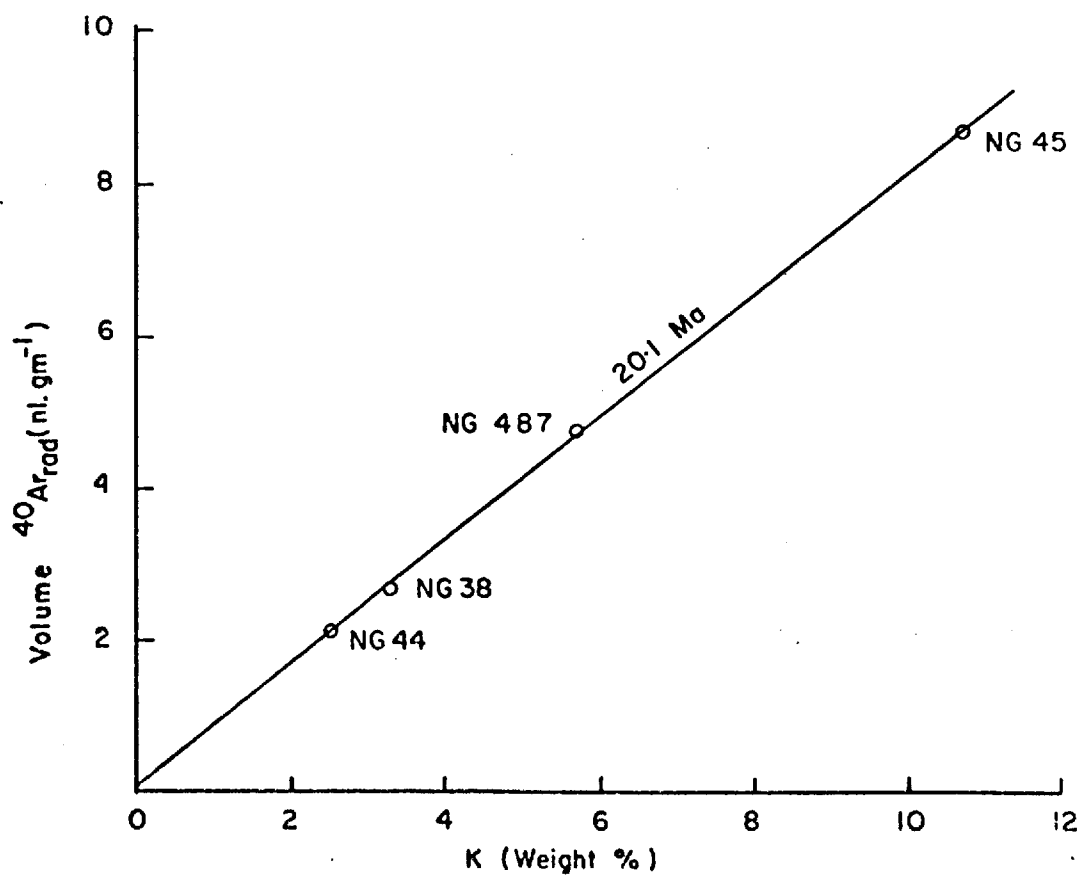


FIG. 5.2. LLALLAGUA - SALVADORA STOCK. K/Ar DATA

A. APPARENT AGE RELATIONSHIPS



B.  $^{40}\text{Ar}/\text{K}$  DIAGRAM



<sup>40</sup>Ar/K diagram is shown in Fig. 5.2B. Although both altered and unaltered samples are included, all plot very close to the least-squares regression line, which passes through the origin (no extraneous argon). The slope of the line gives an age of 20.1 Ma which is in good agreement with the unweighted arithmetic mean age.

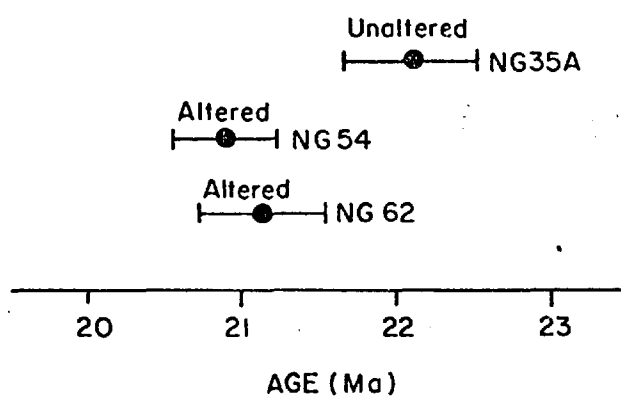
### 5.7.3. Colquechaca

Colquechaca was described by Ahlfeld and Schneider-Scherbina (1964) as a dacite stock, however it has never been geologically mapped in detail. As described in Chapter 2 it is a volcanic complex, probably made up entirely of extrusive rocks. These cover an area of more than 100 km<sup>2</sup> and rest on an irregular basement of folded Palaeozoic and possibly Cretaceous sedimentary rocks. On the southern side there is a lowermost unit of lahar deposits and volcanic breccia. This is overlain by dacitic lavas. In the central part there is a porphyritic quartz-latitude unit which seems to lie conformably beneath the dacite lavas, although an intrusive origin cannot be ruled out. The complex is deeply eroded and the maximum present-day thickness of exposed volcanic rocks is a little over 1000 m. There is an extensive zone of pervasive sericite-tourmaline alteration in the central part of the complex which is cut by small tin-bearing veins. There are a number of much larger sulphide-rich veins which cut the surrounding volcanics. They have well-defined envelopes of sericite-chlorite-carbonate alteration. Much silver was mined from some of these in the past, and base-metals are still being produced. Throughout the remainder of the complex there is widespread

chloritic alteration.

Three samples of the quartz-lattice from the central part of the complex were dated, the locations are shown in Fig. 2.11. Two of these are biotite concentrates; NG 35A(CH) is from virtually unaltered porphyry at the surface, while NG 54 is from a slightly altered rock (chloritized, sericitized) from within the mine, although its potassium analysis does not suggest that the biotite in the concentrate has been significantly chloritized. The third sample (NG 62) is intensely altered (sericitized) whole-rock. They give a spread of ages of just over one million years, from  $20.9 \pm 0.35$  Ma to  $22.1 \pm 0.42$  Ma. The age difference between the unaltered biotite sample and the pervasively sericitized sample is about 1 Ma. The biotite age of NG 54 is very close to the age of the sericitized sample, and it is possible that it suffered argon loss during incipient alteration. However, even adopting the mean age of NG 54 and NG 62 as the age of alteration (20.1 Ma), and 22.1 Ma (NG 35ACH) as the age of formation of the quartz-lattice, the difference between them barely exceeds the critical value (at the 95% confidence level) using a standard error on the age determination of  $\pm 2\%$ . It is concluded that the date of  $22.1 \pm 0.43$  Ma is a reliable estimate of the minimum age of the formation of the quartz-lattice, and that the time difference between this and the pervasive alteration cannot be resolved with confidence. None of the altered rocks associated with the major base-metal veins were dated, but on geological grounds it is unlikely that they are very much younger than the pervasive alteration. The data are plotted in Fig. 5.3.

FIG. 5.3. COLQUECHACA  
APPARENT AGE RELATIONSHIPS



#### 5.7.4. The Potosi region

The Potosi region contains a considerable variety of Andean igneous rocks, and the K-Ar ages reported here indicate a longer history of igneous activity than elsewhere in the southern tin belt. The general geology and locations of the dated samples are shown in Fig. 5.4. Folded Palaeozoic sedimentary rocks form the basement of the region. Previous workers have outlined the following stratigraphic sequence for the Andean rocks from the base upwards (Turneaure, 1960).

##### a) The Chalviri Group

This includes the Agua Dulce and Canteria formations. According to Ahlfeld and Schneider-Scherbina (1964), these consists mainly of andesitic tuffs and lavas, however, the rocks which were dated are rhyodacite tuffs and welded tuffs. Both formations are cut by the Kari-Kari batholith along its western edge, and outcrop over extensive areas farther west.

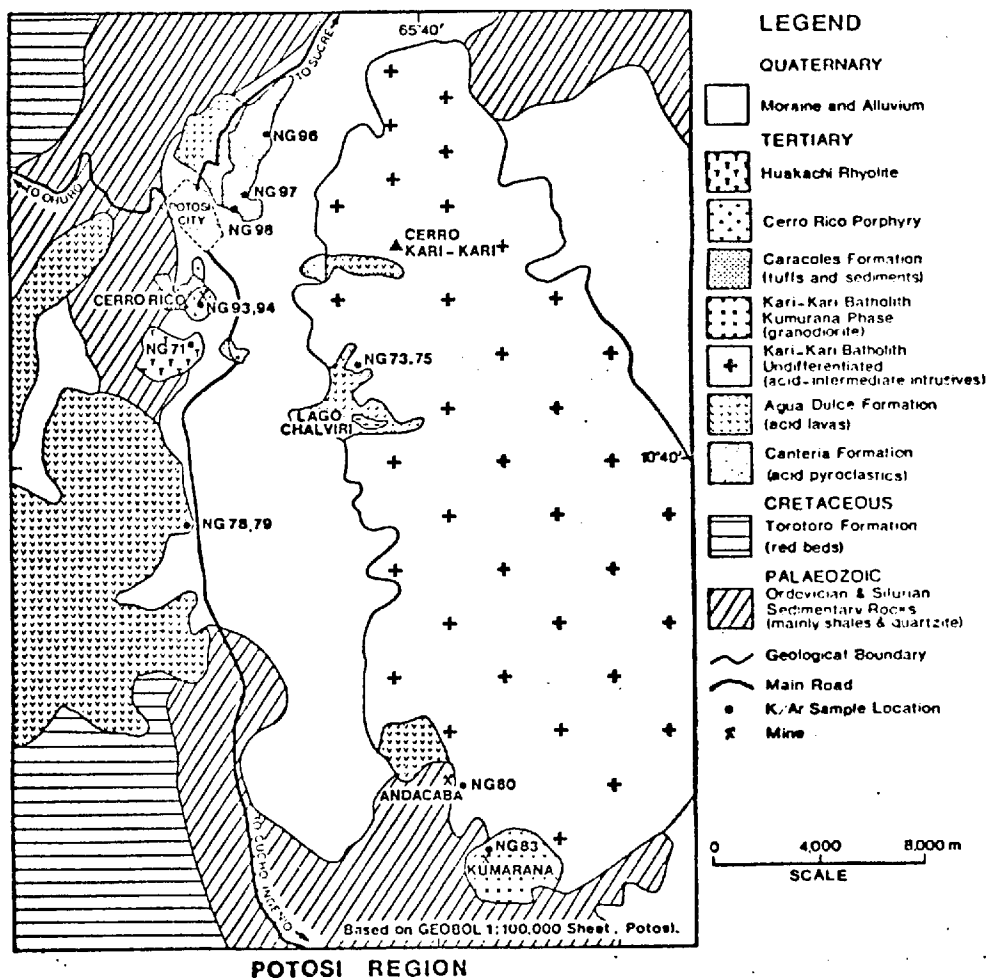
##### b) The Kari-Kari Batholith

This is not in contact with any of the following formations so its upper stratigraphic limit was previously uncertain. Several samples of rhyodacite porphyry from the Lago Chalviri and Andacaba mine areas were dated, and a granodiorite sample from the Kukurana phase at the southern end.

##### c) The Cerro Rico Formation

This includes conglomerates and the plant-bearing tuff beds. They presently outcrop in the immediate vicinity of the Cerro Rico stock, by which they are intruded. No samples from this formation were dated.

FIG.5.4



d) The Cerro Rico Stock

This cuts the Cerro Rico formation in its upper levels and the Palaeozoic sediments at depth. It is about one km in diameter at the surface and narrows rapidly with depth. The rock is a uniform, apparently unbrecciated quartz-porphry which has been intensely sericitized throughout. The veins of the Potosi tin-silver deposit cut the stock in the upper levels, and the Palaeozoic sediments at depth. Two samples of sericitized porphyry from the Pailaviri level of the mine were dated.

e) The Huakachi Rhyolite

This is a rhyolite welded tuff. It overlies rocks of the Cerro Rico formation but is not in contact with the stock. Turneaure (1960) reported pyritized porphyry fragments within it, suggesting a post-mineral age.

The results show that the K-Ar ages of the Kari-Kari batholith, Agua Dulce and Canteria formations are indistinguishable, the differences between them cannot be resolved. The oldest age measured is from the batholith ( $21.7 \pm 0.36$  Ma), but other ages from it overlap with those of other formations. Part of the spread of ages for samples from the batholith is due to partial chloritization of the biotite.

The data for the region are plotted diagrammatically in Fig. 5.5. The  $^{40}\text{Ar}/\text{K}$  diagram for the samples from the Kari-Kari pluton and Agua Dulce and Canteria volcanics is shown in Fig. 5.6. These unaltered rocks all plot close to the regression line, which gives an age of 21.5 Ma.

POTOSI REGION

APPARENT AGE RELATIONSHIPS

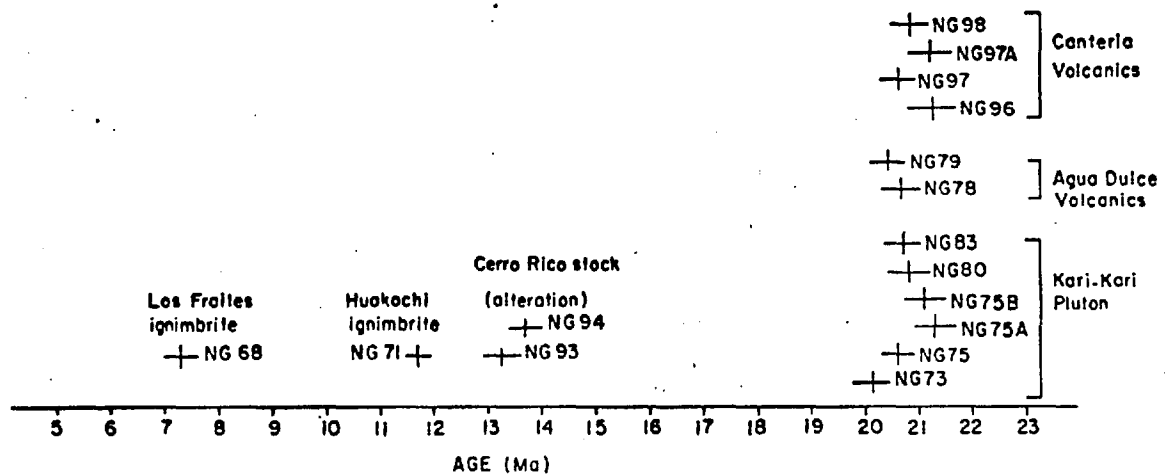


FIG. 5.5



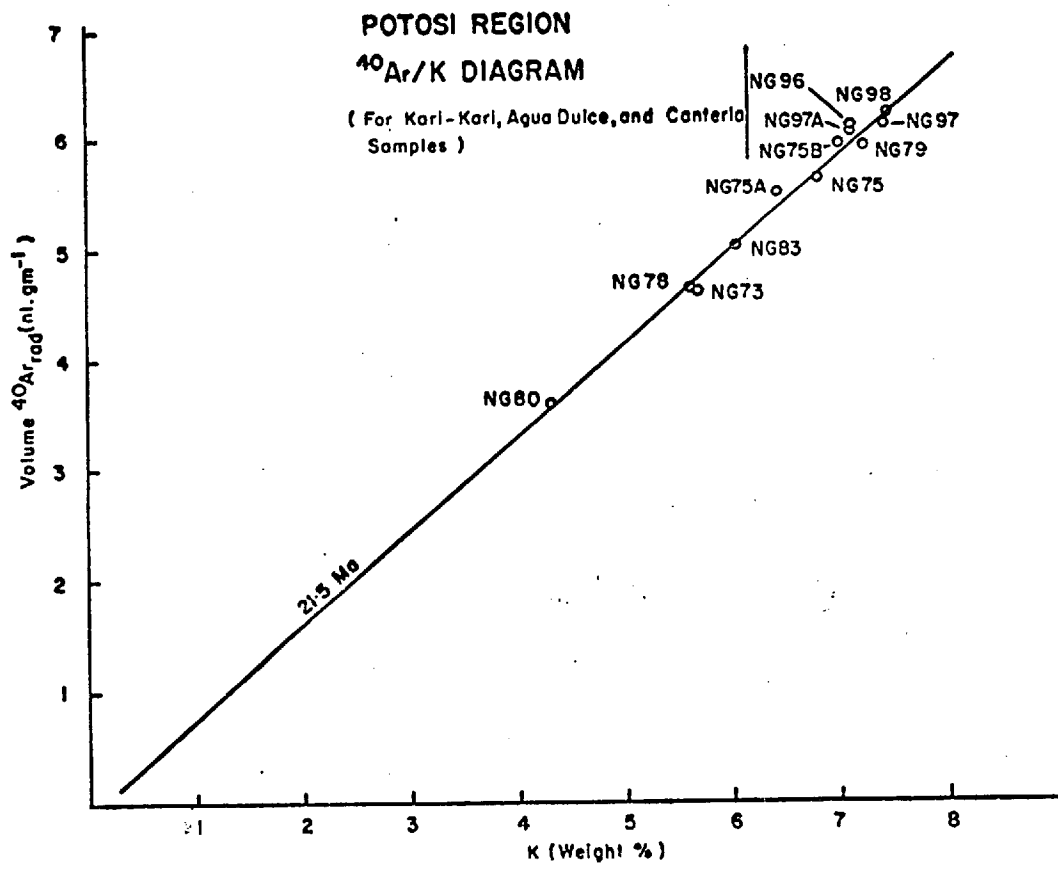


FIG.5.6

It is concluded that the batholith and the volcanics are of closely similar age. The geological relationships show that some of the volcanics of the Agua Dulce formation must have been extruded before the emplacement of at least part of the batholith. However, elsewhere volcanic activity may have been later than the intrusion. This tends to support the field evidence for a very high level of emplacement of the batholith. The data also show that the Kumurana phase is essentially the same age as the rest of the batholith.

The age of the mineralized Cerro Rico stock is indicated by sample NG 93 and NG 94. Both are intensely sericitized and pyritized porphyry. They give an unweighted mean age of  $13.5 \pm 0.3$  Ma. Although no fresh Cerro Rico porphyry has been found, the data from the other altered and mineralized stocks which were dated suggests that it is unlikely that the emplacement of the stock took place much more than 1 Ma before the alteration was complete, and the vein mineralization is unlikely to be much younger.

The Huakachi Rhyolite was dated using a biotite concentrate. The single age determination of  $11.65 \pm 0.22$  Ma (NG 71) is consistent with geological evidence that it is younger than the Cerro Rico porphyry. The Los Frailes ignimbrite was not dated where it outcrops closest to Potosi, but a sample (NG 68) collected about 25 km north of Potosi beside the main road gave a biotite age of  $7.3 \pm 0.20$  Ma. Assuming a similar age for the ignimbrite where it outcrops closer to Potosi, this indicates that the Huakachi Rhyolite is not part of the Los Frailes formation as suggested by Turneáure (1960), but that it is a

separate, distinctly older eruption.

In conclusion the K-Ar ages show that the earliest igneous activity in the Potosi region was associated with the emplacement of the Kari-Kari batholith at about 21 Ma, and this was essentially contemporaneous with eruptions of the Agua Dulce and Canteria volcanics. A time-span of about 6 million years followed in which no igneous activity is recorded. The tuffs of the Cerro Rico formation preceded intrusion of the Cerro Rico stock, which suffered pervasive alteration at 13 - 14 Ma, and the vein mineralization was formed at about that time. Two post-mineral extrusive events followed; first the eruption of the Huakachi Rhyolite at slightly less than 12 Ma, and lastly the Los Frailes ignimbrite eruption whose overall chronology is not known, but which is probably all younger than 8 Ma.

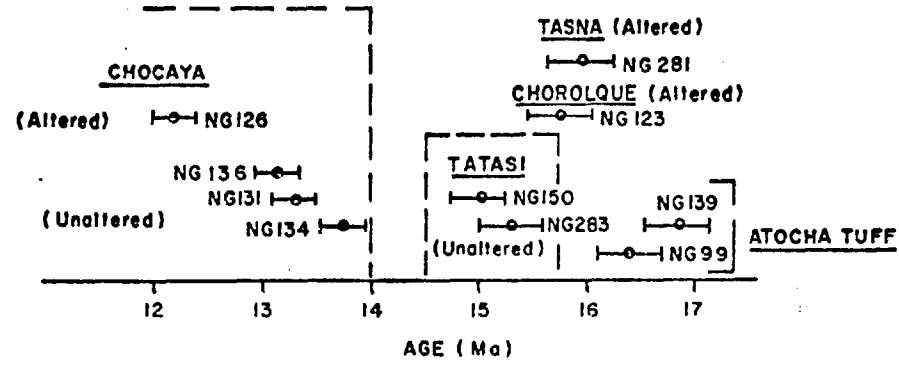
#### 5.7.5. The mineralized igneous centres of the Quechisla region

These include Tasna, Chocaya, Chorolque and Tatasi, which were dated, and a number of other small centres with minor mineralization which have not been dated. The age determinations are plotted diagrammatically in Fig. 5.7.

The region is underlain by folded Lower Palaeozoic shale and sandstone. These were eroded to an irregular plateau before the beginning of igneous activity in the region. The earliest igneous formation is an extensive acid crystal tuff unit which blankets much of the land surface in the Atocha-Telemayu region (Fig. 2.3). Two samples of this tuff (NG 99 and NG 139) were dated. They give an unweighted mean age of  $16.5 \pm 0.3$  Ma. The rocks of the mineralized igneous centres

FIG.5.7

QUECHISLA (ATOCHA) REGION  
APPARENT AGE RELATIONSHIPS



were intruded into the Palaeozoic sediments, or rest unconformably on them. The eastern edge of the Chocaya volcanic complex overlies the crystal tuff unit, but none of the other complexes are in contact with it, or with each other.

At Tasna, the Bi-Cu-Sn veins occur within a several km<sup>2</sup> area of hornfelsed sedimentary rocks. There are some quartz-porphyry dykes, but no large igneous body is exposed at the surface or in the mine workings. One sample from a small dyke on the southern side was dated. The rock was originally a quartz-feldspar-biotite porphyry, probably quartz-latitude, which has been intensely sericitized. The whole-rock analyses duplicate well, giving an unweighted mean age of  $16.0 \pm 0.3$  Ma. This is the minimum age for the alteration of the dyke and surrounding sedimentary rocks, and probably closely approaches the age of the mineralization.

The Chocaya complex is made up almost entirely of extrusive rocks. It now covers an area of over 100 km<sup>2</sup> and has been extensively eroded since its formation. It is made up of rhyodacitic pyroclastics and lavas cut by a few dykes. There is a very extensive zone of strong hydrothermal alteration in the center of the complex (mainly sericite/carbonate and argillic alteration) and the important tin and silver-lead veins lie within this. Both fresh rocks from the outer part of the complex, and an altered sample from the center were dated. The sample locations are shown in Fig. 2.14.

The biotite ages of the three unaltered samples range from  $13.8 \pm 0.2$  (NG 134, mean of duplicate analyses), to

13.2  $\pm$  0.2 (NG 136). The difference between these is less than the critical value so it is concluded that there is no resolvable difference in the ages of the three unaltered samples, and an unweighted mean of 13.4  $\pm$  0.2 Ma can be taken as a good estimate of the minimum age for the eruption of much of the volcanic material at Chocaya. The whole-rock age of the sericitized sample from the pervasive alteration zone is 12.2.  $\pm$  0.24 Ma (NG 126). This age is significantly younger than the biotite ages of the unaltered rocks, and suggests that, as at several other centres, there was a time-span of at least 1 Ma between the eruption of the volcanics and the completion of pervasive alteration.

The Tatasi volcanic complex is similar to Chocaya. It includes acid lavas, lava domes and pyroclastics. Its present extent is over 100 km<sup>2</sup>. Widespread hydrothermal alteration in the core of the complex is generally argillic, and the mineralized veins carry silver and base-metals with little tin. Two separate samples of unaltered rhyodacitic lava from different localities near the edge of the complex (Fig. 2.15) give an unweighted mean age of 15.2  $\pm$  0.3 Ma. No altered rocks from the central region were dated, and thus the overall time-span of igneous activity at Tatasi cannot be estimated.

The Chorolque complex consists of a central core of breccia and intrusive porphyry (the volcanic vent), which is surrounded by acid lavas and pyroclastics which have largely been removed by erosion, exposing the Palaeozoic sediments underneath. The rocks are all altered. The central core is altered to a quartz-tourmaline rock, and the major tin-bearing

veins are within this. It is surrounded by a halo of sericitic alteration which grades out to chloritization. Even in the volcanics farthest from the vent the mafic minerals are chloritized, and the only rocks suitable for K-Ar dating are the sericitized volcanics. Two samples from the sericitic alteration zone have been dated (see Fig. 2.7 for locations). NG 279 gives a whole-rock age of  $17.9 \pm 0.6$  Ma, but this sample proved to have a very high tourmaline content, and is considered to be unreliable. A good estimate of the age of the alteration is given by NG 123 which gave a whole-rock age of  $15.8 \pm 0.3$  Ma (unweighted mean of duplicate analyses). This is considered to be a reliable minimum age for the formation of the Chorolque complex.

## 5.8. Discussion

### 5.8.1. General considerations

The Bolivian tin belt extends for a distance of about 800 km, parallel to the trend of the Eastern Cordillera, at a distance of between 300 and 500 km inland from the coast. The Cordillera is mainly underlain by Lower Palaeozoic sedimentary rocks which have been intruded by acid to intermediate calc-alkaline magmas. The geochronology of the igneous activity is by no means fully understood; however, a number of distinctive features are evident which can be considered in terms of the chronology of magmatic activity in the Eastern Cordillera of the central Andes as a whole.

1. No Palaeozoic ages have been measured on any of the igneous rocks within the tin belt, although the Eastern

Cordillera in both Peru and Argentina has undergone a long and complex history of Palaeozoic igneous activity.

2. The oldest known igneous rocks and ore deposits within the tin belt are the granite-granodiorite batholiths and associated tin-tungsten deposits of the Cordillera Real. These give Triassic to Lower Jurassic K-Ar ages, and were apparently emplaced, at a distance of over 300 km from the coast, at about the same time that volcanic activity was beginning in the coastal regions of southern Peru and northern Chile. That violent volcanic activity is generally taken to mark the beginning of the Andean orogeny (James, 1971b).
3. All later significant igneous activity was Miocene or younger in age.
4. Within the tin belt, presently available age data suggest that magmatic activity took place in a series of relatively discrete pulses. The geographical distribution of dates suggests that each pulse was confined to a limited section of the tin belt, with little overlap except in the case of the youngest event (the post-mineral ignimbrites). Further work may reveal a more complex distribution, particularly in the region to the east of Lake Titicaca where mineralized high-level eruptives have been found, suggesting that the Miocene igneous province may extend northward, parallel with, but to the west of the Mesozoic plutonics.

To the north of the tin belt, in Peru, the Eastern Cordillera



contains a variety of plutonic and volcanic rocks which have given Palaeozoic ages ranging from Ordovician to Permian, and there are also Pliocene volcanics (Stewart et al., 1974). A Permian igneous event seems to have been the most widespread and important, having produced acid and basic volcanics and granitic plutons (Fig. 1.4). The southernmost of the major plutons, the Coasa batholith, has given Permian zircon U-Pb ages ( $238 \pm 11$  Ma, Lancelot et al., 1976). This suggests that the northernmost plutons of the tin belt, which give Triassic K-Ar ages, may be distinctly younger than the Permian plutons of Peru which contain no tin mineralization, and hence that the northern termination of the tin belt corresponds with a significant break in the chronology of igneous activity in this region. The possibility remains, however, that the K-Ar ages of the Bolivian plutons are too young, and they could be contemporaneous with the plutons of southern Peru.

At its southern end, the tin belt terminates just south of the Bolivia-Argentina border. The Eastern Cordillera in northern Argentina has undergone a long and complex history of magmatic activity which is relatively well-documented (Clark et al., 1976). There is a pre-Andean pattern of granitic plutonic belts, of Cambrian to Carboniferous age, oriented NW to SE and becoming progressively younger towards the Chilean border. Some of these plutons have tin-tungsten-bismuth mineralization associated with them. In the Permian there was volcanic and high-level plutonic activity, with associated copper mineralization, in a belt close to the Chilean border. Some Mesozoic ages (Cretaceous) have also been recorded (Sillitoe, 1977).

A northward extension of these older igneous provinces into Bolivia has not been recognised. There are, however, sub-volcanic eruptive complexes of Miocene age in the Eastern Cordillera in northern Argentina (Fig. 1.4). Their ages overlap with those of the southernmost groups of tin-mineralized igneous complexes of the Bolivian tin belt, and they may represent a southward continuation of that igneous province. The Miocene igneous complexes in northern Argentina contain copper mineralization, including a number of porphyry copper deposits (Sillitoe, 1977), thus the southern termination of the Bolivian tin belt seems to be marked by an apparently abrupt change in the metal content of the ore deposits within a continuous magmatic province rather than the termination of a belt of igneous rocks of a particular type or age. However, the lack of age-data and detailed geological investigations in the region of the Bolivia-Argentina border leaves considerable uncertainty regarding the geographical and geochronological relationships of the mineral belts in this area.

At the latitude of northern Argentina, Andean magmatic activity began in the coastal region of Chile in Permo-Triassic time. The focus of magmatism migrated inland across the Western Cordillera, forming a succession of narrow longitudinal igneous belts, parallel with the coast, and decreasing in age eastward. In the Miocene there was an abrupt eastward expansion. Magmatism "broke out" of the Western Cordillera, forming the mineralized eruptive complexes mentioned above (Clark et al., 1976).

Farther north, in the latitude of the Bolivian tin belt, the chronology of igneous activity in the Western Cordillera is

less well known, but a similar pattern apparently exists. The Miocene igneous activity of the Eastern Cordillera, which produced the mineralized plutons and sub-volcanic eruptive complexes of the tin belt to the south of the Cordillera Real, was part of the "break-out" event which lasted into the Pliocene. In the Upper Pliocene there was a contraction of magmatic activity westward, back into the Western Cordillera. This is recognised both in Bolivia and in Argentina. Thus, the igneous geology of the tin belt to the south of the Cordillera Real fits rather well into a coherent pattern of Andean igneous activity which is recognisable throughout the whole region. The same cannot be said of the plutons and associated tin-tungsten deposits of the Cordillera Real whose relationships to the larger pattern of magmatic and tectonic evolution remain obscure.

#### 5.8.2. Geochronology of the southern tin belt

Previous chronological subdivisions of the tin belt, such as those of Schneider-Scherbina (1962), or Ahlfeld (1967), are not consistent with the new age data reported here. The latter proposed two metallogenic epochs for the southern tin belt; a plutonic phase of Miocene age which included the minor mineralization of the Kari-Kari batholith, and an Upper Miocene sub-volcanic phase which included all the important tin deposits, and whose age was based on a 9.4 Ma age for the Llallagua stock. Ahlfeld also proposed that the Mesozoic batholiths of the Cordillera Real with their associated mineralization, were post-tectonic plutons of a 'Variscan' orogeny, which preceded the Andean cycle. Although few radiometric ages were available, he recognised that the more

southerly plutons of the Cordillera Quimsa Cruz, Santa Vera Cruz, and possibly Illimani, were younger and had been emplaced at a higher crustal level than those further north. He also noted the similarity in metal content and certain morphological features shown by the deposits associated with these plutons and the sub-volcanic deposits of the southern tin belt.

The data obtained in this study are plotted diagrammatically in Fig. 5.8. It shows that the ages of mineralized sub-volcanic centres of the southern tin belt fall into two distinct groups. All of the igneous rocks associated with mineralization which have been dated, as far south as Colquechaca, give ages between approximately 23 Ma and 19 Ma. This overlaps with the ages of the plutons of Quimsa Cruz and Santa Vera Cruz. The mineralized centres south of Colquechaca have ages ranging between 17 and 12 Ma, although in the Potosi region, the igneous rocks of the Kari-Kari batholith and Agua Dulce and Canteria formations fall within the older group. This suggests that the Quimsa Cruz, Santa Vera Cruz and Illimani plutons, and the northern sub-volcanic centres, all belong to a distinct province of Lower Miocene age. Although they have not been dated in this study it is probable that the major ore deposits at Colquiri, Oruro, and Huanuni could also be included. If this is the case then this group contains all of the most important predominantly tin-producing deposits of the Bolivian tin belt, while the southern group is characterised by deposits rich in silver and base-metals (Potosi, Chocaya, Tatasi, Tasna). To the north, the Cordillera Real forms a distinct older

**CENTRAL AND SOUTHERN TIN BELT, SUMMARY DIAGRAM - K/Ar AGES**

A = ALTERED SAMPLE

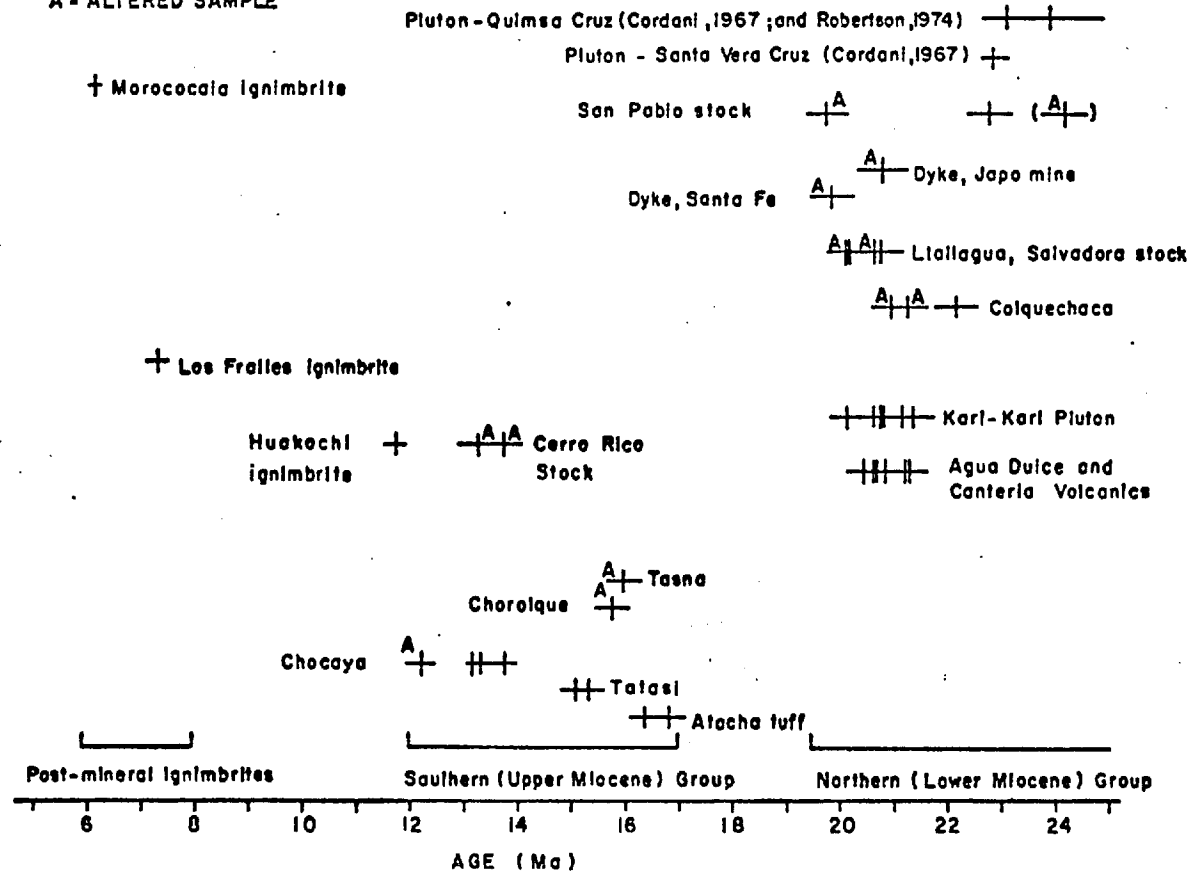


FIG. 5.8

(Mesozoic) province of tungsten-rich deposits. Its geochronology is complex, and although much work has been done to resolve it, the results have not been published yet (Robertson, 1974).

The data show that there was a distinct southward shift in high-level igneous activity in the southern tin belt between 19 Ma and 17 Ma, with overlap of the older and younger age groups in the Potosi region. Considering the tin belt as a whole there is a marked overall trend towards younger ages in the south, with the locus of igneous activity apparently moving southward in a series of discontinuous steps.

There is an overall north to south change in the metal content of the ore deposits. Mineralization associated with the plutonics of the northern tin belt is predominantly of tin-tungsten type. As noted above, the two age groups in the southern tin belt can be broadly distinguished by their differing types of mineralization. The northern group (older than 19 Ma) is made up mainly of deposits associated with high-level plutons or sub-volcanic stocks, and the ores are of quartz-cassiterite type with tin as the dominant economic metal. Included here are the deposits of the Cordillera Quimsa Cruz, the San Pablo stock, Llallagua, the Kari-Kari batholith etc. There are however, exceptions, such as Colquechaca which is a volcanic complex containing sulphide-rich base-metal and silver mineralization with little tin. The Oruro tin-silver deposit also probably belongs with this age group. The southern group (younger than 17 Ma) is dominated by sulphide-rich ores containing important amounts of base-metals and silver in addition to tin, and the deposits are within eruptive complexes of essentially volcanic character. They include the Cerro Rico (Potosi), Chocaya and

Tatasi. Again, there are exceptions, including Chorolque which is a brecciated stock with quartz-cassiterite veins, and also Isca-Isca which is a breccia pipe with tin-tungsten veins. Thus the differences in the style of mineralization and the metal content of the ore deposits within the tin belt are not consistently related to their age, but primarily reflect the depth at which the deposits formed, rather than changes in the geochemistry of the parent magmas with time or space. This argument can not, however, be applied to the northern and southern terminations of the tin belt, which must reflect some more fundamental geochemical factors. The general trend from tungsten, through tin, to silver and base-metals from north to south down the tin belt parallels the decrease in erosion level southward. This does not imply that any individual centre of mineralization is, or was, vertically zoned through the full range of styles and metal associations, from plutonic to volcanic, which are displayed laterally within the tin belt as a whole.

The data also indicate the length of time involved in the development of some of the mineralized sub-volcanic centres of the southern tin belt. In most cases there is little doubt that the pervasive hydrothermal alteration is younger than virtually all the igneous rocks. Thus the alteration ages are minimum ages for the igneous activity. This shows that the maximum probable time between the cooling of the earliest igneous rocks and the completion of the pervasive alteration at a given centre is of the order of 1 Ma, which is similar, for example,

to the measured time-span between porphyry intrusion and pervasive alteration and ore deposition at the Bingham Canyon porphyry copper deposit (Moore et al., 1968).



## CHAPTER 6

SUMMARY AND CONCLUSIONS6.1. Origin of the Tin Belt

Although there are scattered tin deposits at intervals on the continental side of the Cordillera of the western Americas from Alaska to Argentina, the Bolivian tin belt is much more highly mineralized than any other part, and forms a clearly defined metallogenic province. The tin province is only one of several metal provinces within the Andes, the most important of which are all associated with Andean magmatic activity of predominantly calc-alkaline character.

The derivation of calc-alkaline rock suites in island-arcs and active continental margins by processes related to the subduction and partial melting of oceanic lithosphere seems to be beyond doubt (Green and Ringwood, 1968; Ringwood, 1974; Wyllie, 1973). A variety of ore deposits are associated with these igneous rocks world-wide, in particular deposits of copper, molybdenum, gold, lead, zinc, and silver. Although alternative views have been proposed (e.g., Krauskopf, 1967; Jensen, 1971), it is widely accepted that the ore metals were contained in the magmas at the time of their emplacement and derived from the magmas during crystallization (e.g., Holland, 1972). It is also generally assumed that in most cases the metals were incorporated into the magma at the time of its formation and thus that the metals and magma are derived from the same source material. In the case of deposits of the metals

listed above which are associated with calc-alkaline igneous rocks in island-arcs or active continental margins, it is thus generally accepted that the source material for both metal and magma is subducted oceanic lithosphere, and there is no doubt that this material contains sufficient metals to account for the ore deposits. The topmost sedimentary layer of the oceanic crust is particularly metal-rich (e.g., Cronan, 1976; Bostrom et al., 1969). The subduction mechanism for the origin of this type of mineral deposit has been very widely invoked whenever there is evidence for a subduction zone having existed at the appropriate time (e.g., Sillitoe, 1972a, 1972b; Mitchell and Bell, 1973; Strong, 1974; Mitchell and Garson, 1976).

The question of the origin of tin deposits is more complex. Tin is associated with rocks of granitic composition. The typical calc-alkaline plutonic complexes of active continental margin orogens do contain granitic members (e.g., Pitcher, 1978); however, in this setting granites are volumetrically minor, the dominant rock compositions are gabbro-diorite-tonalite, and tin mineralization is absent. Tin is associated with distinctly different rocks; most commonly highly siliceous potassic granites which are geochemically specialized late-stage members of a high-level batholith-forming granodiorite-adamellite-granite suite. In the Andes, and in several other continental margin orogenic belts, these do not overlap in space with the more mafic calc-alkaline suite (although they may be of similar age), but occupy discrete linear belts on the inner, continental side of the orogen. The relationship

of these to subduction processes is not clear.

It has been proposed that siliceous, K-rich magmas can be produced by the partial melting of quartz-eclogite during very deep underthrusting of oceanic lithosphere (Ringwood, 1974). These magmas would be enriched in incompatible elements, perhaps including tin which would be released from the descending slab only when refractory tin-bearing minerals such as phlogopite break down. The special conditions of deep underthrusting required for this to take place would limit the locations in which tin-rich granite magmas could form. This mechanism for the direct derivation of both tin and acid magma from subducted oceanic lithosphere has been advanced for the origin of the Bolivian tin belt (Sillitoe, 1976) and the Malayan tin belt (Bignell and Snelling, 1977). There are, however, several important objections to this. Despite the early experimental work of Green (1972) and Green and Ringwood (1972), the more recent data of experimental petrology suggest that a sub-crustal source for any significant volume of granitic magma is highly unlikely (Wyllie et al., 1976). Petrochemical and isotopic data also generally indicate that there is a substantial crustal melt component in tin granites (e.g., Floyd, 1972; Chappel and White, 1974). A deep rather than shallow region of crustal melting is indicated both by the high level to which tin granite magmas are emplaced, and by the strontium isotope characteristics (Cann, 1970).

There are a variety of possible mechanisms in which crustal melting could be related to subduction. Melting could be triggered by the rise into the crust of large volumes of mafic magma.

This has been proposed to account for the granitic phases of cordilleran calc-alkaline gabbro-tonalite plutons (Presnall and Bateman, 1973). These generally do not have tin associated with them, but it is worth noting that the acid phases of the Bushveld igneous complex of South Africa, which are considered to have formed by a similar mechanism though in a quite different tectonic setting, do have tin deposits associated with them (Hunter, 1976). Underplating of the continental crust, without penetration, by mantle-derived magma would also have the effect of increasing crustal thickness, increasing deep crustal temperature, and so promoting melting (e.g., Brown, 1977). The rise of volatiles alone from a subduction zone might also promote melting in the lower crust; however, the rate of diffusion of volatiles through the mantle wedge above a subduction zone is probably too slow for this mechanism to operate. In all of the above mechanisms, tin could have been supplied from the mantle.

Crustal melting during high-grade metamorphism associated with compressional tectonics, with rise of anatexic magmas along deep-reaching shear zones, is likely as a mechanism for the origin of many granitic plutons. In the case of tin granites this would imply a crustal source for both tin and magma, and the pattern of distribution of tin provinces would perhaps be partly related to an inhomogeneous distribution of tin in the crust. A crustal source for all except very ancient tin deposits has been widely invoked (e.g., Schuiling, 1967). Important lines of evidence include; the very low tin content of oceanic lithosphere as compared with certain rocks now incorporated into continental crust (some shales, granites), the tendency

for tin mineralization to recur in certain areas over a long time-span indicating a source region within the same lithospheric plate, and the absence of tin mineralization in an island-arc setting.

It is also possible that the distinction between tin-associated igneous rocks and others results entirely, or almost entirely, from differences in the history of differentiation and country-rock interaction which the magmas underwent after formation. There is no doubt that tin mineralization is associated with granitoids which are highly geochemically specialized as a result of particularly advanced fractional crystallization (e.g., Tischendorf, 1977; Groves and Mc Carthy, 1978). The processes leading to tin enrichment are probably highly sensitive to rather subtle factors such as the content of  $H_2O$  and other volatiles, and the oxygen fugacity of the magma (Ishihara, 1977). It may be that these are the critical factors in the development of 'tin granites', rather than the chemistry of the magma source region.

In the case of the Bolivian tin belt, any satisfactory model must account in particular for the following features.

- a) Its conformity with the Andean trend, and its limited longitudinal extent.
- b) Its distinctive position on the continental side of the orogen and of the other metal provinces.
- c) The timing of emplacement of the tin-bearing igneous rocks with respect to Andean tectonic/magmatic evolution.

Much of the evidence needed to begin to assess the relative crustal or mantle contributions to the tin-belt magmas is lacking

at present. However, it seems unlikely that a mantle contribution would be completely ruled out by geochemical or isotopic evidence. The simplest model for the source of all the magmas plus the tin at great depth on a subduction zone can probably be rejected on the grounds that the bulk of granitic magmas must be crustally derived. However, the spatial distribution of the tin belt does suggest some degree of control by a segmented descending slab in which maximum underthrusting took place beneath the tin belt, as is the case at the present day. Here, however, the timing of emplacement of the northern tin granites becomes a problem, as they were emplaced at the beginning of Andean subduction, although over 300 km inland from the trench.

The main objection to a simple crustal origin is the parallelism of the tin belt with the Andean trend, its sharp boundary with the polymetallic belt to the west, and its sharply limited longitudinal extent. It seems unlikely that this spatial distribution of tin deposits within the larger pattern of Andean magmatism merely reflects the shape of a tin-rich zone in the lower crust. Furthermore, there is clear evidence that Miocene acid igneous activity in northern Argentina did not lead to tin rejuvenation in that area, where the upper crust at least is tin-rich. It could be, however, that while melting of tin-rich lower crust was relatively widespread during the Andean orogeny, perhaps particularly during the Triassic and Miocene, the magmas were only able to rise to shallow depth in a discrete zone defined by the tin belt, and during those two distinct time periods. A tectonic control, coupled perhaps with subtle

factors of differentiation history etc. may be dominant in both the space and time distribution of the tin mineralization. In this context it is perhaps significant that the extent of the tin belt corresponds broadly with the Altiplano basin, a major tensional tectonic feature. It also corresponds with the axis of the Palaeozoic sedimentary basin, which in turn may have been controlled by deep basement structures.

My conclusions are as follows :

a simple subduction-related mantle origin for the tin-bearing igneous rocks is unlikely; a purely crustal origin is possible, with the processes of melting and magma ascent tectonically controlled, hence indirectly subduction-related, with important secondary controls provided by factors affecting the differentiation history of the magmas. A combined crustal and mantle source cannot be ruled out, perhaps with small quantities of volatile-rich magma rising from the subduction zone and triggering melting in the crust, and perhaps also carrying the tin. A great deal of further work is required before a better understanding can be gained.

#### 6.2. Geochronology of the Southern Part of the Tin Belt

The currently available radiometric age data suggest a 3-fold chronological subdivision of the tin belt as a whole. The plutons and associated mineralization of the northern Cordillera Real (as far south as Mururata-Taquesi) are Triassic in age, and form a distinct tin-tungsten metallogenic sub-province.

The higher-level plutons of Illimani, Cordillera Quimsa Cruz, and Cordillera Santa Vera Cruz are Upper Oligocene

(Illimani) to Lower Miocene in age (26 to 23 Ma), and the new K-Ar data reported here show that there is no time break between these and the sub-volcanic eruptive complexes of the northern part of the southern tin belt. The ages of these range from approximately 23 Ma to 20 Ma. Together, the southern plutons, the northern eruptive complexes (as far south as Colquechaca) and the Kari-Kari pluton form a distinct sub-province which contains most of the major tin deposits of Bolivia, although it does also contain tungsten, tin-silver, and predominantly base-metal deposits.

The mineralized centres from Potosi (Cerro Rico) southward form a distinct younger sub-province, with ages from approximately 16 to 12 Ma. The mineralization typically occupies a high-level position in relatively weakly eroded eruptive complexes, and is characterized by high silver and base-metal content.

The great ignimbrite sheets of Morococala and Los Frailes are distinctly younger than the mineralized eruptive complexes, with an age range of approximately 6 to 8 Ma, and were erupted after the mineralized complexes had been extensively eroded.

The general decrease in the age of mineralization from north to south down the tin belt corresponds with a generalized change from tungsten-rich mineralization in the north to predominantly silver and base-metal rich deposits in the south. In detail, the metal content of the ores of individual eruptive complexes show a distinct relationship to the depth at which the deposits were formed. Thus, the north to south metal zonation of the province as a whole reflects the general



decrease in erosion level southward, and may not be related to any fundamental change in the chemistry of the parent magmas with time or space.

At the sub-volcanic eruptive complexes, the time-span between the beginning of eruptive activity and completion of pervasive alteration is generally less than 2 Ma, in some cases closer to 1 Ma, but the length of time over which the vein mineralization was deposited has not been measured.

### 6.3. A Genetic Model for the Sub-Volcanic Tin Deposits

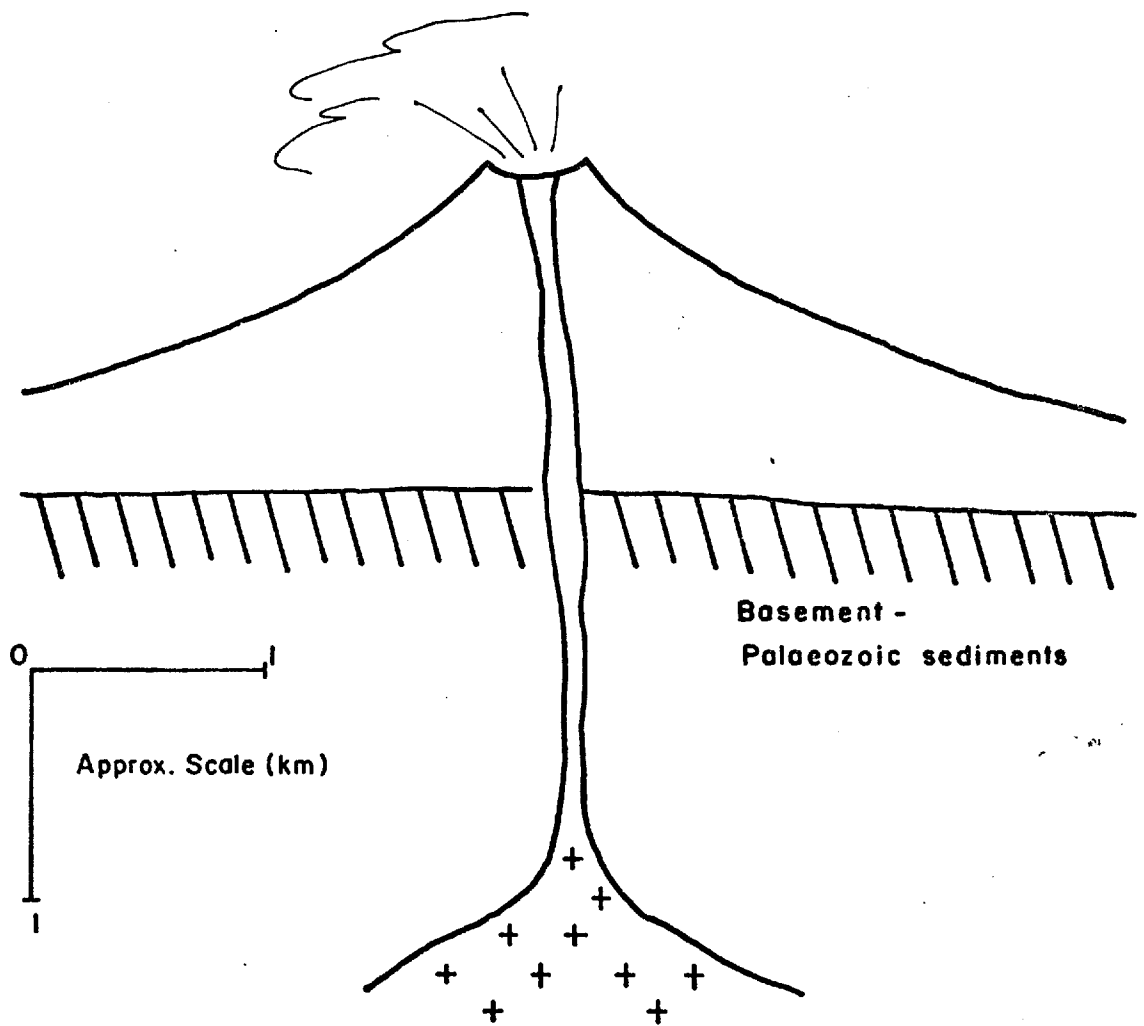
The geological, fluid inclusion, and stable isotope data reported here can be combined to provide a generalized conceptual model for the evolution of the sub-volcanic tin deposits. The data is by no means complete, and the model is partly speculative. In its general aspects it is closely similar to models which have been proposed for the genesis of the porphyry copper-molybdenum deposits, involving a magmatic source of metal-bearing fluid and heat which interacts with meteoric water in a convecting hydrothermal system, to give the characteristic zoned pattern of mineralization and alteration (Taylor, 1974; Gustafson and Hunt, 1975; Henley and Mc Nabb, 1978). The model outlined below for the tin deposits confirms the genetic similarities between these and the porphyry Cu-Mo deposits first postulated by Sillitoe et al., (1975).

The genesis of the sub-volcanic tin deposits can be described in terms of the following overlapping evolutionary stages.

1. The volcanic stage (Fig. 6.1). This involved the construction of a stratovolcano, which was built up of dacite and rhyodacite pyroclastics and lavas, erupted from a central vent.

FIG.6.1

VOLCANIC STAGE - construction of stratovolcano



Dry magma, from large body at depth, erupts at surface

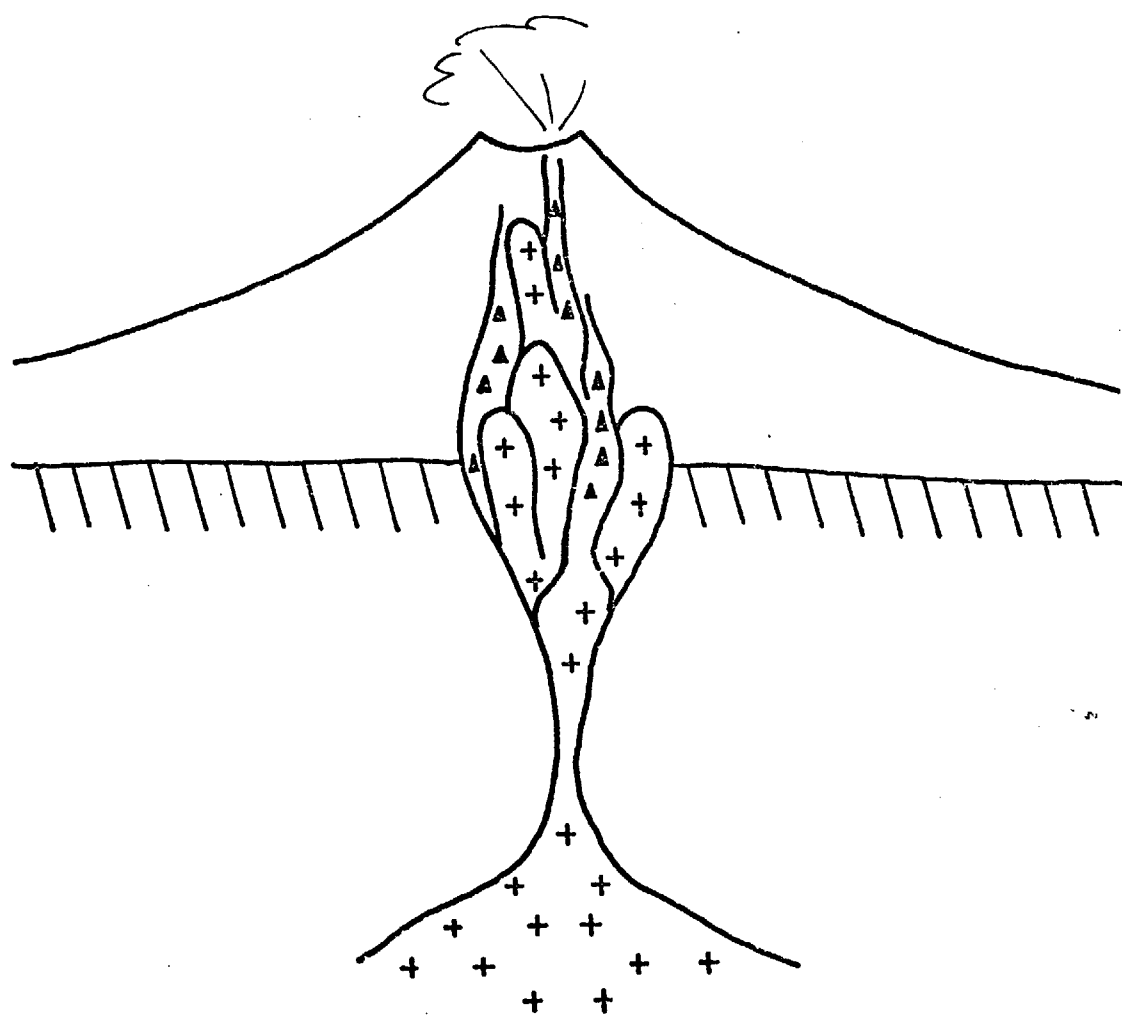
The erupted material was derived from a large magma chamber at depth. From this, dry magma rose and was erupted violently at the surface. This magma was not particularly highly specialized geochemically, although it does show a characteristically low K/Rb ratio and anomalous Sn and Li content.

2. The vent-filling porphyry and breccia stage (Fig. 6.2). As crystallization in the source magma chamber continued, the rest melt became enriched in  $H_2O$ , other volatiles, and Sn etc. Pulses of this more fluid magma rose rapidly in the vent and underwent isothermal vapour saturation at a greater depth than earlier magma. This resulted in violent fluid release, and freezing of the magma as porphyry in the vent. The hydrothermal brecciation which is so characteristic of many of these deposits is an expression on the violent fluid release. The breccias were formed mainly by initial hydraulic fracturing followed by corrosion and fluidization of fragments in an upward-streaming vapour, derived from successive pulses of porphyry emplacement.

3. Pervasive alteration stage (Fig. 6.3). As porphyry intrusion retreated to lower levels in the vent, the brecciated rocks above were altered pervasively. Intense quartz-tourmaline alteration was associated with the high-temperature magmatic fluid. This may have separated directly from magma as a 2-phase fluid, or as a vapour which condensed to a 2-phase fluid (vapour plus highly saline brine) in somewhat cooler regions (Henley and Mc Nabb, 1978). The fluid inclusion data from Chorolque indicate that this alteration took place at temperatures at least as high as  $500^{\circ}C$ , and the isotopic data indicate a magmatic origin for the fluid. No mineralization

FIG.6.2

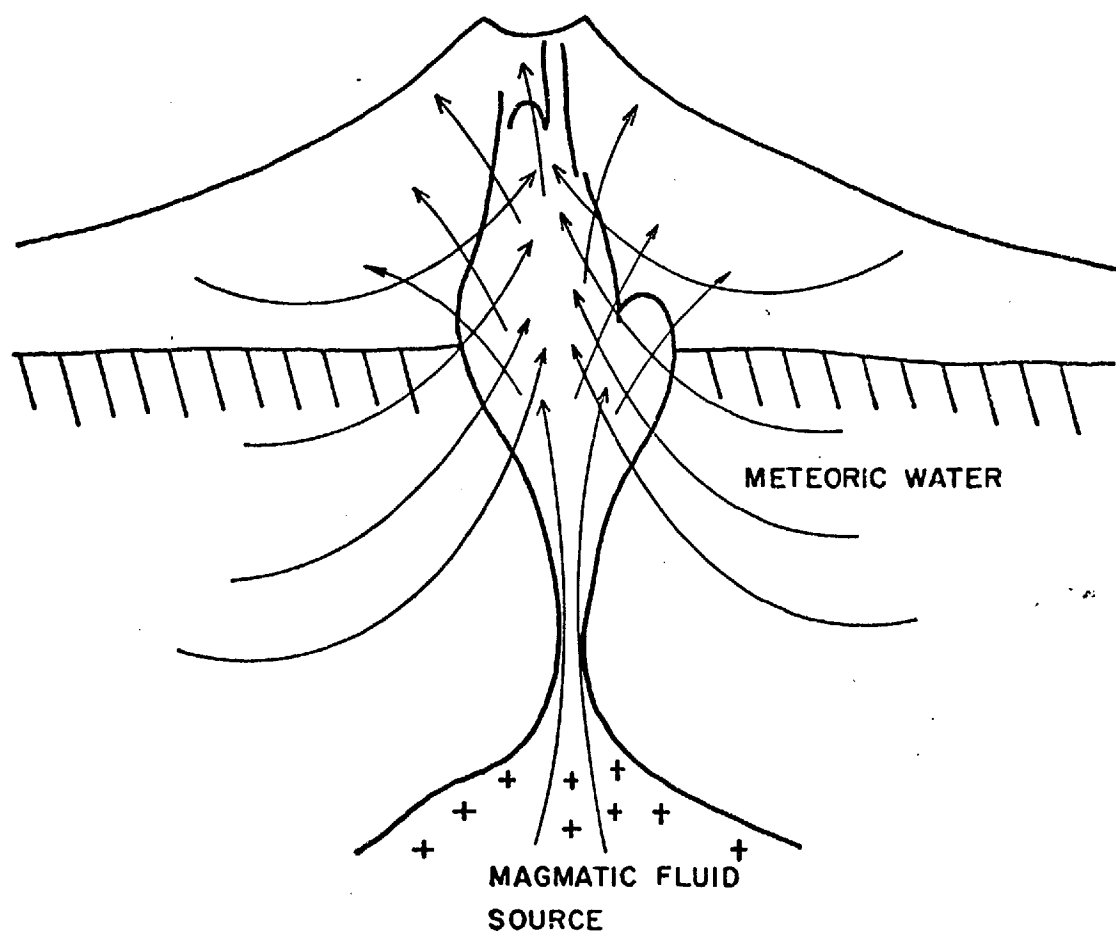
**PORPHYRY INTRUSION STAGE**  
with explosive hydrothermal brecciation



Pulses of volatile-rich more fractionated magma rise rapidly, release vapour explosively, consolidate as porphyry in the vent

FIG.6.3A

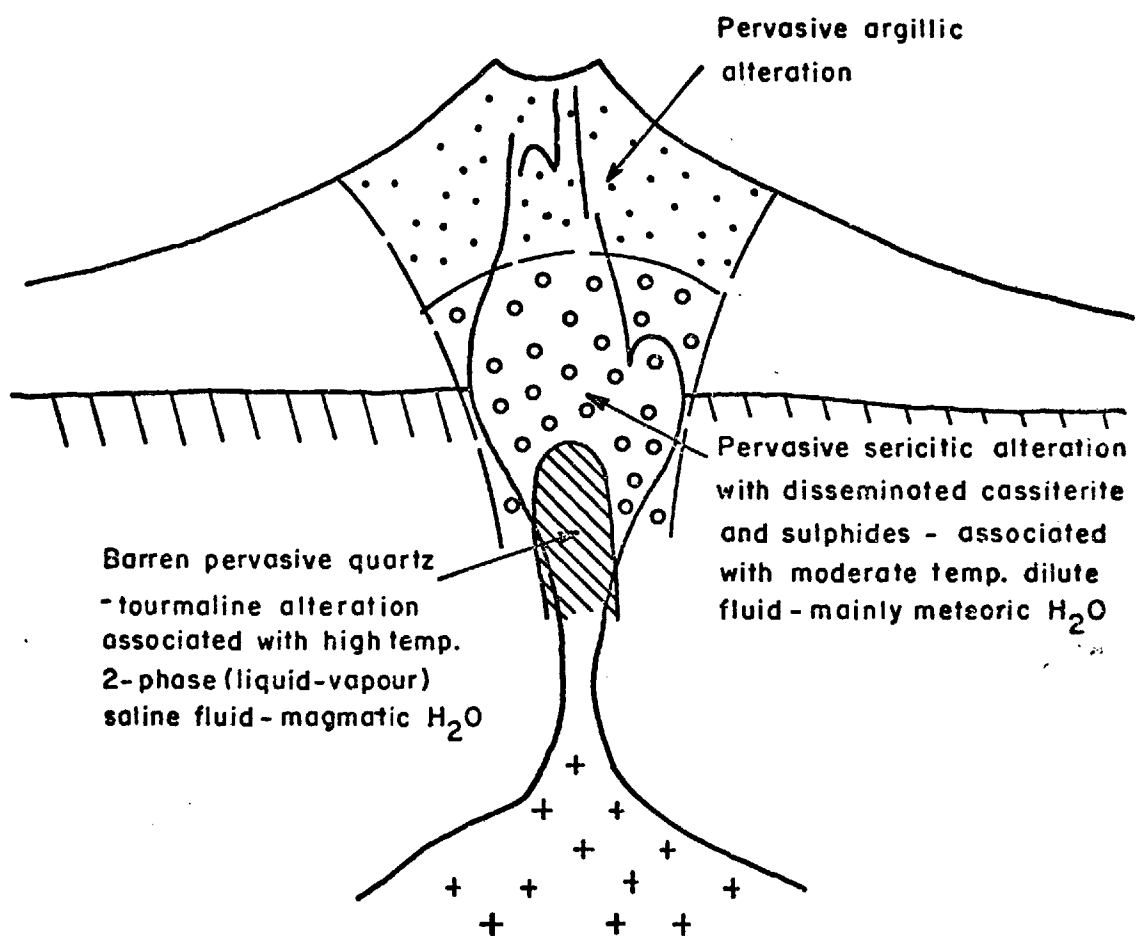
**MAIN HYDROTHERMAL STAGE**  
convective magmatic - meteoric system develops



Widespread pervasive alteration and ore-mineral  
deposition takes place in the upper vent and volcanic  
superstructure

FIG.6.3B

ALTERATION PATTERN produced by the magmatic-meteoric hydrothermal system



was deposited in association with this alteration either because conditions were unsuitable for deposition from the liquid phase (temperature and salinity too high, pH too low) or because the ore metals were transported in the vapour phase to peripheral and higher regions. The permeable vent rocks in this region probably became progressively choked with deposited silica.

The regions surrounding and overlying the 'core' of magmatic fluid contained cool meteoric fluid (groundwater). This mixed with the magmatic fluid at the vent margin and became involved in a convecting hydrothermal system. While quartz-tourmaline alteration took place in the inner regions, sericitic alteration developed in the cooler peripheral and overlying parts of the system where the fluid was dominantly heated meteoric water. Mineralization was deposited in the zones of sericitic alteration mainly in response to the decreasing temperature and salinity resulting from mixing of meteoric water with the original magmatic fluid. This resulted in the zonation of pervasive alteration and mineralization both laterally around the vent (Chorolque) and vertically within it (Llallagua). The temperature and salinity decline from quartz-tourmaline to sericitic alteration is indicated by the fluid inclusion data, and the isotopic data show that the fluid associated with sericitization was clearly different (from the magmatic fluid) and probably, though not definitely, meteoric water.

The convective hydrothermal system was 'driven' by heat and fluid provided by rising and cooling porphyry magma in the vent.

When the supply of porphyry magma ceased, there was a sharp change in the character of the system.

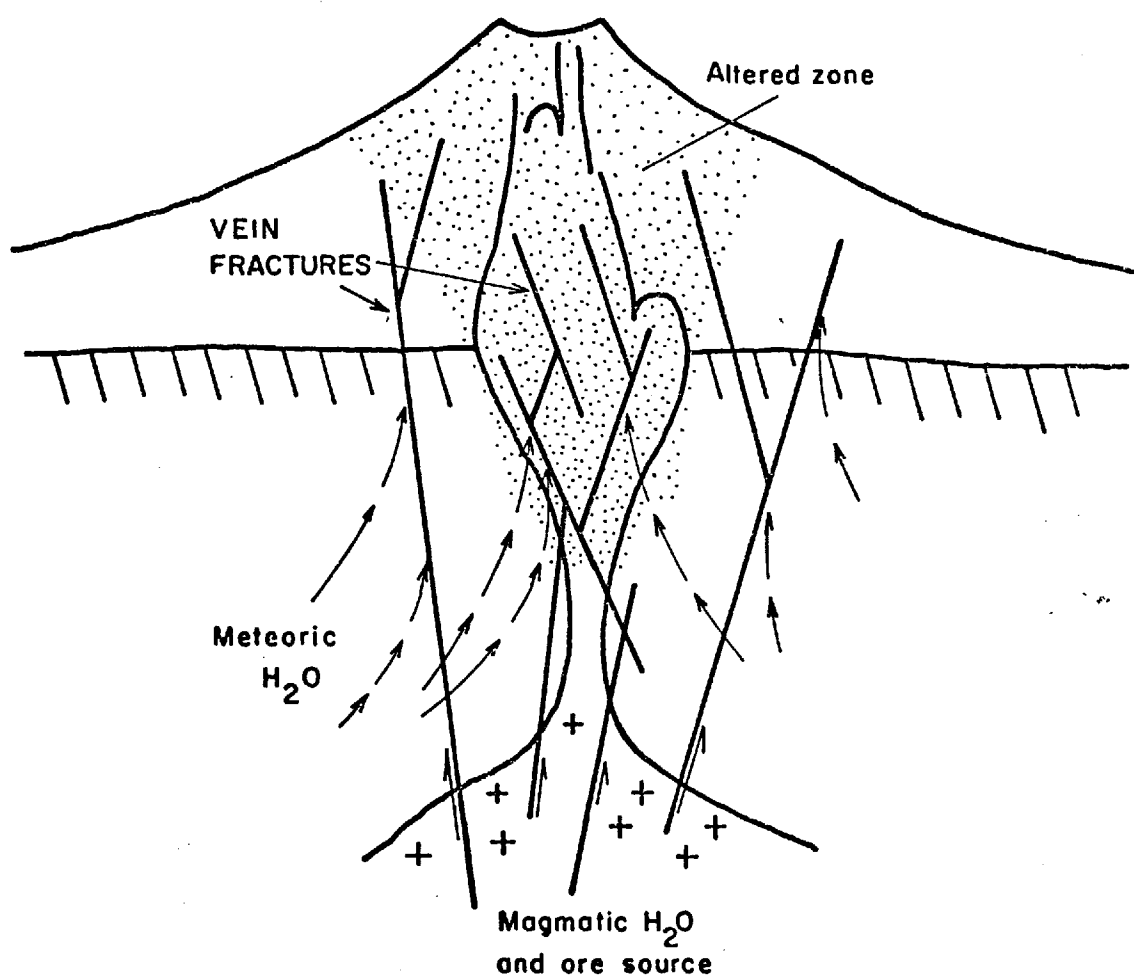
4. The vein stage (Fig. 6.4). Following the cessation of porphyry intrusion, magmatic and hydraulic pressure in the vent region declined, and cooling in the underlying magma chamber led to a marked change in the local stress pattern. A deep-reaching fault system developed in the vent area, this penetrated to the underlying pluton and tapped the continuing supply of metal-bearing fluid which was given off as the pluton crystallized. The probable magmatic origin of the early vein fluids is indicated by the isotopic data. The fluid inclusion data for the veins shows a progressive decline in fluid temperature and salinity during vein growth, and this can most reasonably be attributed to the increased incorporation of meteoric water into the vein system, although there are no isotopic data with which to evaluate this. The interval over which ore deposition took place in the vein system was probably controlled by the pattern of meteoric water mixing and the resulting thermal and salinity gradients in the rising, initially magmatic fluid. These in turn may have influenced the levels at which boiling took place in the vein fluids, and boiling may have been a significant factor in promoting rapid ore deposition and the development of strongly 'telescoped' ore mineral assemblages which are characteristic of these deposits.

Kaolinite was deposited as a final filling in many veins. It may have been a product of supergene weathering, deposited from downward-percolating groundwater during uplift and erosion



FIG.6.4

VEIN STAGE - follows pervasive alteration



Fluid movement becomes restricted to vein structures as temperature falls in the vent - magmatic ore fluid continues to rise in veins from deep plutonic source - with incorporation of meteoric water increasing.

at a much later date. This is most in keeping with the isotopic data.

The genetic model outlined above applies in particular to those mineralized eruptive complexes which have a well-developed porphyry and breccia 'stock' (the vent) with disseminated 'porphyry-tin' mineralization. The very high-level volcanic complexes such as Chocaya and Tatasi appear to lack this, and there was apparently a direct transition from the volcanic stage, with strong mainly argillic alteration, to the vein stage. These complexes contain no porphyry-type mineralization.

#### 6.4 The Transport and Deposition of Tin in Hydrothermal Systems

Various mechanisms, involving both vapour and liquid phase transport have been proposed. In the case of the vapour phase, tin can be transported as simple halide ions in experimental systems, but the presence of  $H_2O$  seems to suppress the volatility, particularly of the chloride (Hurd, 1976). However, it is known that other metals, including copper, can be transported in aqueous vapour as mixed alkali (Na)-chloride complexes (Henley and Mc Nabb, 1978), so the vapour phase transport of tin in multi-component magmatic-hydrothermal systems seems possible at high temperatures.

In the aqueous liquid phase, a variety of tin-transporting complex molecules have been postulated, including hydroxofluoristannate, alkali stannate, alkali thio-stannate and alkali fluor- and chloro-stannate complexes (Smith, 1947; Barsukov and Kuril'chikova, 1966; Hesp and Rigby, 1971; Barsukov and Ryabchikov, 1977; Hesp and Varlamoff, 1977). The importance

of fluorine, which is often associated with tin mineralization, and which has been shown to promote tin solubility in experimental systems, is not clear. However, fluid inclusion studies have shown that natural ore-forming solutions almost invariably contain both chlorine and sodium as principle dissolved elements, and the presence of fluorine may not be essential for tin solubility.

The evidence from fluid inclusion studies of a variety of tin deposits has shown that cassiterite deposition took place both from 2-phase (liquid plus vapour) and single (liquid) phase fluids (e.g., Little, 1960; Kelly and Turneaure, 1970; Jackson et al., 1977). A 2-phase fluid was also commonly associated with ore-mineral deposition in other high-temperature magmatic-hydrothermal deposits. This is usually interpreted as indicating boiling of a liquid ore fluid. An alternative view is that the initial metal-bearing magmatic fluid was dominantly vapour, which condensed and mixed with meteoric water (Henley and Mc Nabb, 1978; White et al., 1971). In either case, the major factors leading to ore-mineral deposition would be temperature decline, pH change, salinity decline and change in  $fO_2$  and  $fS_2$ .

The present study of the Bolivian deposits provides little information on mechanisms of tin transport, beyond confirming the presence of large amounts of Cl, Na, and K in the ore fluid, and the absence of F-bearing minerals in the altered rocks (except perhaps tourmaline, which may contain F).

The most important conclusions in this respect are as follows.

a) Cassiterite was deposited from both 2-phase (liquid plus vapour) and single phase (liquid) solutions, in different

regions and at different times within the same deposit. None of the hydrothermal systems appear to have been vapour-dominated during the main stages of cassiterite deposition (except perhaps at Huanuni, from which only one sample was studied). The data generally indicate liquid ore fluids at the vein stage, with intermittent boiling. Much ore deposition was not accompanied by boiling, which does not appear to have played a particularly important role.

b) There is a distinctive upper salinity limit (approximately 25 equivalent weight percent NaCl), above which cassiterite is not deposited from the ore fluids. Almost all other fluid inclusion studies of tin deposits indicate that ore deposition took place from relatively dilute fluids. The temperature of ore deposition was highly variable, in the Bolivian deposits ranging from over 400°C down to 200°C or even less. The evidence from Chorolque in particular suggests that at least during the early vein stage, the tin was transported in a highly saline liquid, and that the most important factors in causing ore-deposition were the decrease in salinity and temperature and changes in oxygen fugacity and pH which accompanied mixing with dilute, probably meteoric water.

## Appendix 1

## Petrographic (Thin Section) Descriptions of Analysed Rocks.

A. Dated samplesNG 1. Morococala formation ignimbrite, near Japo Mine.

Porphyritic-aphanitic texture; made up of 20% altered plagioclase phenocrysts (to 2 mm length), 20% biotite phenocrysts (to 1 mm length), occasional sanidine and partly chloritized hornblende phenocrysts (to 2 mm length); in a glassy matrix (60%), partly isotropic and crowded with micro-lites. Accessory apatite and zircon.

NG 2. Morococala formation ignimbrite. As NG 1.NG 6. Altered quartz-porphyry, San Pablo stock.

Relict porphyritic-microgranular texture; made up of 10% primary quartz phenocrysts (to 8 mm), patches of fine-grained intergrown tourmaline, minor quartz and sericite (pseudomorphing 5 - 10 mm feldspar phenocrysts, 25%), patches of fine sericite plus rutile and opaques (pseudomorphing 2 - 3 mm biotite phenocrysts, 10%), in a microgranular quartz-rich matrix (55%) flecked with sericite and minor tourmaline. Accessory apatite and zircon.

NG 27. Altered quartz-porphyry, San Pablo stock.

Relict porphyritic-microgranular texture; made up of 10% primary quartz phenocrysts (3 - 6 mm), patches of fine sericite-quartz intergrowth (pseudomorphing 3 - 6 mm feldspar phenocrysts, 30%), patches of sericite plus rutile and Fe-oxides (pseudomorphing 2 - 3 mm biotite phenocrysts, 10%), in a quartz-rich microgranular matrix (50%), flecked with sericite. No tourmaline,

accessory apatite, zircon.

NG 31. Mineral sample (hand picked sanidine macrocrysts), no thin-section.

NG 21. Altered feldspar-porphyry dyke, Japo mine.

Relict porphyritic-microgranular texture; made up of patches of fine intergrown sericite-quartz (pseudomorphing 3 - 6 mm feldspar phenocrysts, 40%), patches of fine intergrown sericite plus rutile and opaques (pseudomorphing 3 - 4 mm biotite laths, 10%) in a granular matrix of quartz with minor sericite. No tourmaline, accessory zircon, apatite.

NG 14. Altered feldspar-porphyry dyke, Santa Fe mine.

As NG 21.

NG 487. Salvadora stock, Llallagua; 650 level, Siglo XX mine.

Unaltered quartz-feldspar porphyry. Porphyritic-microgranular texture; made up of 15% rounded, embayed quartz phenocrysts (to 5 mm), 20% corroded and poorly zoned subhedral plagioclase phenocrysts (approximately andesine composition, 5 - 10 mm) partly replaced by potash feldspar and with very minor alteration to sericite and tourmaline, 20% subhedral sanidine, phenocrysts (5 - 8 mm), 10% brown euhedral biotite phenocrysts (2 - 5 mm), in a mottled, very fine granular quartz-rich matrix (35%). Accessory zircon, apatite.

NG 38. Salvadora stock, Llallagua; 383 level, Siglo XX mine.

Altered quartz-feldspar porphyry. Relict porphyritic-microgranular and brecciated texture. Made up of 15% rounded or fractured angular primary quartz phenocrysts, 40% indistinct rounded patches of fine sericite-quartz-minor tourmaline intergrowths (pseudomorphing 5 - 10 mm feldspar phenocrysts), 10%

patches of fine sericite-rutile-quartz-minor tourmaline intergrowth (pseudomorphing 2 - 5 mm biotite phenocrysts), in a granular quartz-rich matrix flecked with fine sericite and clay.

NG 45. Salvadora stock, Llallagua; from dyke-like offshoot at surface. Very weakly altered quartz-feldspar porphyry.

Similar to NG 487, but coarser phenocryst grain size, and partial alteration of biotite phenocrysts to chlorite plus sericite.

NG 44. Salvadora stock, Llallagua; from surface, central region of the stock.

Intensely altered quartz-feldspar porphyry. As NG 38, with occasional tourmalinized argillite fragments.

NG 68. Los Frailes ignimbrite formation; north of Potosi.

Porphyritic-aphanitic texture, made up of crowded angular quartz phenocrysts, plagioclase, minor sanidine, biotite, and minor brown hornblende phenocrysts in a clay-altered, slightly spherulitic flow-banded shard-rich glassy matrix. A rhyodactic welded tuff, similar to NG 1.

NG 71. Huakachi rhyolite formation; base of Cerro Huakachi immediately south of Cerro Rico, Potosi.

Siliceous (rhyolite) welded tuff; made up of crowded angular to rounded quartz phenocrysts (50%), lesser unaltered plagioclase, sanidine and biotite phenocrysts (20%), numerous tabular argillite fragments (10%) in a glassy, shard-rich matrix.

NG 93 and 94. Cerro Rico stock, Potosi; level Pailaviri O, adjacent to Veta Rica 1 (NG 93) and Veta Rica 3 (NG 94).

Intensely altered quartz-feldspar porphyry. Relict porphyritic-microgranular texture; made up of 25% rounded primary quartz

phenocrysts (3 - 8 mm), 25% patches of fine sericite-quartz-pyrite-clay intergrowth (pseudomorphing feldspar phenocrysts), 10% patches of sericite-rutile-quartz (pseudomorphing biotite phenocrysts), in a fine granular quartz-sericite-clay matrix with patches of coarser pyrite. No tourmaline; accessory zircon and apatite.

NG 73. Kari-Kari pluton; near Lago Chalviri, southeast of Potosi.

Feldspar-biotite porphyry (granodiorite). Porphyritic-microgranular texture, slightly brecciated; made up of 30 to 40% angular, fractured, zoned plagioclase phenocrysts (2 - 4 mm) slightly sericitized; 5 to 10% subhedral brown biotite phenocrysts (1 - 3 mm) with narrow rims altered to chlorite plus opaques; occasional broken K-feldspar (sanidine) phenocrysts; accessory garnet, apatite, zircon; in a granular quartz-feldspar matrix.

NG 75, 75A, 75B. Kari-Kari pluton; near Lago Chalviri.

Feldspar-biotite porphyry, essentially as NG 73, with variable degrees of chloritization of biotite (always less than 20% of total).

NG 80. Kari-Kari pluton; near Lago Chalviri.

Feldspar-biotite porphyry (granodiorite), as NG 73, with partly cataclastic texture.

NG 83. Kari-Kari pluton, near southern end, Kumurana.

Equigranular granodiorite with strongly cataclastic texture; made up of quartz (10 - 20%), plagioclase (60 - 70%), potash feldspar (10%) and biotite (10%). Plagioclase is weakly sericitized, biotite is essentially unaltered. All are partly granulated, crushed; traversed by zones of very fine quartz-chlorite.

NG 78 and 79. Agua Dulce volcanic formation, south of Potosi.



Porphyritic-aphanitic texture; made up of broken, angular quartz phenocrysts (1-3 mm, 15%), plagioclase phenocrysts (2 - 5 mm, 20%), biotite laths (unaltered, 10%), sanidine phenocrysts partly altered to clay (3 - 5%), in a glassy, shard-rich, flow-banded matrix. A rhyodacite welded tuff.

NG 96, 97 and 98. Canteria volcanic formation, north of Potosi.

Porphyritic-aphanitic texture, made up of rounded quartz phenocrysts (2 mm, 20%), biotite flakes (1 to 3 mm, unaltered, 10 to 15%), patches of carbonate-clay-sericite intergrowth (pseudomorphing feldspar phenocrysts, 30%), in a shard-rich glassy matrix partly altered (weathered) to clay. Occasional small argillite fragments, and accessory apatite, garnet.

NG 35A (CH). Colquechaca, cirque south of Cerro Hermosa.

Quartz-feldspar porphyry; porphyritic-microgranular texture; made up of rounded, embayed, 3 to 5 mm quartz phenocrysts (5%), subhedral unaltered 3 to 8 mm sanidine phenocrysts (5%), subhedral 3 to 8 mm weakly sericitized plagioclase (andesine) phenocrysts (35%), biotite laths (15%) with minor alteration of rims to chlorite plus rutile and opaques, in a fine granular quartz-rich matrix. Accessory apatite, zircon.

NG 54. Colquechaca, Mina Descubridora adit.

Quartz-feldspar porphyry, as NG 35A (CH), with increased alteration of biotite to chlorite.

NG 62. Colquechaca, below Cerro Yanakaka.

Intensely altered (sericitized) quartz-feldspar porphyry.

Relict porphyritic texture; made up of 20% rounded primary quartz phenocrysts, 20 to 30% indistinct patches of fine sericite-quartz intergrowth (pseudomorphing feldspar phenocrysts), 10%

patches of intergrown sericite plus rutile-quartz-opaques (pseudomorphing biotite phenocrysts), in a fine grained quartz-sericite-clay matrix. Accessory apatite (common), tourmaline, zircon.

NG 131, 134, 136. Chocaya, unaltered acid volcanics.

Porphyritic-aphanitic texture, typically made up of 5% rounded, embayed quartz phenocrysts (to 3 mm), occasional sanidine phenocrysts, 10 to 20% biotite laths (to 2 mm) with rims altered to chlorite plus opaques, in a glassy matrix showing patchy devitrification. Accessory zircon, apatite.

NG 126. Chocaya, surface sample at Mina Animas.

Intensely altered (sericitized) quartz-porphyry; made up of 10% rounded quartz phenocrysts, 30% patches of fine intergrown sericite-quartz plus carbonate (pseudomorphing feldspar phenocrysts), in a microgranular quartz-rich matrix flecked with sericite, clouded with clay. No tourmaline, accessory apatite, zircon.

NG 123. Chorolque, surface sample near Santa Barbara.

Intensely altered (sericitized) quartz-porphyry; made up of 20% broken quartz phenocrysts in a fine granular matrix of sericite-quartz. Original feldspar phenocryst texture largely obscured. Biotite sites partly recognizable by presence of clustered fine rutile grains. Occasional green-brown tourmaline blades, scattered opaques (pyrite), accessory apatite.

NG 279. Chorolque, surface sample near Mina Siete.

Intensely altered quartz-porphyry; made up of 15% rounded or broken quartz phenocrysts, 20% patches (to 5 mm) of sericite-tourmaline-quartz intergrowth (pseudomorphing feldspar phenocrysts), 10% patches of fine tourmaline-sericite-rutile-opaques-

quartz intergrowth (pseudomorphing biotite phenocrysts) in a granular quartz-rich matrix flecked with fine tourmaline and sericite and clouded with clay. Accessory apatite, zircon.

NG 283 and 150. Tatasi, unaltered acid volcanics.

Porphyritic-aphanitic texture; typically made up of 10% rounded quartz phenocrysts (4 mm), 10% subhedral (5 mm) plagioclase phenocrysts (oligoclase to andesine composition), occasional 5 mm sanidine phenocrysts, 10% biotite laths (3 mm) with very minor alteration of rims to Fe-oxides; in a microgranular quartz-feldspar groundmass. Accessory apatite, zircon.

NG 281. Tasna, altered quartz-porphyry dyke (surface).

Relict porphyritic texture; made up of 1 to 2% rounded 1 to 5 mm quartz phenocrysts, 20% patches of fine intergrown sericite-quartz (pseudomorphing 2 - 8 mm feldspar phenocrysts), 10% patches of fine intergrown pale tourmaline plus sericite-rutile-quartz intergrowth (pseudomorphing biotite phenocrysts); in a granular quartz-rich matrix flecked with tourmaline, sericite. Accessory zircon, apatite.

NG 99 and 139. Friable crystal tuffs, made up of angular quartz fragments, argillized feldspar and fresh biotite phenocrysts (2 - 4 mm) in an argillized matrix (no thin-sections).

B. Undated samples; whole-rock analyses reported in Chapter 2.

NG 243 and 250. Chorolque, underground samples from central quartz-tourmaline altered vent.

Granular recrystallized texture; made up of irregular quartz intergrown with coarse bladed pleochroic green-brown tourmaline. Some primary rounded quartz phenocrysts are

recognisable, overgrown with rims of secondary quartz. Original biotite sites occasionally indicated by patches of fine rutile. Accessory zircon, altered cordierite. Proportion of tourmaline to quartz varies widely, some distinct tourmaline-rich patches reflect breccia texture. Occasional lakes of clear, inclusion-free quartz intergrown with fine, almost colourless tourmaline needles.

NG 255. Chorolque, underground sample, Chimborazo adit, in vent contact region.

Intensely altered quartz-porphyry; fragmental texture; made up of broken quartz phenocrysts, patches of fine intergrown tourmaline (pseudomorphing feldspar and biotite phenocrysts), in a quartz-clay matrix. Much sulphide throughout, as disseminated grains and patches.

NG 482 and 488. Llallagua, Salvadora stock; 650 level, Siglo XX mine.

Altered quartz-porphyry; made up of quartz phenocrysts, patches of tourmaline-sericite-quartz (pseudomorphing feldspar and biotite phenocrysts), in a microgranular quartz-rich matrix flecked with sericite and tourmaline.

NG 494. Llallagua, Salvadora stock; 650 level, Siglo XX mine.

A fine fragmental rock made up of 60% angular to rounded quartz grains, occasional rounded zircon grains, in a matrix of fine pale-green matted tourmaline grains.

## Appendix 2

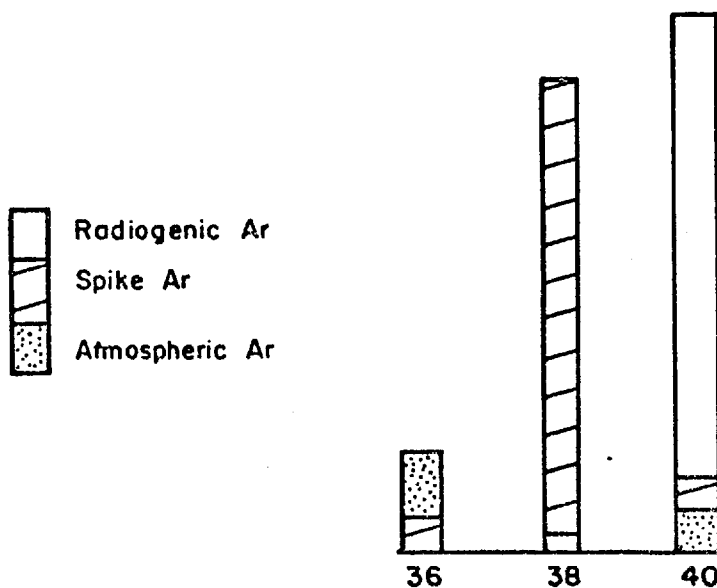
## Calculations in Potassium-Argon Dating.

A. Determination of the volume of radiogenic  $^{40}\text{Ar}$ .

In order to determine a K-Ar age, it is necessary to know the weight ratio of radiogenic  $^{40}\text{Ar}$  to  $^{40}\text{K}$  in the sample, i.e., the volume of radiogenic  $^{40}\text{Ar}$  must first be determined. In the isotope dilution method this is done using a known volume of  $^{38}\text{Ar}$  as a tracer or 'spike', then

$$\text{Vol. radiogenic } ^{40}\text{Ar} = \frac{\text{radiogenic } ^{40}\text{Ar}}{\text{spike } ^{38}\text{Ar}} \times \text{Vol. spike } ^{38}\text{Ar}$$

However, the argon isotopic spectrum measured in the mass spectrometer includes not only radiogenic and spike contributions, but also atmospheric contributions of all three argon isotopes from air which can never be totally excluded from the measuring system. Further, the spike itself is not pure  $^{38}\text{Ar}$  but contains a small proportion of the other isotopes. The mass spectrum can be represented diagrammatically as follows :



The amount of  $^{40}\text{Ar}$  in the spike is very small compared with the radiogenic and atmospheric contributions and can be ignored, except in dating very young samples, where the radiogenic component is very small. Also, the volume of atmospheric  $^{38}\text{Ar}$  is very small compared with the amount of spike  $^{38}\text{Ar}$ , and is usually ignored.

From the mass spectrum measured by the instrument, the ratios  $^{40}\text{Ar}/^{38}\text{Ar}$  (Measured) and  $^{36}\text{Ar}/^{38}\text{Ar}$  (Measured) are obtained. Using the letters M to indicate measured ratios, S for spike contributions, A for atmospheric contributions and R for radiogenic contributions, these become

$$^{40}\text{Ar}/^{38}\text{Ar} (M) = \frac{^{40}\text{Ar}(R) + ^{40}\text{Ar}(A)}{^{38}\text{Ar}(S)} \dots\dots\dots (a)$$

$$^{36}\text{Ar}/^{38}\text{Ar} (M) = \frac{^{36}\text{Ar}(A) + ^{36}\text{Ar}(S)}{^{38}\text{Ar}(S)} \dots\dots\dots (b)$$

From (a)

$$^{40}\text{Ar}(R)/^{38}\text{Ar}(S) = ^{40}\text{Ar}/^{38}\text{Ar}(M) - ^{40}\text{Ar}/^{38}\text{Ar}(S) \dots\dots\dots (c)$$

From (b)

$$^{36}\text{Ar}(A)/^{38}\text{Ar}(S) = ^{36}\text{Ar}/^{38}\text{Ar}(M) - ^{36}\text{Ar}/^{38}\text{Ar}(S) \dots\dots\dots (d)$$

The ratio  $^{36}\text{Ar}/^{38}\text{Ar}(S)$  is known and constant for a given spike and measuring system (the value used at the IGS is 0.000056), as is the ratio  $^{40}\text{Ar}/^{36}\text{Ar}(A)$  for which a value of 296 is used at the IGS. Thus

From (d)

$$^{36}\text{Ar}(A)/^{38}\text{Ar}(S) = ^{36}\text{Ar}(M)/^{38}\text{Ar}(M) - 0.000056$$

and

$$^{40}\text{Ar}(A)/^{38}\text{Ar}(S) = \left( ^{36}\text{Ar}(M)/^{38}\text{Ar}(M) - 0.000056 \right) 296.$$

Substituting in (c)

$${}^{40}\text{Ar}(\text{R})/{}^{38}\text{Ar}(\text{S}) =$$

$${}^{40}\text{Ar}/{}^{38}\text{Ar}(\text{M}) - \left( {}^{36}\text{Ar}/{}^{38}\text{Ar}(\text{M}) - 0.000056 \right) 296$$

from which the volume of radiogenic  ${}^{40}\text{Ar}$  is obtained by multiplying by the volume of spike  ${}^{38}\text{Ar}$ .

#### B. The spike system

The  ${}^{38}\text{Ar}$  tracer is contained in a sealed reservoir of constant volume. For each age determination, an aliquot of the tracer is extracted by allowing the gas first to expand into a small space between two valves (the pipette). After pressure and isotopic equilibration, the pipette is isolated from the reservoir and opened to the extraction system.

If the initial pressure in the reservoir is  $P$ , and its volume is  $V$ , after the first expansion into the pipette (of volume  $v$ ) the pressure in the reservoir will be  $P_1$

$$\text{and, } PV = P_1(V + v)$$

$$\text{so } P_1 = \frac{PV}{V + v}$$

If the gas in the pipette is pumped away and the process repeated,

$$P_1V = P_2(V + v)$$

$$P_2 = \frac{P_1V}{V + v} = \frac{PV}{V + v} \times \frac{V}{V + v} = P \left( \frac{V}{V + v} \right)^2$$

and in the general case,

$$P_n = P \left( \frac{V}{V + v} \right)^n = P \cdot K^n$$

where  $n$  is the number of extractions.

Taking logs (base e) gives

$$\begin{aligned}\log P_n &= \log P + n \cdot \log K \\ &= \log P + nK^1\end{aligned}$$

Since  $K^1 = \log \left( \frac{V}{V+v} \right)$ ,  $K^1$  must be negative, so

$$\log P_n = \log P - nK^1$$

$$\text{and } P_n = P e^{-nK^1}$$

This means that the pressure of gas in the pipette decreases exponentially with each extraction, and since the volume is constant, the actual volume of gas in each aliquot also decreases exponentially, so

$$V_n = V \cdot e^{-nK^1}$$

and  $\log V_n = \log V - nK^1$ , which is the equation of a straight line.

The system is calibrated by measuring, at regular intervals, the volume of the spike released. This is done by isotope dilution, using the known atmospheric argon content and isotope ratios of a measured volume of air. The air is introduced into the measuring system in a sealed glass capsule of known volume, which is then broken in the presence of the  $^{38}\text{Ar}$  spike aliquot. The logs of the measured spike volumes lie on a straight line whose slope and intercept can be determined by least squares analysis. The calibration procedure is normally carried out on every 20<sup>th</sup> spike aliquot. The volumes of successive spikes can be read from the graph, or calculated from the equation of the line.

#### C. Determination of $^{40}\text{K}$ .

The value taken for the atomic proportion of  $^{40}\text{K}$  in normal potassium is 0.0119 (Nier, 1950). This means that 1 gm of normal K



contains

$$\frac{0.0119 \times \text{atomic weight } ^{40}\text{K}}{\text{atomic weight normal K} \times 100}$$

$$= \frac{0.0119 \times 40}{39.096 \times 40} = 1.2175 \times 10^{-4}$$

1% K is equivalent to  $10^{-2}$  gm K/gm sample and will be equivalent to  $1.2175 \times 10^{-6}$  gm  $^{40}\text{K}$ /gm sample, i.e., 1.2175 ppm. Thus  $1.2175 \times \%K$  gives the ppm  $^{40}\text{K}$  directly.

#### D. Calculation of the ratio $^{40}\text{Ar}_{\text{radiogenic}}/^{40}\text{K}$

The conversion of the measured volume of  $^{40}\text{Ar}_{\text{radiogenic}}$  to weight is as follows :

1 gm. atomic weight of any gas occupies 22.4 litres (at standard temperature and pressure).

$$\text{i.e., } 40 \text{ gm } ^{40}\text{Ar occupies } 22.4 \times 10^9 \text{ nl and } 1 \text{ nl. } ^{40}\text{Ar weighs}$$

$$\frac{40}{22.4} \times 10^{-9} \text{ gm.}$$

$$= 1.785 \cdot 10^{-9} \text{ gm}$$

Using the ratio for the weight of  $^{40}\text{K}$  per unit weight of normal K derived above, the ratio  $^{40}\text{Ar}_{\text{radiogenic}}/^{40}\text{K}$  is :

$$\frac{\text{Vol } ^{40}\text{Ar(R) in nl/gm} \times 1.785 \cdot 10^{-9}}{\%K \times 1.217 \times 10^{-6}}$$

$$= 1.466 \times 10^{-3} \times \frac{\text{Vol } ^{40}\text{Ar}_{\text{radiogenic}} \text{ (nl/gm)}}{\%K}$$

This can then be applied to the age equation (see Chapter 5), and using the known decay constants gives the age  $t$ , in years  $\times 10^6$

$$= 1885.4 \ln \left[ 1 + 9082 \left( 1.466 \times 10^{-3} \cdot \frac{\text{Vol } ^{40}\text{Ar(R) in nl/gm}}{\%K} \right) \right]$$

#### E. Errors.

The error on a K-Ar age can be determined by combining the errors on the separate K and  $^{40}\text{Ar}$  determinations. For young samples such as those considered here, the error on the age is

given by the square root of the sum of the squares of the separate errors.

1. Errors in the argon determination.

Errors are enhanced when a subtraction is involved, and this is a particular problem in the error on the argon determination, since the radiogenic argon is approximately the difference between the total argon and the atmospheric argon.

The volume of radiogenic argon is equal to

$$\text{Vol. } ^{38}\text{Ar in spike} \times \text{the expression } R \text{ where } R \text{ is}$$

$$\left[ \frac{^{40}\text{Ar}}{^{38}\text{Ar}}(\text{M}) - 296 \left( \frac{^{36}\text{Ar}}{^{38}\text{Ar}}(\text{M}) - \frac{^{36}\text{Ar}}{^{38}\text{Ar}}(\text{S}) \right) \right]$$

(see Appendix 2 section A above).

If  $a$  is the % error on  $R$  and  $b$  is the % error on the spike  $^{38}\text{Ar}$  volume, the error on the  $^{40}\text{Ar}$  radiogenic volume =  $\sqrt{a^2 + b^2}$

The error on the spike is derived from repeated calibrations (in this case a value of  $\pm 1\%$  is used). The error on the expression  $R$  is made up of the combined errors on the ratios in the expression. Of these, the errors on  $\frac{^{40}\text{Ar}}{^{36}\text{Ar}}(\text{A})$  and  $\frac{^{36}\text{Ar}}{^{38}\text{Ar}}(\text{S})$  can be ignored as the ratios are constants, essentially without errors. Error magnification in the subtraction  $\frac{^{36}\text{Ar}}{^{38}\text{Ar}}(\text{M}) - \frac{^{36}\text{Ar}}{^{38}\text{Ar}}(\text{S})$  is small as the error on  $\frac{^{36}\text{Ar}}{^{38}\text{Ar}}(\text{S})$  is very small. However, the product  $296 \left( \frac{^{36}\text{Ar}}{^{38}\text{Ar}}(\text{M}) - \frac{^{36}\text{Ar}}{^{38}\text{Ar}}(\text{S}) \right)$  is directly proportional to the volume of contaminating atmospheric  $^{40}\text{Ar}$ , and significant error magnification can take place in the subtraction of this from the  $\frac{^{40}\text{Ar}}{^{38}\text{Ar}}(\text{M})$ , since the numbers are of similar magnitude. If  $\frac{^{40}\text{Ar}}{^{38}\text{Ar}}(\text{M}) = T$  and  $296 \left( \frac{^{36}\text{Ar}}{^{38}\text{Ar}}(\text{M}) - \frac{^{36}\text{Ar}}{^{38}\text{Ar}}(\text{S}) \right) = A$  a general equation can be derived giving the percentage error on  $R$  :

$$\% \text{ error on } R = \frac{\sqrt{\left(x^2 + \left(\frac{A}{T}\right)^2 y^2\right)}}{1 - \frac{A}{T}}$$

where  $x$  is the % error on  $T$ , and  $y$  is the % error on  $A$  (Snelling, pers.comm.). The most important aspect of this is that as the proportion of atmospheric contamination ( $A$ ) increases, the denominator of the equation approaches 0 and the error approaches infinity. Thus, in order to minimise the error the operator must minimise the amount of atmospheric argon in the measuring system.

In the present investigation the mean values of  $x$  and  $y$  (in 56 age determinations) were  $\pm 0.08$  and  $\pm 0.51$  respectively, and  $A/T$  varies from 0.14 to 0.84, giving a range of  $R$  from  $\pm 0.125\%$  to  $\pm 2.724\%$ . By adopting  $\pm 1\%$  as the error on the potassium determinations and  $\pm 1\%$  as the error on the spike volume (see below) this gives an error range on the age determinations of from  $\pm 1.4\%$  to  $\pm 3.1\%$ .

The validity of this method of determining the error on the argon analyses can be checked by using the pooled standard deviation of the numerous duplicate analyses which were carried out.

The pooled standard deviation of a set of duplicate analyses is determined as follows (Bennett and Franklin, 1954)

$$\text{The pooled variance } S^2 = \frac{\sum(\text{differences}^2)}{2K}$$

where  $K$  = the number of pairs of analyses.

The pooled standard deviation is the square root of this, and the 95% confidence limits are given by  $\pm t_k \cdot \frac{S}{\sqrt{2}}$

where  $t$  is the  $t$ -value appropriate to  $K$ .

A total of seventeen samples were analysed for  $^{40}\text{Ar}_{\text{rad}}$  in duplicate. Ten biotite samples gave  $^{40}\text{Ar}_{\text{rad}}$  contents ranging

from 3.02 nl/gm to 6.11 nl/gm, mean 4.55 nl/gm. The pooled standard deviation is 0.1075 nl/gm or 2.36% of the mean. Seven whole rock samples gave  $^{40}\text{Ar}_{\text{rad}}$  ranging from 1.23 nl/gm to 2.77 nl/gm, mean 2.02 nl/gm. The pooled standard deviation is 0.0373 nl/gm or 1.84% of the mean. Adopting a standard error on the duplicated argon determinations of  $\pm 2.5\%$  and on potassium determinations of  $\pm 1\%$  gives an error on the age of  $\pm 2.7\%$ , which is in agreement with the range of errors obtained by combining the error on R, the spike volume and the potassium analysis. This indicates that the latter method is indeed valid.

## 2. Errors in the potassium determination.

The error in the K determination can be estimated from repeated analyses of standard samples. In the present study, the errors on the ages were determined using a value of  $\pm 1\%$  for the error on K. A total of 19 separate determinations were made by the writer on the Bern 4M muscovite standard which has a recommended value of 8.70%K. The mean of the 19 determinations was 8.703%K, standard deviation 0.097, i.e., a one standard deviation error of  $\pm 1.1\%$ .

Individual age determinations were made using duplicate K analyses. The large number of pairs can be used to determine a pooled standard deviation and 95% confidence limits. The samples have been divided into two groups. The biotites (26 samples), give a pooled standard deviation of 0.056%. Their average potassium value is 6.62% giving an error of  $\pm 0.85\%$ . The whole rock and sericite samples (13) give a pooled standard deviation of 0.033%. Their average potassium value is 3.46%, giving an error of  $\pm 0.95\%$ . This confirms the validity

of using a value of  $\pm 1\%$  as the error on the K determinations.

3. Error in the spike volume.

This is derived from the repeated calibrations, which are usually made on every 20<sup>th</sup> spike aliquot. The records indicate an error of  $\pm 1\%$  for the IGS argon measuring system, and this value was used in all calculations.

## REFERENCES

- Ahlfeld, F., 1967, Metallogenetic epochs and provinces of Bolivia: Mineralium Deposita, v. 2, p. 291 - 311.
- Ahlfeld, F., 1972, Geologia de Bolivia: Encyclopedia Boliviana, Eds. Los Amigos del Libro, Cochabamba, Bolivia.
- Ahlfeld, F., and Branisa, L., 1960, Geologia de Bolivia: Inst. Boliv. Petrol., La Paz, 240 p.
- Ahlfeld, F., and Schneider-Scherbina, A., 1964, Los yacimientos minerales y de hidrocarburos de Bolivia: Dep. Nacional de Geol., La Paz, Boletin 5, 388 p.
- Aldrich, L.T., Davis, G.L., and James, H.L., 1965, Ages of minerals from metamorphic and igneous rocks near Iron Mountain, Michigan: Jour. Petrology, v. 6, p. 445 - 472.
- Angellini, V., Fernandez Lima, J.C., Herrera, A., and Aristarian, L., 1970, Descripcion del mapa metalogenetico de la Republica Argentina: Minerales metaliferos: Dir. Nac. Geol. Min., Anales 15, Buenos Aires, 172 p.
- Audebaud, E., Laubacher, G., and Marocco, R., 1976, Coupe geologique des Andes du sud du Perou de l'Ocean Pacifique au bouclier Bresilien: Geol. Rundschau, v. 65, p. 223 - 264.

Avila, W., 1975, Un modelo de tectonica de placas para el origen del cinturón estanífero boliviano: Soc. Geol. Boliv. Bol. No. 21.

Baker, I., Gale, N.H., and Simons, J., 1967, Geochronology of the St. Helena volcanoes: Nature, Lond., v. 215, p. 1451 - 1456.

Barnes, H.L., 1975, Zoning of ore deposits: types and causes: Roy. Soc. Edinburgh Trans., v. 69, p. 295 - 311.

Barsukov, V.L., and Kuril'chikova, G., 1966, On the forms in which tin is transported in the hydrothermal solutions: Geochem. Int., v. 3, p. 759 - 764.

Barsukov, V.L., and Ryabchikov, I.D., 1977, Physical - chemical factors of migration and concentration of metals: in, Metallization Associated With Acid Magmatism, v. 2, Geol. Surv., Prague, p. 99 - 104.

Barth, T.F.W., 1952, Theoretical petrology: New York, John Wiley.

Barton, P.B., and Skinner, B.J., 1967, Sulphide mineral stabilities: in, Barnes, H.L., ed., Geochemistry of hydrothermal ore deposits: New York, Holt, Rinehart, and Winston, p. 238 - 333.

Bennett, C.A., and Franklin, N.L., 1954, Statistical analysis in chemistry and the chemical industry: New York, John Wiley,

- Berry, E.W., 1937, The fossil flora of Potosi, Bolivia: The John Hopkins Univ., Studies in geology No. 13, p. 6 - 67.
- Bigeleisen, J., Perlman, M.L., and Prosser, H.C., 1952, Conversion of hydrogenic materials to hydrogen for isotopic analysis: *Analyt. Chem.*, v. 24, p. 1356.
- Bignell, J.D., and Snelling, N.J., 1977, Geochronology of Malayan granites: *Inst. of Geol. Sciences, Overseas geology and mineral resources No. 47*, London, H.M. Stationery Office.
- Bostrom, K., Joensuu, O. and Fisher, D.E., 1969, Aluminium-poor ferromanganoan sediments on active oceanic ridges: *Jour. Geophys. Res.*, v. 74, p. 3261 - 3270.
- Brooks, R., Horton, A.T., and Torgesen, U.C., 1968, Occlusions of mother liquor in solution-grown crystals: *Jour. Crystal Growth*, v. 2, p. 279 - 283.
- Brown, G.C., 1977, Mantle origin of Cordilleran granites: *Nature, Lond.*, v. 265, p. 21 - 24.
- Bryant, D.G., 1968, Intrusive breccias associated with ore, Warren (Bisbee) mining district, Arizona: *Econ. Geol.*, v. 63, p. 1 - 12.
- Bryner, L., 1968, Proposed terminology for hydrothermal breccias and conglomerates: *Econ. Geol.*, v. 63, p. 692 - 693.
- Buckley, H.E., 1951, *Crystal growth*: New York, John Wiley.



- Buddington, A.F., 1935, High-temperature mineral associations at shallow to moderate depths: *Econ. Geol.*, v. 30, p. 205 - 222.
- Burnham, C.W., 1962, Facies and types of hydrothermal alteration: *Econ. Geol.*, v. 57, p. 768 - 784.
- Campbell, D.F., 1942, The Oruro silver-tin district, Bolivia: *Econ. Geol.*, v. 37, p. 87 - 115.
- Camus, F., 1975, Geology of the El Teniente ore body with emphasis on wall-rock alteration: *Econ. Geol.*, v. 70, p. 1341 - 1372.
- Cann, J.R., 1970, Upward movement of granite magma: *Geol. Mag.*, v. 107, p. 335 - 340.
- Chappel, B.W., and White, A.J.R., 1974, Two contrasting granite types: *Pac. Geol.*, v. 8, p. 173 - 174.
- Chase, F.M., 1948, Tin-silver veins of Oruro, Bolivia: *Econ. Geol.*, v. 43, p. 333 - 383, 435 - 470.
- Clark, A.H., and Farrar, E., 1973, The Bolivian tin province; notes on the available geochronological data: *Econ. Geol.*, v. 68, p. 102 - 106.
- Clark, A.H., Farrar, E., Caelles, J.C., Haynes, S.J., Lortie, R.B., Mc Bride, S.L., Quirt, G.S., Robertson, R.C.R., and Zentilli, M.,

- 1976, Longitudinal variations in the metallogenetic evolution of the central Andes: A progress report: in, Strong, D.F., ed., *Metallogeny and Plate Tectonics*; Geol. Assoc. Canada Sp. Paper No. 14, p. 22 - 58.
- Clayton, R.N., and Mayeda, T.K., 1963, The use of bromine pentafluoride in the extraction of oxygen from oxides and silicates for isotopic analysis: *Geochim. Cosmochim. Acta*, v. 27, p. 43 - 53.
- Cobbing, E.J., and Pitcher, W.S., 1972a, Plate tectonics and the Peruvian Andes: *Nature, Lond.*, v. 240, p. 51 - 53.
- Cobbing, E.J., and Pitcher, W.S., 1972b, The coastal batholith of central Peru: *Jour. Geol. Soc. Lond.*, v. 128, p. 421 - 460.
- Cordani, U., 1967, Unpublished letter in library of the Servicio Geologico de Bolivia, La Paz.
- Coveney, R.M., and Kelly, W.C., 1971, Dawsonite as a daughter mineral in hydrothermal fluid inclusions: *Contr. Mineral. and Petrol.*, v. 32, p. 334 - 342.
- Creasy, S.C., 1959, Some phase relations in hydrothermally altered rock of porphyry copper deposits: *Econ. Geol.*, v. 54, p. 351 - 373.
- Crerar, D.A., and Barnes, H.L., 1976, Ore solution chemistry, V. Solubilities of chalcopyrite and chalcocite assemblages in

hydrothermal solutions at 200° to 350°C: *Econ. Geol.*,  
v. 71, p. 772 - 794.

Cronan, D.S., 1976, Basal metalliferous sediments from the  
eastern Pacific: *Geol. Soc. America Bull.*, v. 87, p. 928 -  
934.

Dalrymple, G.B., and Lanphere, M.A., 1969, Potassium-argon dating:  
San Fransico, Freeman and Co., 258 p.

Damon, P.E., and Kulp, J.L., 1958, Excess helium and argon in  
beryl and other minerals: *Am. Min.*, v. 43, p. 433 - 459.

Deicha, G., 1955, Les lacunes des cristaux et leurs inclusions  
fluides; signification dans la genèse des gîtes minéraux  
et des roches: Paris, Masson et Cie.

Deicha, G., and Sella, C., 1962, Lacunes de cristallisation et  
structure mosaïque du chlorure de sodium étudiées par  
microscope électronique: *Acad. Sci. Comptes rendus*, v. 255,  
p. 975 - 977.

Dewey, J.F., and Bird, J.M., 1970, Mountain belts and the new  
global tectonics: *Jour. Geophys. Res.*, v. 75, p. 2625 - 2647.

Dickinson, W.R., 1970, Relations of andesites, granites, and  
derivative sandstones to arc-trench tectonics: *Rev. Geophys.*  
*Space Phys.*, v, 8, p. 813 - 860.

- Dickinson, W.R., and Hatherton, T., 1967, Andesitic volcanism and seismicity around the Pacific: *Science*, v. 157, p. 801 - 803.
- Eadington, P.J., 1974, Microprobe analysis of the non-volatile constituents in fluid inclusions: *N.Jb. Miner. Mh.*, v. 11, p. 518 - 525.
- Ellis, A.J., 1967, The chemistry of some explored geothermal systems: in, Barnes, H.L., ed., *Geochemistry of hydrothermal ore deposits*: New York, Holt, Rinehart, and Winston, p. 465 - 514.
- Epstein, S., and Mayeda, T., 1953, Variation in  $^{18}\text{O}$  content of waters from natural sources. *Geochim. Cosmochim. Acta*, v. 4, p. 213 - 224.
- Eremin, N., 1975, Quantitative analysis by means of the laser microanalyser LMA-1: *Min. Mag.*, v. 40, p. 312 - 314.
- Evans, D.L., 1940, Structure and mineral zoning of the Pailaviri section, Potosi, Bolivia: *Econ. Geol.*, v. 35, p. 737 - 750.
- Evernden, J.F., 1961, Edades absolutas de algunas rocas igneas en Bolivia por el metodo potasio-argon: *Soc. geol. Boliviana*, Not. No. 2, p. 3.
- Evernden, J.F., Kriz, S.J., Cherroni, C., 1977, Potassium-argon ages of some Bolivian rocks: *Econ. Geol.*, v. 72, p. 1042 - 1061.

- Farrar, E., Clark, A.H., Haynes, S.J., Quirt, G.S., Conn, H., and Zentilli, M., 1970, K-Ar evidence for the post-Palaeozoic migration of granitic intrusion foci in the Andes of northern Chile: *Earth Planet. Sci. Lett.*, v. 10, p. 60 - 66.
- Fisher, J.R., 1976, The volumetric properties of H<sub>2</sub>O, a graphical portrayal: *Jour. Research U.S. Geol. Survey*, v. 4, No. 2, p. 180 - 193.
- Floyd, P.A., 1972, Geochemistry, origin and tectonic environment of the basic and acidic rocks of Cornubia, England: *Proc. Geologists Assoc.*, v. 83, p. 385 - 404.
- Fournier, R.O., 1972, The importance of depth of crystallization on the character of magmatic fluids: in, 24th Int. geol. Congr. (Montreal), pt. 10, p. 214 (Abstract).
- Fyles, J.T., Harakal, J.E., and White, W.H., 1973, The age of sulphide mineralization at Rossland, British Columbia: *Econ. Geol.*, v. 68, p. 23 - 33.
- Gansser, A., 1973, Facts and theories on the Andes: *Jour. Geol. Soc. Lond.*, v. 129, p. 93 - 131.
- Gordon, S.G., 1944, The mineralogy of the tin mines of the Cerro de Llallagua, Bolivia: *Acad. Nat. Sci. Philadelphia Proc.*, v. 96, p. 279 - 359.

- Gough, D.I., 1973, Dynamic uplift of Andean mountains and island arcs: *Nature, Lond.*, v. 242, p. 39 - 41.
- Grant, J.N., and Neilsen, R.L., 1975, Geology and geochronology of the Yandera porphyry copper deposit, Papua New Guinea: *Econ. Geol.* v. 70, p. 1157 - 1174.
- Green, T.H., 1972, Crystallization of calc-alkaline andesite under controlled high-pressure conditions: *Contrib. Mineral. Petrol.*, v. 34, p. 150 - 166.
- Green, T.H., and Ringwood, A.E., 1968, Genesis of the calc-alkaline rock suite: *Contrib. Mineral. Petrol.*, v. 18, p. 105 - 162.
- Green, T.H., and Ringwood, A.E., 1972, Crystallization of garnet-bearing rhyodacite under high pressure hydrous conditions: *Jour. Geol. Soc. Australia*, v. 19, p. 203 - 212.
- Groves, D.I., 1972, The geochemical evolution of tin-bearing granites in the Blue Tier batholith, Tasmania: *Econ. Geol.*, v. 67, p. 445 - 457.
- Groves, D.I., and Mc Carthy, T.S., 1978, Fractional crystallization and the origin of tin deposits: *Mineralium Deposita*, v. 13, p. 11 - 26.
- Gustafson, L.B., and Hunt, J.P., 1975, The porphyry copper deposit at El Salvador, Chile: *Econ. Geol.*, v. 70, p. 857 - 912.

- Haas, J.L., 1971, The effect of salinity on the maximum thermal gradient of a hydrothermal system at hydrostatic pressure: *Econ. Geol.*, v. 66, p. 940 - 946.
- Hanson, G.N., and Gast, P.W., 1967, Kinetic studies in contact metamorphic zones: *Geochim. et Cosmochim. Acta*, v. 31, 1119 - 1153.
- Hart, S.R., 1964, The petrology and isotopic-mineral age relations of a contact zone in the Front Range, Colorado: *Jour. Geol.*, v. 72, p. 493 - 525.
- Helgeson, H.C., 1970, A chemical and thermodynamic model of ore deposition in hydrothermal systems: *Mineralog. Soc. America Spec. Paper* 3, p. 155 - 186.
- Hemley, J.J., and Jones, W.R., 1964, Chemical aspects of hydrothermal alteration with emphasis on hydrogen metasomatism: *Econ. Geol.*, v. 59, p. 538 - 569.
- Henley, R.W., 1973, Some fluid dynamics and ore genesis: *Trans. Inst. Min. Metall. (Sect. B)*, v. 82, p. B1 - B7.
- Henley, R.W., and Mc Nabb, A., 1978, Magmatic vapor plumes and ground-water interaction in porphyry copper emplacement: *Econ. Geol.*, v. 73, p. 1 - 20.
- Herron, E.M., 1972, Sea-floor spreading and the Cenozoic history of the east-central Pacific: *Geol. Soc. America Bull.*, v. 83, p. 1671 - 1692.

- Hesp, W.R., and Rigby, D., 1971, The transport of tin in acid igneous rocks: *Pac. Geol.*, v. 4, p. 135 - 152.
- Hesp, W. R., and Varlamoff, N., 1977, Temporal and spatial relations between the formation of acid magmatic rocks and deposits: in, *Metallization Associated With Acid Magmatism*, v. 2, *Geol. Surv.*, Prague, p. 23 - 40.
- Hoefs, J., 1973, *Stable isotope geochemistry*: New York, Springer - Verlag, 140 p.
- Holland, H.D., 1965, Some applications of thermochemical data to problems of ore deposits, II. Mineral assemblages and the composition of ore-forming fluids: *Econ. Geol.*, v. 60, p. 1101 - 1166.
- Holland, H.D., 1967, Gangue minerals in hydrothermal deposits: in, Barnes, H.L., ed., *Geochemistry of hydrothermal ore deposits*: New York, Holt, Rinehard, and Winston, p. 382 - 436.
- Holland, H.D., 1972, Granites, solutions and base metal deposits: *Econ. Geol.*, v. 67, p. 281 - 301.
- Howell, F.H., and Molloy, J.S., 1960, Geology of the Braden ore body, Chile, South America: *Econ. Geol.*, v. 55, p. 863 - 905.
- Hunter, D.R., 1976, Some enigmas of the Bushveld complex: *Econ. Geol.*, v. 71, p. 229 - 248.



- Hurd, N.J., 1976, The role of fluorine and chlorine in late-stage magmatic processes: an experimental study: Min. Soc. London, General Meeting, June, 1976 (unpublished).
- Ineson, P.R., and Mitchell, J.G., 1972, Isotopic age determinations on clay minerals from lavas and tuffs of the Derbyshire orefield: Geol. Mag., v. 109, p. 501 - 512.
- Ineson, P.R., and Mitchell, J.G., 1974, K-Ar isotopic age determinations from some Scottish mineral localities: Trans. Inst. Min. Metall. (Sect. B), v. 83, p. B13 - B18.
- Irvine, T.N., and Baragar, W.R.A., 1971, A guide to the chemical classification of the common volcanic rocks: Canadian Jour. Earth Sci., v. 8, p. 523 - 548.
- Ishihara, S., 1977, The magnetite series and ilmenite series granitic rocks: Mining Geology, v. 27, p. 293 - 305.
- Jackson, N.J., Moore, J.McM., and Rankin, A.H., 1977, Fluid inclusions and mineralization at Cligga Head, Cornwall, England: Jour. Geol. Soc. Lond., v. 134, p. 343 - 350.
- Jakeš, P., and White, A.J.R., 1971, Composition of island arcs and continental growth: Earth Planetary Sci. Letters, v. 12, p. 224 - 230.
- Jakeš, P. and White, A.J.R., 1972, Major and trace element abundances in volcanic rocks of orogenic areas: Geol. Soc.

America Bull. v. 83, p. 29 - 40.

James, D.E., 1971a, Andean crustal and upper mantle structure:

Jour. Geophys. Research, v. 76, p. 3246 - 3271.

James, D.E., 1971b, Plate tectonic model for the evolution of

the Central Andes: Geol. Soc. America Bull., v. 82, p.

3325 - 3346.

Jaskolski, S., 1933, Les gisements argento-stannifères de Potosí

en Bolivie: Soc. Sci. Varsovie Archives Mineralogie, v. 11,

p. 24 - 102.

Jenks, W.F., and Harris, E.G., 1953, Plutonics near Arequipa as

a petrologic sample of the coastal batholith of Peru: Bol.

Soc. Geol. Peru, Lima, v. 26, p. 79 - 94.

Jensen, M.L., 1971, Provenance of cordilleran intrusives and

associated metals: Econ. Geol., v. 66, p. 34 - 42.

Johnston, W.P., and Lowell, J.D., 1961, Geology and origin of

mineralized breccia pipes in Copper Basin, Arizona: Econ.

Geol., v. 56, p. 916 - 940.

Keevil, N.B., 1942, Vapour pressures of aqueous solutions at high

temperatures: Jour. Am. Chem. Soc., v. 64, p. 841 - 850.

Kelly, W.C., and Turneure, F.S., 1970, Mineralogy, paragenesis and geothermometry of the tin and tungsten deposits of the eastern Andes: *Econ. Geol.*, v. 65, p. 609 -680.

Kennedy, G.C., 1950a, "Pneumatolysis" and the liquid inclusion method of geologic thermometry: *Econ. Geol.*, v. 45, p. 533 - 547.

Kennedy, G.C., 1950b, Pressure-volume-temperature relations in water at elevated temperatures and pressures: *Am. Jour. Sci.*, v. 248, p. 540 - 564.

Kennedy, G.C., 1954, Pressure-volume-temperature relations in  $\text{CO}_2$  at elevated temperatures and pressures: *Am. Jour. Sci.*, v. 260, p. 115 -141.

Khitarov, N.I., 1958, Phase equilibria in the system  $\text{H}_2\text{O} - \text{CO}_2$ : *Geochem. Int.*, v. 7, p. 846 - 848.

Koslowski, R., and Jaskolski, S., 1932, Les gisements argento-stannifères d'Oruro en Bolivie: *Soc. Sci. Varsovie Archives Mineralogie*, v. 8, p. 1 - 121.

Krauskopf, K.B., 1967, *Introduction to geochemistry*: New York, Mc Graw-Hill Book Company.

Lacy, W.C., 1958, Porphyry copper deposit, Cuajone, Peru: *Mining Engineering*, v. 10, p. 104 - 107.

- Landis, G.P., and Rye, R.O., 1974, Geologic, fluid inclusion and stable isotope studies of the Pasto Bueno tungsten-base metal ore deposit, northern Peru. *Econ. Geol.*, v. 69, p. 1025 - 1059.
- Larson, R.L., and Pitman, W.C., 1972, World-wide correlation of Mesozoic magnetic anomalies, and its implications: *Geol. Soc. America Bull.*, v. 83, p. 3645 - 3662.
- Lancelot, J.R., Laubacher, G., Marocco, R., and Renaud, J., 1976, U/Pb radiochronology of two granitic plutons from the eastern cordillera (Peru)- extent of Permian magmatic activity and consequences: Montpellier, Centre Geologique et Geophysique, Contribution No. 222, 5 p.
- Le Bel, L., 1976, Note preliminaire sur la mineralogie des phases solides contenus dans les inclusions des phenocristaux de quartz du porphyre cuprifere de Cerro Verde/Santa Rosa, Perou meridional: Universite de Lausanne, Laboratoires de geologie, mineralogie, geophysique et du musee geologique; Bulletin No. 220, p. 201 - 208.
- Lemmlein, G.G., and Klevtsov, P.V., 1961, Relations among the principal thermodynamic parameters in a part of the system  $H_2O - NaCl$ : *Geochemistry*, No. 2, p.148 - 158.
- Lindgren, W., 1933, *Mineral deposits* (4<sup>th</sup> edition): New York, Mc Graw - Hill Book Company.

- Lindgren, W., and Abbott, A.C., 1931, The silver-tin deposits of Oruro, Bolivia: *Econ. Geol.* v. 26, p. 453 - 479.
- Lindgren, W., and Creveling, J.G., 1928, The ores of Potosí, Bolivia: *Econ. Geol.*, v. 23, p. 233 - 262.
- Little, W.M., 1960, Inclusions in cassiterite and associated minerals: *Econ. Geol.*, v. 55, p. 485 - 509.
- Llambías, E.J., and Malvicini, L., 1969, The geology and genesis of the Bi-Cu mineralized breccia pipe, San Francisco de los Andes, San Juan, Argentina: *Econ. Geol.*, v. 64, p. 271 - 286.
- Locke, A., 1926, The formation of certain ore bodies by mineralization stoping: *Econ. Geol.*, v. 21, p. 431 - 453.
- Lowell, J.D., and Guilbert, J.M., 1970, Lateral and vertical alteration-mineralization zoning in porphyry ore deposits: *Econ. Geol.*, v. 65, p. 373 - 408.
- Malinin, S.D., 1959, The system water-carbon dioxide at high temperatures and pressures: *Geochem. Int.*, v. 3, p. 292 -306.
- Mc Culloch, D.S., 1959, Vacuole disappearance temperatures of laboratory-grown hopper halite crystals: *Jour. Geophys. Res.*, v. 64, p. 849 - 854.
- Mc Intyre, D.B., 1963, Precision and resolution in geochronometry: in, Albritton, C.C., ed., *The fabric of geology*; Reading,

- Mass., Addison-Wesley, p. 112 - 134.
- Megard, F., Dalmayrac, B., Laubacher, G., Marocco, R., Martinez, C., Paredes, J., and Tomasi, P., 1971, La chaîne Herciniennne au Pérou et en Bolivie: premiers résultats: Cah. OSTROM, sér. Geol. III, v. 1, p. 5 - 44.
- Metzger, F.W., Kelly, W.C., Nesbitt, B.E., and Essene, E.J., 1977, Scanning electron microscopy of daughter minerals in fluid inclusions: Econ. Geol., v. 72, p. 141 - 152.
- Meyer, C., and Hemley, J.J., 1967, Wall-rock alteration: in, Barnes, H.L., ed., Geochemistry of hydrothermal ore deposits: New York, Holt, Rinehart, and Winston, p. 166 - 235.
- Mills, J.W., 1972, Origin of copper-bearing breccia pipes: Econ. Geol., v. 67, p. 533 - 535.
- Mitcham, T.W., 1974, Origin of breccia pipes: Econ. Geol., v. 69, p. 412 - 413.
- Mitchell, A.H., and Bell, J.D., 1973, Island-arc evolution and related mineral deposits: Jour. Geol., v. 81, p. 381 - 405.
- Mitchell, A.H., and Garson, M.S., 1976, Mineralization at plate boundaries: Minerals Sci. Engng., v. 8, p. 126 - 169.
- Moenke, L., and Moenke, H., 1968, Laser microspectrochemical analysis (in German): English translation 1973, London,

Adam Hilger Ltd.

- Moore, W.J., Lanphere, M.A., and Obradovich, J.D., 1968, Chronology of intrusion, volcanism, and ore deposition at Bingham, Utah: *Econ. Geol.*, v. 63, p. 612 - 621.
- Moore, W.J., and Nash, T.J., 1974, Alteration and fluid inclusion studies of the porphyry copper ore body at Bingham, Utah: *Econ. Geol.*, v. 69, p. 631 - 645.
- Mon, R., 1976, The structure of the eastern border of the Andes in northwestern Argentina: *Geol. Rundschau*, v. 65, No. 1.
- Myashiro, A., 1974, Volcanic rock series in island arcs and active continental margins: *Am. Jour. Sci.*, v. 274, p. 321 - 355.
- Nash, J.T., and Cunningham, C.G., 1974, Fluid inclusion studies of the porphyry copper deposit at Bagdad, Arizona: *U.S. Geol. Survey Jour. Research*, v. 2, p. 31 - 34.
- Nash, J.T., and Theodore, T.G., 1971, Ore-fluids in the porphyry copper deposit at Copper Canyon, Nevada: *Econ. Geol.*, v. 66, p. 385 - 399.
- Nier, A.O., 1950, A redetermination of the relative abundances of the isotopes of carbon, nitrogen, oxygen, argon, and potassium: *Phys. Rev.*, v. 77, p. 789 - 793.

- Noble, D.C., Mc Kee, E.H., Farrar, E., and Petersen, V., 1974, Episodic Cenozoic volcanism and tectonism in the Andes of Peru: *Earth Planet. Sci. Lett.*, v. 21, p. 213 - 220.
- Norton, D.L., and Cathles, L.M., 1973, Breccia pipes - products of exolved vapour from magma: *Econ. Geol.*, v. 68, p. 540 - 546.
- Ocola, L.C., Meyer, R.P., and Aldrich, L.T., 1971, Gross crustal structure under Peru - Bolivia altiplano: *Earthquake Notes, Seis. Soc. America*, v. 42, p. 3 - 4.
- O'Neill, J.R., and Chappell, B.W., 1977, Oxygen and hydrogen isotope relations in the Berridale batholith: *Jour. Geol. Soc. Lond.*, v. 133, p. 559 - 572.
- Park, C.F., and MacDiarmid, R.A., 1964, *Ore deposits (1st edition): San Francisco, Freeman and Co., 475 p.*
- Petersen, U., 1965, Regional geology and major ore deposits of central Peru: *Econ. Geol.*, v. 60, p. 407 - 476.
- Phillips, W.J., 1973, Mechanical effects of retrograde boiling and its probable importance in the formation of some porphyry ore deposits: *Trans. Inst. Min. Metall. (Sec. B)*, v. 82, p. B90 - 98.
- Pitcher, W.S., 1978, The anatomy of a batholith: *Jour. Geol. Soc. Lond.*, v. 135, p. 157 - 182.



- Potter, R.W., 1977, Pressure corrections for fluid inclusion homogenization temperatures based on the volumetric properties of the system NaCl - H<sub>2</sub>O: Jour. Research U.S. Geol. Surv., v. 5, p. 603 - 607.
- Poty, B., Leroy, J., and Jachimowicz, L., 1976, Un nouvel appareil pour la mesure des températures sous le microscope: l'installation de microthermométrie Chaixmeca: Bull. Soc. fr. Mineral. Cristallog., v. 99, p. 182 - 186.
- Presnall, D.C., and Bateman, P.C., 1973, Fusion relations in the system NaAlSiO<sub>8</sub> - CaAl<sub>2</sub>Si<sub>2</sub>O<sub>8</sub> - KAlSi<sub>3</sub>O<sub>8</sub> - SiO<sub>2</sub> - H<sub>2</sub>O and generation of granite magmas in the Sierra Nevada batholith: Geol. Soc. America Bull., v. 84, p. 3181 - 3202.
- Radelli, L., 1966, New data on tectonics of Bolivian Andes from a photograph by Gemini 5, and field knowledges: Trav. Lab. Geol. Grenoble, v. 42, p. 237 - 261.
- Richard, K., and Courtright, J.H., 1958, Geology of Toquepala, Peru: Mining Eng., v. 10, p. 262 - 266.
- Ringwood, A.E., 1974, The petrological evolution of island-arc systems: Jour. Geol. Soc. Lond., v. 130, p. 183 - 204.
- Roberts, M., 1901, Chorolque tin mines and alluvial deposits: Trans. Inst. Min. Metall., v. 9, p. 373 - 376.

- Robertson, R., 1974, Notas sobre el metodo del K-Ar de datacion de rocas e interpretacion de edades obtenidas hasta ahora: Inf. Prelim., Proy. Plutonismo, Geobol, La Paz (Unpublished).
- Roedder, E., 1958, Technique for the extraction and partial chemical analysis of fluid-filled inclusions from minerals: Econ. Geol., v. 53, p. 235 - 269.
- Roedder, E., 1962, Studies of fluid inclusions, I: Low temperature application of a dual-purpose freezing and heating stage: Econ. Geol., v. 57, p. 1045 - 1061.
- Roedder, E., 1963, Studies of fluid inclusions, II: Freezing data and their interpretation: Econ. Geol., v. 58, p. 167 - 211.
- Roedder, E., 1967, Fluid inclusions as samples of ore fluids: in, Barnes, H.L., ed., Geochemistry of hydrothermal ore deposits: New York, Holt, Rinehart and Winston, p. 515 - 574.
- Roedder, E., ed., 1968, 1969, 1970a, 1971a, 1972a, Fluid inclusion research, Proceedings of COFFI (annual summary of world literature, privately printed and available from the editor).
- Roedder, E., 1970b, Application of an improved crushing microscope stage to studies of the gases in fluid inclusions: Schweizer. Mineralog. Petrog. Mitt., v. 50, pt. 1, p. 41 - 58.
- Roedder, E., 1971b, Fluid inclusion studies on the porphyry-type ore deposits at Bingham, Utah; Butte, Montana; and Climax,

Colorado: Econ. Geol., v. 66, p. 98 - 120.

Roedder, E., 1972b, The composition of fluid inclusions, Chapter JJ, in Fleischer, M., ed., Data of geochemistry, sixth edition: U.S. Geol. Surv. Prof. Paper 440 JJ, 164 p.

Roedder, E., 1977, Fluid inclusions as tools in mineral exploration: Econ. Geol., v. 72, p. 503 - 525.

Roedder, E., and Coombs, D.S., 1967, Immiscibility in granitic melts, indicated by fluid inclusions in ejected granite blocks from Ascension Island: Jour. Petrology, v. 8, p. 417 - 451.

Roedder, E., Ingram, B., and Hall, W.E., 1963, Studies of fluid inclusions, III: Extraction and quantitative analysis of inclusions in the milligram range: Econ. Geol., v. 58, p. 353 - 374.

Roedder, E., and Skinner, B.J., 1968, Experimental evidence that fluid inclusions do not leak: Econ. Geol., v. 63, p. 715 - 730.

Rose, A.W., 1970, Zonal relations of wall-rock alteration and sulphide distribution at porphyry copper deposits: Econ. Geol., v. 65, p. 920 - 936.

Rose, A.W., and Baltosser, W.W., 1966, The porphyry copper deposit at Santa Rita, New Mexico: in, Titley, S.R., and Hicks, C.L.,

- eds., *Geology of the porphyry copper deposits, southwestern North America: Tucson, Arizona, The University of Arizona Press, p. 205 - 220.*
- Ruiz, F.C., Aquirre, L., Corvalán, J., Klohn, C., Klohn, E., and Levi, B., 1965, *Geología y yacimientos metalíferos de Chile: Santiago, Inst. Invest. Geol., 350 p.*
- Rutland, R.W.R., Guest, J.E., and Grasty, R.L., 1965, *Isotopic ages and Andean uplift: Nature, Lond., v. 208, p. 677 - 678.*
- Rye, R.O., and O'Neil, J.R., 1968, *The <sup>18</sup>O content of water in primary fluid inclusions from Providencia, north-central Mexico: Econ. Geol., v. 63, p. 232 - 238.*
- Rye, R.O., and Sawkins, F.J., 1974, *Fluid inclusion and stable isotope studies on the Casapalca Ag-Pb-Zn-Cu deposit, central Andes, Peru: Econ. Geol., v. 69, p. 181 - 205.*
- Samoyloff, V., 1934, *The Llallagua-Uncia tin deposit: Econ. Geol., v. 29, p. 481 - 499.*
- Savin, S.M., and Epstein, S., 1970, *The oxygen and hydrogen isotope geochemistry of clay minerals: Geochim. et Cosmochim. Acta, v. 34, p. 25 - 42.*
- Schlatter, L., and Nederlof, M., 1966, *Bosquejo de la geología y palaeogeografía de Bolivia: La Paz, Geobol Bol. No. 8.*

Schneider - Scherbina, A., 1962, Uber metallogenetische Epochen Boliviens und den hybriden charakter der sogenannten "Zinn-Silber-Formation": Geol. Jahrb., v. 81, p. 157 - 170.

Schneider, H-J., and Lehmann, B., 1977, Contribution to a new genetical concept on the Bolivian tin province: in, Klemm, D., and Schneider, H-J., eds., Time and strata-bound ore deposits: Berlin, Springer - Verlag, 444 p.

Schuiling, R.D., 1967, Tin belts on the continents around the Atlantic ocean: Econ. Geol., v. 62, p. 540 - 550.

Segerstrom, K., 1967, Geology and ore deposits of central Atacama province, Chile: Geol. Soc. America Bull., v. 78, p. 305 - 318.

Sheppard, S.M.F., 1977a, Identification of the origin of ore-forming solutions by the use of stable isotopes: in, Geol. Soc. London Spec. Publication No. 7, p. 25 - 41.

Sheppard, S.M.F., 1977b, The Cornubian batholith, S.W. England: D/H and  $^{18}\text{O}/^{16}\text{O}$  studies of kaolinite and other alteration minerals: Jour. Geol. Soc. London, v. 133, p. 573 - 592.

Sheppard, S.M.F., and Gustafson, L.B., 1976, Oxygen and hydrogen isotopes in the porphyry copper deposit at El Salvador, Chile: Econ. Geol., v. 71, p. 1549 - 1559.

Sheppard, S.M.F., Neilsen, R.L., and Taylor, H.P., 1969, Oxygen and hydrogen isotope ratios of clay minerals from porphyry

copper deposits: *Econ. Geol.*, v. 64, p. 755 - 777.

Sheppard, S.M.F., Neilsen, R.L., and Taylor, H.P., 1971, Hydrogen and oxygen isotope ratios in minerals from porphyry copper deposits: *Econ. Geol.*, v. 66, p. 515 - 542.

Schlichta, P.J., 1968, Growth, deformation, and defect structure of salt crystals: *Geol. Soc. America Spec. Paper* 88, p. 597 - 617.

Sillitoe, R.H., 1972a, Relation of metal provinces in western America to subduction of oceanic lithosphere: *Geol. Soc. America Bull.*, v. 83, p. 813 - 818.

Sillitoe, R.H., 1972b, A plate tectonic model for the origin of porphyry copper deposits: *Econ. Geol.*, v. 67, p. 184 - 197.

Sillitoe, R.H., 1973, The tops and bottoms of porphyry copper deposits: *Econ. Geol.*, v. 68, p. 799 - 815.

Sillitoe, R.H., 1974, Tectonic segmentation of the Andes: Implications for magmatism and metallogeny: *Nature, Lond.*, v. 250, p. 542 - 545.

Sillitoe, R.H., 1976, Andean mineralization: A model for the metallogeny of convergent plate margins: in, Strong, D., ed., *Metallogeny and plate tectonics*; *Geol. Assoc. Canada Sp. Paper No. 14*, p. 59 - 100.

- Sillitoe, R.H., 1977, Permo-Carboniferous, Upper Cretaceous, and Miocene porphyry copper-type mineralization in the Argentinian Andes: *Econ. Geol.*, v. 72, p. 99 - 103.
- Sillitoe, R.H., Halls, C., and Grant, J.N., 1975, Porphyry tin deposits in Bolivia: *Econ. Geol.*, v. 70, p. 913 - 927.
- Sillitoe, R.H., and Sawkins, F.J., 1971, Geologic, mineralogic and fluid inclusion studies relating to the origin of copper-bearing tourmaline breccia pipes, Chile: *Econ. Geol.*, v. 66, p. 1028 - 1041.
- Skinner, B.J., 1953, Some considerations regarding liquid inclusions as geologic thermometers: *Econ. Geol.*, v. 48, p. 541 - 550.
- Smith, F.G., 1947, Transport and deposition of the non-sulphide vein minerals: II, cassiterite: *Econ. Geol.*, v. 42, p. 251 - 262.
- Smith, F.G., 1949, Transport and deposition of the non-sulphide vein minerals: IV, tourmaline: *Econ. Geol.*, v. 44, p. 186 - 192.
- Smith, F.G., 1953, Historical development of inclusion thermometry: Toronto, Univ. of Toronto Press, 149 p.
- Sorby, H.C., 1858, On the microscopical structure of crystals, indicating the origin of minerals and rocks: *Geol. Soc. London Quart. Jour.*, v. 14, p. 453 - 500.

- Sourirajan, S., and Kennedy, G.C., 1962, The system  $H_2O - NaCl$  at elevated temperatures and pressures: *Am. Jour. Sci.*, v. 260, p. 115 - 141.
- Stauder, W., 1973, Mechanism and spatial distribution of Chilean earthquakes with relation to subduction of the oceanic plate: *Jour. Geophys. Res.*, v. 78, p. 5033 - 5061.
- Steinmann, G., 1922, Über die junge Hebung der Kordillera Südamerikas: *Geol. Rundschau*, v. 13, p. 1 - 9.
- Steinmann, G., 1930, *Geologia del Peru*: Heidelberg, Carl Winters Universitatbuchhandlung, 448 p.
- Stewart, J.W., Evernden, J.F., and Snelling, N.J., 1974, Age determinations from Andean Peru: A reconnaissance survey: *Geol. Soc. America Bull.*, v. 85, p. 1107 - 1116.
- Stoll, W.C., 1964, Metallogenic belts, centers, and epochs in Argentina and Chile: *Econ. Geol.*, v. 59, p. 126 - 135.
- Stoll, W.C., 1965, Metallogenic provinces of South America: *Mining Mag.*, v. 112, p. 22 - 23, 90 - 99.
- Strong, D.F., 1974, Plate tectonic setting of Appalachian - Caledonian mineral deposits as indicated by Newfoundland examples: *Soc. Mining. Eng. AIME, Trans.* v. 256, p. 121 - 128.



- Suzuoki, T., and Epstein, S., 1976, Hydrogen isotope fractionation between OH-bearing silicate minerals and water: *Geochem. Cosmochim. Acta*, v. 40, p. 1229 - 1240.
- Swift, S.A., and Carr, M.J., 1973, The segmented nature of the Chilean deep seismic zone: Conference on Geodynamics, Int. Union. Geodesy, Geophys., Lima, Aug. 1973, CGD-24.
- Takenouchi, S., and Kennedy, G.C., 1964, The binary system  $H_2O - CO_2$  at high temperatures and pressures: *Am. Jour. Sci.*, v. 262, p. 1055 - 1074.
- Takenouchi, S., and Kennedy, G.C., 1965, The solubility of carbon dioxide in NaCl solutions at high temperatures and pressures: *Am. Jour. Sci.*, v. 263, p. 445 - 454.
- Taylor, H.P., 1967, Oxygen isotope studies of hydrothermal mineral deposits: in, Barnes, H.L., ed., *Geochemistry of hydrothermal ore deposits*: New York, Holt, Rinehart, and Winston, p. 109 - 142.
- Taylor, H.P., 1968, The oxygen isotope geochemistry of igneous rocks: *Contrib. Mineral. Petrol.*, v. 19, p. 1 - 71.
- Taylor, H.P., 1974, The application of oxygen and hydrogen isotope studies to problems of hydrothermal alteration and ore deposition: *Econ. Geol.*, v. 69, p. 843 - 883.

- Taylor, H.P., 1977, Water/rock interactions and the origin of H<sub>2</sub>O in granitic batholiths: Jour. Geol. Soc. London, v. 133, p. 509 - 559.
- Taylor, S.R., 1965, The application of trace element data to problems in petrology: Physics and Chemistry of the Earth, v. 6, p. 133 - 213.
- Tischendorf, G., 1977, Geochemical and petrographic characteristics of silicic magmatic rocks associated with rare - element mineralization: in, Mineralization Associated With Acid Magmatism, v. 2, Prague, Geol. Surv., p. 41 - 98.
- Touret, J., 1977, The significance of fluid inclusions in metamorphic rocks: in, Fraser, D.G., ed., Thermodynamics in geology, Dordrecht - Holland, D. Reidel Publishing Co., p. 203 - 227.
- Tsui, T.F., Holland, H.D., and Snetsinger, K.G., 1975, Laser microprobe analysis of fluid inclusions: Geol. Soc. America, Annual Meeting, Abstracts with programs, v. 7, p. 1304 - 1305.
- Turneure, F.S., 1935, The tin deposits of Llallagua, Bolivia: Econ. Geol., v. 30, p. 14 - 60, 170 - 190.
- Turneure, F.S., 1960, A comparative study of the major ore deposits of central Bolivia: Econ. Geol., v. 55, p. 217 - 254, 574 - 606.

Turneaure, F.S., 1971, The Bolivian tin-silver province: *Econ. Geol.*, v. 66, p. 215 - 225.

Turneaure, F.S., and Welker, K.K., 1947, The ore deposits of the Eastern Andes, Bolivia. *The Cordillera Real: Econ. Geol.*, v. 42, p. 595 - 625.

Turner, J.C., 1970, The Andes of northwestern Argentina: *Geol. Rundschau*, v. 59, p. 1028 - 1063.

Velasco, J.R., 1966, Geology of the Cananea district: in, Titley, S.R., and Hicks, C.L., eds., *Geology of the porphyry copper deposits, southwestern North America: Tucson, Arizona, The University of Arizona Press*, p. 245 - 250.

White, D.E., Muffler, L.J.P., and Truesdell, A.H., 1971, Vapor-dominated hydrothermal systems compared with hot-water systems: *Econ. Geol.*, v. 66, p. 75 - 97.

Whitney, J.A., 1975, Vapour generation in a quartz-monzonite magma: A synthetic model with applications to porphyry copper deposits: *Econ. Geol.*, v. 70, p. 346 - 358.

Wyllie, P.J., 1973, Experimental petrology and global tectonics, a preview: *Tectonophysics*, v. 17, p. 189 - 209.

Wyllie, P.J. Huang, W-L., Stern, C.R., and Maaloe, S., 1976, Granitic magmas: possible and impossible sources, water contents, and crystallization sequences: *Canadian Jour. Earth Sci.*, v. 13, p. 1007 - 1019.

Yermakov, N.P., 1965, Research on the nature of mineral-forming solutions, with special reference to data from fluid inclusions: International Series of Monographs in Earth Sciences; New York, Pergamon Press, v. 22, 743 p.

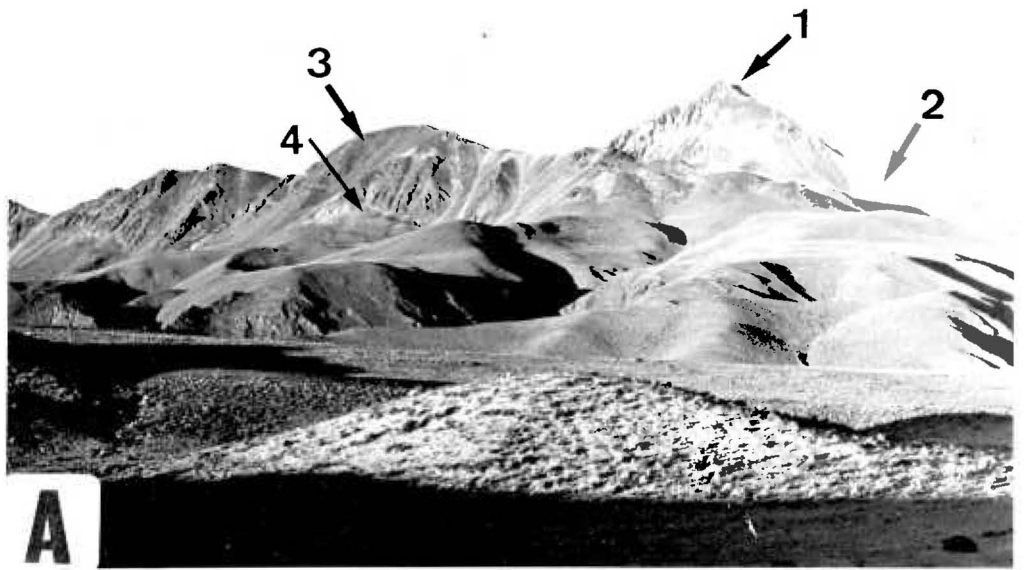
York, D., and Farquhar, R.M., 1972, The earth's age and geochronology: Oxford - Pergamon Press, 178 p.

Ypma, P.J.M., 1963, Rejuvenation of ore deposits as exemplified by the Belledonne metalliferous province: Thesis, Univ. of Leiden, Netherlands.

## PLATE 1

A. View of the Chorolque complex from the west. Cerro Chorolque (1) is made up of quartz-tourmaline altered breccia and porphyry of the central vent, with pale sericitized acid volcanics on its immediate flanks (2). The nearer hills are outlying slightly chloritized acid volcanics (3), resting unconformably on folded Palaeozoic sedimentary rocks (contact at 4) which make up the middle distance. In the foreground are acid crystal tuffs of the (16.9 Ma) 'Atocha' tuff unit.

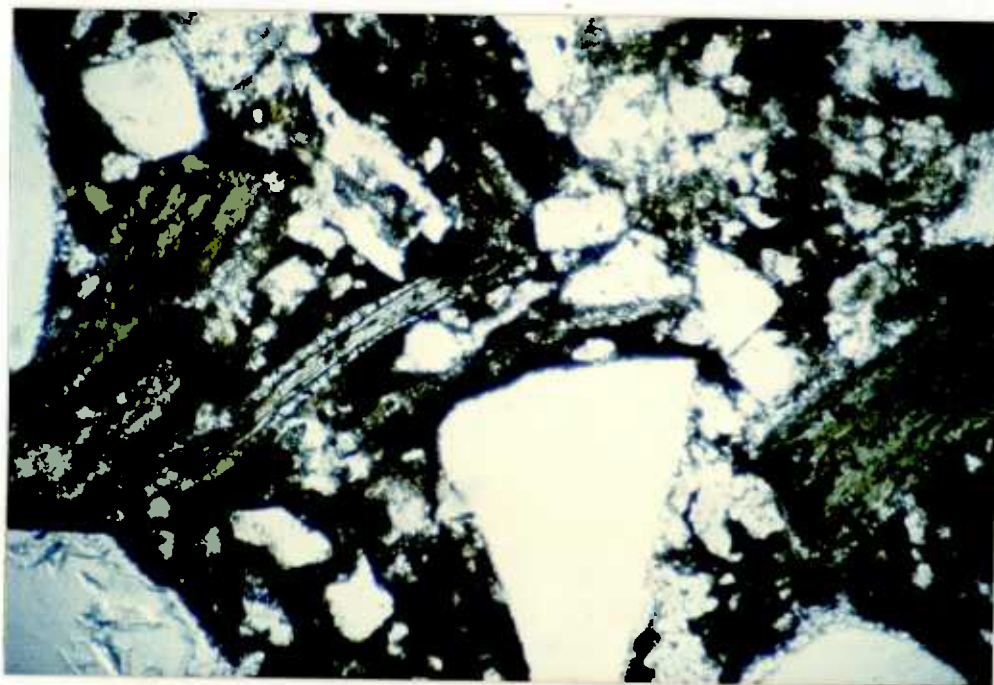
B. Cerro Chorolque from Cerro Espiritu Santu (point 3 in Plate A above), with the mining camp of Santa Barbara in the foreground. The vent contact lies at the foot of the rocky outcrops on the left flank of the Cerro, and continues horizontally across the slope above Santa Barbara where it is marked by a distinct colour change. The sericitic zone in the flanking volcanics (pale colour) extends down slope as far as the buildings.



## PLATE 2

A. Chorolque: Transmitted light photomicrograph of typical volcanic rock distant from the vent. Angular broken quartz phenocrysts (white), chloritized biotite laths (green), in an almost opaque clay-rich matrix (altered glassy material). Plane polarized light, X10.

B. Chorolque: Typical quartz-tourmaline altered vent breccia; Cerro Chorolque summit. Dark tourmaline-rich fragments with relict quartz phenocrysts in a pale quartz-rich matrix.

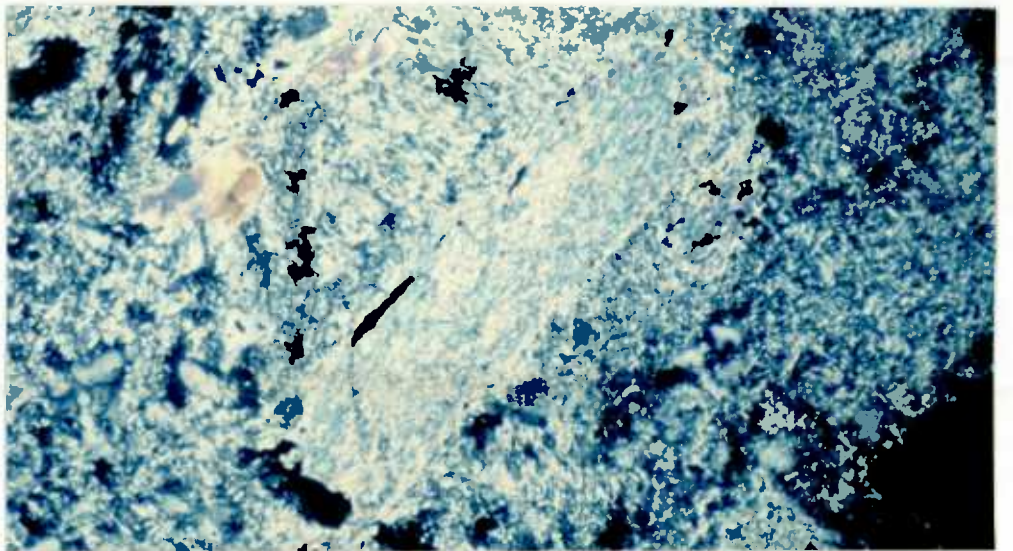
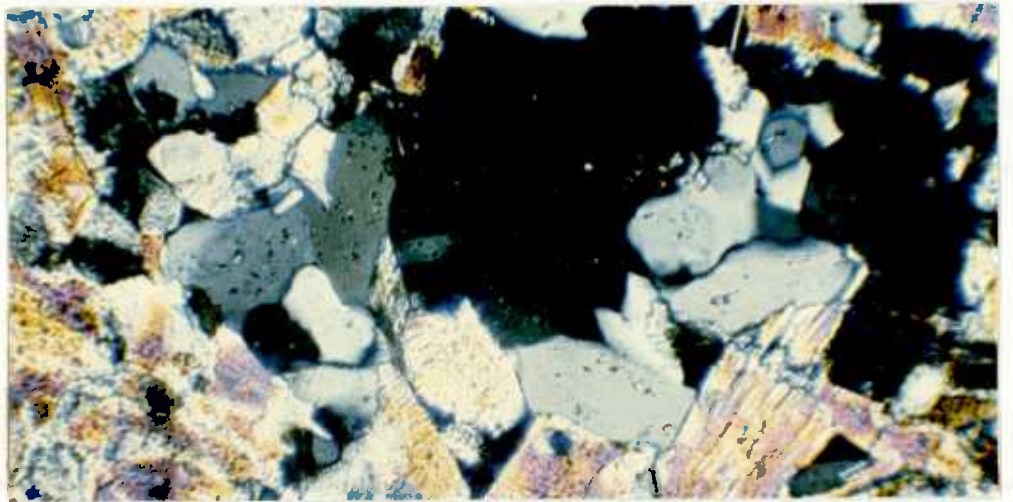
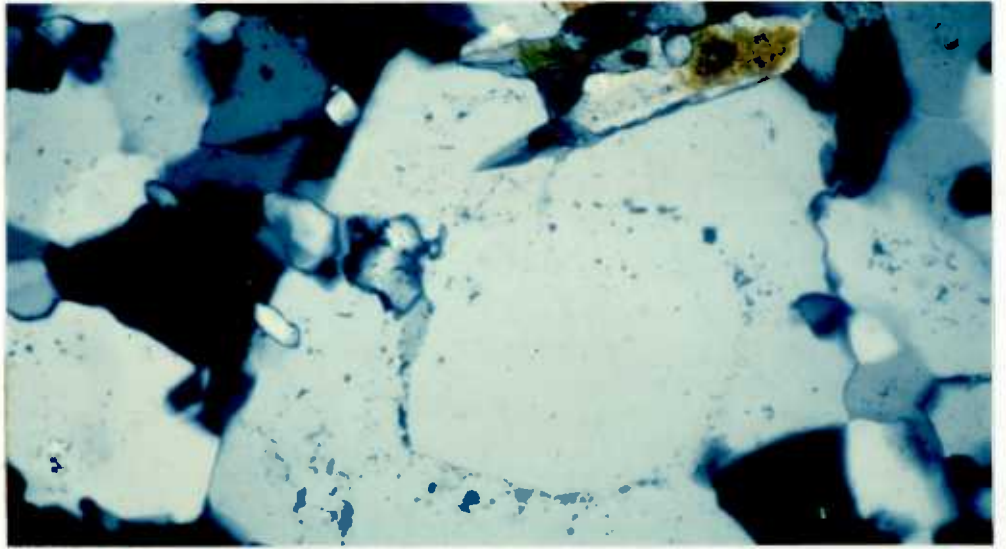




## PLATE 3

## Chorolque: Petrography of altered rocks

- A. Transmitted light photomicrograph of quartz-tourmaline altered vent rock, showing a relict primary igneous quartz phenocryst (outlined by solid and fluid inclusions) overgrown by secondary quartz. Crossed polars, X60.
- B. Transmitted light photomicrograph of typical quartz-tourmaline altered vent rock, consisting of fine intergrown quartz and tourmaline. Crossed polars, X60.
- C. Transmitted light photomicrograph of typical altered volcanic rock from the zone of sericitization peripheral to the vent. The large lath-shaped relict phenocryst is a sericite-quartz intergrowth replacing feldspar. The groundmass is also fine intergrown sericite and quartz, with occasional tourmaline grains (high relief, high birefringence). Crossed polars, X60.



Salvadora stock, Llallagua: Igneous breccia.

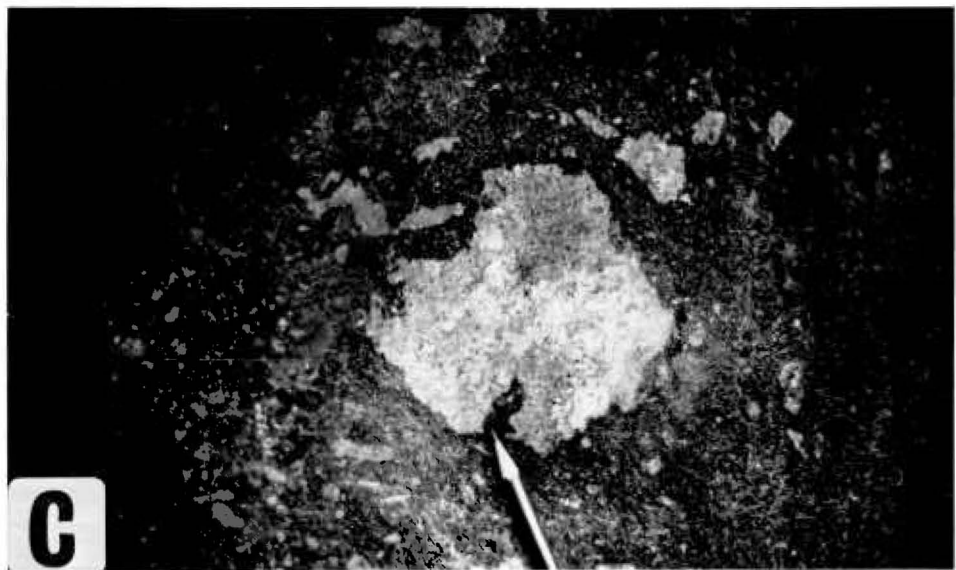
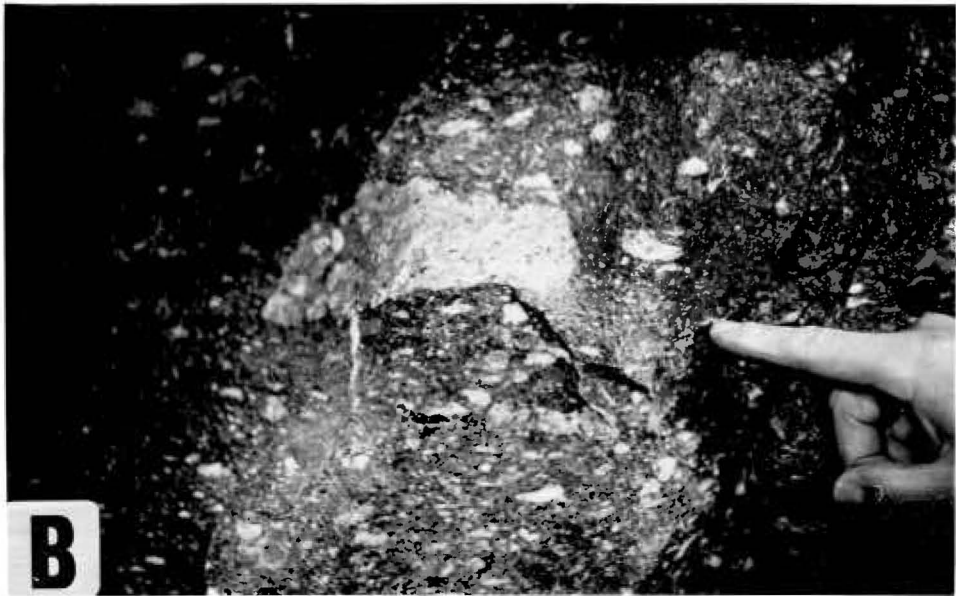
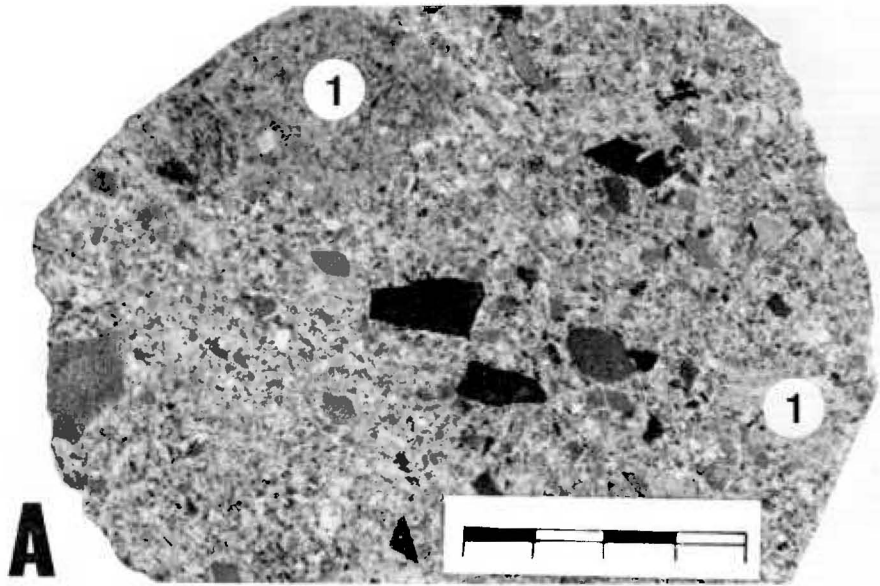
A. Typical igneous breccia. Indistinct fragments of porphyry (1) and dark argillite fragments in a quartz-porphyry matrix.

Scale in cm.

B. Igneous breccia, near Animas office, 383 level, Catavi mine.

Oriented fragments of porphyry (pale) in a fine dark siliceous porphyry matrix.

C. As Above, showing corrosion of fragments by the matrix.



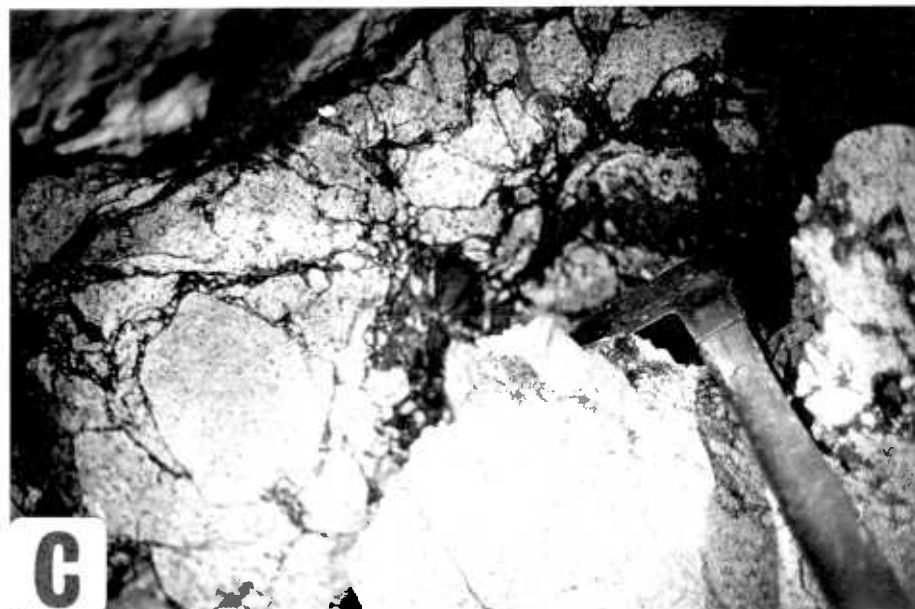
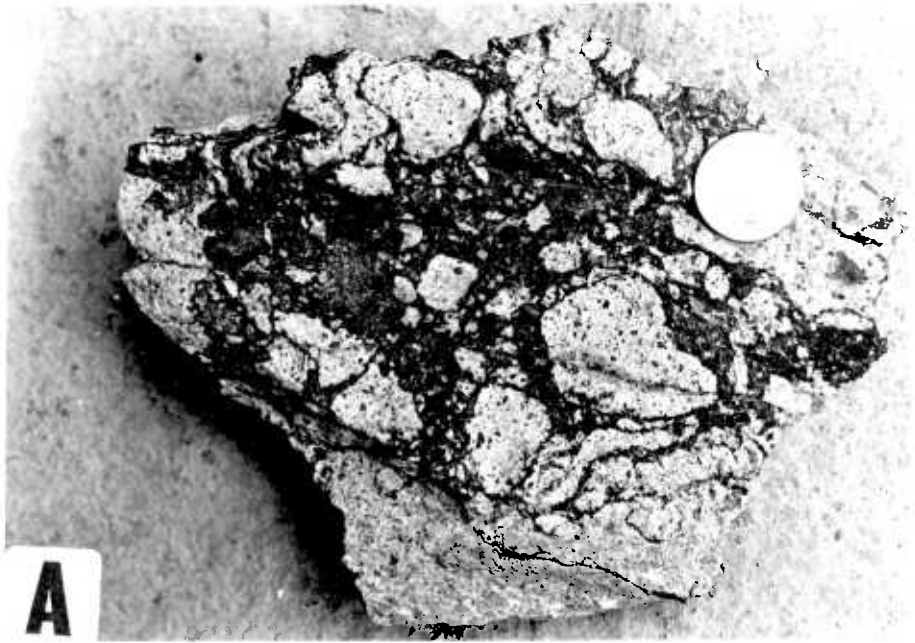
## PLATE 5

Salvadora stock, Llallagua: Hydrothermal breccia.

A. Silicified porphyry breccia. Pale rounded fragments of silicified quartz-porphyry in a black, fine quartz-tourmaline matrix crowded with fine rock fragments. In this example the fragments are relatively well rounded. Coin diameter is 2.7 cm.

B. Silicified porphyry breccia, near Old Salvadora shaft, 383 level, Catavi mine. Shows gradation from network fracturing and penetration of matrix material, to rounded isolated fragments in 'channelway'.

C. As above, showing network fracturing and penetration of matrix material without much movement of the fragments.

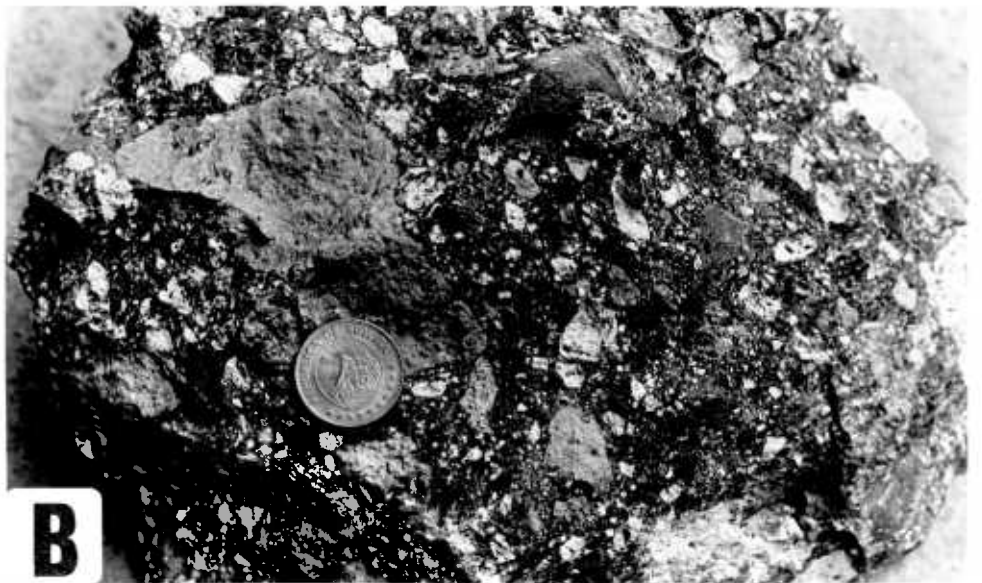
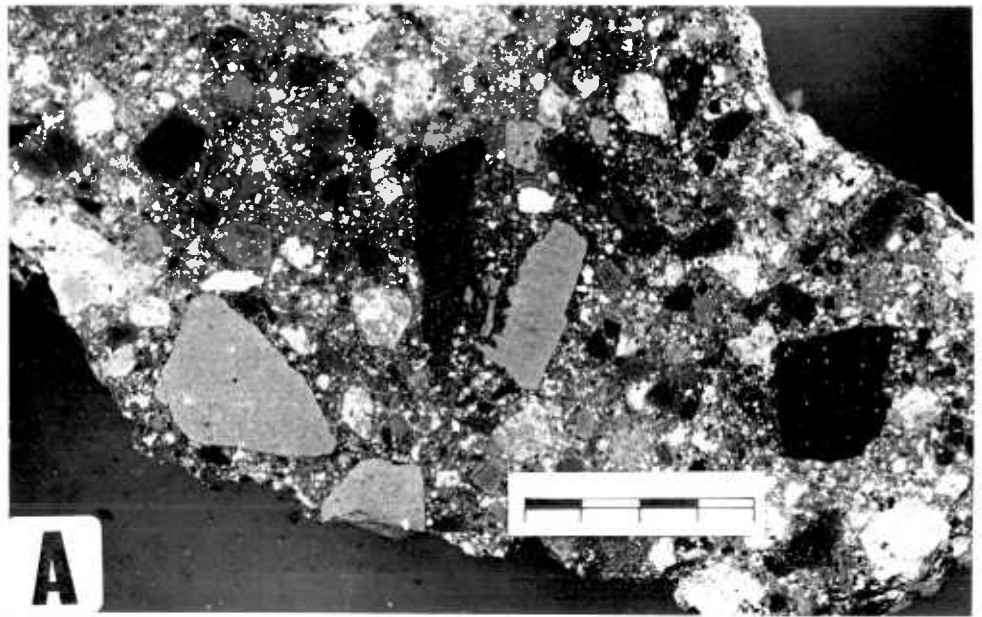


## PLATE 6

Salvadora stock, Llallagua: Hydrothermal breccia.

A. Typical polymict breccia, from eastern part of the stock, 411 level, Catavi mine. Consists of fragments of sericitized and argillized quartz-porphyry (white), fine feldspar porphyry (medium grey) and argillite (dark grey to black), in a clastic matrix of fine rock fragments cemented by tourmaline. Scale in cm.

B. As above. Coin diameter is 2.7 cm.



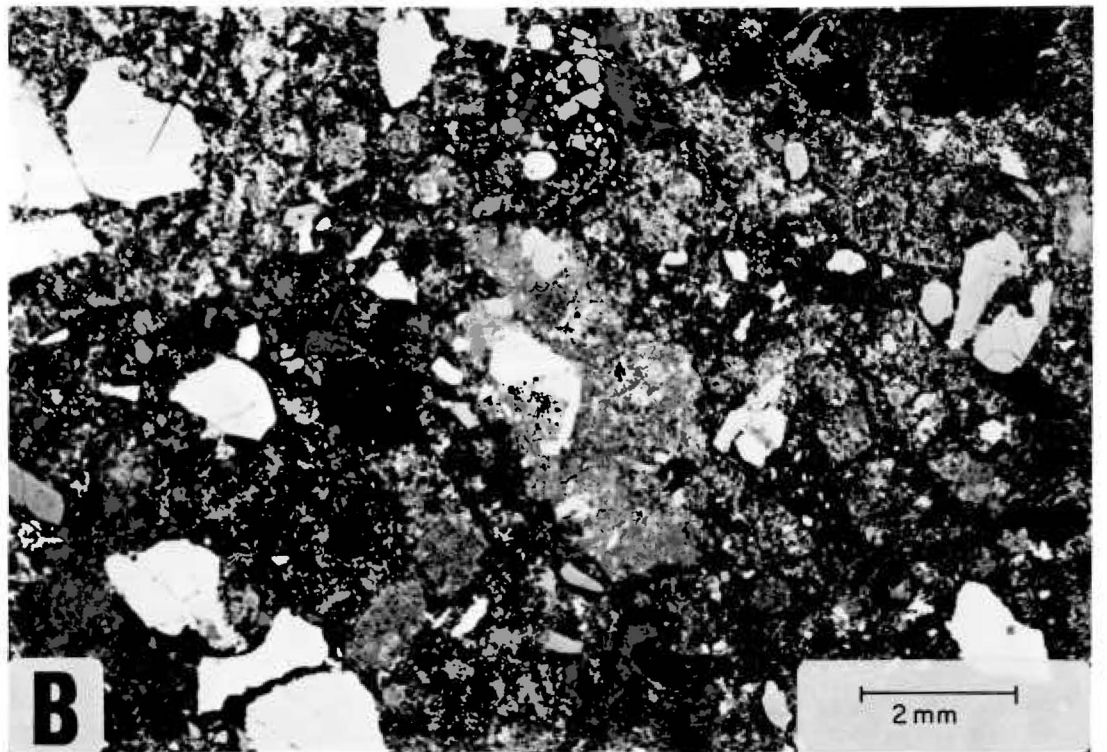
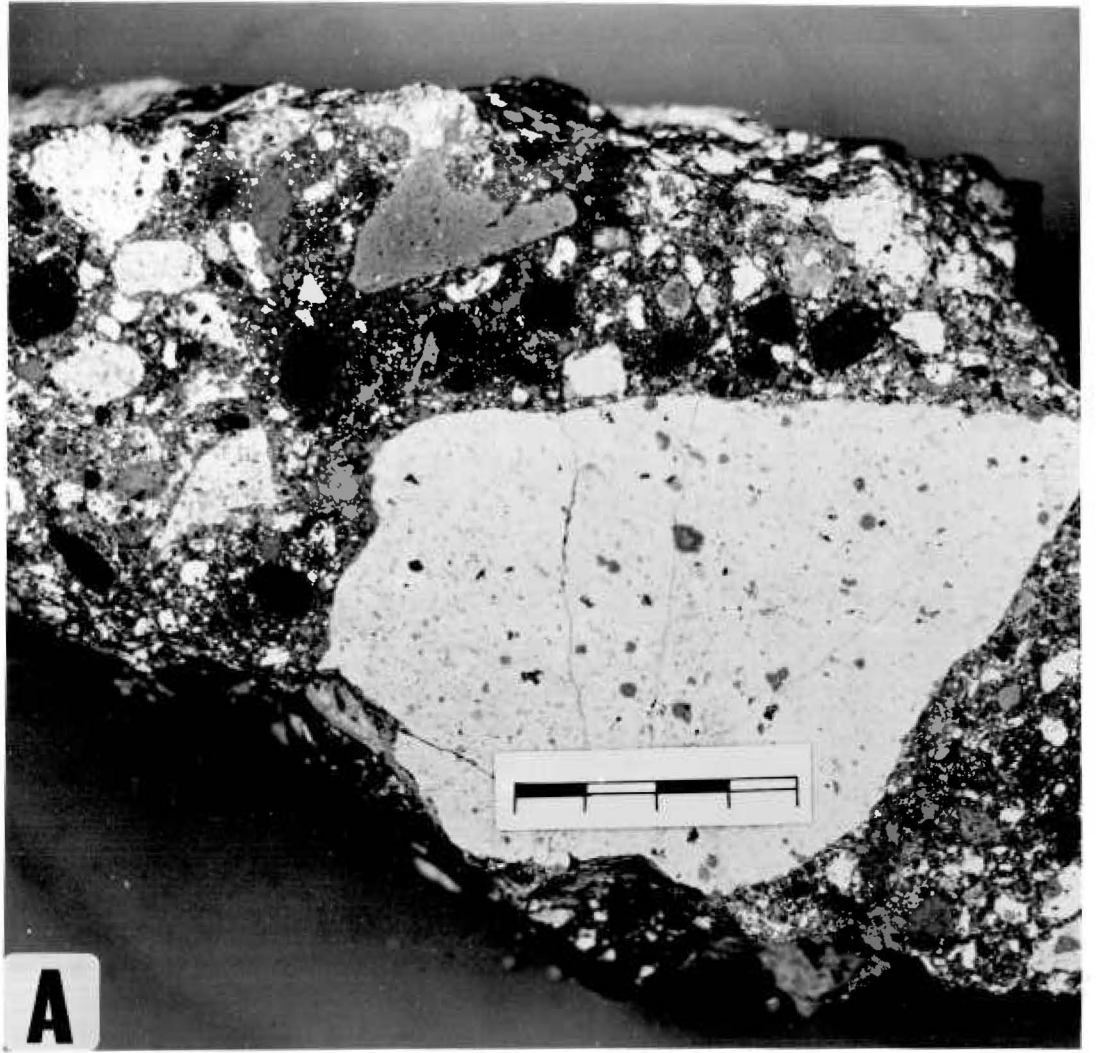


## PLATE 7

Salvadora stock, Llallagua: Hydrothermal breccia.

A. Typical polymict breccia, from eastern part of the stock, 411 level, Catavi mine. Fragments of sericitized and argillized quartz-porphyry (white), fine feldspar porphyry (medium grey) and argillite (dark grey) in a clastic matrix of fine rock fragments and quartz grains cemented by fine tourmaline. Scale in cm.

B. Hydrothermal breccia matrix. Transmitted light photomicrograph showing clastic texture of broken remnant quartz phenocrysts and fine rock fragments in (dark) cement of fine intergrown tourmaline.

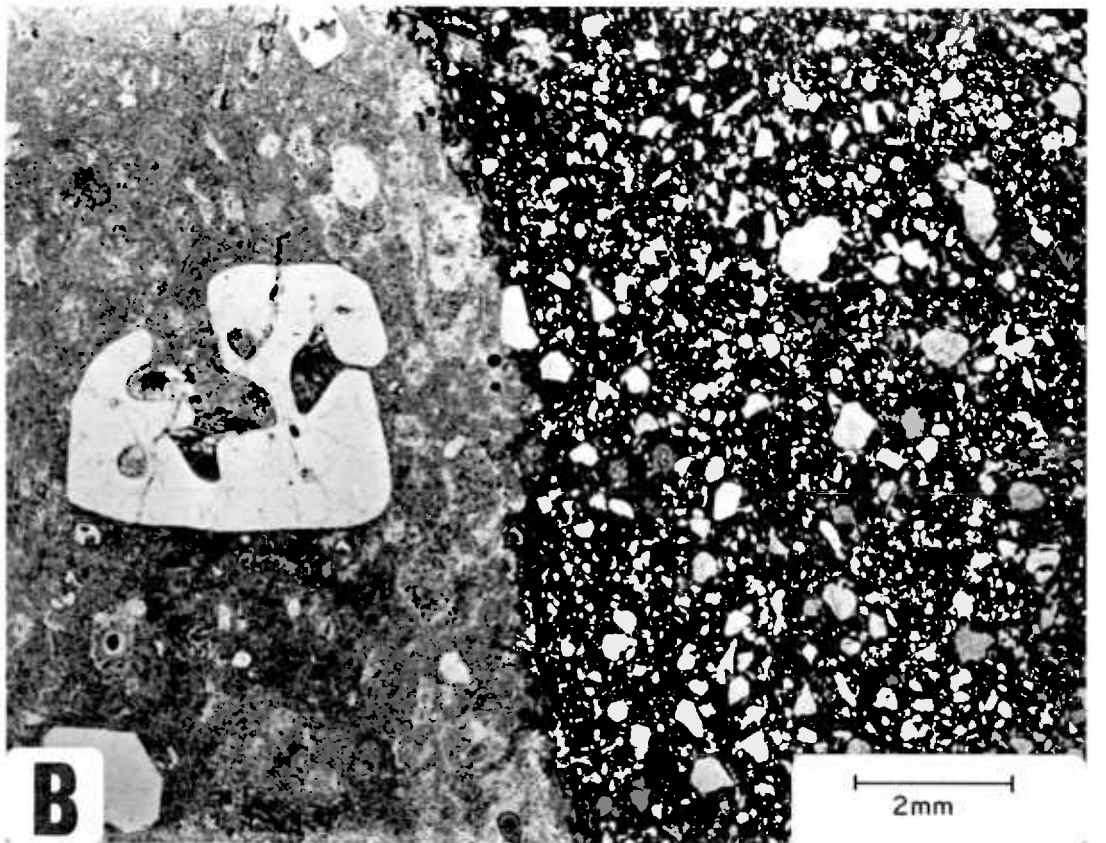
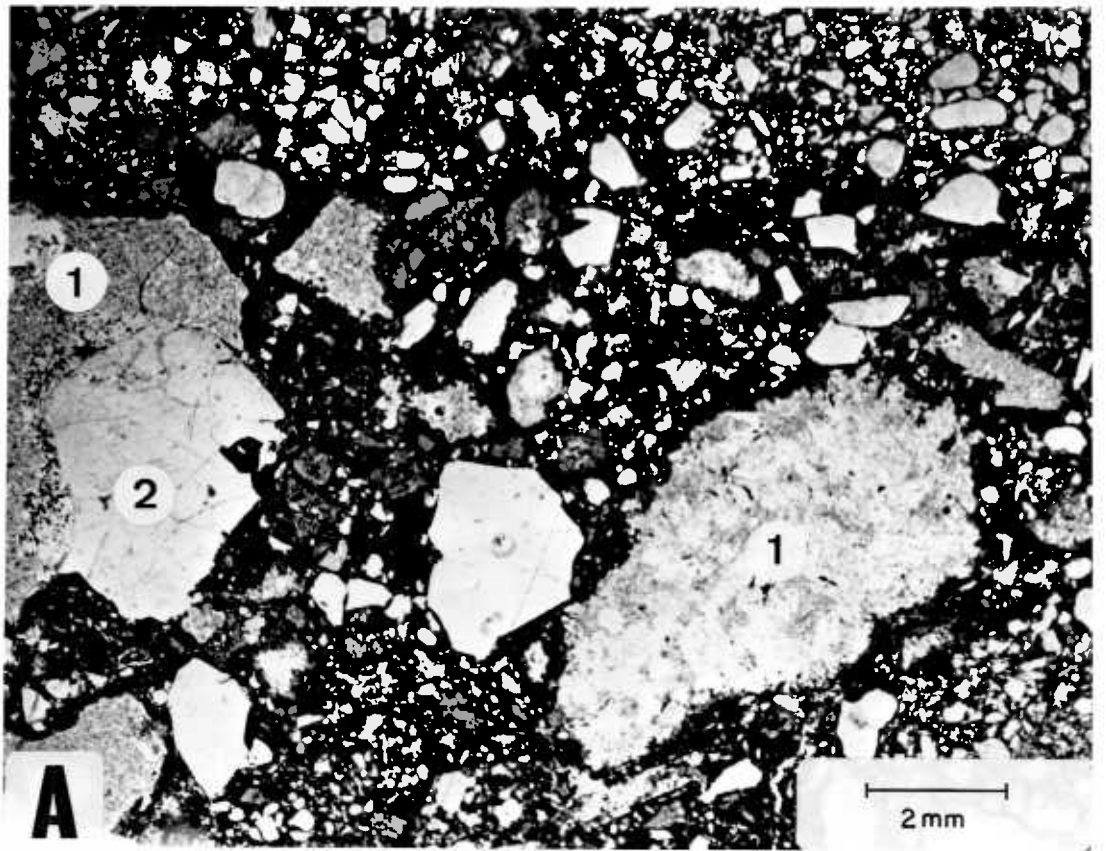


## PLATE 8

Salvadora stock, Llallagua: Hydrothermal breccia.

A. Transmitted light photomicrograph of breccia matrix. Fine ragged fragments of silicified rock (1), one of which is porphyry with remnants of a primary quartz phenocryst (2), in a matrix of quartz grains (residual quartz phenocrysts) cemented by fine tourmaline (black). Clavo San Jose, 586 level, Siglo XX mine.

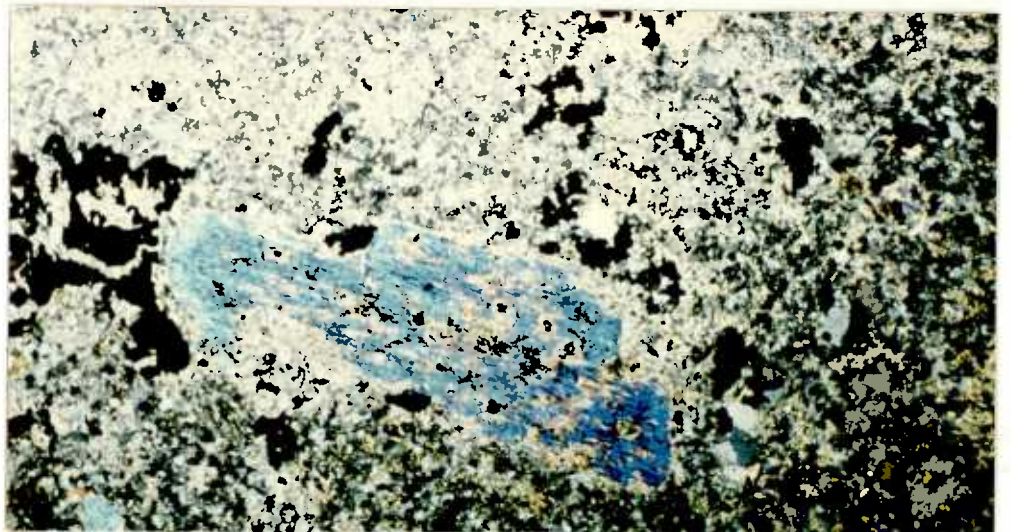
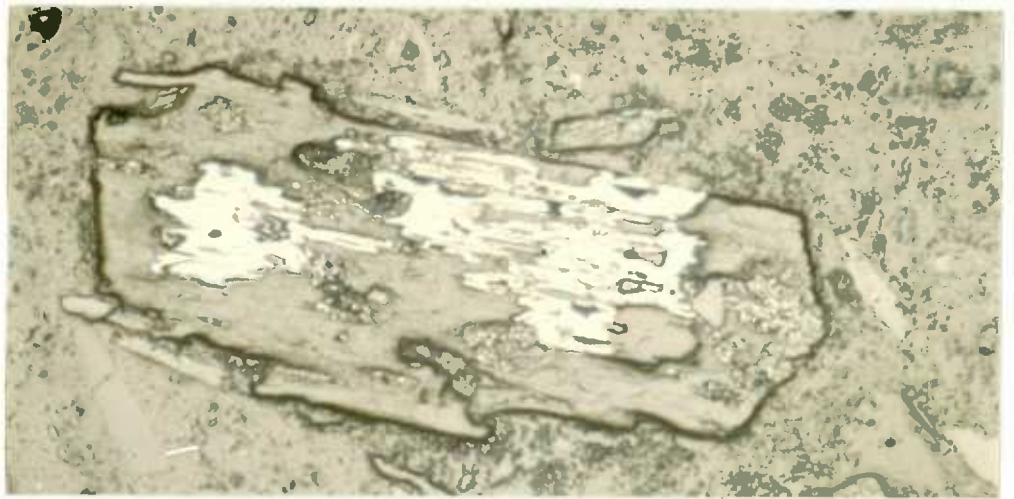
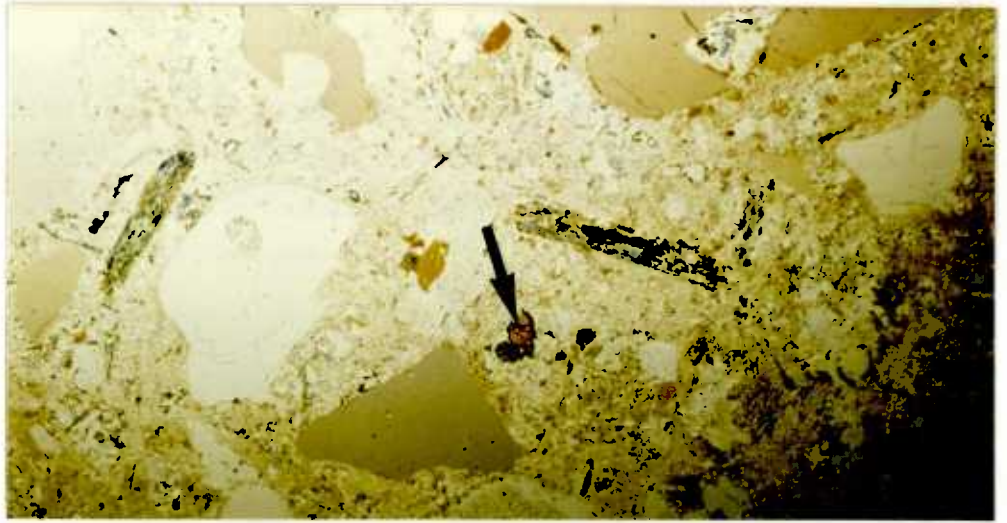
B. Transmitted light photomicrograph of a 'black dyke' (right) cutting quartz-porphyry. The dyke consists of quartz grains cemented by fine tourmaline (black), and is interpreted as hydrothermal breccia matrix material which has undergone advanced corrosion and abrasion, leaving only rounded residual quartz phenocrysts. These have been injected along fractures as a fluidized slurry, and cemented by tourmaline.



## PLATE 9

## Llallagua: Disseminated mineralization types

- A. Transmitted light photomicrograph showing typical habit of cassiterite (arrowed) in sericitized quartz-feldspar porphyry of the Salvadora stock. Blue-green laths are tourmalinized biotite, matrix is strongly sericitized. Plane polarized light, X60.
- B. Reflected light photomicrograph showing pyrrhotite (white) replacing biotite phenocryst, associated with tourmalinization of the biotite. Typical habit of early disseminated sulphide in the tourmaline-rich rocks of the lowest mine levels. X100.
- C. Transmitted light photomicrograph showing disseminated sulphide (pyrite, black) in intensely sericitized quartz-feldspar porphyry. Typical of the peripheral parts of the middle and upper levels of the Salvadora stock. Crossed polars, X20.



## PLATE 10

A. Colquechaca. Cerro Yanakaka, a glacially eroded remnant of a thick columnar-jointed dacite flow, cut by tin-bearing veins. The rocks below the Cerro are pervasively sericitized and carry disseminated cassiterite and sulphide mineralization, and are cut by small tin veins.

B. San Pablo stock. Hydrothermal brecciation of quartz-porphyry with subsequent intense sericitic alteration.

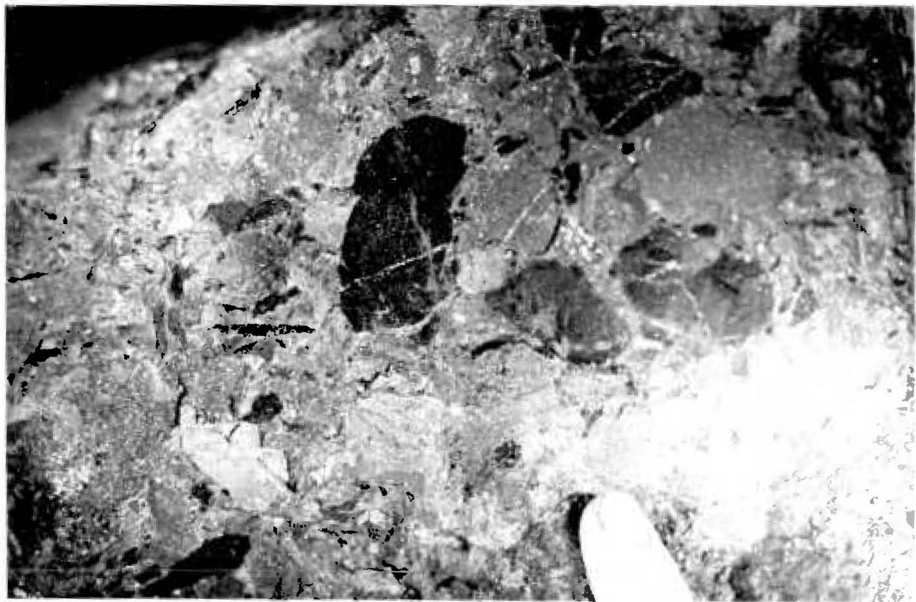
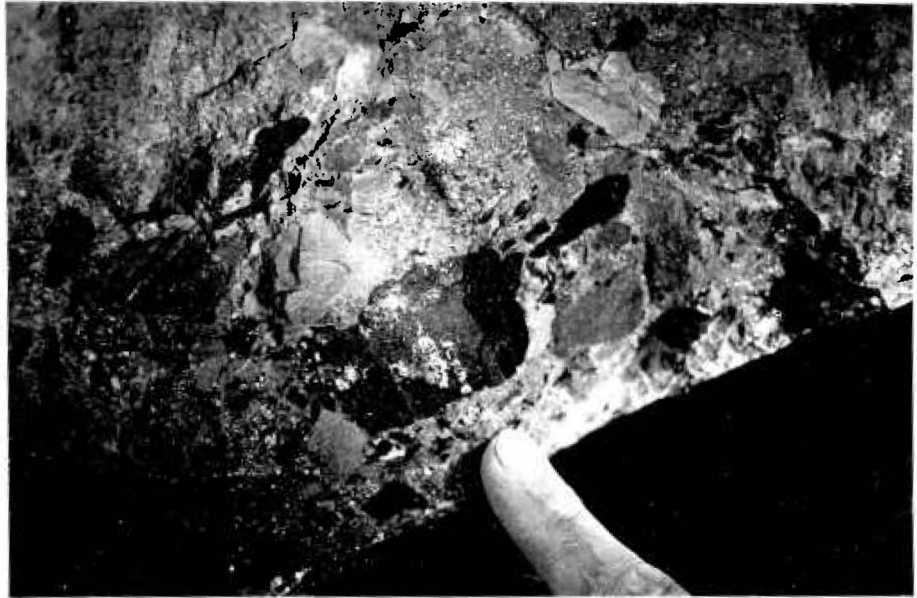
C. San Pablo stock. Pervasive alteration of quartz-porphyry. Sanidine phenocrysts replaced by tourmaline (black). The remainder of the rock is pervasively sericitized.





## PLATE 11

Santa Fe mine, pebble dyke (hydrothermal breccia) crossing the Veta Boyadora, level 170. Argillite and quartzite fragments in a clayey clastic matrix, with both pre- and post-breccia sulphide mineralization.

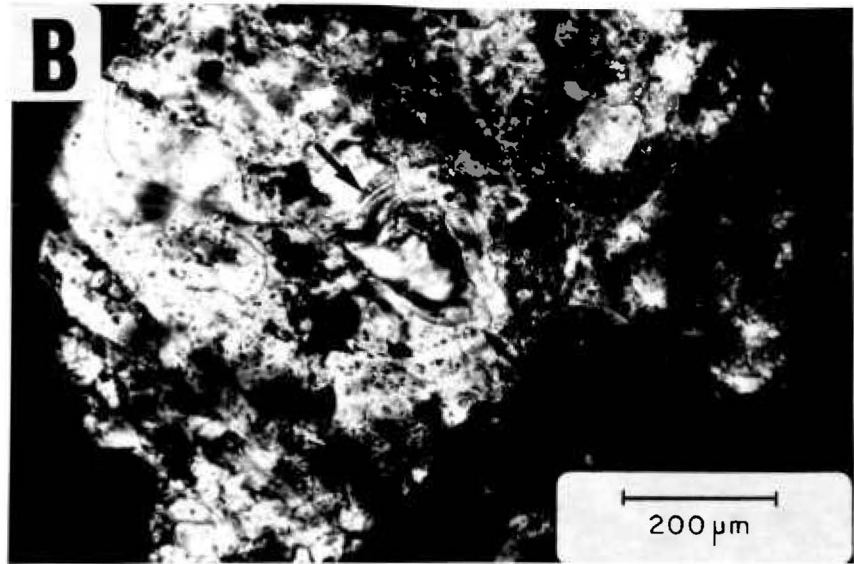
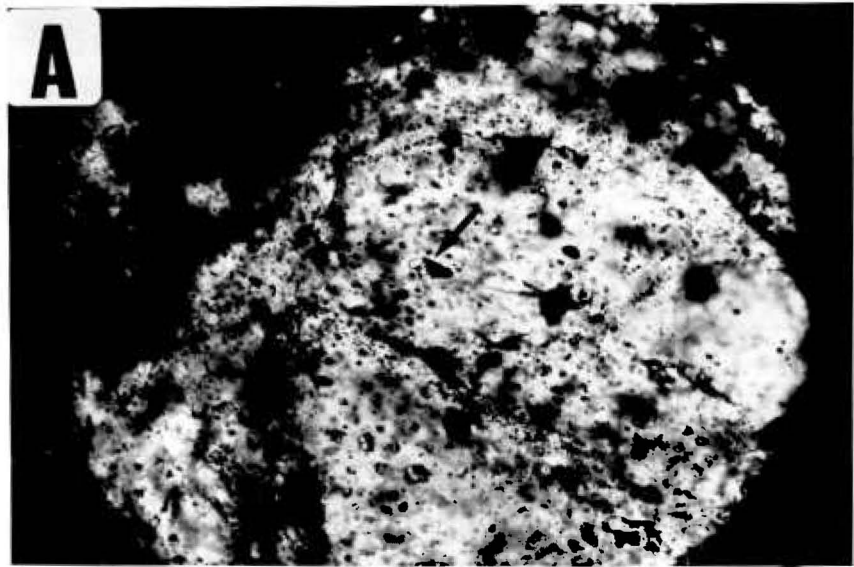


## PLATE 12

Fluid inclusion analysis by laser microprobe.

A. Transmitted light photomicrograph taken through the laser microprobe optical path prior to firing. The specimen is a  $\frac{1}{2}$  mm doubly polished slice of quartz from the quartz-tourmaline zone of the Chorolque vent, containing numerous coexisting highly saline brine inclusions with many daughter minerals (Type VI) and vapour-filled inclusions (Type V). The target (arrowed) is a large multi-daughter inclusion. Scale as for B.

B. Transmitted light photomicrograph taken after firing the laser, showing the large size of the resulting crater (arrows at opposite ends) relative to the inclusion size.



## PLATE 13

## Fluid inclusion analysis by laser microprobe.

A. Scanning electron microscope (SEM) image of a crater produced by laser microprobe shot at a minute pyrite grain enclosed in quartz. This shows that much of the cratering effect is the result of mechanical fracturing. The 'burn' hole produced by vaporization of the sample is visible in the center of the crater, and is small compared with the total crater volume. The splashed material on the crater sides is iron from the incompletely vaporized pyrite target grain.

B. Detail of above.

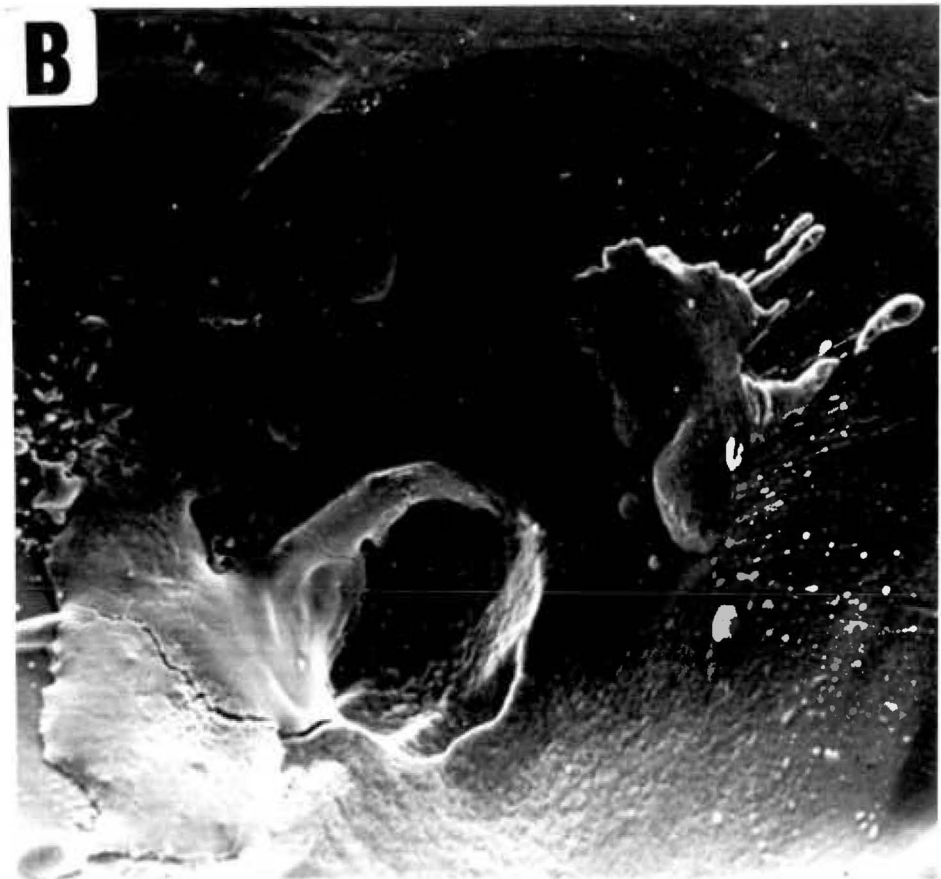
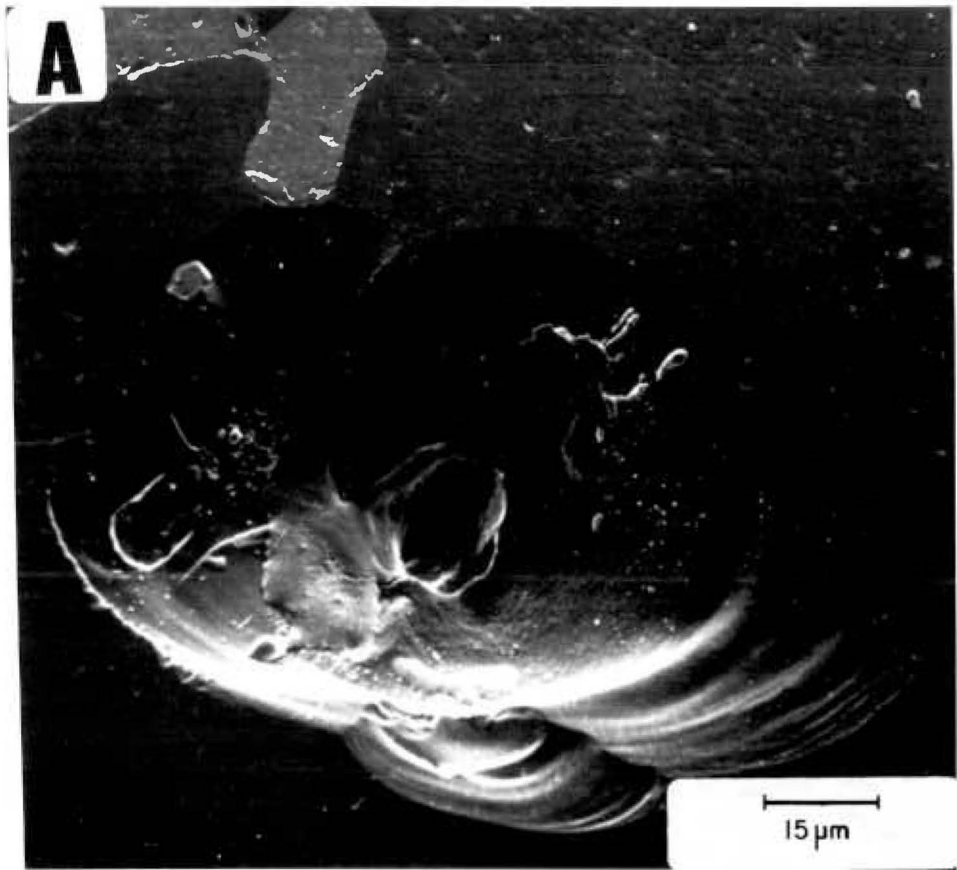
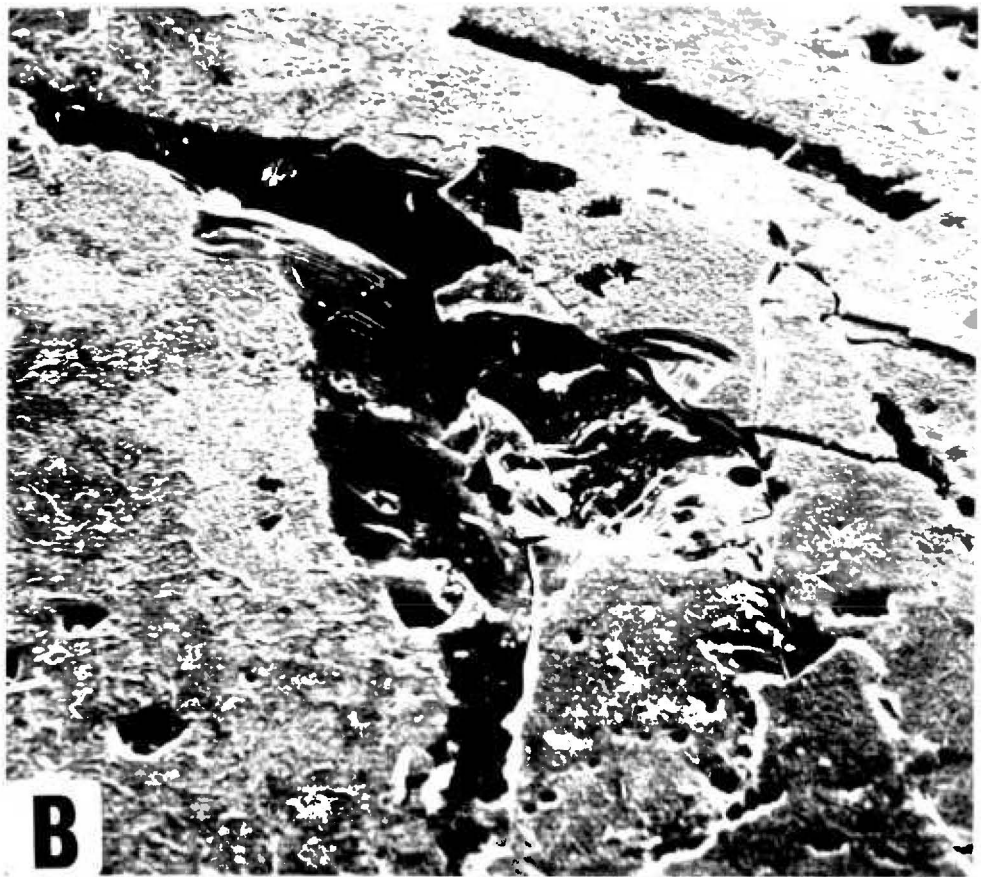
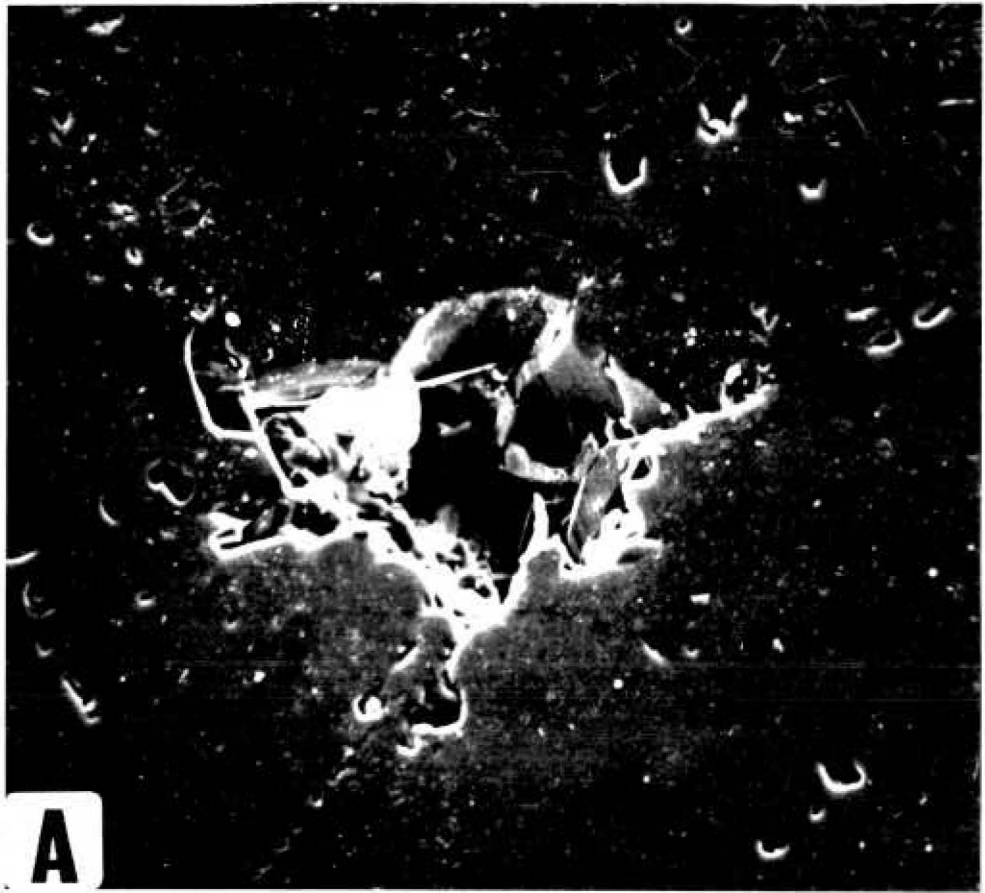


PLATE 14

Fluid inclusion analysis by laser microprobe.

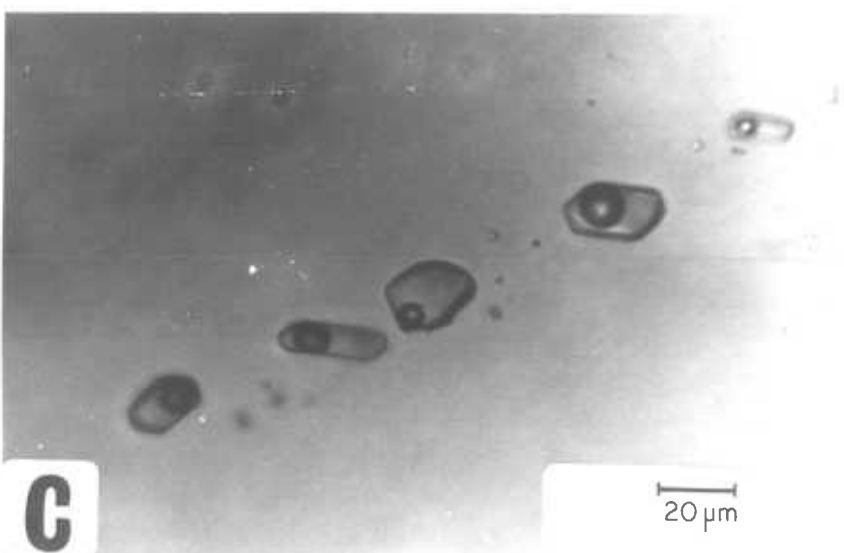
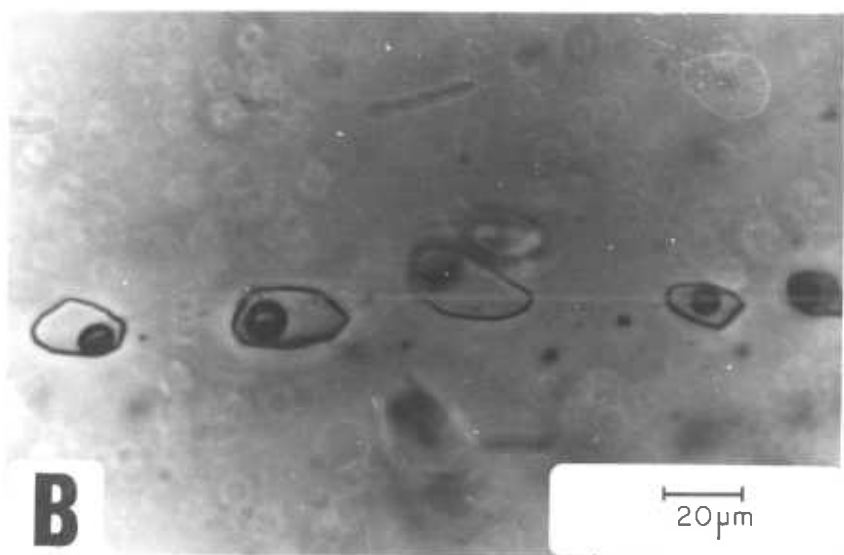
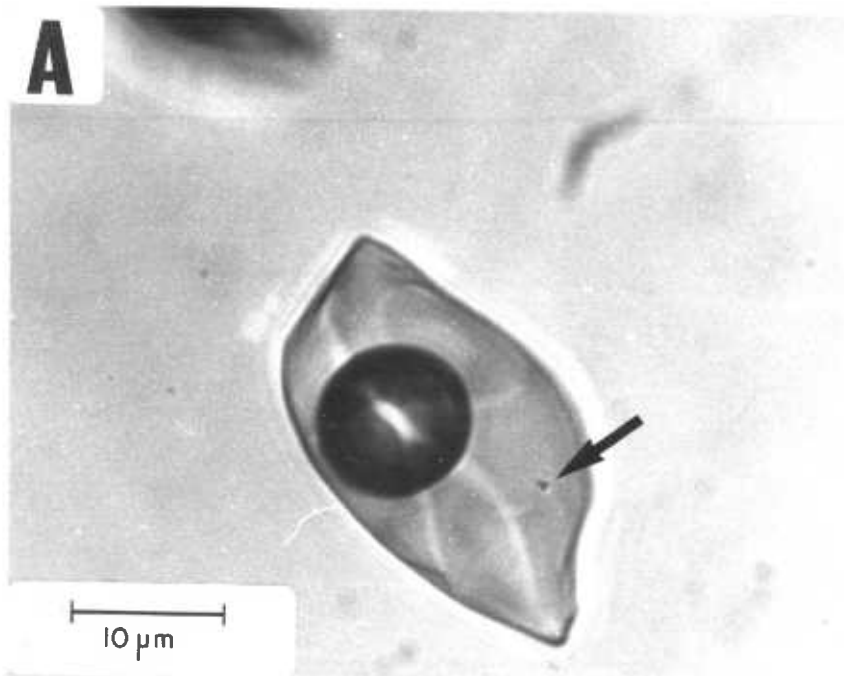
A. SEM image of crater in quartz produced by laser shot at multi-daughter inclusion, illustrating the mechanical fracturing effect. Magnification X1000.

B. As above (a different specimen). Magnification X1500.





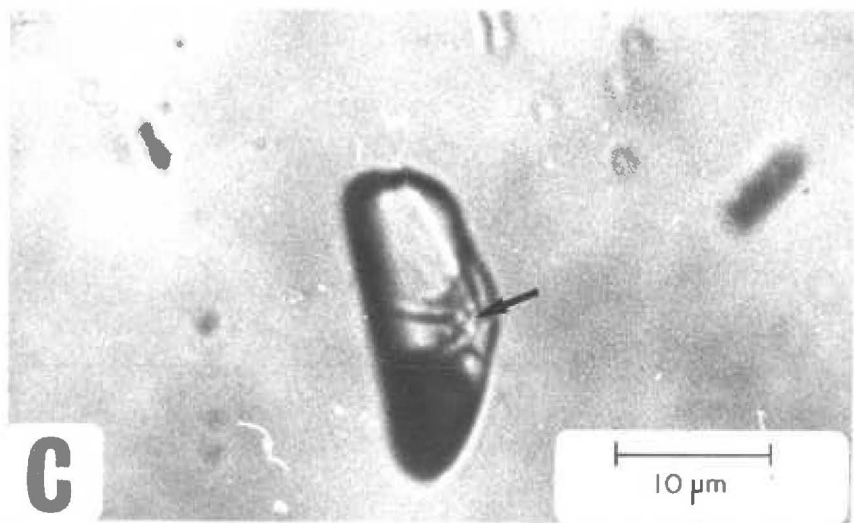
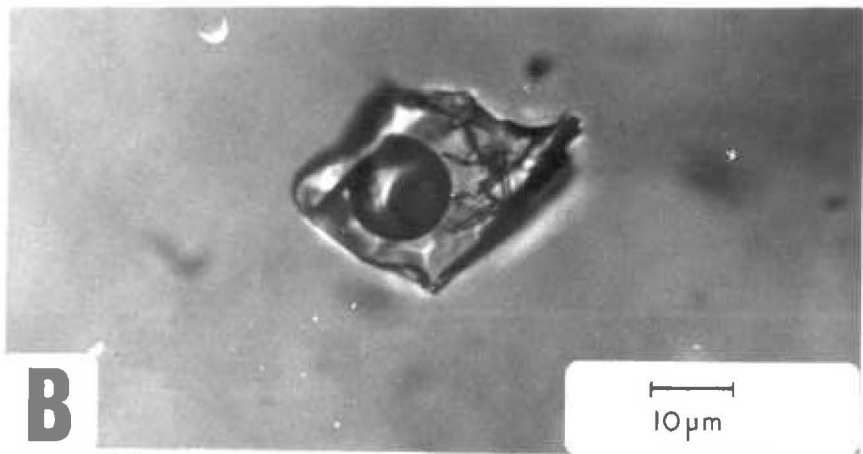
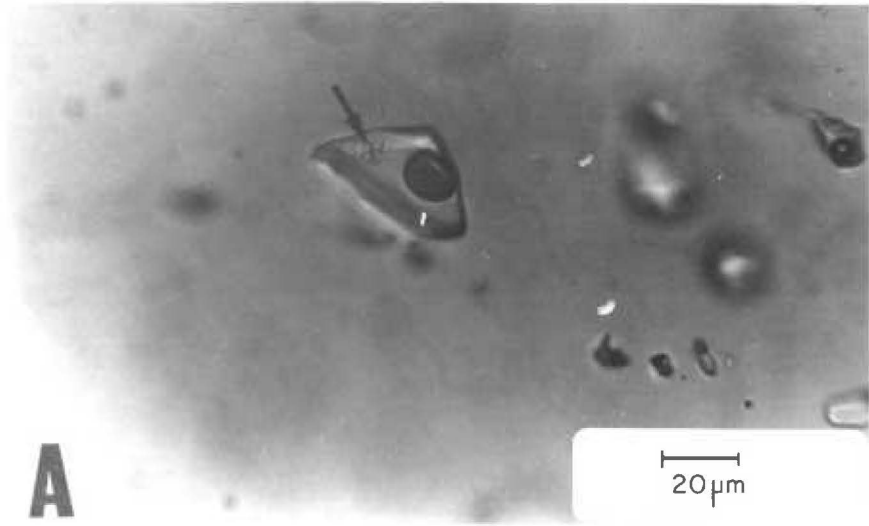




## PLATE 16

Chorolque: Fluid inclusion types.

- A. Typical primary Type II inclusion in vein quartz, showing a cluster of needle-shaped daughter mineral grains (arrowed).
- B. As above. The daughter mineral is weakly birefringent, faintly greenish in colour, and is probably dawsonite-  $\text{NaAlCO}_3(\text{OH})_2$ .
- C. As above, showing spray of acicular daughter mineral crystals (arrowed).



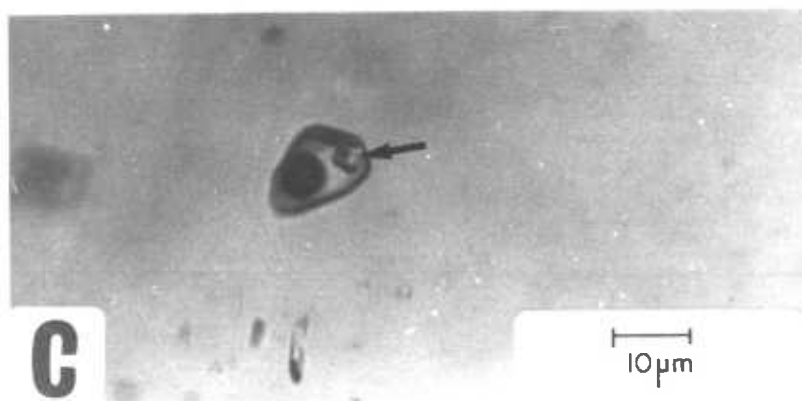
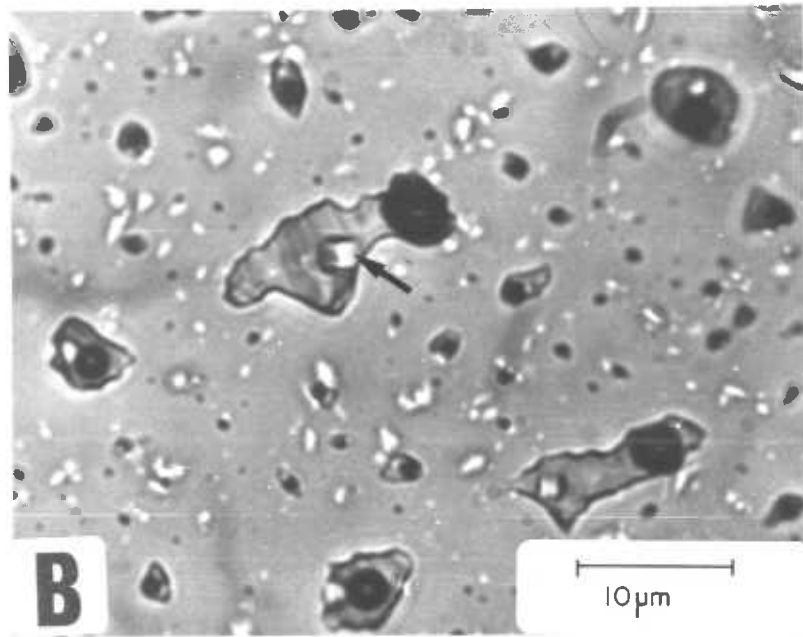
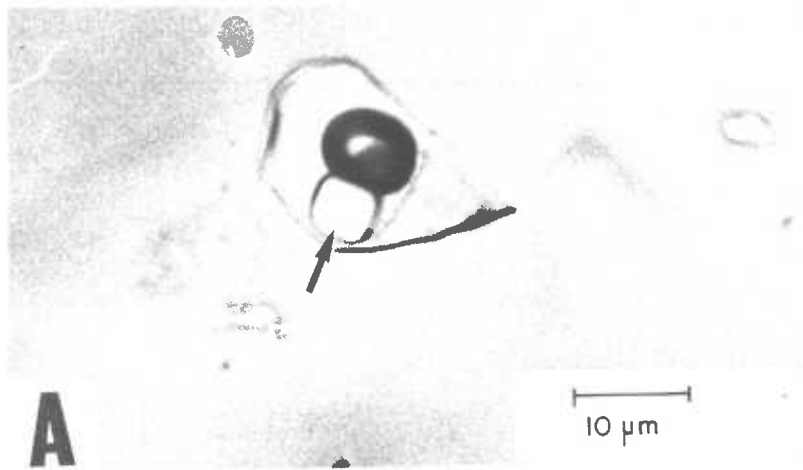
## PLATE 17

Chorolque: Fluid inclusion types.

A. Typical primary Type III inclusion in vein quartz, showing cubic daughter mineral (halite, arrowed).

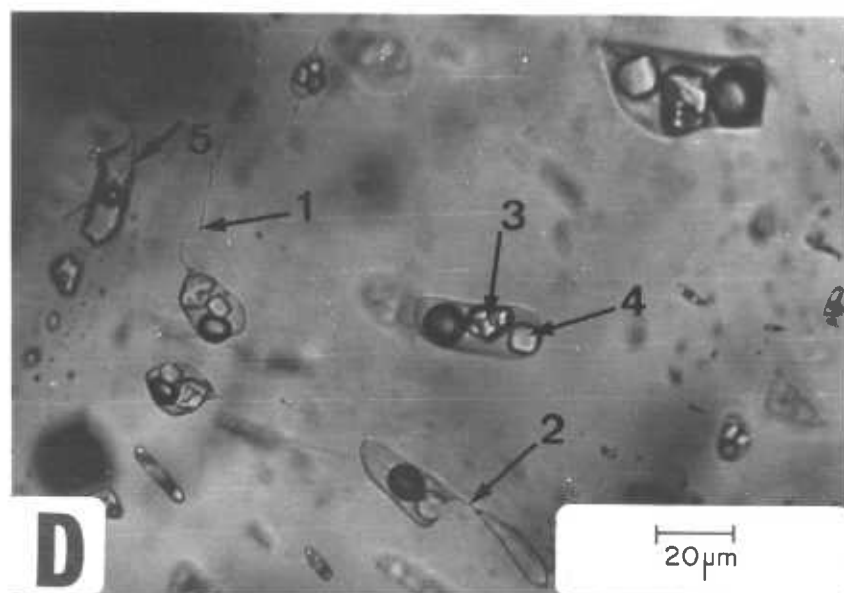
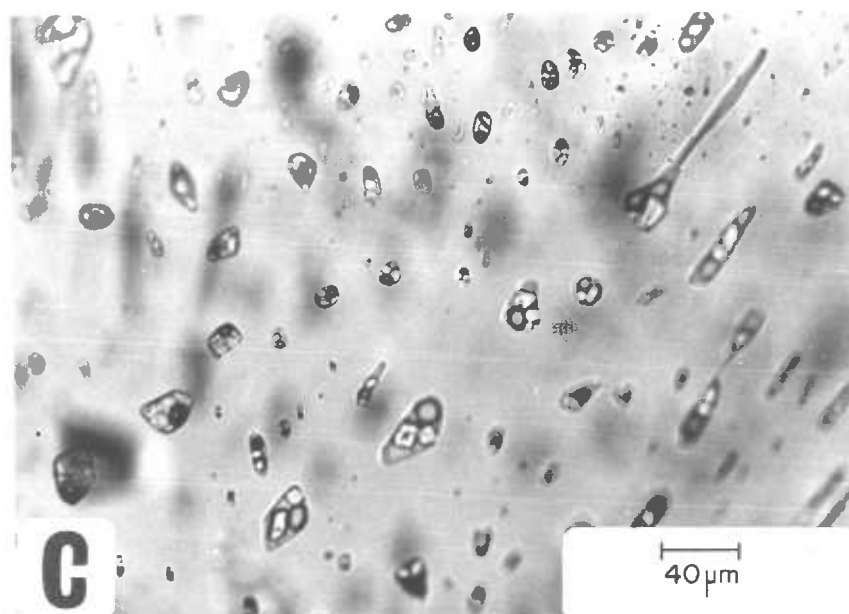
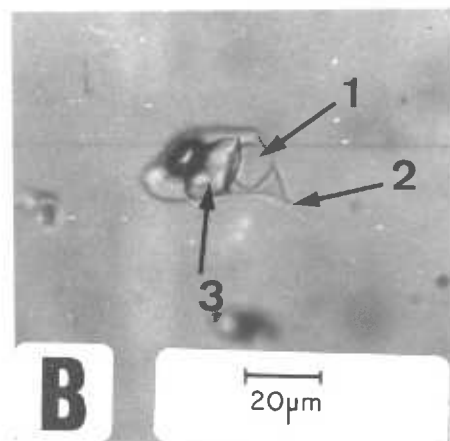
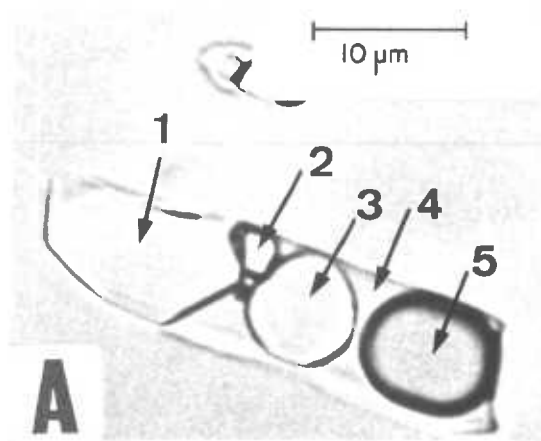
B. Plane of pseudosecondary Type III inclusions in vein quartz, with cubic daughter minerals (halite, arrowed).

C. Small primary Type III inclusion in vein quartz. Halite cube arrowed.



Chorolque: Fluid inclusion types.

- A. Typical primary Type IV multi-daughter inclusion in vein quartz. 1-large, pale greenish birefringent salt (hydrous iron chloride); 2-unidentified; 3-isotropic salt (halite); 4-liquid; 5-contraction vapour bubble.
- B. Pseudosecondary Type IV inclusion in vein quartz. 1-isotropic cubic daughter mineral (halite); 2-'tailed-off' shape of inclusion indicates that necking has taken place; 3-large daughter mineral grain, probably hydrous iron chloride.
- C. Plane of pseudosecondary Type IV inclusions in vein quartz. These contain 2 daughter minerals (as in B above), halite and hydrous iron chloride. Some show evidence of necking, but in general the phase ratios are constant.
- D. Pseudosecondary Type IV inclusions in vein quartz, showing good evidence of necking. 1-neck tube and tailed-off shape; 2-partially completed necking; 3- and 4-halite and hydrous iron chloride daughter minerals in un-necked inclusion; 5-separate plane of Type I inclusions.



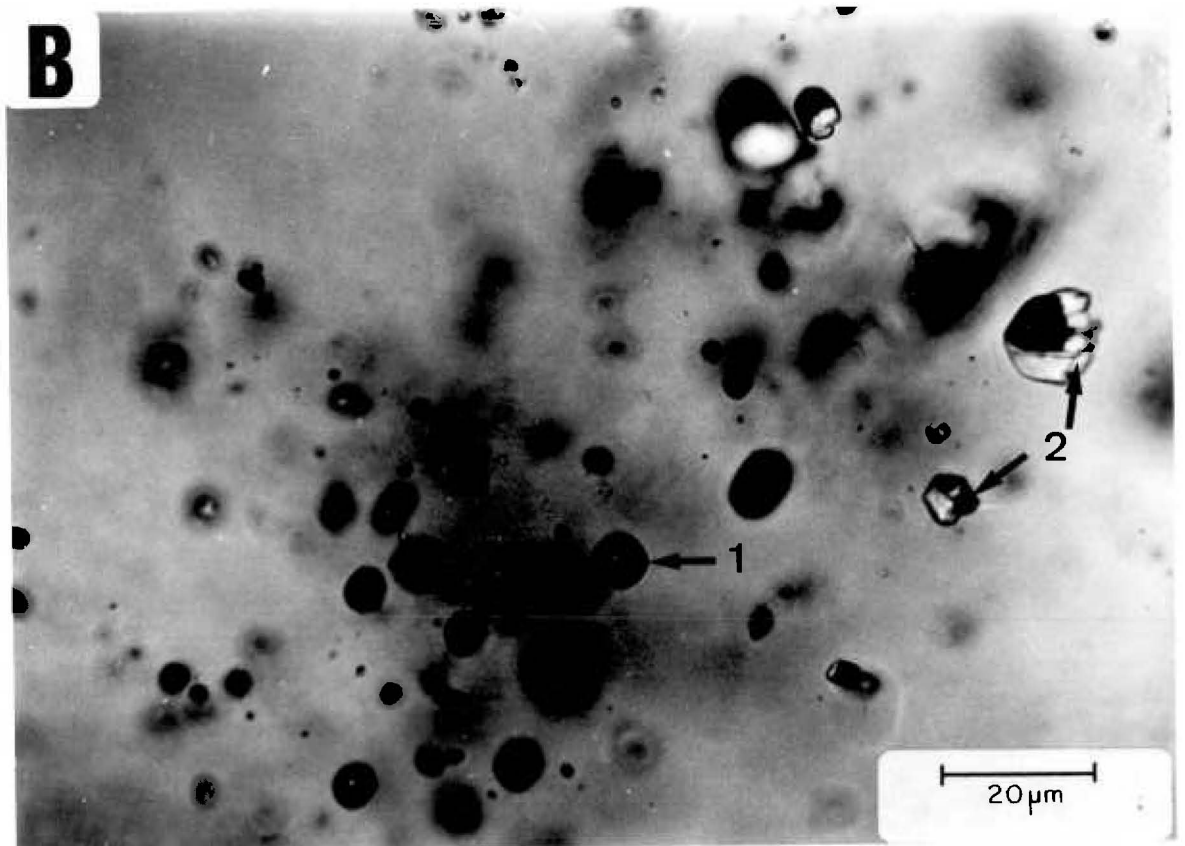
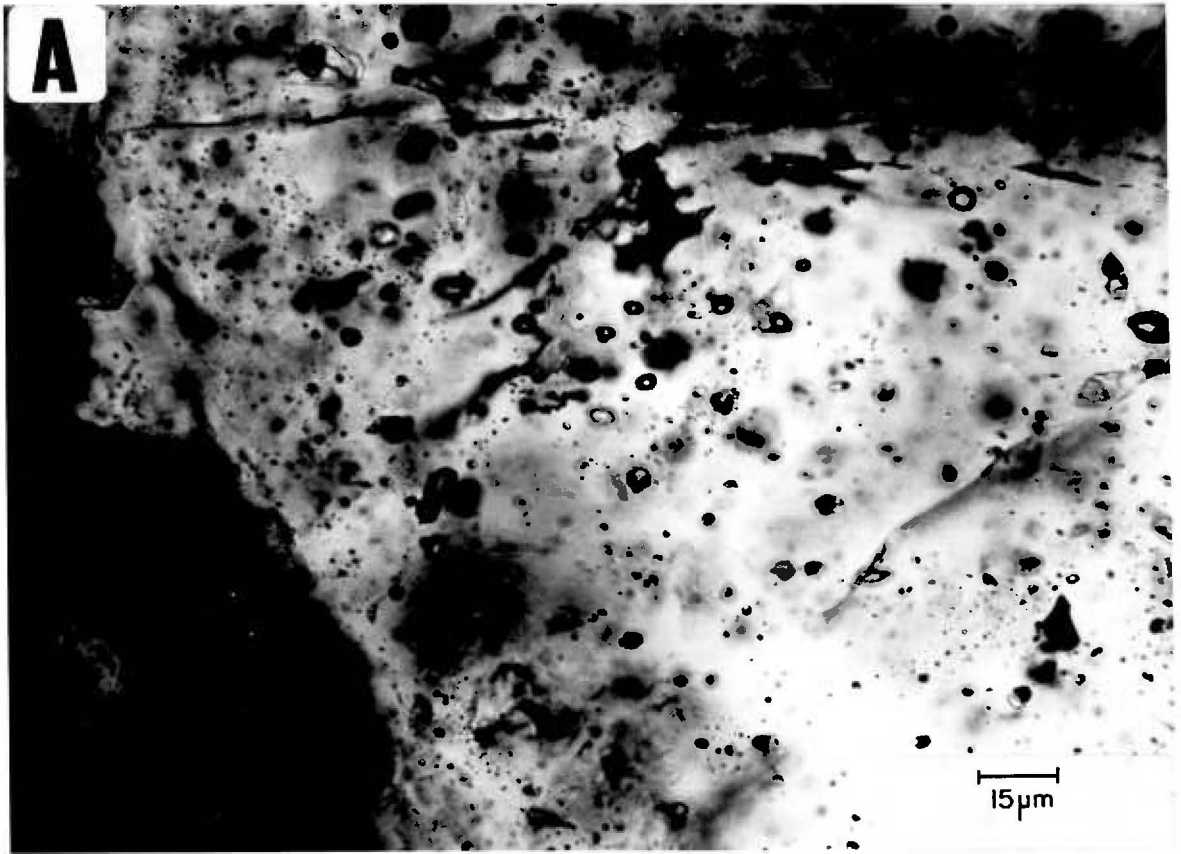


## PLATE 19

Chorolque: Fluid inclusion types.

A. Mainly primary vapour-filled Type V inclusions in quartz of the quartz-tourmaline alteration zone.

B. Detail of same specimen, showing co-existing vapour-filled Type V inclusions (1) and highly saline multi-daughter Type VI inclusions (2). A typical 2-phase (boiling) assemblage.



## PLATE 20

Chorolque: Fluid inclusion types.

A. Detail of primary Type V vapour-filled inclusions in quartz of the quartz-tourmaline alteration zone.

B. Detail of a primary Type VI inclusion in quartz of the quartz-tourmaline zone. The inclusion is packed with daughter minerals (2, 3, 4) which can not be individually identified. The vapour bubble (1) is distorted by the daughter minerals, and no liquid phase is visible at room temperature.

C. Two Type VI inclusions (arrowed) in a healed fracture traversing a quartz phenocryst overgrown with secondary quartz, in the quartz-tourmaline alteration zone. The inclusions are packed with daughter salts, have distorted vapour bubbles and no visible liquid phase at room temperature.

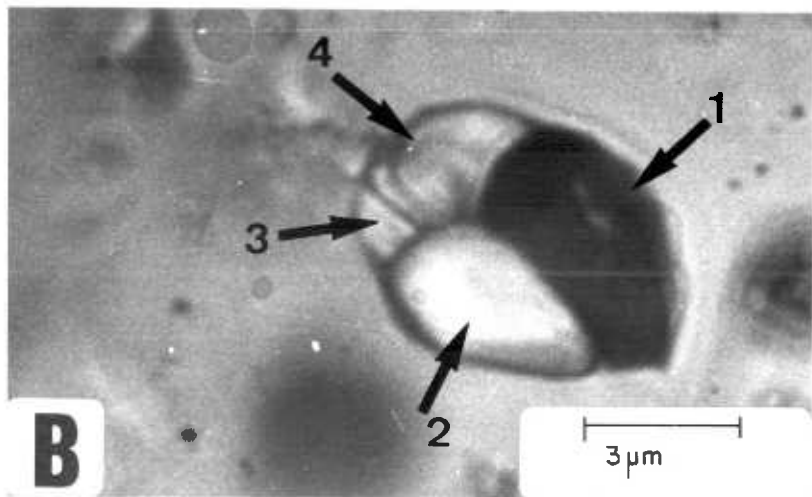
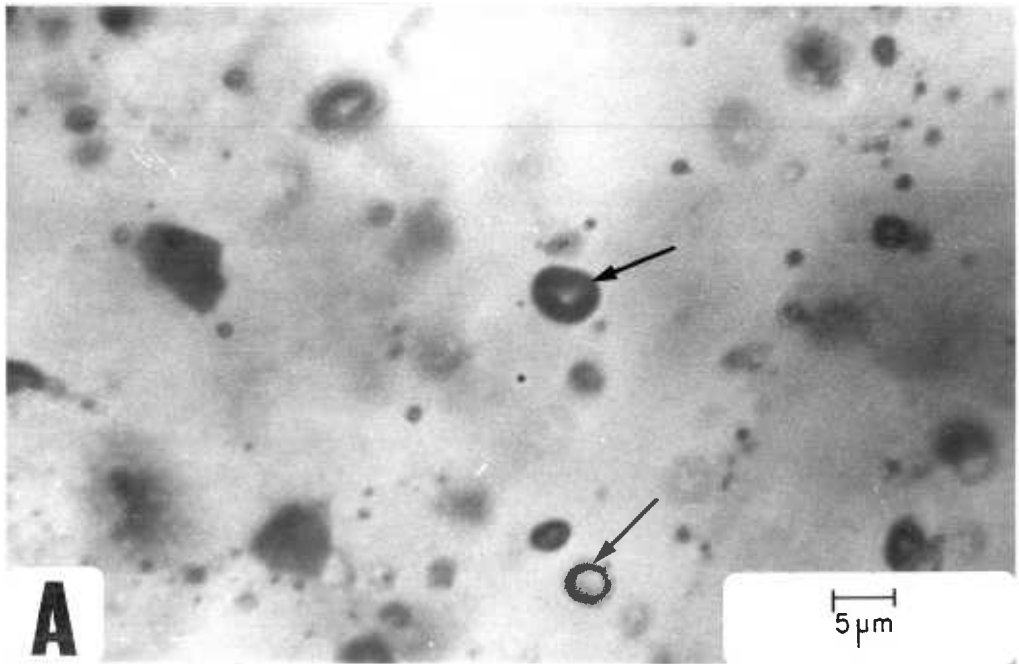


PLATE 21

Chorolque: Fluid inclusion types.

A. Two pseudosecondary Type VI inclusions, packed with daughter salts; in earliest vein quartz from Veta Colon. Plane polarized light.

B. As above, with crossed polars, showing the birefringence of one of the daughter salts (probably hydrous iron chloride).

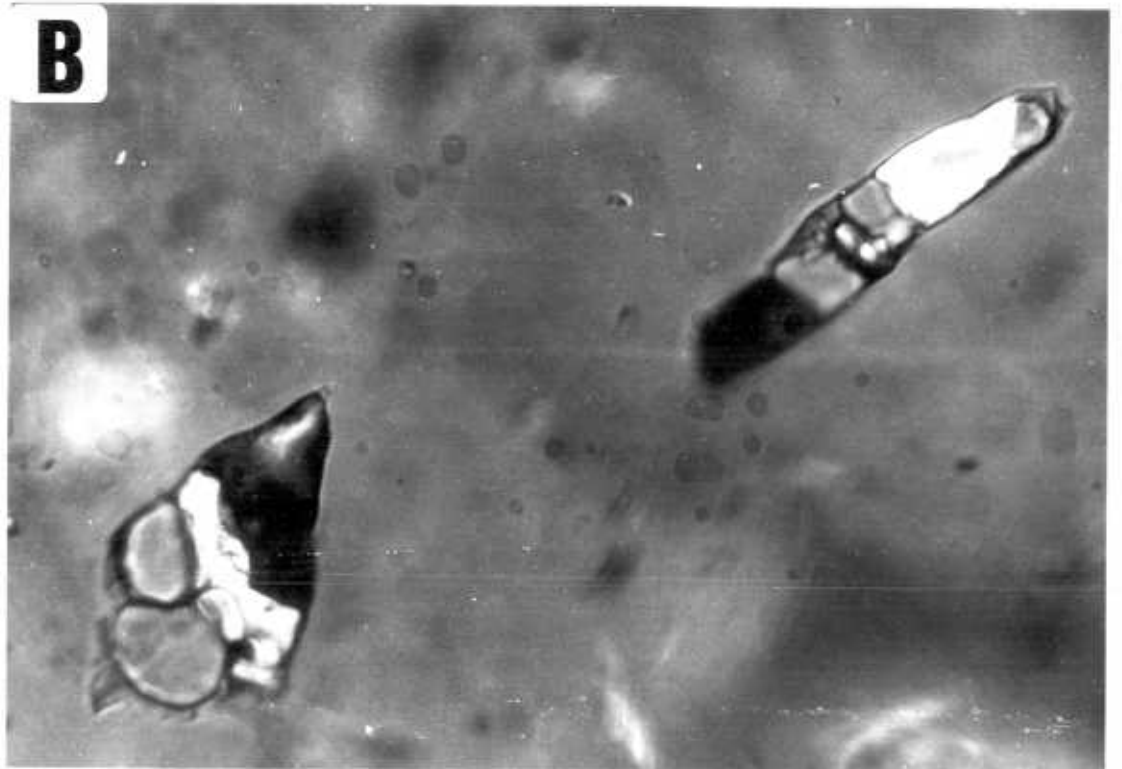
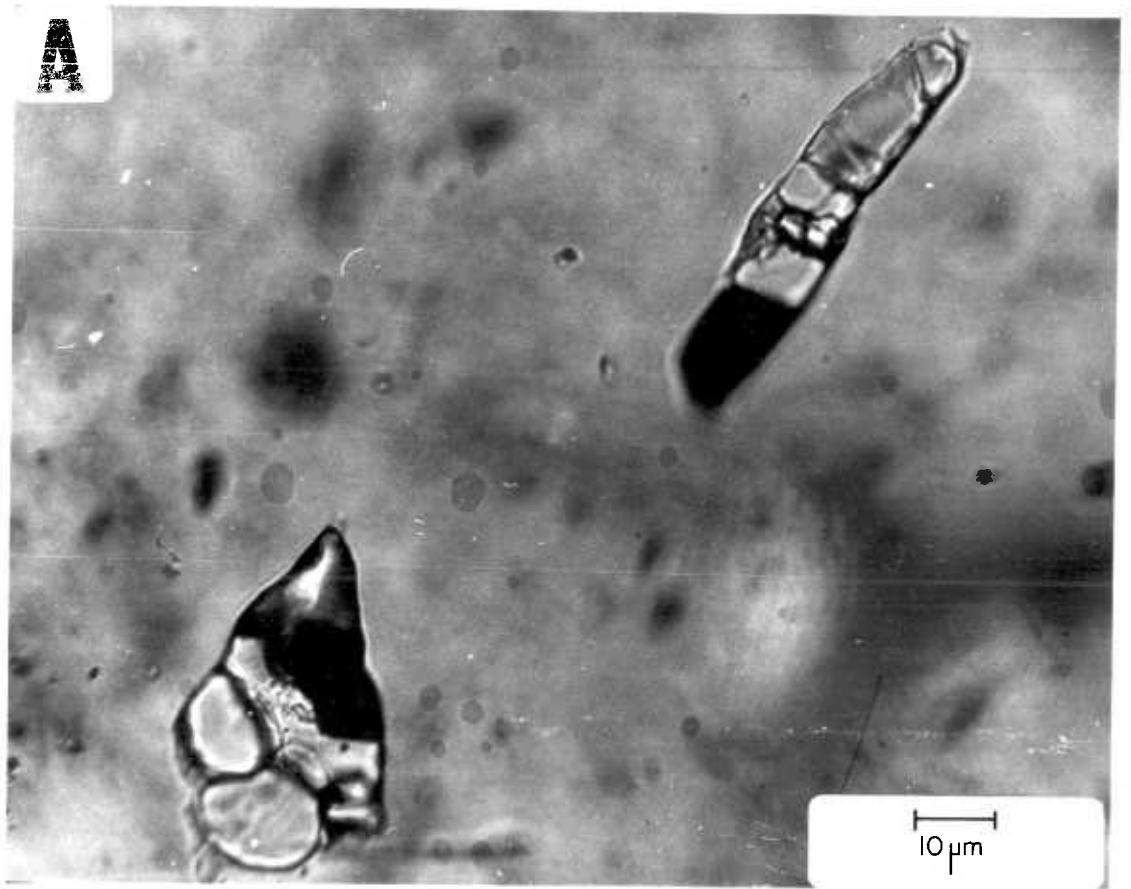


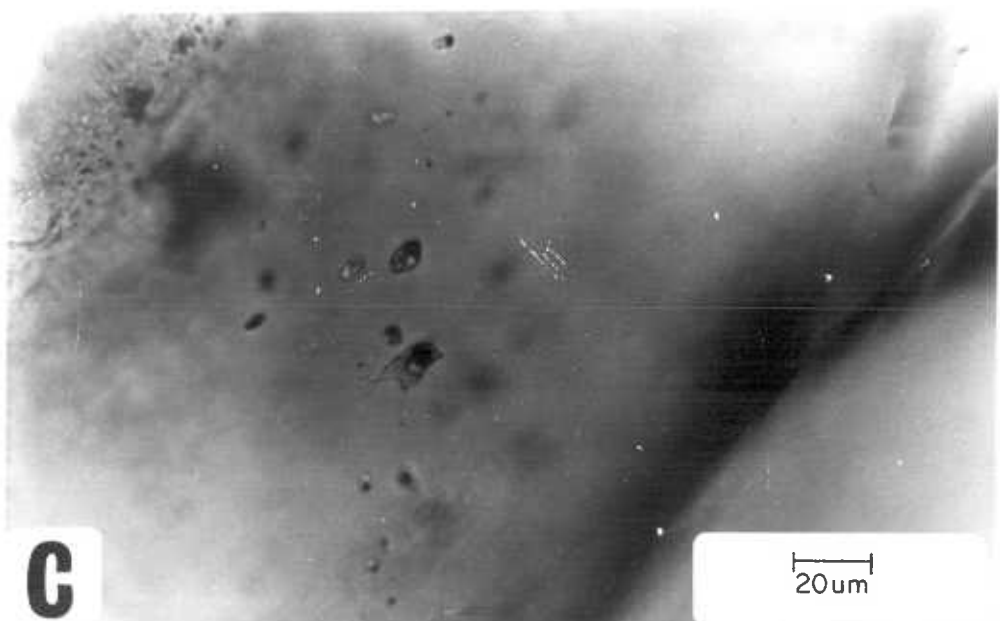
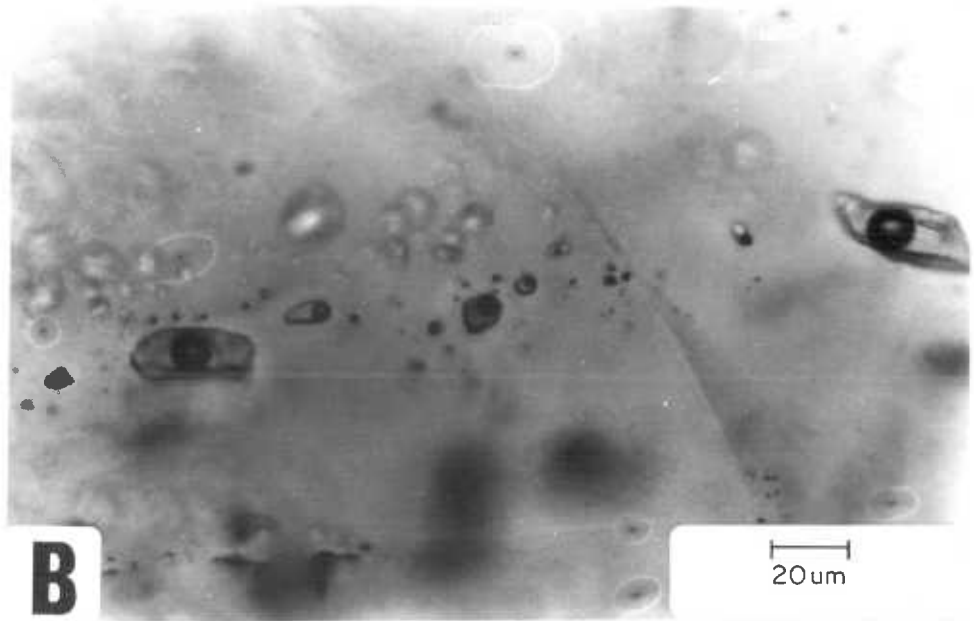
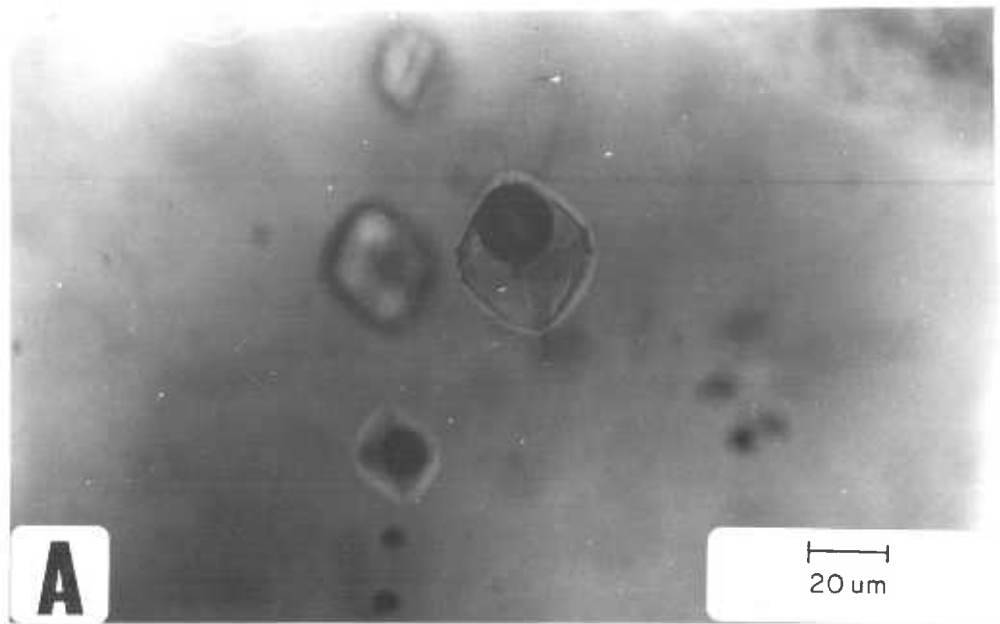
PLATE 22

Chorolque: Fluid inclusions in the sericitized volcanics.

A. Primary glass inclusion in quartz phenocryst.

B. Secondary Type I inclusions (liquid plus contraction vapour bubble) in quartz phenocryst.

C. Secondary Type IV inclusions in quartz phenocryst.





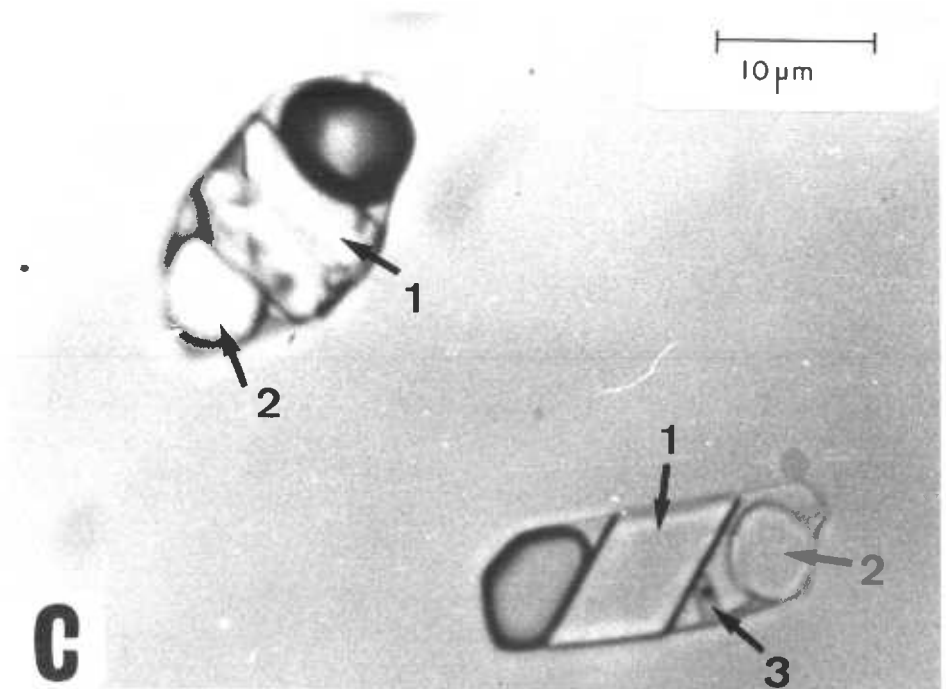
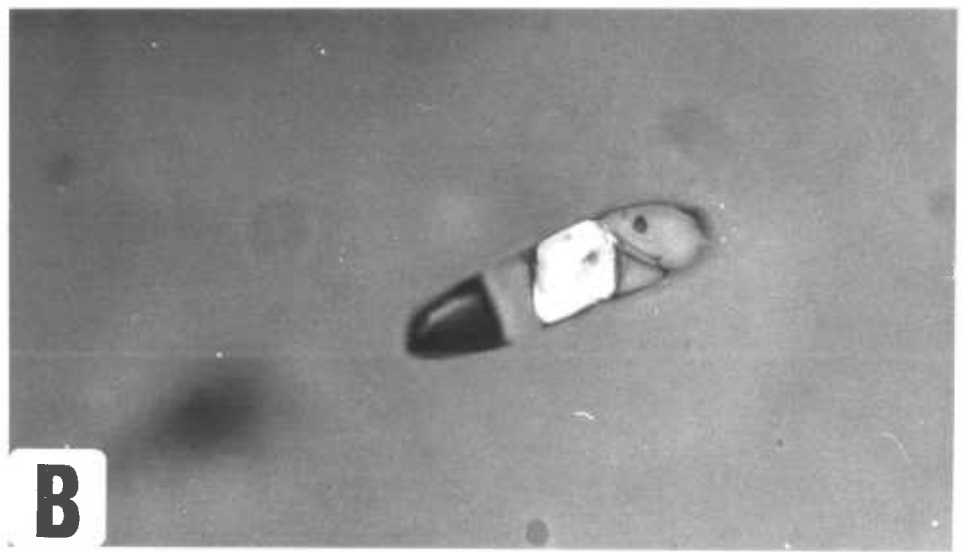
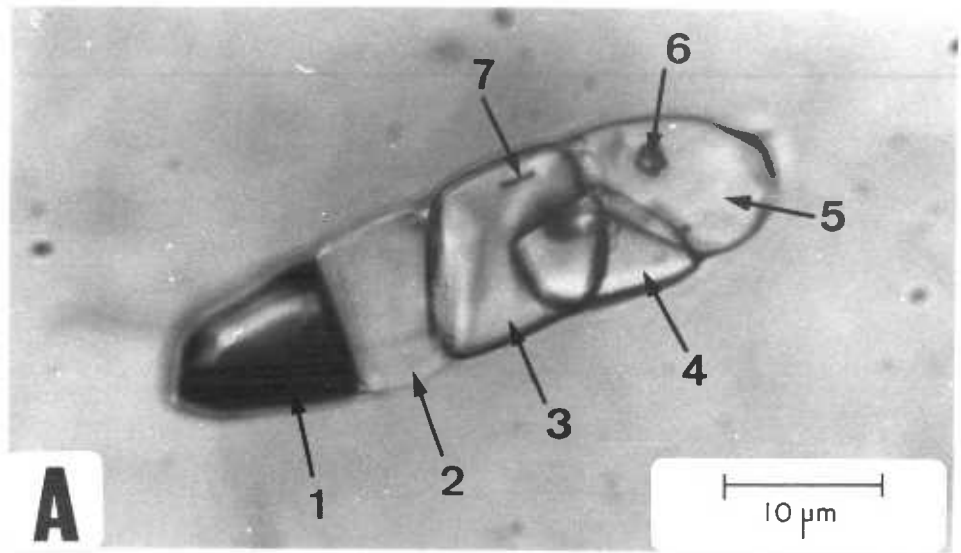
## PLATE 23

Chorolque: Daughter minerals in Type IV and VI inclusions.

A. Type VI inclusion in earliest vein quartz, Veta Colon. 1-distorted vapour bubble; 2-cubic salt with refractive index very close to that of quartz (halite); 3-rhombic birefringent salt (hydrous iron chloride); 4-unknown; 5-isotropic salt, possibly sylvite (KCl); 6- and 7-unknowns. Plane polarized light.

B. The same inclusion, crossed polars; showing the birefringence of the rhombic salt.

C. Type IV inclusions in vein quartz. 1-rhombic birefringent salt (hydrous iron chloride) showing twinning in the upper inclusion; 2-cubic salt (halite); 3-unknown transparent salt and very small opaque grain.

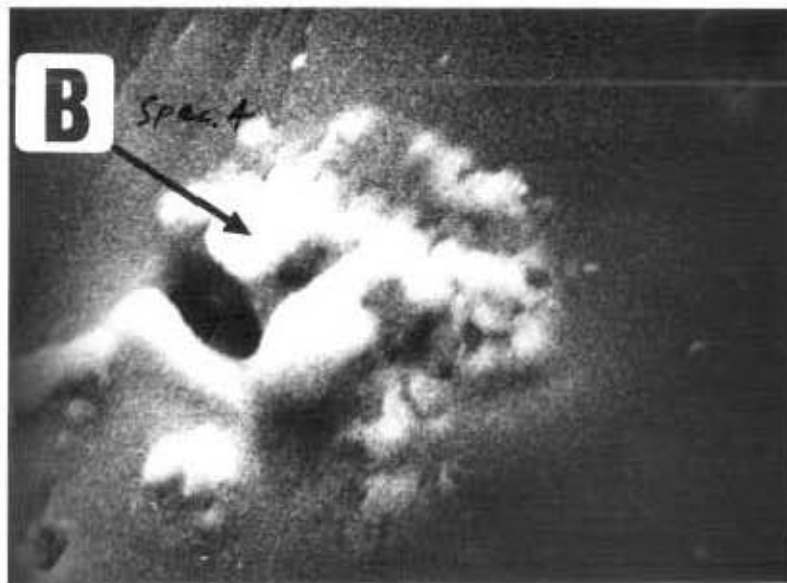
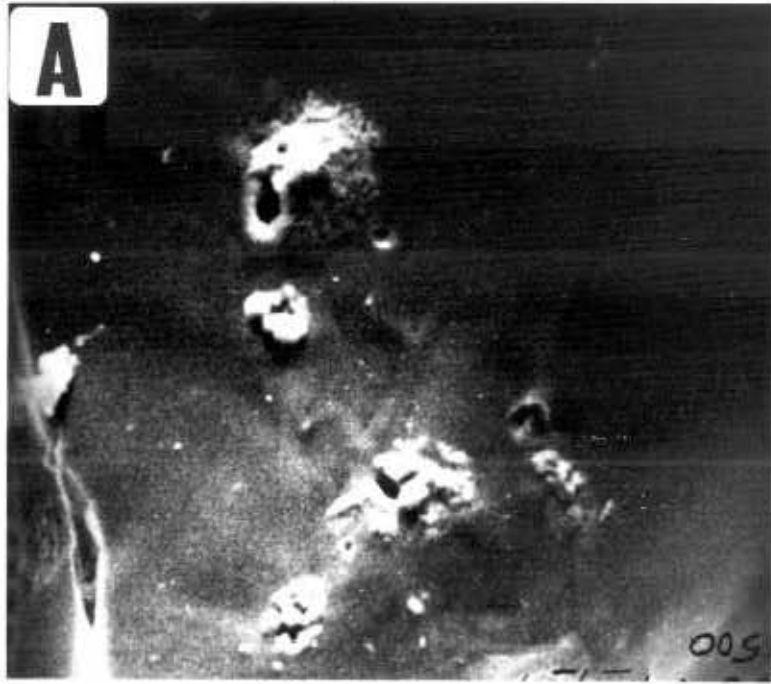


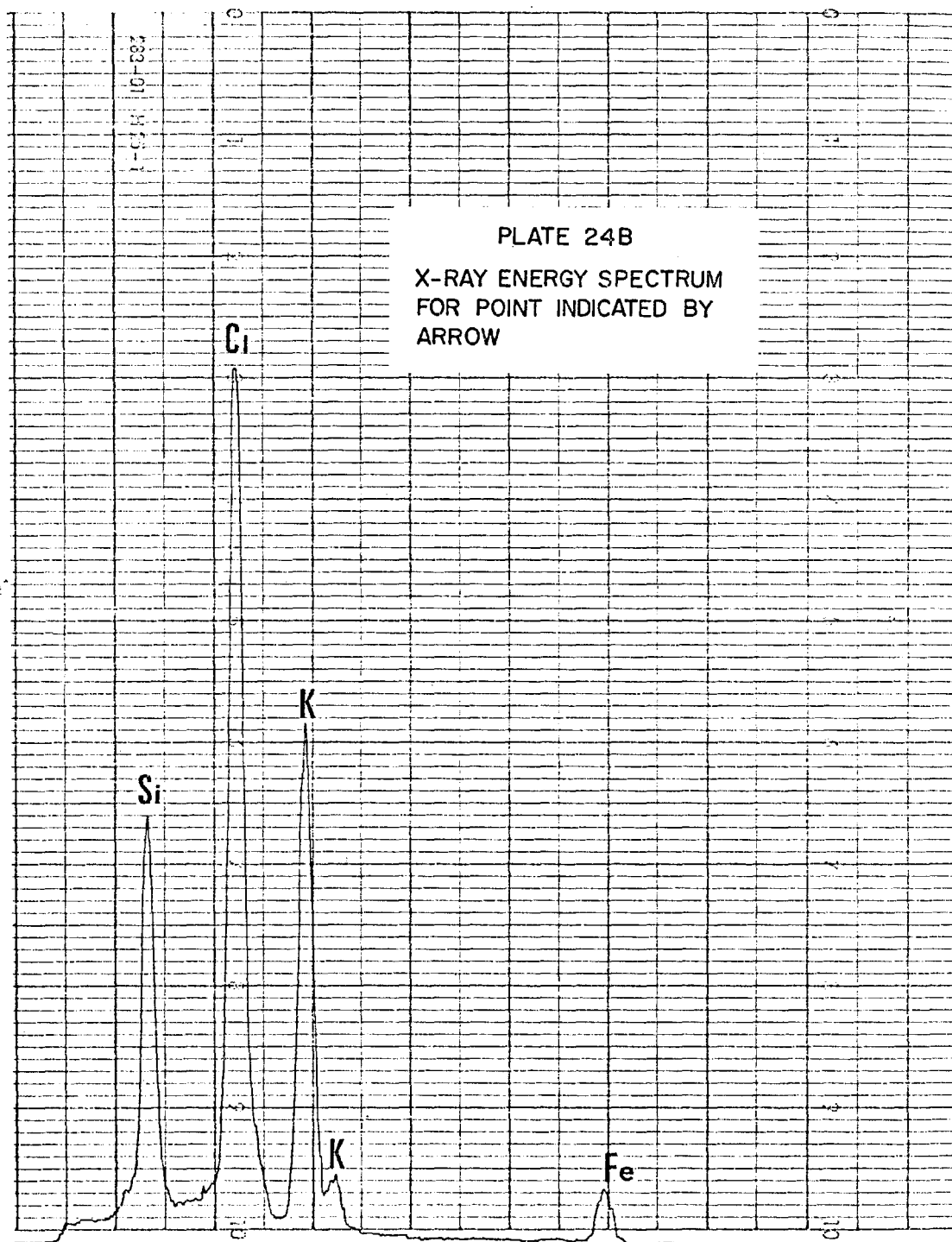
## PLATE 24

Scanning electron microscope investigation of daughter minerals:  
Chorolque, quartz-tourmaline altered vent rocks.

A. Low magnification view (X500) of broken surface of quartz sample showing several opened inclusion cavities with apparently extruded daughter salt material.

B. Detail of one inclusion (X1500), showing the formless appearance of the daughter salt material. The major components are potassium and chlorine, arrow indicates analysed point, see following page for X-ray spectrum.



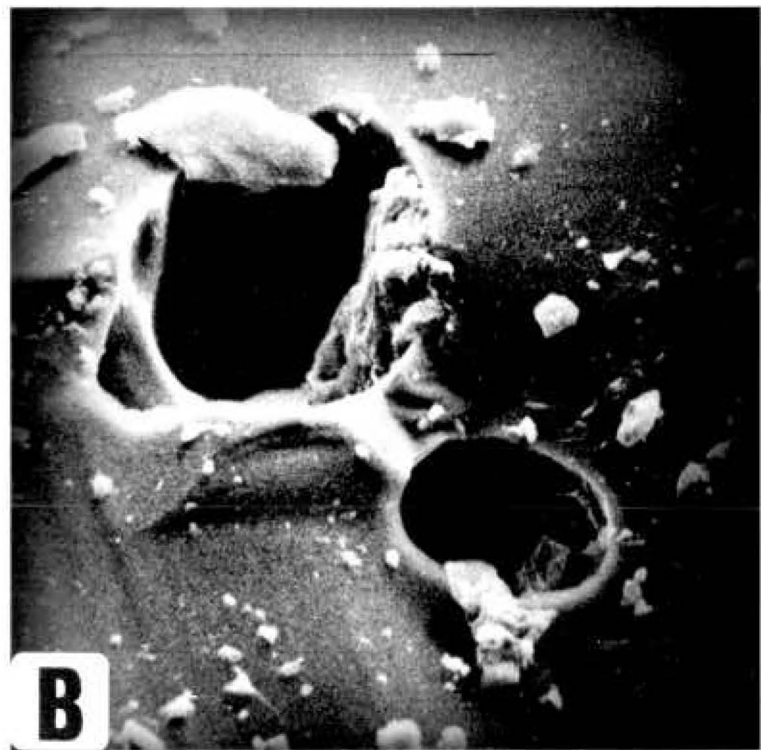


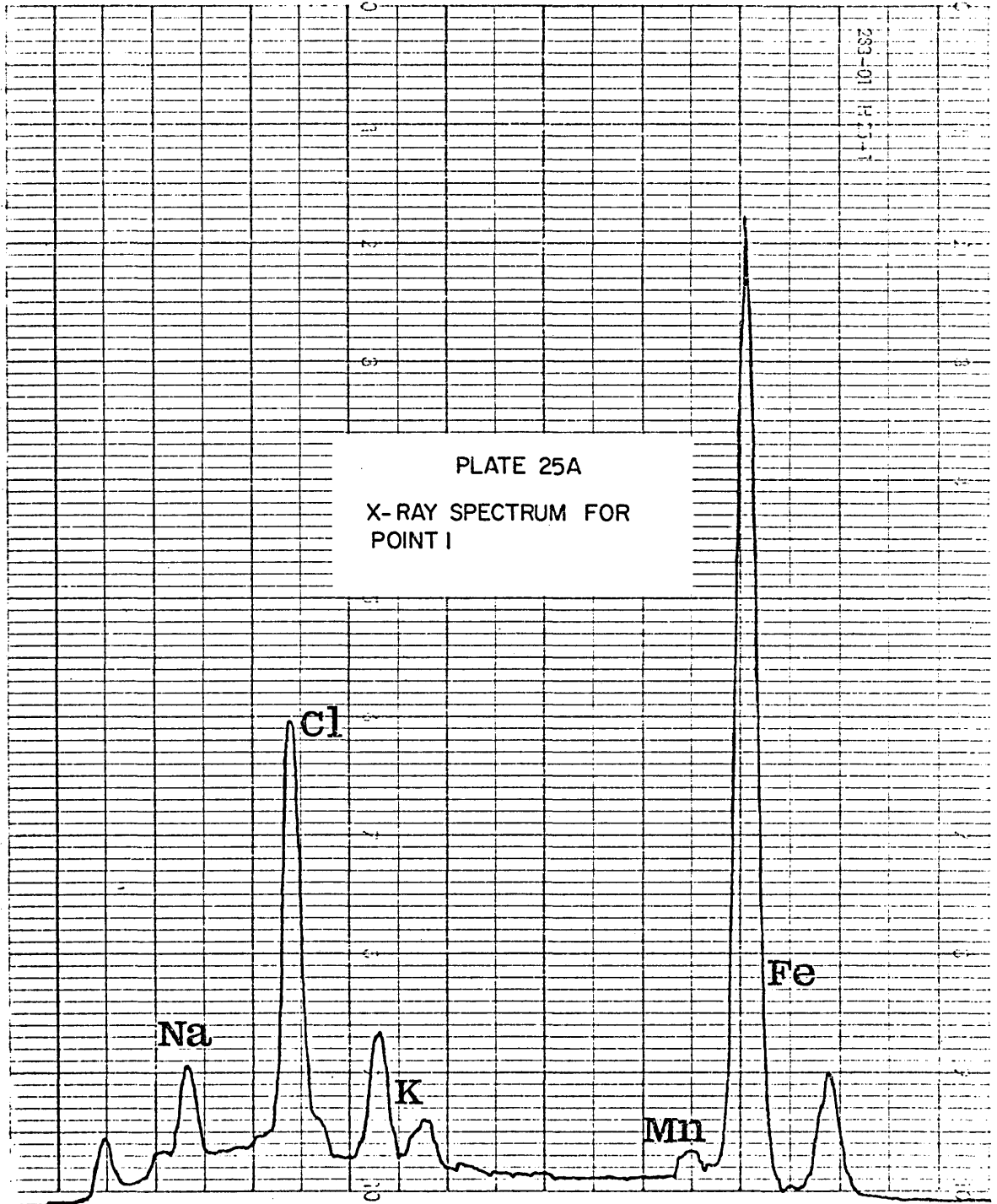
## PLATE 25

SEM investigation of daughter minerals: Chorolque, quartz-tourmaline altered vent rocks.

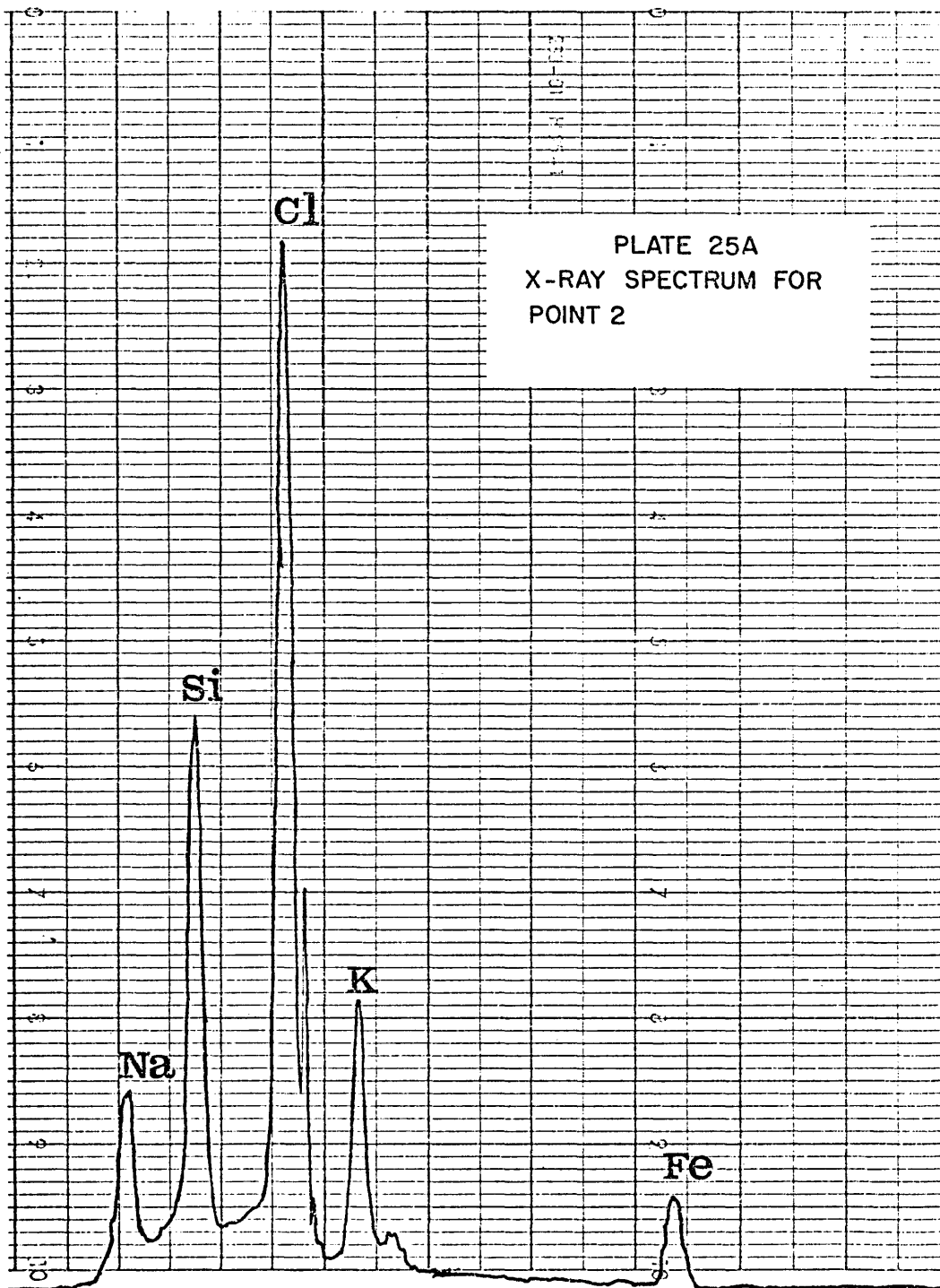
A. Single inclusion cavity in quartz, with daughter minerals in-situ. Arrows indicate analysed points (see following pages for X-ray spectra). Most of the grains on the surface surrounding the cavity are quartz fragments produced during the opening process. X1500.

B. Two inclusion cavities in quartz, with some daughter salt material adhering to the cavity sides. X1500.









## PLATE 26

SEM investigation of daughter minerals: Chorolque, quartz-tourmaline altered vent rocks.

A. Type VI inclusion cavity crowded with daughter mineral grains. The X-ray spectrum from scanning the entire inclusion cavity (see following page) indicates that the major components are; iron, potassium, chlorine, sodium, and sulphur. Silicon comes mainly from quartz fragments and the cavity walls. X2500.

B. Inclusion cavity with much daughter salt material. X-ray spectra from scanning the entire cavity , and from individual points (arrowed) are shown on the following pages. Major components are iron, chlorine, potassium, sodium, and sulphur. X1500.

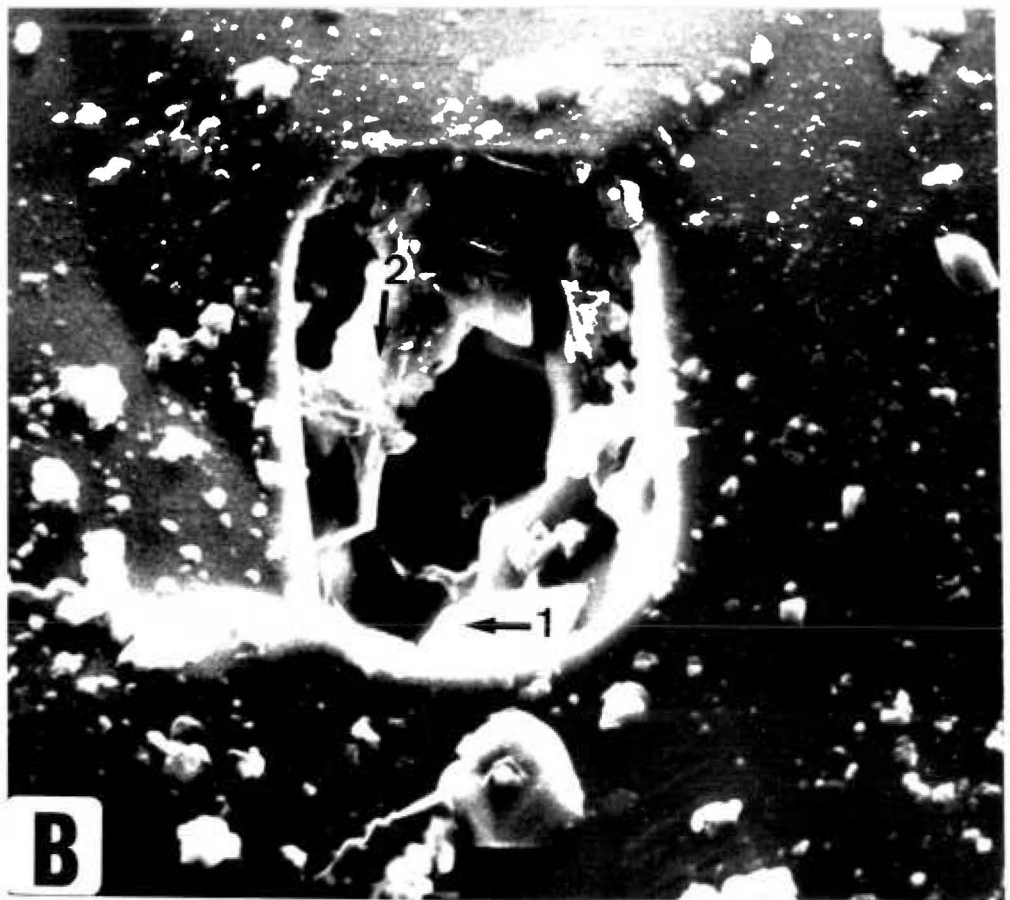
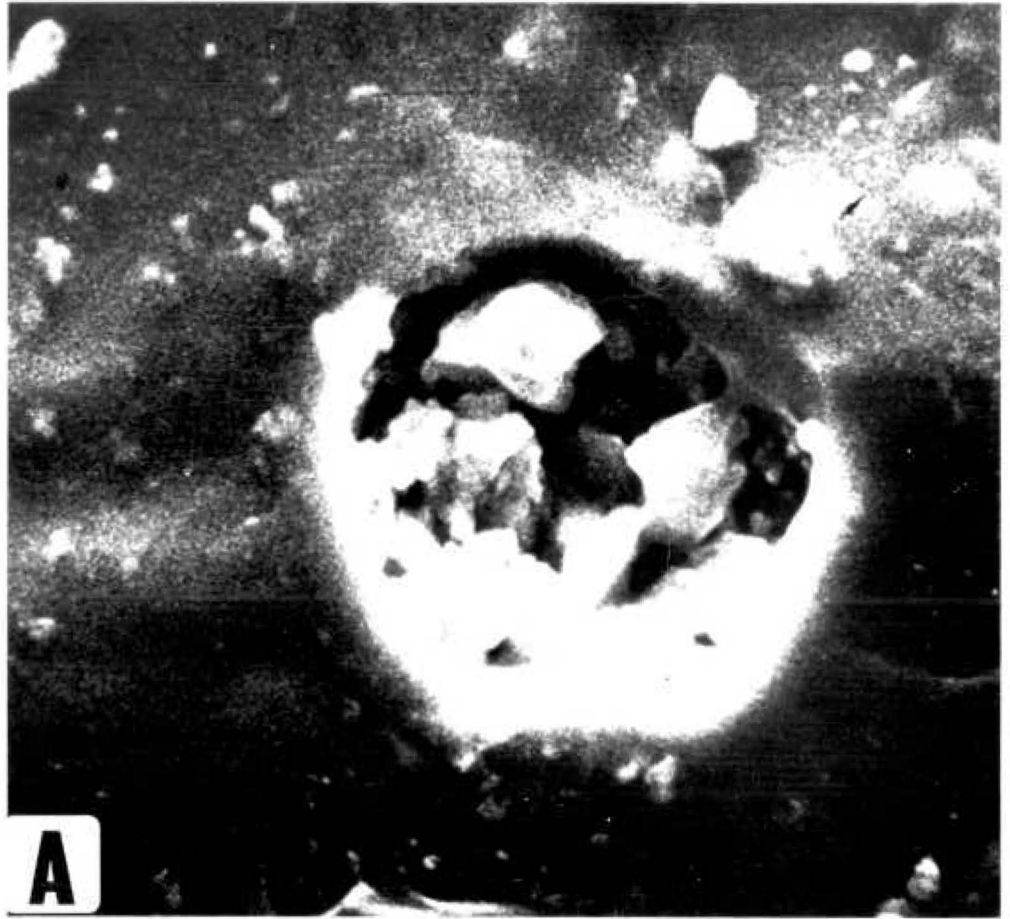
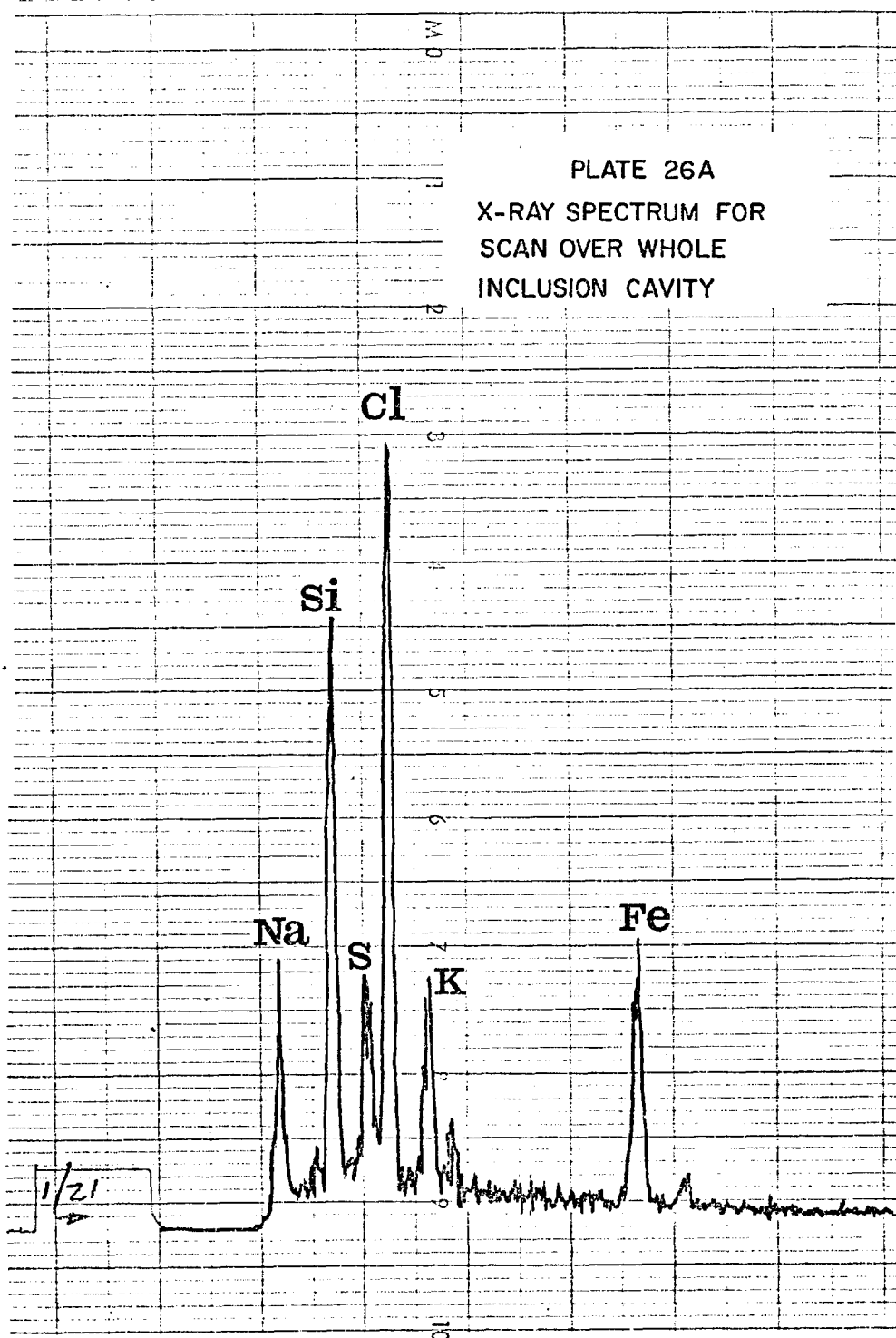
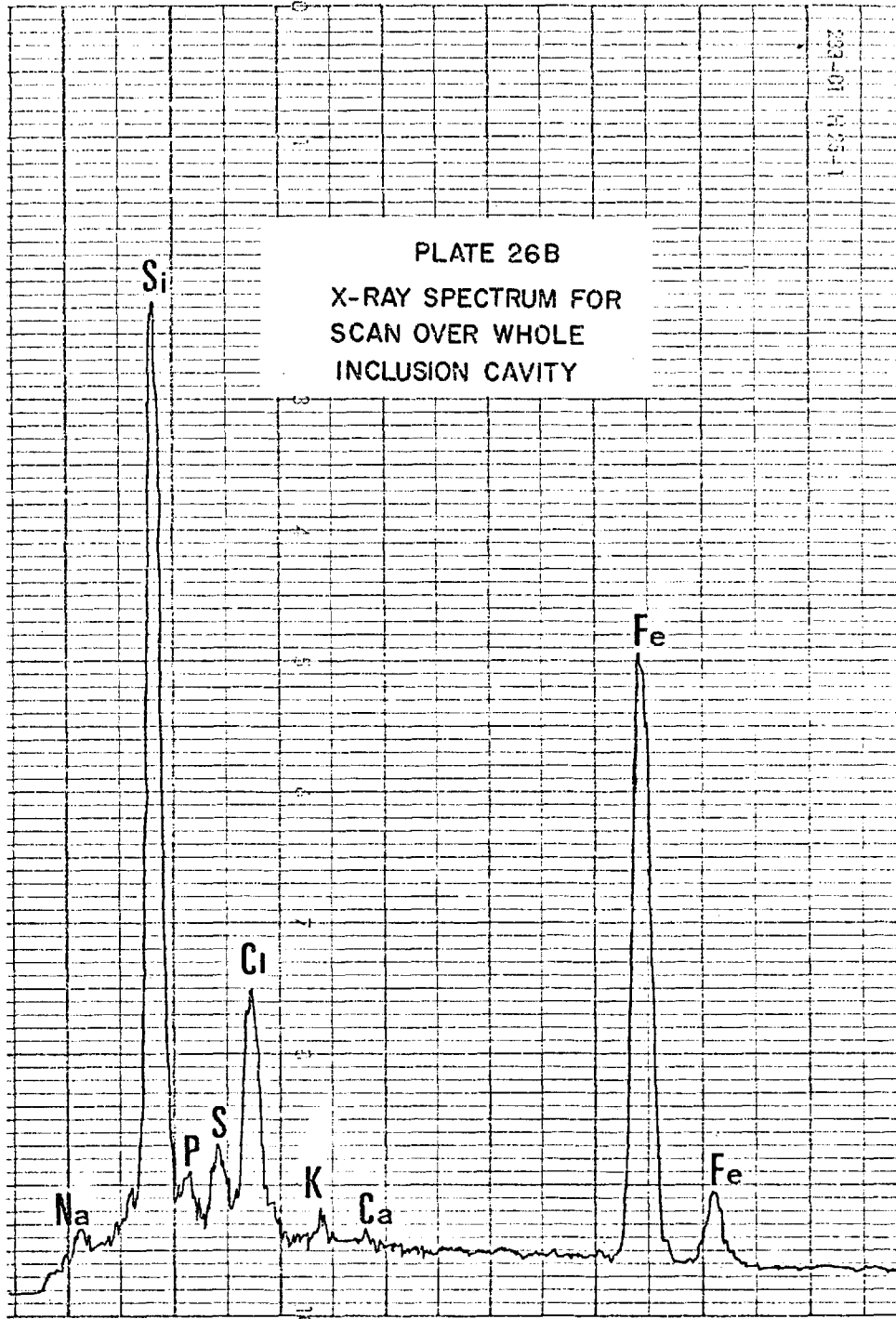
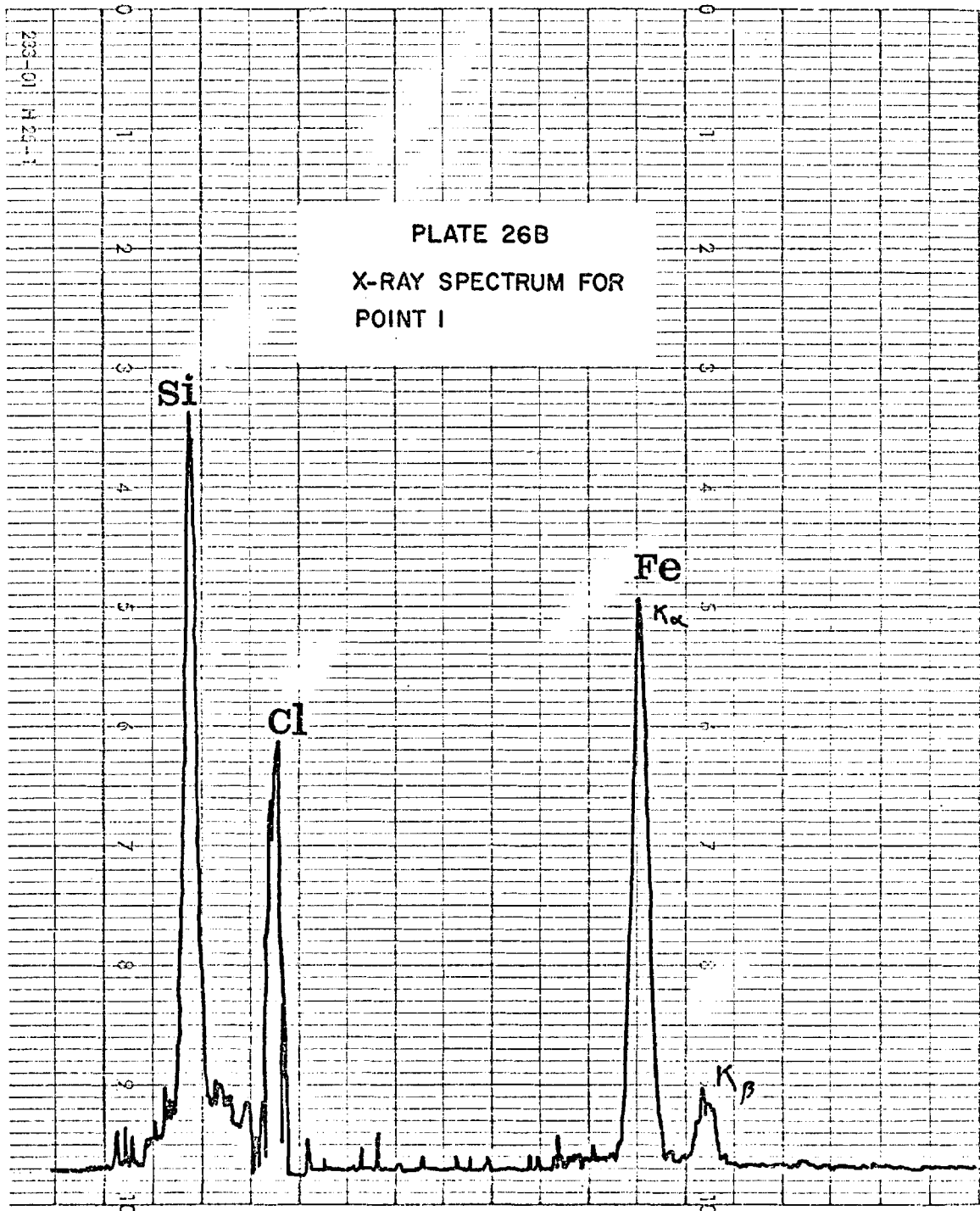


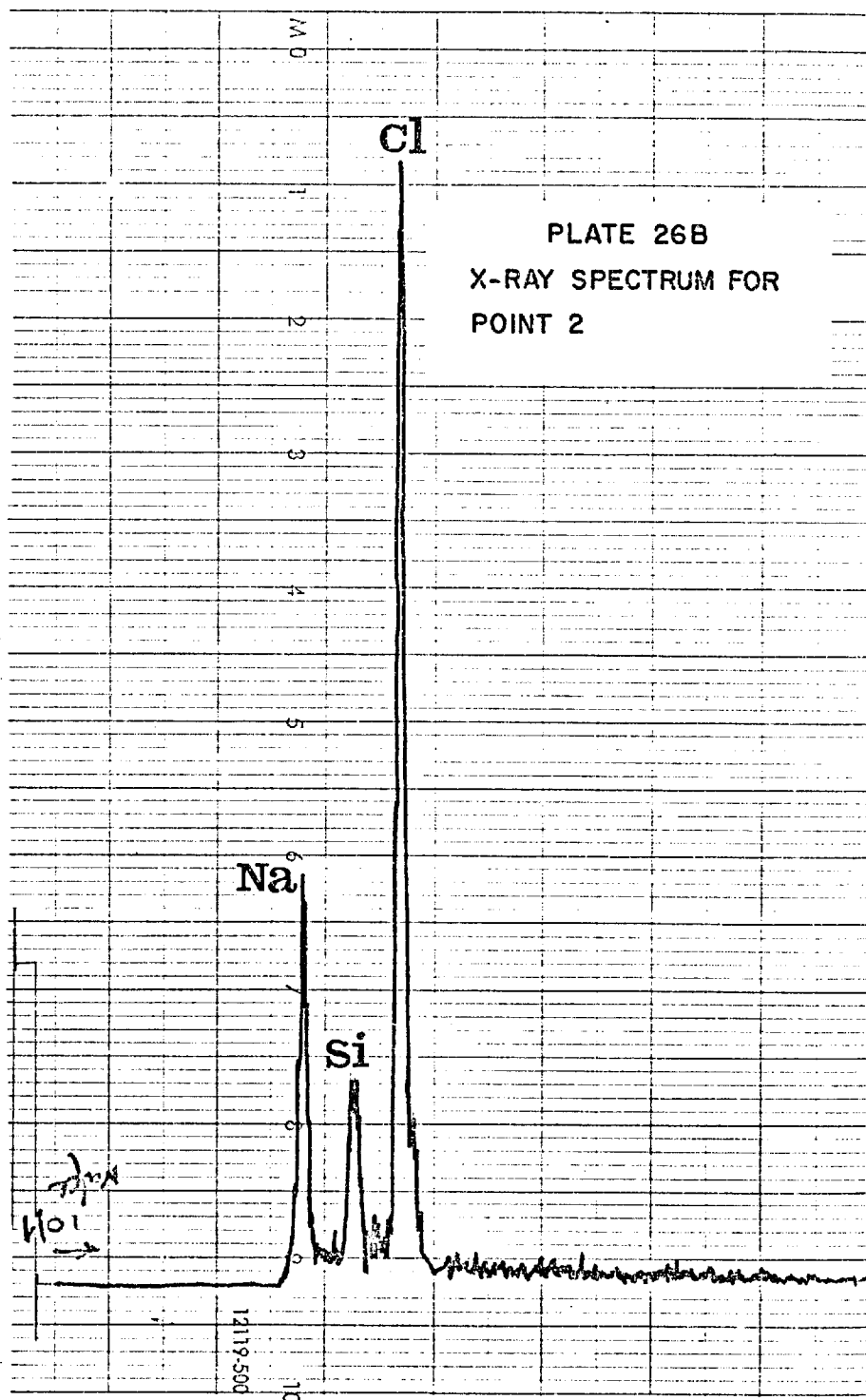
PLATE 26A  
X-RAY SPECTRUM FOR  
SCAN OVER WHOLE  
INCLUSION CAVITY



25







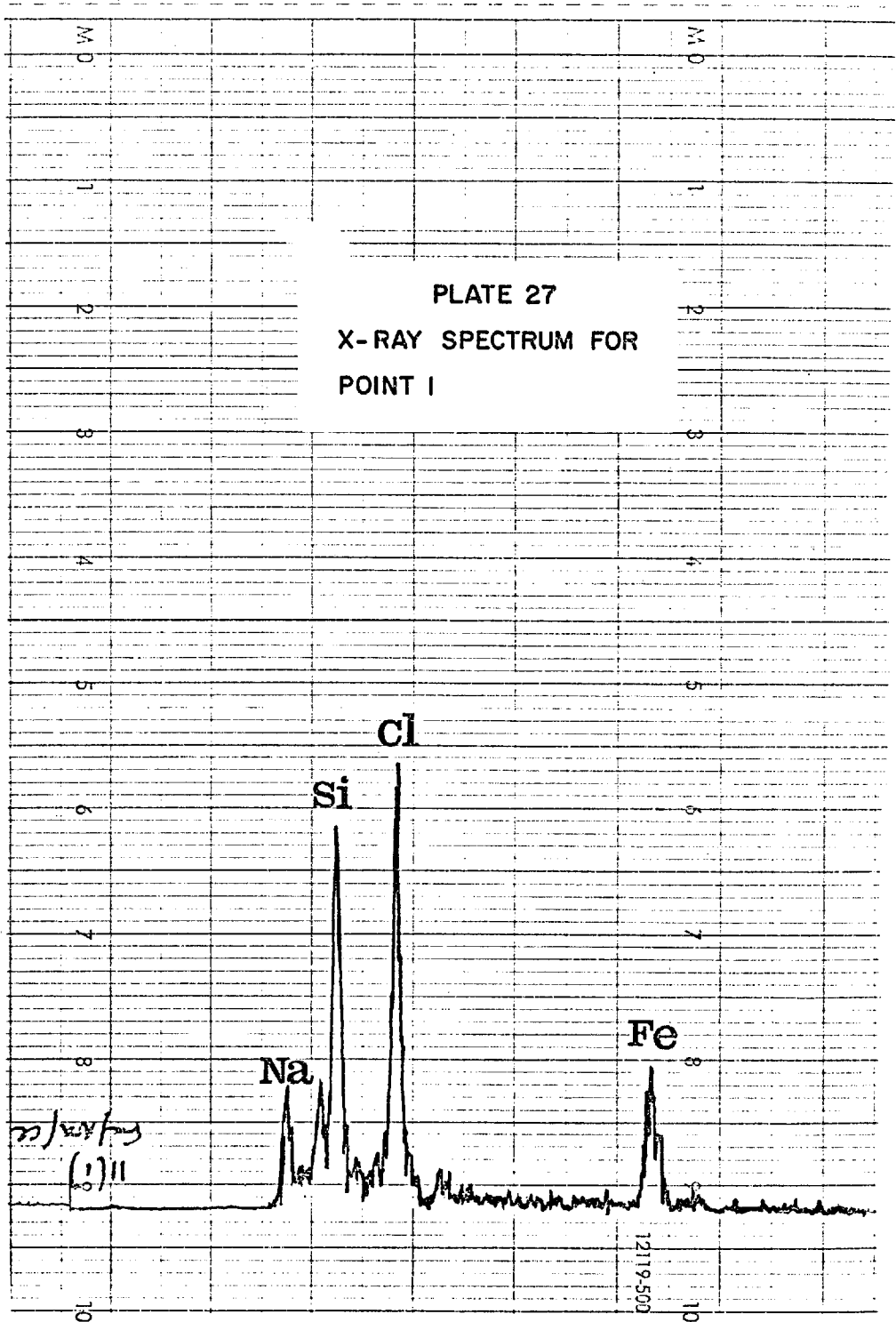
## PLATE 27

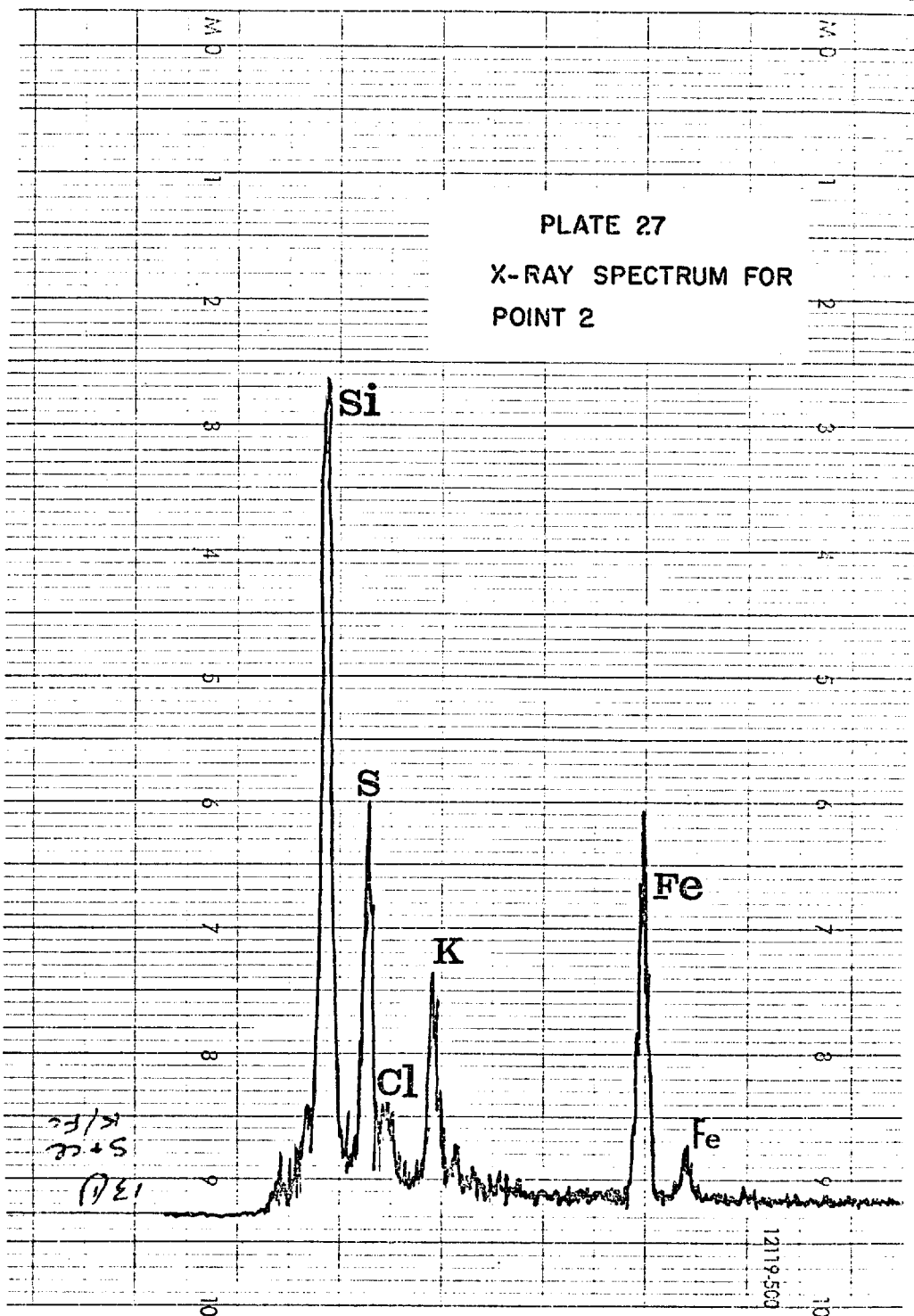
SEM investigation of daughter minerals: Chorolque, quartz-tourmaline altered vent rocks.

Inclusion cavity with much rather formless daughter salt material. X-ray spectra for point analyses (1 and 2 ) are shown on the following pages.









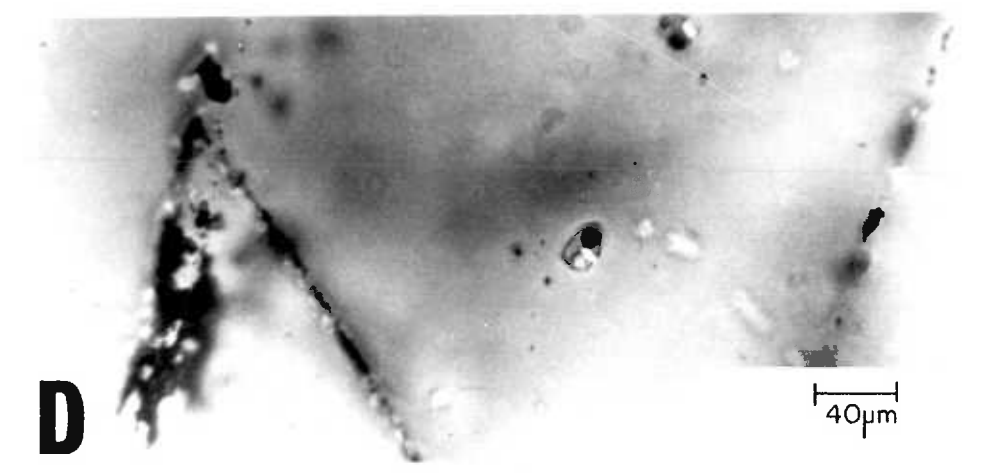
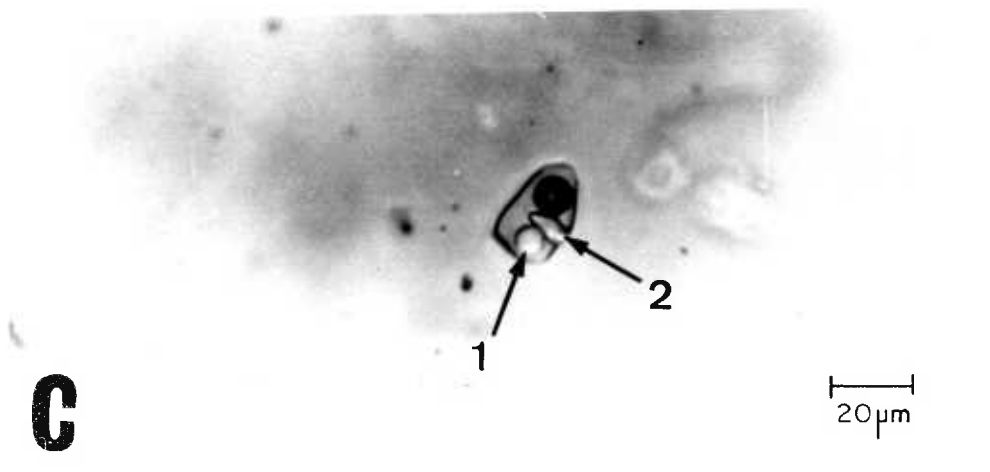
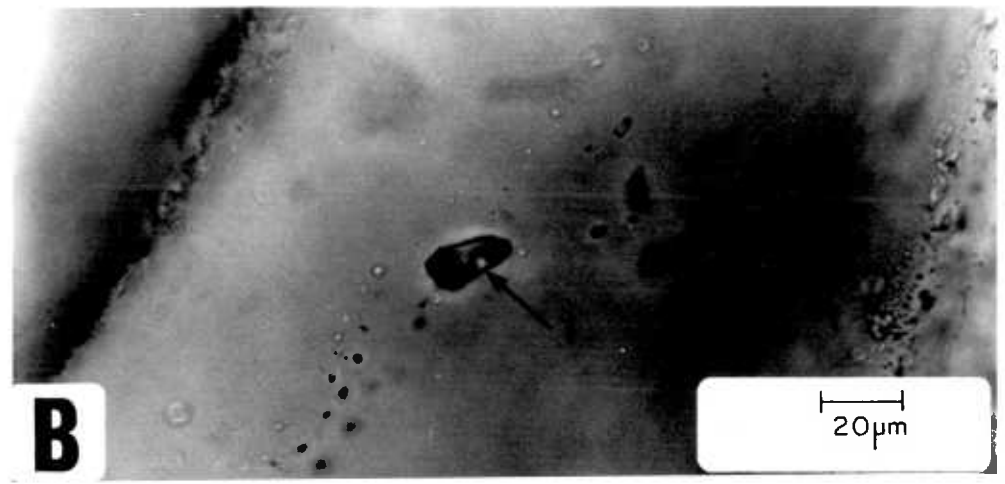
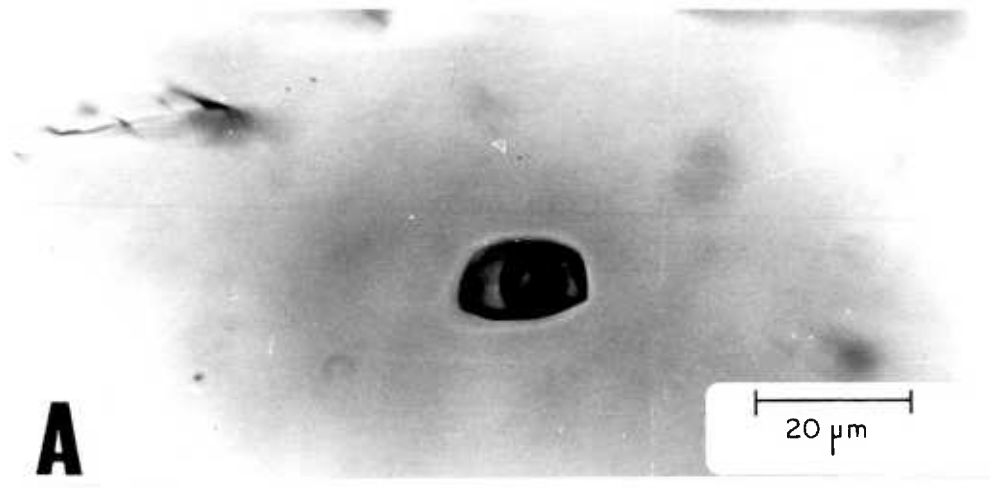
Llallagua, Salvador stock: Typical fluid inclusions in sericite-tourmaline altered quartz porphyry (secondary inclusions in quartz phenocrysts).

A. Type I inclusion.

B. Type III inclusion with halite daughter mineral (1).

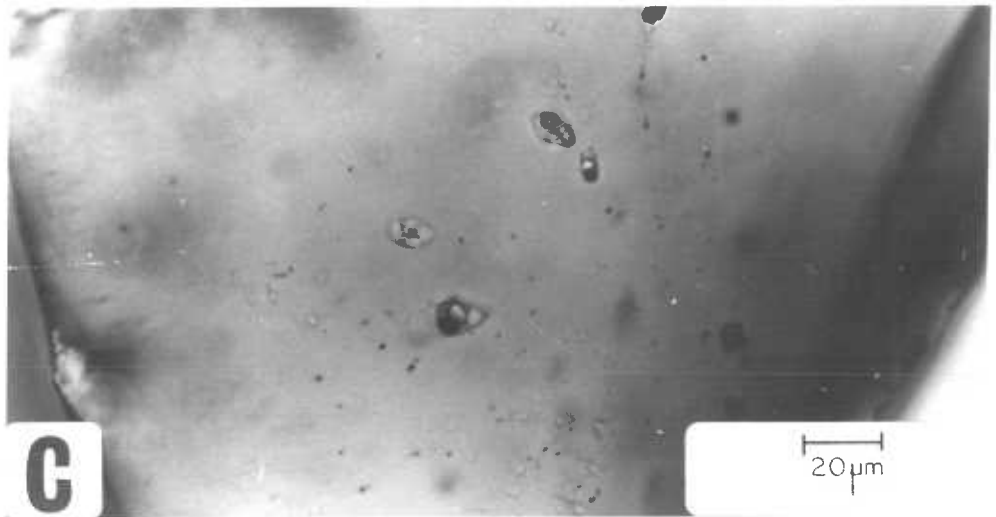
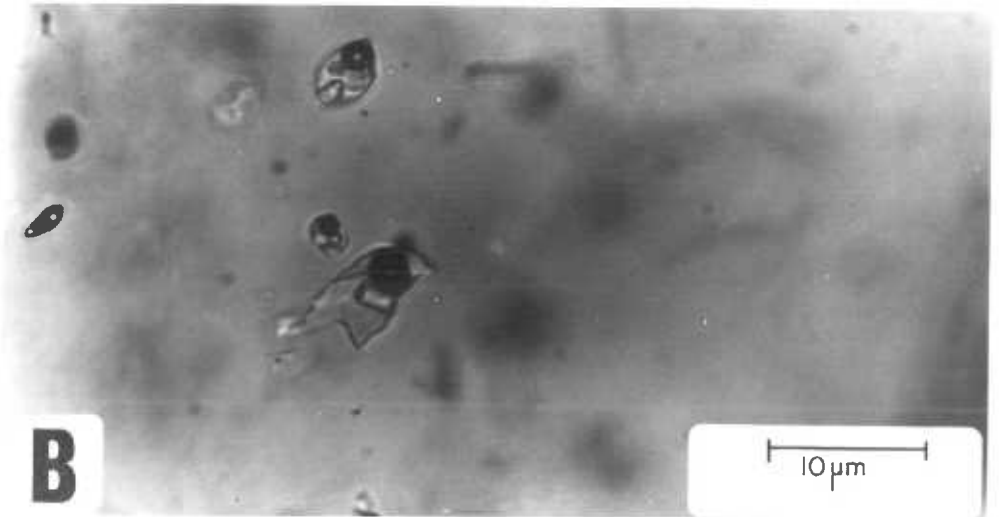
C. Type IV inclusion with halite (1) and rhombic birefringent (probably hydrous iron chloride) daughter (2). Plane polarized light.

D. Same inclusion as above, crossed polars, showing birefringence of rhombic daughter mineral.



Potosi: Fluid inclusion types.

- A. Typical very small primary or pseudosecondary inclusions in vein quartz intergrown with cassiterite and pyrite (black). Type I inclusions.
- B. Examples of the rare Type IV inclusions in quartz phenocrysts in the sericitized quartz-porphyry of the Cerro Rico stock.
- C. As above (B).



## PLATE 30

Huanuni: Fluid inclusions in vein quartz intergrown with cassiterite. A rare example of unequivocal primary inclusions in quartz.

A. Typical appearance of the vein quartz; primary vapour-rich inclusions (1) and numerous large irregular liquid-rich secondary inclusions (2).

B. Primary vapour-rich (low density fluid) inclusions oriented parallel to growth zoning in the quartz.

C. Primary vapour-rich inclusions (1) and primary liquid-rich inclusions (2) in separate growth zones.



